THE UNIVERSITY OF
SYDNEY

THE STRUCTURAL AND METAMORPHIC PETROLOGY OF THE MT. ROBE

DISTRICT, BROKEN HILL, N.S.W.

A thesis submitted for the Degree of Doctor of Philosophy,

Sydney University, 1966.

8 6 3 0 6 5

I hereby state that the results contained in this thesis and the
accompanying map, unless otherwise acknowledged, are my own.

 Specific references are made in the text to the published works of
other authors. This thesis, in part or whole, has not been submitted
previously for academic qualification at any institution.

A B S T R A C T

The tectonic and metamorphic histories of a portion of the Willyama Complex around Mt. Robe, Broken Hill, are clarified and described. Four generations of folds are recognised. The first generation of folds are isoclinal and transposed layering to parallel a schistosity that is axial surface to the folds. Analysis of the various sub-fabrics contributing to the triclinic symmetry of the fold system suggests the existence of an even earlier phase of folding. The second generation of folds are also isoclinal, but lack any penetrative foliation resulting from deformation.

The third and fourth generations of folds are characterised by the development of a conjugate set of kink bands in their hinges. The style of the folds is very variable and reflects the properties of the initial fabric on which the folds were imposed. The preferred orientation of basal deformation lamellae in quartz in a fourth generation fold allows the fixing of the principal axes of stress for the deformation. The minor and major axes are sub-horizontal and the intermediate axis plunges steeply parallel to the fold axes. A study of the geometry of two sets of deformation lamellae in a single grain indicates that they may be parallel to a number of the common forms of quartz. The major structure of the area is determined by one first generation fold, two fourth generation folds and an inhomogeneous fold-fault structure.

Metamorphism to produce mineral assemblages of the almandine-amphibolite facies followed or accompanied the first generation of folds. The area can be zoned with respect to the distribution of andalusite and sillimanite. Interfacial tension played a significant role in determining the shapes of grains but probably did not alter the shape of aggregates determined by deformation. The relative magnitudes of interfacial tensions, determined from the measurement of interfacial angles at triple junctions, of quartz-quartz and quartz-muscovite are the most important factors determining grain shapes.

Local metamorphism associated with the intrusion of pegmatites and a more general retrogression, followed the first phase of metamorphism. The various phases of folding and metamorphism probably represent two major and distinct episodes in the history of the Willyama Complex.

I N D E X

CHAPTER 4   THE MACROSCOPIC STRUCTURE

CHAPTER 5   METAMORPHIC PETROLOGY

CHAPTER 1

Introduction

This thesis is concerned with the structural and metamorphic history of the small portion of the Willyama Complex surrounding Mt. Robe, Broken Hill, N.S.W. (Map 1).

The Willyama Complex is a heterogeneous mass composed of regional metamorphics and intrusive rocks (Andrews, 1922) and is overlain unconformably by the sediments of the Torrowangee Beds. Radioactive dating gives an age of approximately 1600 million years for the primary regional metamorphism of the Willyama Rocks and ages of 1350-1600 million years for some of the acid intrusive rocks (pers. communication R. Pidgeon, 1964). The primary metamorphism produced sillimanite schists, pyroxene gneisses and amphibolites over the area of exposed Willyama Rocks (Andrews, 1922; Browne, 1922; Binns, 1963). The intrusive rocks are predominantly acid pegmatites although granitic rocks and dolerites have also been recognised.

Previous Literature

The first comprehensive map of the Willyama Complex was presented by E. C. Andrews in 1922. Andrew's work revealed the existence of a large, open fold closing to the north of Mt. Robe and dominating the structure in the north-western* portion of the Willyama Complex. This fold was named the Mt. Robe Basin by Andrews (Andrews, 1922, p.115). As such, the Mt. Robe Basin was one of a "group of basins, irregular in form, and of a complex nature, connected by ridges and by zones of flowage and dislocation" (Andrews, 1922, p.111) that formed the major structures of the metamorphic rocks. It is clear in the text that Andrews recognised that the structure may be very complex within small areas.

*
Roughly the area considered in this thesis.
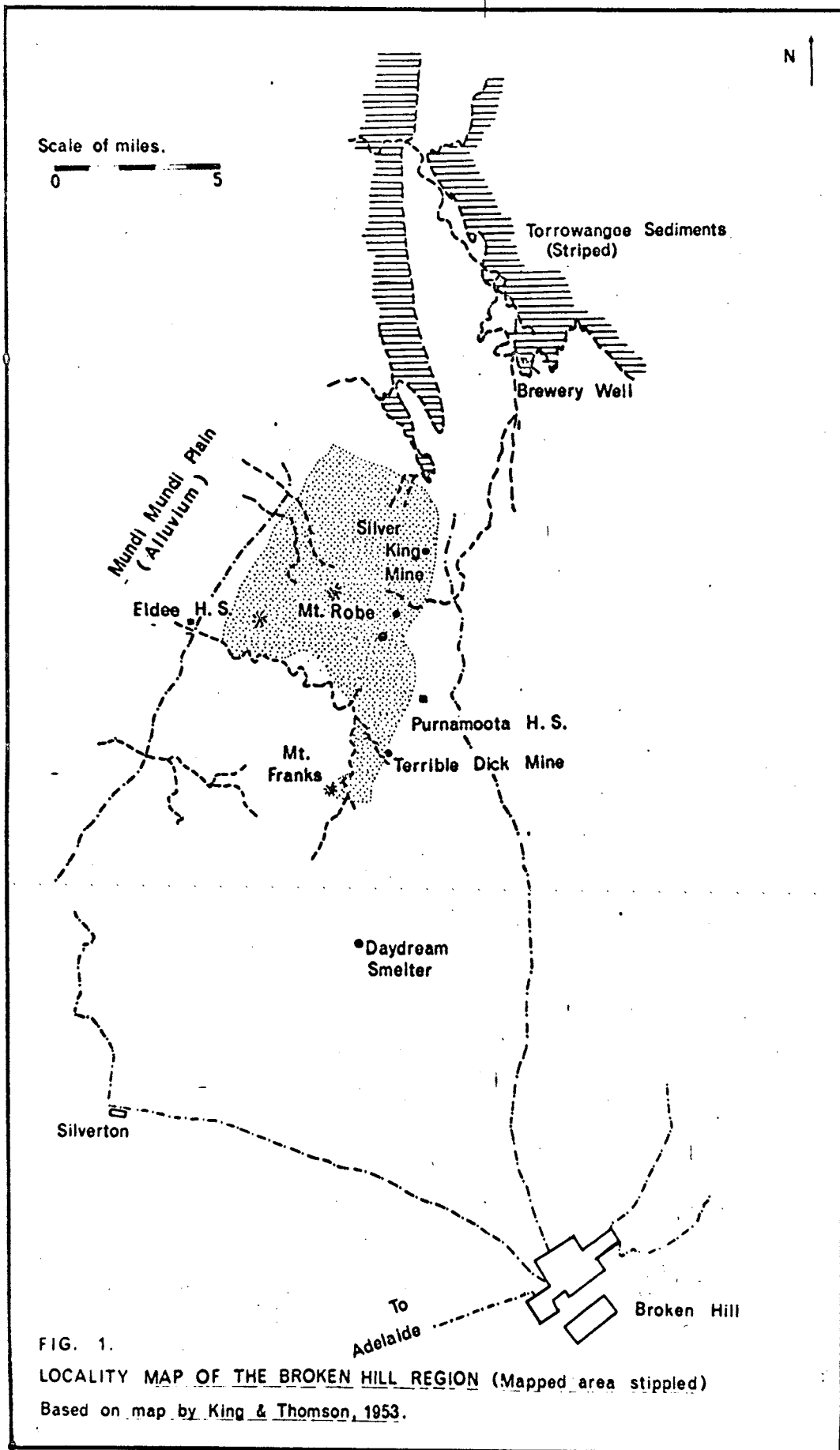
FIG. 1.

LOCALITY MAP OF THE BROKEN HILL REGION (Mapped area stippled)

Based on map by King & Thomson, 1953.

Andrew's regional map was not superseded until 1953 by a map published by King and Thomson (1953). Except for the recognition of some folds with steeply plunging axes and some details of fold shapes, the structural picture of King and Thomson differs very little from that of Andrews (1922). King and Thomson noted some minor complications in the western limb of the Mt. Robe Basin which they renamed the Mt. Robe Syncline.

The most complete structural analysis of a part of the Willyama Complex yet published is that of Gustafson, Burrell and Garretty (1950). Their report deals only with the structure of the rocks enclosing the Broken Hill Lode. With the abundant data available in the mines, Gustafson, Burrell and Garretty were able to construct three dimensional blocks of the folds in this area. As a result they recognised;

(i)   steeply plunging isoclinal folds with attenuated limbs,

(ii)   complicated relationships between minor and major folds with smaller folds "spiralling" across the larger folds in part of the area (Fig. 23, p.1413,

(iii) a second generation of folds, mainly irregular buckles which are apparently connected with faulting of the area.

Leslie and White (1955) also recognised the existence of steeply plunging folds (50°) in an area south of Brewery Well (Map 1), which almost adjoins the area covered by the present map.

Gustafson, Burrell and Garretty (1950) believed that the Willyama Rocks surrounding the ore body had been subjected to intense folding. In contrast some later workers (King and Thomson, 1953; Condon, 1958; Carruthers and Pratten, 1961; Thomas, 1961; but excluding Leslie and White, 1955, and Den Tex

1958) have tended to emphasise the stratigraphic complexity of the Willyama rocks and to minimise the effects of folding. This trend is noted specifically by Thomas (1961). Den Tex (1958) in a study of the preferred orientation of quartz and biotite in some Broken Hill rocks accepted the structural interpretations of Gustafson, Burrell and Garretty (1950).

Two authors, Browne (1922) and Binns (1962, 1963) have attempted to summarise the metamorphic history of the Willyama Complex. Both authors have recognised more than one phase of metamorphism, but differ over the classification of various rocks and mineral assemblages. Browne and Binns are also the only authors to have commented on the petrology of the Mt. Robe District. One of the important differences between Browne and Binns is the classification of the andalusite schists which outcrop in a belt from Mt. Franks to Brewery Well (Browne, 1922, Binns, 1962, 1963). The inclusion of the andalusite schists in the first phase of metamorphism proposed in Chapter 5 of this thesis differs again from the conclusions of the authors above.

The contributions of Browne and Binns will be reviewed more fully in Chapter 5. Meanwhile the few brief statements below, which are broad enough to be common to both Browne and Binns, are sufficient background for the reading of Chapters 2,3, and 4.

The primary regional metamorphism of the Willyama rocks (termed the Willyama Metamorphism by Binns, 1964) was followed by various types of retrogression. Intense retrogressive metamorphism has occurred along narrow zones, but of more importance in the Mt. Robe District is a less intense and more widespread retrogression. The last type of retrogression tends to destroy the foliated fabric of the high grade rocks.

It is not difficult to establish the existence of a large scale fold of the

type described by Andrews (1922) and King and Thomson (1953) in the Mt. Robe District. Nor is it very difficult to prove that this fold has a relatively shallow plunge in a south-west direction. However, a sampling of the fabric of the schists as observed in continuous outcrops and hand specimens (i.e. at the mesoscopic scale of Weiss, 1959), shows a surprising diversity of small scale folds and other structures (foliation and lineation etc.); the complexity of the mesoscopic fabric is difficult to reconcile with the apparent simplicity of the Mt. Robe Syncline. As many as three lineations can be observed on some schistosity surfaces. So far the microscopic and mesoscopic fabric have been largely ignored in assessing the structural history of the Willyama Complex. However, the fabrics at both scales have much information to offer and a proper understanding of the tectonic history must include these structures. The microscopic-mesoscopic fabric also provides a convenient framework for investigating the metamorphic history of the area. Correlation of the metamorphic and tectonic history of the area is attempted in Chapters 5,6.

Acknowledgements

CHAPTER 2

THE MICROSCOPIC AND MESOSCOPIC FABRIC OF THE METAMORPHIC ROCKS

2.10   Introduction

In this and the following Chapter the fabric of the metamorphic rocks
as observed in thin sections, hand specimens and single continuous outcrops
is described. At the same time definitions and symbols are given for the
various structural elements that are important in the geometrical analysis
of the area (Chapter 4). The description is divided into three parts, each
part of which corresponds to a group of mesoscopic folds of a distinctive style.

2.20   Definition and description of S, S_1, L and L_1

The symbol S will be used to denote the surface between two layers of
different composition and grainsize at the mesoscopic scale. Layers in the
metamorphic rocks which are laterally continuous for more than a few centi-
metres seldom have a thickness of less than two millimetres. The upper limit
for the continuity and thickness of layers whose interfaces define S is set
only by the limit of continuous outcrop. A microscopic compositional
layering, (to be referred to as metamorphic lamination) visible in polished
hand specimens (at low magnifications) or in thin sections is not included in
the definition of S_1 and will be discussed separately below. The metamorphic
laminations are much finer than the minimum dimensions of layers used to
define S.

When the surface S results from the contact of quartz-feldspar rocks or
quartzites against schists, the ultimate nature of the surface is probably
bedding, although there is no direct evidence (such as sedimentary structures
or conglomerate layers) to confirm this. Where S is an amphibolite versus
schist contact the nature of the surface is less obvious and interpretation
depends on both structural and petrological arguments.

In referring to this surface the term litholo gical layering is to be
preferred to bedding, partially because of the lack of evidence noted above.

In addition, in the following pages almost complete transposition of this surface during deformation is demonstrated, nullifying many of the stratigraphic concepts intrinsic in the term bedding (Turner and Weiss, 1963, p.92). The nature of S now mainly reflects the effects of the transposition and it is only with the greatest difficulty that anything can be inferred of the disposition and nature of stratigraphic units before deformation.

S_1 is a foliation* defined in the schists by the average preferred orientation of tabular (parallel to {001}) grains of mica; the term schistosity refers explicitly to this surface. Other features which serve to emphasise, but not to define S_1 are:

(1). Preferred orientation of quartz and feldspar grain boundaries in some schists - especially those rich in micas.

(2). Metamorphic lamination.

The intersection of S and S_1 produces the lineation L which appears as a banding on the S_1 surface.

Where retrogressive metamorphism or later deformation have not strongly altered the schists, a well developed lineation L_2, which can be identified with the same deformation that formed S_1, can be found. In andalusite schists L_1 appears as a "mineral streaking" on the S_1 surface, whereas in sillimanite schists, in addition to the mineral streaking, L_2 is also represented by a preferred orientation of cylindrical aggregates of sillimanite. As a general rule andalusite schists are well foliated and weakly lineated, whereas the fabrics of many sillimanite schists are almost totally composed of linear elements.

S_1 and L_2 are possibly the most important structural elements in the area ,

*Note that, by definition foliation refers only to surfaces believed to be of metamorphic and tectonic origin (Turner and Weiss, 1963, p.98). The definitions and names of structural elements used in this thesis are in accord with suggestions made by Turner and Weiss (1963).

as one or both are present in nearly every outcrop of schists. In mica-rich schists S_1 is penetrative on all scales; where the schists are composed of laminae of quartz (with little or no mica) and micaceous layers, there is a penetrative repetition of these layers, and hence the preferred orientation of the micas, at all but the finest microscopic scale. S_1 in hand specimen (except where affected by later deformation) is a more or less planar surface of parting, but on a finer scale S_1 often has a distinctly "platey" aspect. For the remainder of this section the discussion is confined to well foliated schists; rodded sillimanite schists will be dealt with separately in the next section.

The nature of the S_1 fabric at a microscopic scale is shown in Fig. 2.1 in sections parallel and normal to the lineation L_2 and normal to S_1 taken from a well foliated and lineated quartz-muscovite schist. A distinct and systematic variation in S_1 can be seen in the section normal to L_2, whereas S_1 is essentially homogeneous in the section parallel to L_2. The style is slightly different in micaceous layers with little or no quartz. Two trends in the orientation of the micas are clearly discernible (in sections normal to L_2) but the micas are not organised in trains as above. In either case, plots of the orientation of the $\{001\}$ cleavage of the muscovite are asymmetric[*](Fig. 2.2), confirming the visual impression that micas of one orientation predominate.

Another important aspect of many S_1 tectonites is the concentration of quartz (and in other specimens feldspar) into rod-like aggregates or lenticular, prismatic laminae (referred to above as metamorphic

---

* Specimen numbers refer to specimens submitted to the collection of the Geology Department, Sydney Univeristy. References to localities are given by reference to the coordinate system on Map 1 (back pocket thesis). The first five digits give the distance west of zero.

** All data are plotted on the lower hemisphere of an equal area net, unless otherwise noted.

(a)

(b)

2 mm.
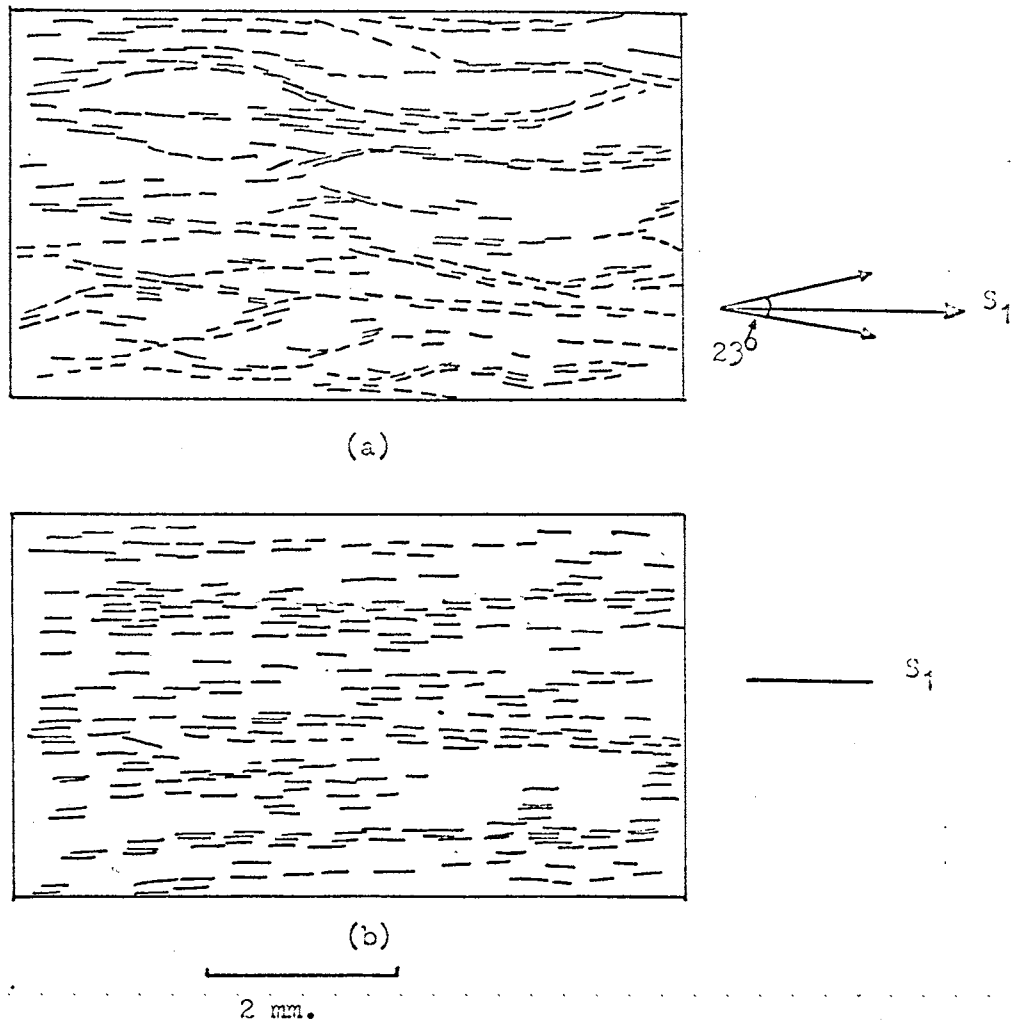
FIGURE 2.1

Style of S_1 in a quartz-mica schist;

(a) in a section normal to the foliation and lineation. The mean trend of S_1 is suggested by the large arrow,

(b) in a section normal to the foliation and parallel to the lineation.

Dashed lines represent the trace of the basal cleavage of muscovite in individual flakes on the plane of the section (Details drawn on an enlarged photograph. Spec. from Location 22300 123400).

(a)

(b)
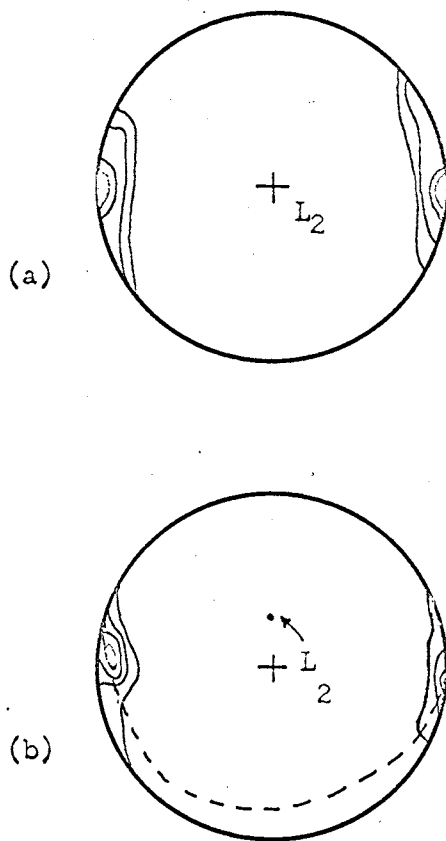
FIGURE 2.2

Preferred orientation of the {001} cleavage of micas in two schists:

(a). 100 poles to {001} from the specimen illustrated in Fig. 2.1.
(Contours, 25, 20, 4, 1% per 1% area).

(b). 125 poles to {001} of biotite from specimen 28350 , in which micas of different orientations are spread uniformly throughout the rock (Con. 50, 33, 25, 1% per 1% area).

The data in both cases are derived from two sections normal to the foliation (one also normal to L_2). Examination of a third section parallel to the foliation revealed no measurable micas. Both plots have monoclinic symmetry, with the single plane of symmetry normal to L_2.

2

lamination). The optimum development of this type of fabric is in mica-rich

schists; but it is one of the most obvious aspects of the fabric of most

samples of schists. The shape of the aggregates can be deduced from the two

sections in Fig. 2.3. The maximum dimension of the rods or laminae is parallel

to L_2, while the minimum dimension is perpendicular to both L_2 and S_1. The

distinction between rods and laminae is quite abritrary and depends only on

the relative dimensions normal and parallel to S_1. The laminae have absolute

dimensions less than 1 cm. (parallel to S_1) by 2 mm.(thick) and there is a

discontinuity in sizes between the laminae and fine compositional layering (S).

The bulk lithology and the relative distribution of quartz and mica are

important in determining the fabric of the schists. Rods are prominent in

schists in which the ratio of quartz and feldspar to mica is equal to, or

greater than, one to one, provided the micas are differentiated into distinct

laminae. However, micas in some very quartz and/or feldspar rich schists

(quartz-feldspar to mica ratio equals 4:1) are isolated along the grain

boundaries of the quartz and feldspar grains. Rodding is absent in these schist

but laminae are dominant in mica schists in which the quartz-feldspar to mica

ratio is less than one to one. Rods are associated with a maximum variation

in the trend of S_1 from point to point and the laminae with a minimum variation

of S_1, and hence to some extent the two elements are mutually exclusive.

The mineral streaking and L_2 is a complex lineation formed from a number of

elements:

(1), the principal element is the rod-like aggregates described above,

(2), the intersection of micas of one orientation on a parting surface

(a)
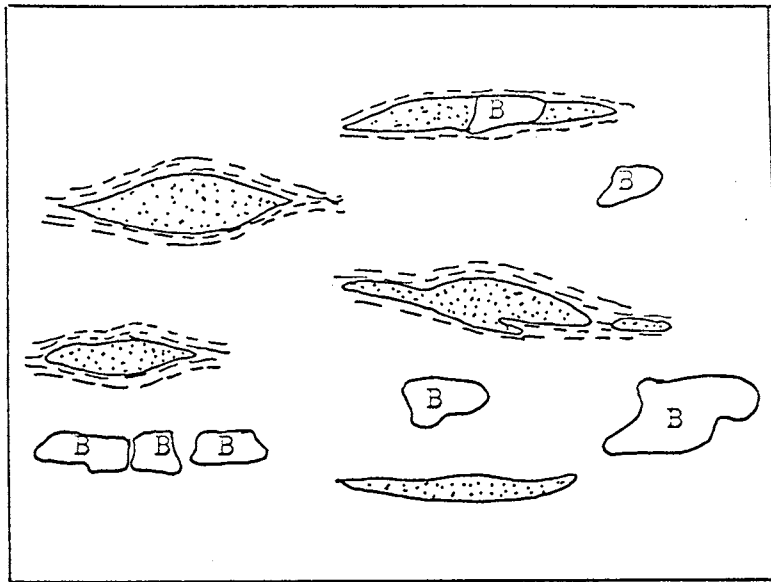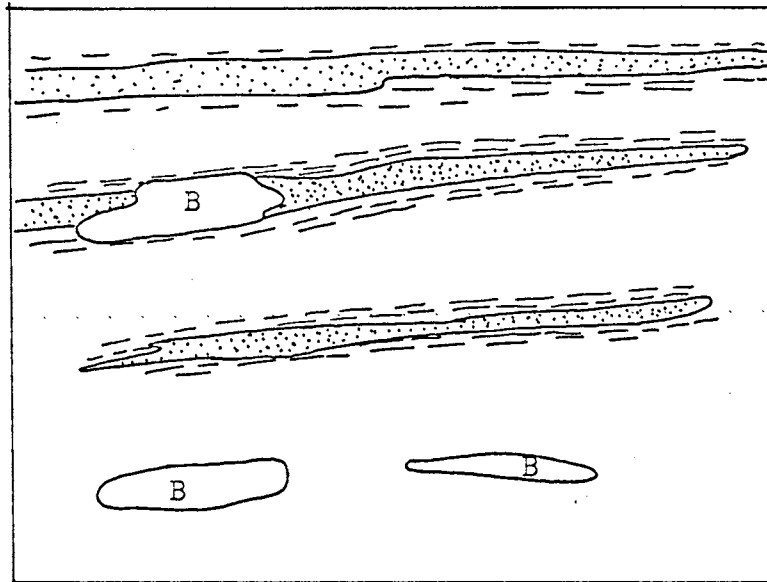
FIGURE 2.3   (b)

Shape of quartz aggregates (stipled) and biotite flakes (B) in sections

normal to the foliation and normal to L $_2$ (a) and parallel to L $_2$ (b). Traces

of {001} cleavage of micas are shown as dashes (From Spec. 28372; detail

imposed on enlarged photograph).

predominantly parallel to micas of another orientation. This produces

a fine streaking on the broken surface,

(3), the average dimensional elongation of mica porphyroblasts (mainly

biotite, Fig. 2.3), rods of sillimanite (see below), and occasionally prisms

of andalusite. 'The extent of preferred orientation of the c-axes of

andalusite porphyroblasts is variable - except that in most schists the c-axes

tend to lie preferentially in the S_1 surface. However, the arrangement in S_1

may be either haphazard or strongly aligned parallel to the other elements of

L_2. It is only rarely that the andalusite lacks any preferred orientation.

The lineations defined by each of the above elements separately are all

parallel. A specimen of a well foliated and lineated schist is illustrated

in Fig. 2.4, Plate 1.

2.21   Rodded sillimanite schists

The fabric of a typical rodded sillimanite schist can be seen in Fig. 2.5,

Plate 1. The exposed surface is a crude S_1 surface, within which are scattered

cylindrical aggregates of fibrous sillimanite. The cylinders have a mean

diameter of 1-3 mm. and a length of 5-10 cm., and occasionally bifurcate.

The fabric of the rodded schists is dominated by linear elements. Rods of

quartz and plagioclase, parallel to sillimanite rods, are prominent. Trains

of muscovite and biotite diverge about both types of rods and where two

trains meet, form linear concentrations of mica. Metamorphic laminae of

biotite are found in biotite-rich varieties of the schists, but otherwise

laminae are lacking.

2.30 $B_S^{S_1}$ folds in schists

The first recognisable generation of mesoscopic folds in S have S_1

parallel to their axial surfaces, and may be symbolised (Weiss and

FIGURE 2.4 (PLATE 1)

Specimen of a well foliated,lineated quartz-muscovite-biotite andalusite schist from exposures in the creek approximately 200 yards east of the Black Prince Mine. The lineation L_2, is visible as a faint streaking parallel to the vertical edges of the photograph. L_2 lineation in the andalusite schists or quartz-muscovite schists is seldom better developed than in the sample illustrated.

(Lens cap is two inches in diameter)

FIGURE 2.5   (PLATE 1)

Well rodded quartz-muscovite-biotite-sillimanite schist, collected in
the creek below the main adit of the Mt. Robe Mine. The cylindrical
aggregates of sillimanite are white and oriented parallel to the pencil.
Note the dark coloured aggregate of biotite with minor muscovite and quartz
in most rods (especially in the aggregate at the right end of the pencil).
A rod bifurcating can be seen just to the right, and slightly above the line,
of the pencil.

(The pencil is approximately six inches long)
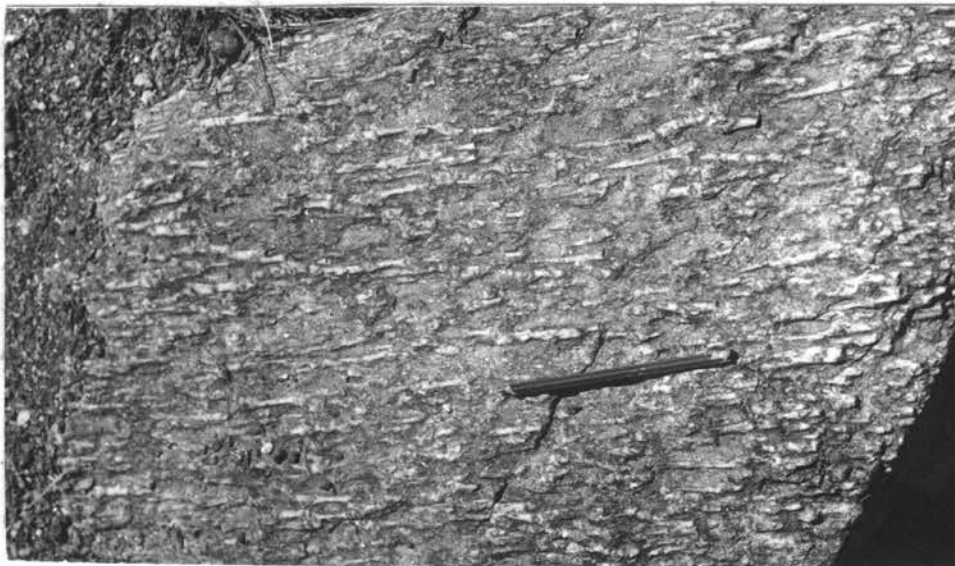
Turner, 1963, p.131) as $B_S^{S_1}$ folds. The symbol B_1 will be used as an equivalent to $B_S^{S_1}$ *.

Representative examples of the styles of B_1 folds are illustrated in Fig. 2.6. The complete folds all have the same basic style with one limb virtually parallel to S_1 and the other limb gradually curving away from the hinge region to an orientation close to S_1. Minor folds near the hinge of a larger fold may have both limbs at an angle to S_1 (Figs. 2.6, a,c).

Some features of the folds are:

(1). Quartz and feldspar rich units more than a few centimetres thick in the schists have a prominent fracture cleavage parallel to S_1 in the hinge region of the folds and are strongly jointed elsewhere (Fig. 2.6f). The formation of mullions of quartzite parallel to the fold axis and the L_2 lineation in the schists is common (Fig. 2.6a). Fragmentation of the quartzite unit by penetration of the schists between the mullions and along fracture cleavage planes in the mullions (Fig. 2.7) with irregular warping in the vicinity of the mullions is also common.

(2). Layers may merge together in the limb parallel to S_1 of folds in the micaceous schists to produce a new layering parallel to S_1 (Fig. 2.6b). Alternatively, individual layers may lose their continuity by separating into lenses parallel to S_1 (Fig. 2.8). Although the individual lenses in Fig. 2.8 are parallel to S_1, the total array of lenses is slightly oblique to S_1.

(3). The style of B_1 folds can vary considerably along the axial surface in a direction normal to the fold axis (Fig. 2.6, 2.9). This is a characteristic of concentric folds (Turner and Weiss, 1963, p.470). However

---

* The symbol $B_S^{S_1}$ is read as: a fold in the surface S, the axial surface of which is S_1. In later generations of folds it is convenient to have a symbol to designate all the folds in different surfaces that have the same axial surface. Thus B (Chapter 3) is the group $B_S^{S_4}$, $B_{S_1}^{S_4}$, $B_{S_2}^{S_4}$, and $B_{S_3}^{S_4}$. In the first generation of folds B_1 contains only $B_S^{S_1}$ folds. Note that B_1 has S_1 as axial surface, B_2 has S_2 , B_3 has S_3 etc.

FIGURE 2.6

The style of mesoscopic $B_S{}^1$ folds (as seen in section normal to the fold axes; S_1 shown in micaceous rocks as a dashed line):

(a), in quartzite layers in mica schists at Loc. 27500104000; note the formation of the detached mullions on the right hand side (sketch).

(b), in a biotite-muscovite-quartz schist from Mt. Franks (Loc. 3640037400, drawn from a polished slab; biotite layers black).

(c), in layered calc-silicate, eastern side of Mt. Franks (drawn from photograph of thin section).

(d), in quartz-plagioclase layers in mica schist at Loc. 35100134700. The pegmatite vein is located along a glide surface disrupting the fold. There is no layering in the schists to the right of the vein (drawn from photograph).

(e), in biotite schist (dashed) and quartz-plagioclase rock (stipled) at Loc. 36300131900.

(f)(g), in quartz-plagioclase layers in mica schists at Loc. 36700133300. The "rootless" fold (g) is slightly warped about a set of kink bands formed during a later deformation.

(a)

(b)

(c)

1 in.

1 in.

1 foot.

(d)

1 foot.

(e)

1 foot.

(f)

1 foot

(g)

1 foot.
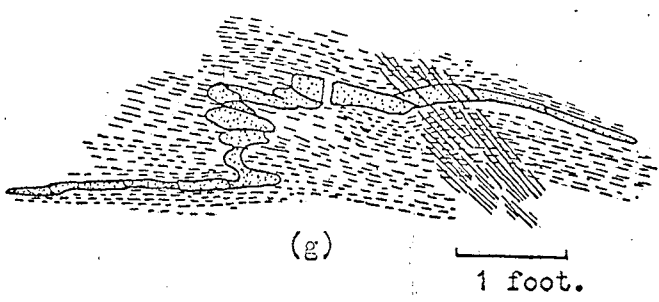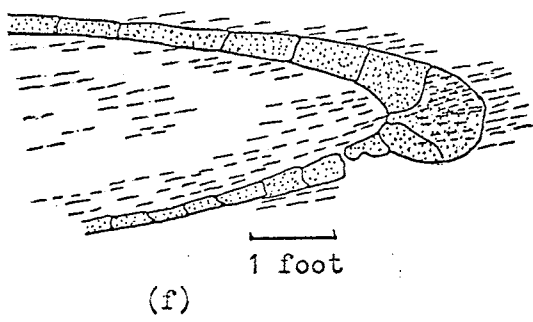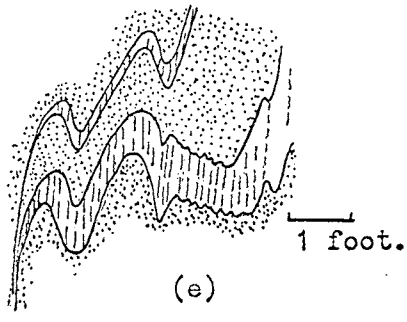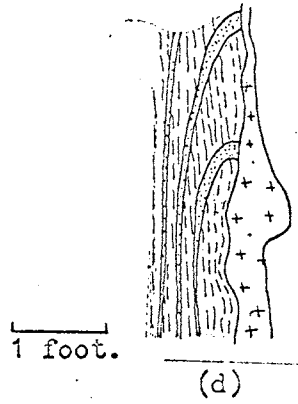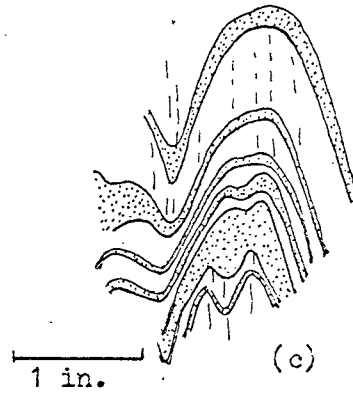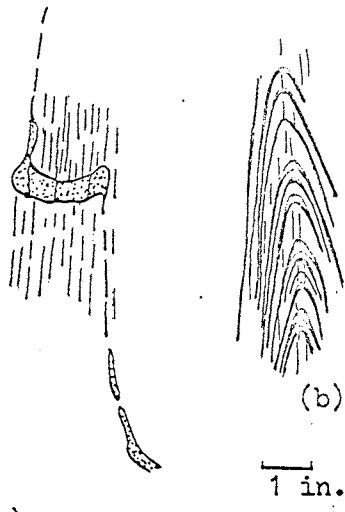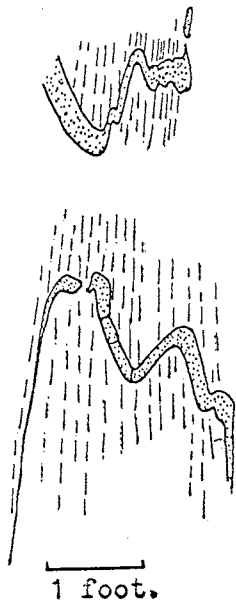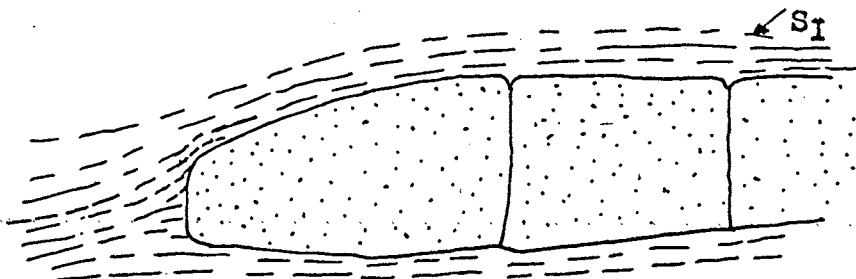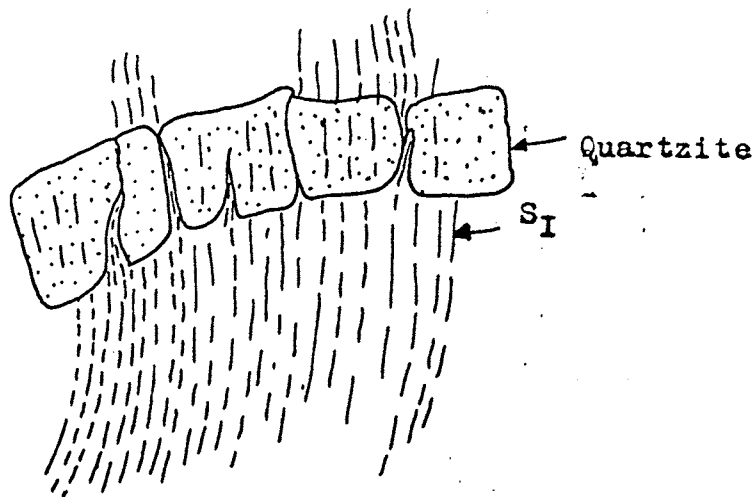
FIGURE 2.7

(a)   Section through a hand specimen containing quartzite mullions from

Loc. 27500104000.   Section is normal to the axes of the mullions.   Note how

S₁ (dashed) penetrates the mullions and deviates from its homogeneous orient-

ation near the mullions (Traced from rock surface, actual scale)

(b)   Schistosity swinging around the termination of a quartz-plagioclase

layer.   Section is normal to L   (Sketch, approx. actual scale; Loc. 363001 31900
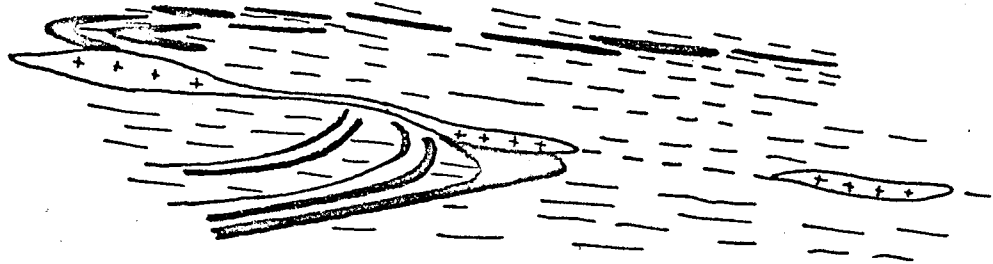
FIGURE 2.8

Details of a B $\frac{S_1}{S}$ fold in specimen 28350 (Loc. 53400107000) a quartz-plagioclase-biotite schist. The fold is disrupted by a glide surface that is nearly parallel to S_1. Patches of pegmatite are concentrated along the glide surface. The fold is outlined by a number of biotite-rich layers (black) and in one limb the layers are broken up into a series of lenses that trend across S_1 at a low angle. L_2 is at an angle to L_1 in this specimen (see text) and homogeneous throughout the specimen proving there is no rotational movement on the glide surface (section normal to fold axes, natural scale).

individual units are thickened (measured normal to S) in the hinge areas of the folds and attenuated in both limbs, so that the folds also have the character of similar folds.

(4). The continuity of B_1 folds is often disrupted by a glide surface (or series of glide surfaces) sub-parallel to S_1 (Figs. 2.6, 2.8). The glide surface is often the site of a pegmatite dyke. Bulges in the pegmatite dyke are accompanied by slight warping of S_1.

A very common structure in outcrops of schists corresponds with the upper part of the fold in Fig. 2.6, in which S changes slightly in trend before terminating abruptly. The closure in the lower part of Fig. 2.6d is obvious, but the origin of the structure is not obvious in many outcrops.

The glide surfaces pre-date the conclusion of high grade metamorphism (Chapter 5), and post-date the initial stages of B_1 folding. Thus, from the relationship between the high grade metamorphism and B_1 folding deduced in Chapter 5, the glide surfaces are probably an integral part of B_1 folding.

Two lineations (L_1 and L_2) at an angle of 50° are present on the S_1 surfaces of the specimen illustrated in Fig. 2.8. These two lineations, and the fold axes in the specimen are still parallel on either side of the glide surface that traverses the specimen, so that there has been no rotational movement on the glide surface. There is a large component of displacement in a direction normal to the fold axes (in S_1) in most instances but it is impossible to determine if this has been accompanied by a component of displacement parallel to the fold axes.

Further details of the relationship between S, S_1 and B_1 folds are revealed on the slopes of Mt. Franks. S, defined by thin units of quartz-biotite

schist, swings continuously across the northern and north-eastern slopes

of the mountain (Chapter 4) and intersects S_1 over a whole range of angles.

One of three different fabrics are found in the delicate layers (1-2 mm. thick)

that are abundant within single units of the quartz-biotite schist:

(1). The internal layers are parallel to the external contact between the

quartz-biotite schists and the andalusite schists,

(2). The internal layers are intensely folded into $B_S^{S_1}$ folds which are cut

by numerous glide surfaces sub-parallel to S_1 (Fig. 2.9, Plate 1). The

nature of the folding changes rapidly from point to point in the type of fabric

illustrated in Fig. 2.9, Plate 1. For example, in the upper left hand corner

the folds are isoclinal, and many individual layers in the limbs of the folds

are discontinuous. Except for fold closures the layering in such an area is

parallel to S_1. In the centre portion of the plate, the folds are more open

and individual layers are more continuous.

The contact of the quartz-biotite schist in the outcrop in Fig. 2.9, Plate 1

is nearly planar and free of mesoscopic B_1 folds. However, this is not always

the case and the external contact may be deformed in a similar manner (Fig. 2.10)

(3). The internal layering is almost exclusively parallel to S_1 except for

isolated closures of isoclinal, and often rootless, $B_S^{S_1}$ folds. Commonly the

external contact in these circumstances has the form shown in Fig. 2.10, but

may be undeformed.

One other feature of the fabric at Mt. Franks is the presence of structures

that resemble current bedding in the internal layering of the quartz-biotite

schists (this type of structure is especially abundant on the eastern buttress

of the mountain). However the surface of contact between the two sets of

FIGURE 2.9 (PLATE 1)

$B_S^{S_1}$ folds in a quartz-muscovite-biotite-plagioclase schist at Mt. Franks (Loc. No. 36400 87400). The folds are outlined by alternate layers rich in plagioclase or biotite. The contact of the above unit with quartz-muscovite-andalusite schists slants (to the left) across the top of the photograph, and is unfolded at the mesoscopic scale (the match is 2 inches long).

(a)

(b)

2 inches
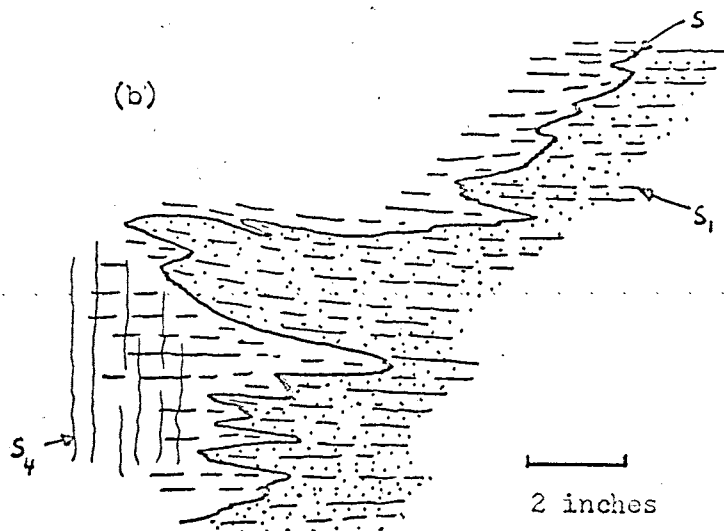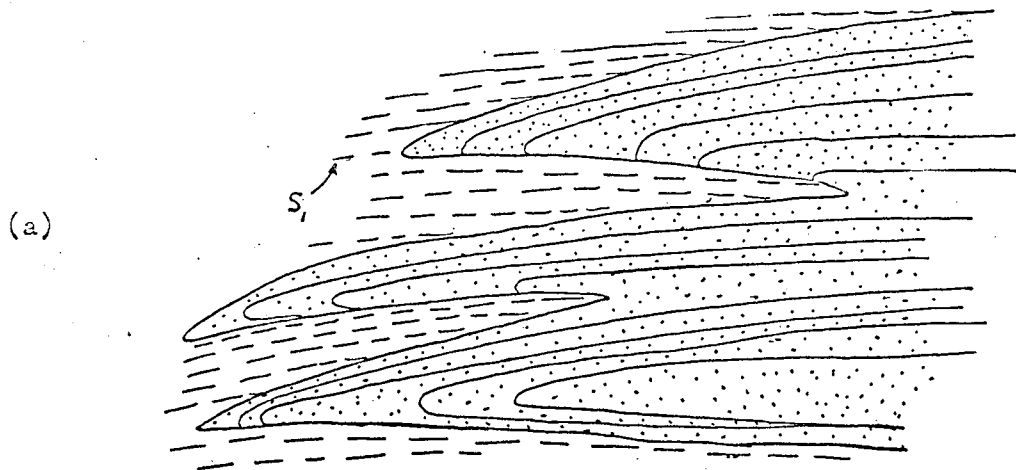
FIGURE 2.10 (a,b)   Contact between andalusite schist (dashed parallel to

S_1) and quartz-muscovite-biotite schist (stipled);

(a)   at Loc. 3640087400. The solid lines represent biotite-rich laminae

in the quartz-muscovite-biotite schist. The contact is sliced by several

glide surfaces sub-parallel to S_1 (Sketch; half scale).

(b)   at Loc. 3760087400. S_4 is a surface formed during a later deformation

(Chapter 3; details superimposed on a photograph; scale shown).

laminae always seems to be sub-parallel to S_1 and not S. This suggests that the structure is due to the bringing together of different portions of B_1 folds along glide surfaces (See Fig. 2.8). No structures that can be classified as sedimentary structures have been found at Mt. Franks or elsewhere within the mapped area.

In one respect the outcrops at Mt. Franks are atypical. Elsewhere in the area, except for isolated outcrops containing $B_S^{S_1}$ folds, the typical mesoscopic fabric has S parallel to S_1. This is true whether S is defined by laminae a few millimetres thick or units. Mt. Franks is the only area (within the mapped area) in which S intersects S_1 consistently in outcrops over an area of more than a few hundred square feet (as compared to 1500 square yards at Mt. Franks). The paucity of B_1 folds at the mesoscopic scale is well illustrated by the strip along the eastern edge of the Mt. Robe Pegmatite Stock from the Black Prince to the Golden Crest Group of mines, in which fewer than a dozen outcrops contain clearly visible $S-S_1$ intersections. However, microscopic fold hooks are fairly abundant in the quartz-schists of this area.

It appears from the material above that the typical mesoscopic fabric - with S sensibly parallel to S_1 - is the result of transposition* of S during B_1 folding. The three different fabrics at Mt. Franks (1-3 on the preceeding page) could well represent successive stages in the evolution of the transposed fabric. Over most of the area transposition (at the mesoscopic scale) is so effective as to produce a fabric resembling "bedding-plane schistosity" However the persistence of fold hooks (or rootless folds), the occasional intersection of S and S_1 against glide surfaces, the presence of a systematic group of folds transposing S and the widespread intersection of S and S_1 at Mt. Franks leave no doubt that S_1 is not a "bedding-plane" schistosity. At the commencement

* Turner and Weiss, 1964, p.92.

of B_1 folding S was at some angle to the final orientation of the imposed

surface S_1. The importance of recognising the almost complete transposition

of S at the mesoscopic scale cannot be overemphasised, as this governs the

whole approach to the analysis of the macroscopic fabric (Chapter 4).

2.31 The mesoscopic fabric of the amphibolites

Thin units of amphibolite (less than 20' thick) are not present in the

mapped area, which combined with the scarcity of internal layering, makes the

amphibolites much less productive than the schists for the analysis of the

mesoscopic fabric.

The question of whether the contact of the amphibolites (at the mesoscopic

scale) has the same geometric significance as lithilógical layering in the

schists presents immediate difficulties. The amphibolites might have resulted

from the metamorphism of either basic igneous or sedimentary rocks (including

basic tuffs or calcareous rocks). Unfortunately neither the chemistry nor the

petrography of the amphibolites allows any clear distinction between these

possibilities (Chapter 5). Clearly if the amphibolites were derived from

intrusive basic igneous rocks which cut partially or wholly across the bedding

of the sediments, then it cannot be equated with S in the schists in the

macroscopic analysis..

The amphibolite-schist contacts observed in continuous outcrop are locally

planar and no examples of irregular projections of the amphibolite into the

schist (or vica-versa) have been found. Without exceptions the contact is

parallel to S, transposed or untransposed, in the contiguous schists. Generally

the amphibolite contact is parallel to S_1 in the schists; the only exceptions to

this occur in the hinges of regular macroscopic folds which have S_1 as axial

surface (Chapter 4). Wherever it is observed at the mesoscopic scale the schist-

amphibolite contact is equivalent to S in the schists.

S_1 in the amphibolites is a foliation defined mainly by thin (< 2 mm.), discontinuous laminae of hornblende versus plagioclase (and sometimes quartz). This fabric is very similar in sytle to the metamorphic lamination in the schists. In some amphibolites which lack a lineation, S_1 is also a "surface of splitting" due to the preferred orientation of the c-axes of hornblende randomly in the S_1 surface. The foliation in the amphibolites near the margin is always parallel to S_1 in adjacent schists. Where internal layering in the amphibolites cut S_1, structures which are reminiscent of transposition structures in the schists are found (Fig. 2.11).

The preferred orientation of the c-axes of hornblende grains (which is accompanied by dimensional orientation of the grains) in the amphibolite gives rise to a lineation. This arrangement of the hornblende grains is more common than the preferred orientation (in S_1) mentioned above. Again the reason for regarding this lineation as equivalent to L_2 in the schists must be deferred until Chapter 4. Often L_2 in the amphibolite must be carefully distinguished from a "false" lineation that is observed on a joint surface that intersects S_1 at a very acute angle. The joint surface is oriented so closely to S_1 that the impression can easily be created that the lineation is being observed on S_1. The lineation, which appears as a streaking on the joint surface, is due to the intersection of S_1 with the joint.

2.32   The mesoscopic fabric of the calc-silicate rocks

The thicker units of calc-silicate rocks are always strongly laminated with laminae less than 2 cm. thick. The laminae are discontinuous over distances of

more than 20-30 cm. (usually less) and are often highly irregular in detail,

particularly in the vicinity of quartz aggregates in the calc-silicates. Only

one outcrop of calc-silicates (at Mt. Franks, Fig. 2.6) contains recognisable

folds. These are almost certainly the same as $B_S^{S_1}$ folds in the schists; at this

outcrop the axial surfaces of the folds are parallel to S_1 in the schists. Else-

where the layering in the calc-silicates is parallel to S_1 in the adjacent schists

2.33   Boudinage structures of calc-silicate rocks in the schist

A type of boudinage structure of thin layers ($<$ 1 foot) of calc-silicate rocks

in the schists is often encountered. The usual form is a boudin with a shape

approximating to a prolate ellipsoid. The shape departs from that of a perfect

ellipsoid in three respects; (i) the extremities (Fig. 2.12, 2.1 3) are not

enclosed by a continuously curved surface; (ii) in some forms, as in Fig. 2.13,

the extremities tend to be cylindrical rather than ellipsoidal; (iii) a few are

elliptical or nearly circular cylinders, rather than ellipsoids. However, the

approximation to an ellipsoid of most specimens is sufficient to warrant the use

of the term.

The boudins are invariably oriented with their major and intermediate axes in

S_1 and their minor axis perpendicular to S_1 in the enclosing schists. The major

axis also parallels S_1 in the schists and the mean trend of a faint lineation

which is occasionally present on the external surface of the ellipsoid. The

absolute dimensions of the axes are variable; major axes as long as six feet have

been found, but three to four feet is more common. The intermediate axis ranges

from 0.5 feet to 3 feet and the minor axis from 0.5 feet to 1.5 feet. It is

seldom that the complete length of all three axes can be measured simultaneously.

The ratio of the three axes is only known in a few instances, but consideration

of these alone indicates the lack of a consistent ratio.

The ellipsoids commonly break on a joint surface perpendicular to the major

axis. This section and exposure surfaces through the ellipsoids always reveal

the presence of compositional layering, which is entirely closed in two dimensions. The central layers are completely closed surfaces in three dimensions, as can be seen very clearly in Fig. 2.14, which is a reconstruction of the layers exposed in the ellipsoid of Plate 1, Fig. 2.13. The inner layers are spherical while the outer layers successively approximate to the general shape of the ellipsoid. All layers in some specimens are ellipsoidal. Often the outmost layers that extend to the extremities of the ellipsoid are not closed, but instead form a layered cylinder.

If biotite mica is present in any of the layers it has a preferred orientation of $\{001\}$ parallel to S_1 in the schists. The intersection of this foliation with the external surface of the ellipsoid produces the lineation mentioned previously. (This lineation of course will be more or less curved depending on the shape of the ellipsoid.)

The ellipsoids occur in concentrations which often form crude layers within which the individual ellipsoids all have a common orientation. The layers extend in the same direction as the intermediate axis of each ellipsoid and parallel to S_1 and transposed S in the schists. How extensive the layers are parallel to the major axes of the ellipsoids is not known. A few examples have been found of a transition between continuous layers of calc-silicate rocks and layers of ellipsoids.

It is proposed that the ellipsoids were formed during B_1 folding by the dissociation of continuous sheets of calc-silicate rock into boudins. The symmetrical relationship of the boudins to L_2 and S_1 and their disposition in layers all support this conclusion. The schistosity of the enclosing schists curves around the ellipsoids, but has the same micro-structure and fabric as schists at some distance from the boudins, so that the ellipsoids
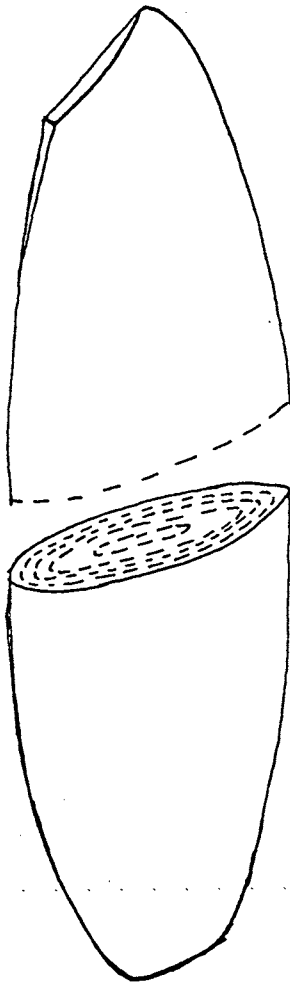
FIGURE 2.12

Details of a boudin excavated from schists south of the Black Prince Shafts
(Loc. 25700102600). Bothe ends of the boudin are broken on a joint that
slants at an angle across the boudin. No boudin was found beneath the
bottom end of the boudin extracted and it appears that the outermost layers
are not closed. The boudin is 23 inches long, 9 inches wide and 5 inches thick.

FIGURE 2.13 (PLATE 1)

Layer of ellipsoids exposed in a small creek near the north-eastern extremity of the area (see next figure for locality co-ordinates). The form of layering in the ellipsoid in the bottom right corner of the photograph is beautifully exposed; a reconstruction of the layers of this ellipsoid is given in the following figure. The layer of ellipsoids, in which four other ellipsoids are visible, passes from the bottom-right hand corner of the plate to the middle-upper left corner. A fifth ellipsoid is obscured by grass in the centre of the plate.
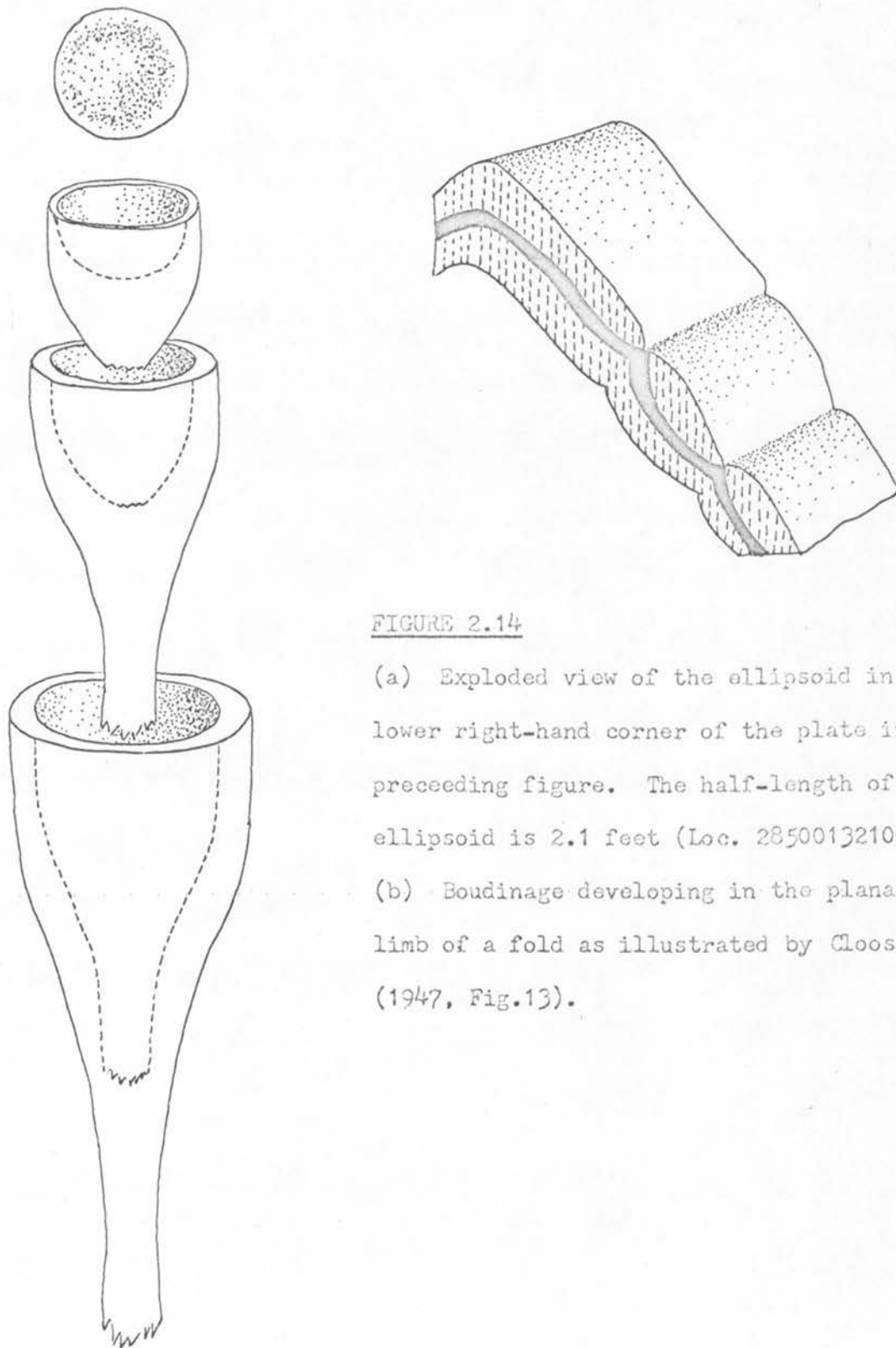
FIGURE 2.14

(a) Exploded view of the ellipsoid in the lower right-hand corner of the plate in the preceeding figure. The half-length of the ellipsoid is 2.1 feet (Loc. 28500132100).

(b) Boudinage developing in the planar limb of a fold as illustrated by Cloos (1947, Fig.13).

must have had their present shape at the conclusion of the metamorphism and deformation associated with B_1 folding (Chapter 5). The ellipsoids are also deformed by a phase of folding that post-dates B_1 folds (Fig. 2.15).

The ellipsoids are broadly similar in cross section to boudins described by Cloos (1947, Figs. 12, 13, and 16), de Sitter (1960, p.87-88) and Ramberg (1955); however, there is apparently no change of shape along the length of any of the boudins in the examples quoted. The boudins are restricted to the calc-silicates, whose initial composition was probably that of an impure limestone, and are apparently the response of this particular rock type to B_1 folding. A similar restriction of boudinage to calcium rich rocks has been noted by Ramberg (1955).

The initial shape suggested for the transformation to an ellipsoid is:

(i) a continuous sheet; examples of a transformation of this type are figured by Cloos (1947, Fig. 13; this text, Fig. 2.14b),

(ii) a prism, bounded by surfaces of layers and joint surfaces.

Either of the transformations suggested for the formation of the ellipsoids involves an inhomogeneous strain. The ellipsoids, although similar in shape, are not strain ellipsoids for B_1 folding, since the former are only sensible for homogeneous deformation of a sphere. In any case, evaluation of strain requires knowledge of the absolute and relative dimensions of a body before and after deformation. Even if the shapes of the layers that yielded the ellipsoids were known with certainty, there is no way of determining the original dimensions of these layers, or the effects of volume changes during metamorphism. Any statement concerning strain can only be a tentative deduction based on information from other sources.

The boudins are comparable in shape to boudins produced in extension
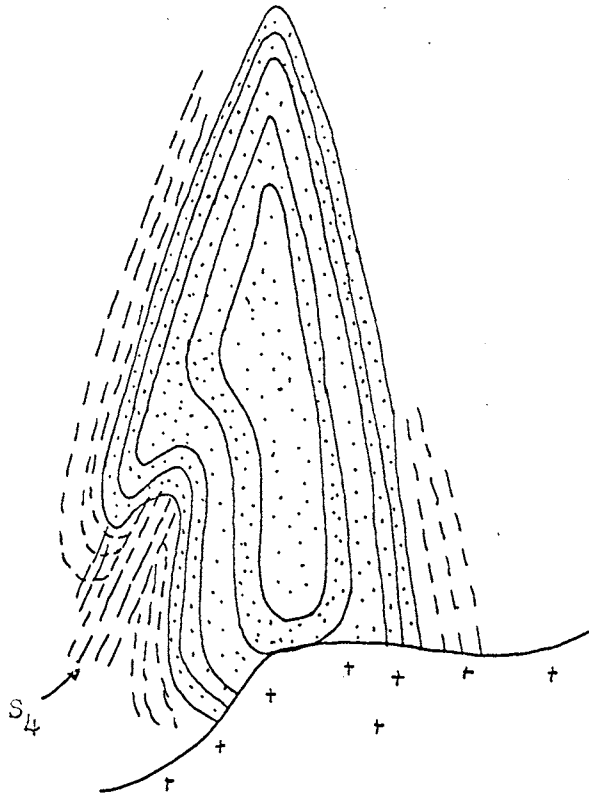
FIGURE 2.15

Sketch of an oblique section through a boudin exposed in Eldee Creek
(loc. 52200107100). The boudin is deformed on the bottom left-hand side by
a fold that, in the schists, has kink bands (S_4) parallel to its axial surface.
The fold belongs to the fourth generation of folds ($B_{S_1}^{S_4}$ fold, Chapter 3).
The boudin is 16 inches from top to bottom in the exposed section.
(boudin, stipled; schists, dashed parallel to trace of S_1)

experiments by Griggs and Handin (1960, Plates 9 and 10). Griggs and Handin
extended cylinders of dolomite enclosed within cylinders of marble by the
application of a uniaxial stress field. Prominent necking occurred in
specimens deformed at $800^{\circ}C$ (2000 and 5000 bars), with flow of the marble
into the neck region. The resultant structure is very similar to the
cylindrical termination of the ellipsoidal boudins. Quartzite rods enclosed
within Yule Marble and extended under similar conditions failed to form
boudins similar to the dolomite. In this respect the differing reactions of
the quartzite and dolomite are comparable with the behaviour of quartzite and
calc-silicates at Broken Hill.

Ramberg (1955) also produced structures similar to boudinage experimentally,
by extension parallel to the axis of the boudin.

Comparison of the experimental and natural boudins renders it likely
that the boudins are the result of extension parallel to the major axis of the
ellipsoid. The presence of a well developed joint normal to this axis,
especially in the cylindrical extremities of the ellipsoids tends to support
this conclusion. The tendency for ellipsoids to separate slightly within a
layer normal to the major axis, combined with fragmentation of continuous
layers into ellipsoids may indicate extension in the S_1 surface normal to the
major axis of the ellipsoids; the glide surfaces disrupting $B_S^{S_1}$ folds are
compatible with extension in this direction.

2.34   The relationship between L_2 and $B_S^{S_1}$ - (and $L_{1_{S_1}}$)

L_2 is visibly parallel to the axes of mesoscopic $B_S^{S_1}$ folds in some occurrences.
However, in many instances there is a clearly discernible angle between L_2 and
$B_S^{S_1}$ and/or L_2. Two examples are:

(1). Numerous mesoscopic $B_S^{S_1}$ folds in an area of several hundred square

yards just to the south of the exit of Little Aller Creek onto the Mundi

Mundi Plain have their axes at an angle to L_2. The folds are in thin

quartz-schist and quartzite horizons in rodded sillimanite schists in which

S_1 is visible albeit poorly developed. There is no trace of later deformation

in the area from which data were collected.

The geometry of the area is summarised in Fig. 2.16. S_1 has a fairly

constant dip of 35-194°, and L_2 lineations are distributed very slightly in

the average S_1 surface. One fold axis coincides with the cluster of L_2

lineations, but the other axes are at an average angle of 80° to the

lineations.

(2). The second example is a single hand specimen of a $B_S^{S_1}$ fold (the fold

illustrated in Fig. 2.8) in a quartz-plagioclase-biotite schist. L_2 is

represented by the trace of S on the S_1 surface and, of geometrical necessity,

parallels the fold axes. L_2, a very fine mineral streaking on S_1, accompanied

by alignment of biotite flakes, is at an angle of 50° to L_1. Again there are

no traces of superposed deformation (and L_1, L_2 and $B_S^{S_1}$ are homogeneous

throughout the specimen).

Further examples of divergence between $B_S^{S_1}$ and L_2 can be found in the

rodded sillimanite schists in the valley bounding the western side of Mt. Robe.

A marked discrepancy and variable angle between L_1 and L_2 also occurs in

andalusite to the north and north-east of Mt. Franks (around loc.34500085000),

but there are no definite $B_S^{S_1}$ folds in this area.

The lineation L_2 is an integral part of the foliation S_1, and it follows

from the transposition of S to parallel S_1 in the $B_S^{S_1}$ folds, that $B_S^{S_1}$, L_1,

L_2, and S_1 are all genetically related to the deformation that created $B_S^{S_1}$ folds.
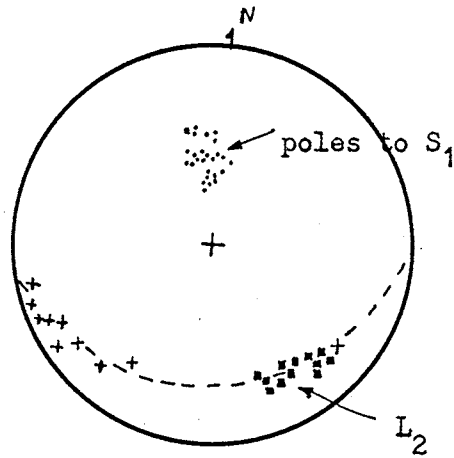
FIGURE 2.16

Angle between B_S^{S1} and L_2 at locality 45700126500 (poles to S_1, dots; L_2 lineations, squares; B_S^{S1}, crosses). Data from an area approximately 100x100 yards square of continuous outcrop. See text for description.

Also the metamorphic laminae are part of the schistosity and the maximum

continuity of the laminae, like that of the rods to which they are trans-

itional, is always coincident with L_2 . This remains true whether L_2 is or

is not parallel to L_1 . Hence the metamorphic laminae are not the result of

transposition of fine layering in the original rocks, since in these circum-

stances the direction of maximum continuity of the laminae would have to

parallel $B_S^{S_1}$. A similar argument applies to the orientation of sillimanite

rods in sillimanite schists.

It is unfortunate that no calc-silicate boudins have been found in areas

where L_1 and L_2 are known to intersect. At the locality south of Mundi Mundi

Creek mentioned above, mullions in the quartzite horizons are oriented parallel

to L_1 ; presumably the ellipsoids would be oriented in a similar fashion. The

pattern of layering in the ellipsoids in these circumstances might provide

interesting information about its origin.

Paterson and Weiss (1961) have suggested that it is possible to sort the

various structural elements of a deformed rock into inherited, composite, and

imposed elements. Thus in B_1 tectonites the fabric elements S_2 and L_2 are

possibly imposed elements (related only to the deformation); $B_S^{S_1}$ and L_1 are

composite elements due to the interaction of the imposed elements and the surface

S_1 inherited from the undeformed rock. The ellipsoids and quartz mullions can

be classed as composite elements. One other useful imposed element that can

be investigated is the preferred orientation of quartz.

2.35   Quartz sub-fabrics and discussion

The preferred orientation of $\{0001\}$ in quartz is shown in Figs. 2.17 and 2.18.

The data for each specimen are from measurements in three sections at right

angles to each other, and are projected on the plane normal to L_2 (except in Fig. 2.18). The main features of the diagrams are reproduced by partial diagrams containing 100-150 grains. L_2 is sensibly parallel to L_1 in all the specimens for which results are given in Fig. 2.17. The diagrams in Fig. 2.17 have imperfect orthorhombic symmetry (D_{2h}). One symmetry plane is normal to L_2, a second plane is normal to mesoscopic foliation and contains L_2. In Fig. 2.17a, the plane of symmetry coincides with a plane defined by the maximum for the preferred orientation of {001} of micas in this specimen (Fig. 2.2a). From a visual inspection only, the same is true for the second specimen measured (Fig. 2.17b). There is a marked discrepancy between the third plane of symmetry in Fig. 2.17c and the foliation in the vicinity of the specimen from which the measurements were obtained (a quartzite mullion). However, S_1 in the immediate vicinity of the quartzite mullion is slightly different to that which prevails in surrounding schists (Fig. 2.7). The orientation of the symmetry plane seems to agree with the latter.

The data for the diagram in Fig. 2.18 were taken from a hand specimen (see last section) in which L_1 is at an angle to L_2. Again the preferred orientation pattern has orthorhombic symmetry. One of the planes of symmetry parallel the mean foliation plane in the specimen (Fig. 2.18). A second symmetry plane is normal to L_2 and coincides with the single plane of symmetry in the mica sub-fabric.

The symmetries of the various fabric elements in B_1 tectonites are:

(i)   a system of B_1 folds - triclinic symmetry*

(ii)   foliation S_1 - monoclinic (C_{2h}; symmetry of the mica sub-fabric)

(iii) L_1 and L_2 - axial symmetry (D_{2h})

(iv)   quartz sub-fabric - orthorhombic (D_{2h})

*From diagram 2.16. The styles are asymmetric in profile and their axes are inconsistent although S_1 and L_2 are constant. There are no planes of symmetry in the fabric of S.
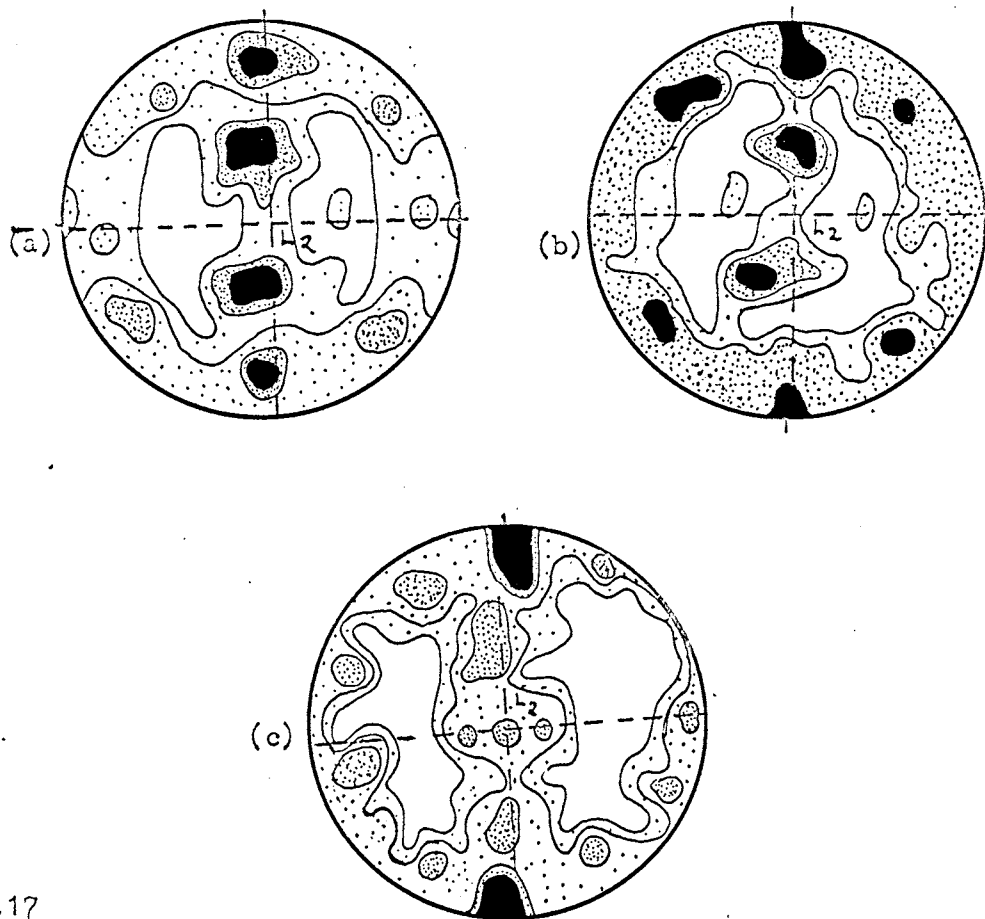
FIGURE 2.17

Preferred orientation of c-axes of quartz in some B$^{S_1}_S$ tectonites. All data

are from three sections at right angles and are projected onto a plane normal

to L.. In each case the primitive circle represents one plane of symmetry; the
2

other two symmetry planes are shown by dashed lines.

(a)   651 c-axes from quartz-mica schist from Loc. 22300123400, Cont. 2, 1,

0.6, 0.3% per 1% area).

(b)   450 c-axes from a rodded sillimanite schist collected several hundred

yards west of the Mt. Robe Mine (Cont. 2, 1, ½% per 1% area)

(c)   450 c-axes from a quartzite mullion from Loc. 27500104000 (Cont. 3, 2, 1,

½% per 1% area).
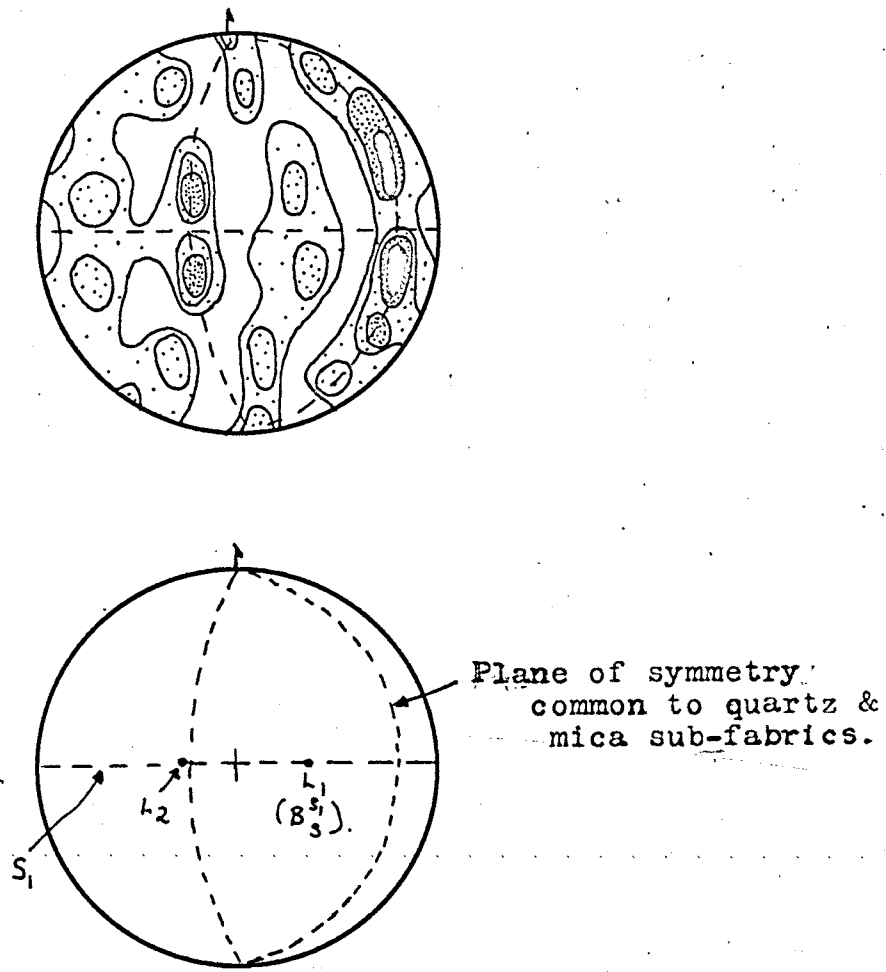
FIGURE 2.18

(a) Preferred orientation of c-axes of quartz in Spec. No. 28350 (Data measured from three sections at right angles; 450 grains, contours: 2, 1.4, 1.2 1, 0.5% per 1% area).

(b) Symmetry planes (dashed lines) in diagram (a) and their relationship to L_1 (=B^{S_1}) and L_2 in the specimen. Symmetry plane normal to L_2 is also present in the mica sub-fabric (Fig. 2.2a).

Where L_2 is parallel to L_1 the total fabric may be monoclinic. Thus at locality 27500104000, all the visible fold axes are homogeneous in orientation and parallel to L_2. However, triclinic symmetry is more general.

The use of symmetry arguments in interpreting fabrics has been set out in detail by Paterson and Weiss (1962) and again by Turner and Weiss (1963). The guiding principle in the use of symmetry arguments is - "The symmetry of any physical system must include those symmetry elements that are common to all the independent factors (physical fields and physical properties of the medium) that contribute to the system, and it may include additional symmetry elements; however, any symmetry elements absent in the system must also be absent in at least one of the independent contributing factors" (Paterson and Weiss, 1962, p.859). Factors which must be considered in the deformation of a body - as given by Paterson and Weiss (1962, p.876), are set out schematically below:

External Factors

General tectonic situation
|
System of forces applied to
the given body of rock

Internal
Factors

Stress field within the rock   Mechanical properties
                                       of the rock
Deformation
("Movement picture")   Initial fabric

Observed fabric
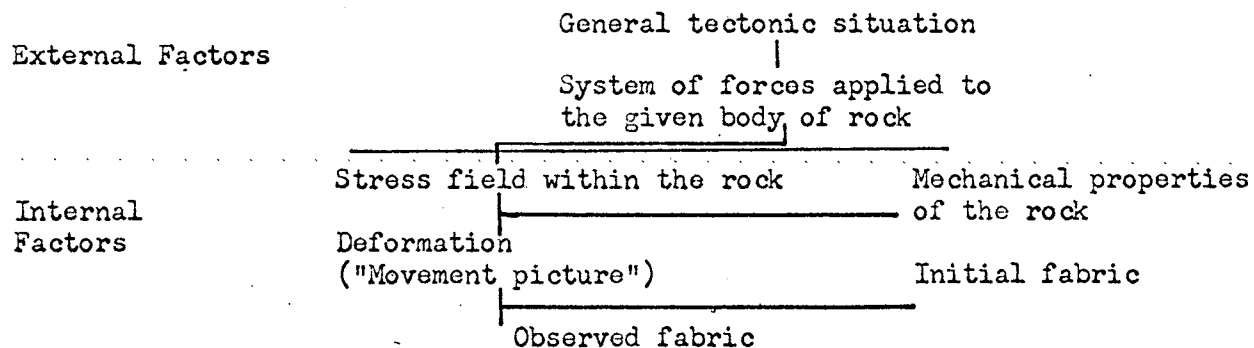
A fabric element of the initial fabric whose mechanical properties can significantly influence the course of deformation is said to be "kinematically active"; elements that serve only as markers, without influencing the deformation, are referred to as "kinematically passive" (Turner and Weiss, 1963, p.383). Lithological layering cannot have been entirely passive during B_1 folding. The schistosity is disturbed in the vicinity of mullions (see Fig. 2.7) and curves

around the termination of layers. In both cases the layering is exerting some influence on the final fabric. This type of behaviour is shown by quartzites.

The most important features to be considered are the discordant symmetries of the inherited sub-fabric (S) and quartz and mica sub-fabrics, and the different symmetries of the last two sub-fabrics. We may also note one important difference between mica and quartz. For mica, preferred orientation of the lattice may be an incidental result of dimensional orientation; in this way mica, by mimetic crystallisation, may emphasise anisotropic features inherited from the original rock. Quartz is not susceptible to dimensional orientation. It is clear that the quartz and mica sub-fabrics are recording different portions of a deformation, although an examination of their mutual microstructure leaves no doubt that both minerals are the result of the same tectonic and metamorphic episode (Chapter 5).

It is doubtful that the interaction of an initial fabric containing only compositional layering could have produced the final fabric observed. (In the following discussion we shall assume a general system of stresses with orthorhombic symmetry, although more special stress systems, such as uniaxial stress, may have higher symmetry). For deformation of kinematically passive layering the stress, strain, movement picture and imposed sub-fabrics would all have concordant orthorhombic symmetry. The symmetry of the inherited sub-fabric would depend on the number of symmetry planes common to layering and stress at the commencement of deformation. The inherited and imposed sub-fabrics need not be concordant or even of the same symmetry, but the quartz and mica sub-fabrics (both imposed) should both have orthorhombic symmetry. For kinematically active layering the symmetries of the imposed and inherited sub-fabrics (and the movement picture) would be concordant and of the same type

(as above, the symmetry would depend on the number of planes of symmetry common to layering and stress). This is obviously not the case.

One model that may be considered involves the transposition of a foliation present in the initial fabric. Some of the micas are now emphasising relicts of the old foliation, while the bulk are oriented in a new (transposed) foliation. The intersection of the new and old foliations is the lineation L_2. If the old foliation was parallel to the axial surfaces of a system of folds in layering, then L_1 ($B_S^{S_1}$) and L_2 would not necessarily be parallel after B_1 folding. Indeed they would only be parallel if the new foliation intersected the old in an axis parallel to the old fold axes. We may expect that if B_1 were superposed on an earlier set of folds of this type, that L_2 would represent a relatively fixed direction and L_1 would vary. Because of folding after B_1 folding in the mapped area, it is no longer possible to test directly the geographic orientation of L_1 and L_2 at the conclusion of B_1 folding. However, the situations south of Little Aller Creek, west of Mt. Robe and north-east of Mt. Franks, where L_2 now has a constant orientation (but different for each area) and L_1 varies suggests that the above is the case. Also, it can be inferred from the distribution of L_2 in later folds that it must have had a fairly constant orientation at the end of B_1 folding over a large portion of the mapped area (see discussion of sub-areas 5 and 14, Chapter 4).

The model of superposed folding requires that the old foliation be passive, since a kinematically active foliation would create a movement picture with monoclinic symmetry, and this would be reflected in the symmetry of the quartz sub-fabric. However, judging from the style of the final fabric, the old foliation must have been more or less penetrative. For a penetrative foliation to remain passive probably requires that the deformation (B_1 folding) have

proceeded mainly by indirect componental movements (e.g. diffusion),since a penetrative foliation normally imparts a distinct mechanical anisotropy to the rock. Some further evidence to support this idea is given below.

There is an alternative. Transposition has brought the old foliation to an orientation where, with L_2, it has approximate orthorhombic symmetry concordant with the quartz sub-fabric (as the relicts of the old foliation disappear). As the foliation approached the final state of complete transposition, it may, if initially active, have exerted a diminishing influence on the course of the deformation. It is this final state, along with the calc-silicate boudins, that the quartz sub-fabric is recording.. Except for mimetic crystallisation, the mica sub-fabric would also have finished with orthorhombic symmetry.

The model of superposed folding also requires that layering have been kinematically passive during the deformation. Otherwise the final sub-fabrics would have symmetries concordant with the inherited sub-fabric of S. However, we have already noted that layering is not entirely passive. However, behaviour of this type is very local and there is no significant change in orientation or style of S_1 from areas where layers are present to adjacent areas where layering is lacking. It is possible then that layering may have bee passive, particularly, as is the general case, the various layers in the schist differ little from the average bulk composition of the schists. Mullions, boudinage and formation of the parasitic folds in $B_S^{S_1}$ folds are peculiar to quartzites and calc-silicates and are not a general feature of layering in the schists.

The symmetry of one other element is concordant with that of the quartz sub-fabric. Layering in the ellipsoids has overall orthorhombic symmetry (D_{2h}) (made up of all layers with orthorhombic symmetry, or central layers with spherical symmetry K_h and outer layers with orthorhombic symmetry).

It seems that no simple process of folding can entirely account for the closed layering of the ellipsoids in three dimensions. A process that might partially account for their form is formation of isoclinal fold hinges followed by closing of the "tail" of the hinge by compression. But layers of boudins should then trend at an angle across S_1, which is contrary to the observation that they always parallel S_1. Moreover, there is a frequently observed pattern in the composition of the internal layers. The outer layers usually contain a higher proportion of the calc-silicate minerals (diopside, epidote, garnet) whereas the inner layers are richer in quartz. The number and order of the internal layers are variable but the above generalisation holds. It is unlikely that layering inherited from the rock prior to metamorphism and deformation could be so regular in the large number of ellipsoids scattered over the mapped area. It appears that a diffusion process, coupled to imposed stress, may have controlled the shape and compositional distribution of internal layers in the boudins. And since the internal layers conform with the shape of the external surfaces of the boudins, the diffusion process may have been an important mechanism in the actual deformation that produced the boudins.

The ellipsoids are not true imposed elements, for processes responsible for their shape have operated on a shape at least partially inherited from the initial fabric. However, if the ellipsoids developed from layers in the transposed limbs of B_1 folds, neither single ellipsoids nor a layer of ellipsoids need record all of the symmetry of the inherited fabric. The initial layers from which the boudins developed, in this case, have axial symmetry and if subject to an influence with orthorhombic or higher symmetry (stress), the resultant fabric would have orthorhombic or higher symmetry. However, the total disposition of all layers of ellipsoids, although individually they

they may parallel S_1, may exhibit the total symmetry of folding. The ellipsoids and the quartz sub-fabrics seem to reflect the symmetry of the stress system responsible for deformation.

The direction of movement on the glide surfaces cannot be fixed, but from symmetry arguments it must be normal or parallel to L_2. The existence of the glide surfaces argues for a monoclinic rather than an orthorhombic movement picture, for, locally the glide surfaces may be as penetrative as B_1 folds. Still the quartz sub-fabric will reflect the symmetry of stress.

In this case the principal axes of stress for B_1 folding were oriented normal and parallel to schistosity with one axis coinciding with the lineation L_2. At least in the transposed limbs of B_1 folds the principal axes of strain were oriented in a similar fashion and extension parallel to the lineation (boudinage) was an important component of strain. Extension normal to L_2 in S_1 (from separation of boudins) was also important. By implication the third axis of strain normal to S_1 was an axis of shortening which, in turn, implies that the major axis of stress may have been normal to S_1.

The most basic criterion that can be brought against the model of superposed folding is the lack of folded folds (by B_1) in the mesoscopic fabric. Given the penetrative nature of B_1 folds and glide surfaces these may be difficult to detect, but if not directly observed, should appear as rapid variations in the orientation of $B_S^{S_1}$ at the mesoscopic scale. No examples have been found although at a larger scale the area south of Little Aller Creek may be an example.

2.40 $B\frac{S_2}{S}$ and $B\frac{S_2}{S_1}$ folds

The surfaces S and S_1 are folded and the lineation L_2 redistributed (no example of folded L_1 has been found) by a second generation of folds, designated $B_S\frac{S_2}{}$ or $B_{S_1}\frac{S_2}{}$ folds for folds in S and S_1 respectively. The group of all folds with S_2 as axial surface is termed B_2 folds. No example has been discovered of a combined $B_S\frac{S_2}{}$ and $B_{S_1}\frac{S_2}{}$ fold in which the two fold axes are not parallel; although such folds might be expected. B_2 folds are noticeably lacking in areas where S_1 intersects S, even though they may be common in adjacent rocks.

B_2 folds are the least common of the mesoscopic folds and their occurrence is limited to the north-west portion of the area. They are particularly common around the margins of the Aller Creek Pegmatite; bodies of schist included in the pegmatite are also commonly deformed by B_2 folds.

The style of B_2 folds is shown in Fig.2.19 . The folds are often nearly isoclinal, with a difference in orientation of S or S_1 of less than 10° in each limb at some distance from the hinge. B_2 folds are never penetrative and usually occur in isolation. Complicated faulting in the hinge region is also common (e.g. in $B\frac{S_2}{S_1}$ folds exposed on the road to the adit of the Mt. Robe Mine).

The most acceptable evidence that B_2 folds post-date B_1 folds - the folding of mesoscopic B_1 folds about a mesoscopic B_2 fold - is lacking. However other evidence suggests the relationship proposed above is correct. Single rods of sillimanite (L_2) and flakes of muscovite (at locality 285001,32200 in particular and in the specimen illustrated in Fig. 3.12c) are bent across the hinge of mesoscopic B_2 folds. The rods and the mica are both the product of a metamorphism that outlasted B_1 folding (M_1 metamorphism, Chapter 5) and their

(a)

1 foot

(b)

2 inches
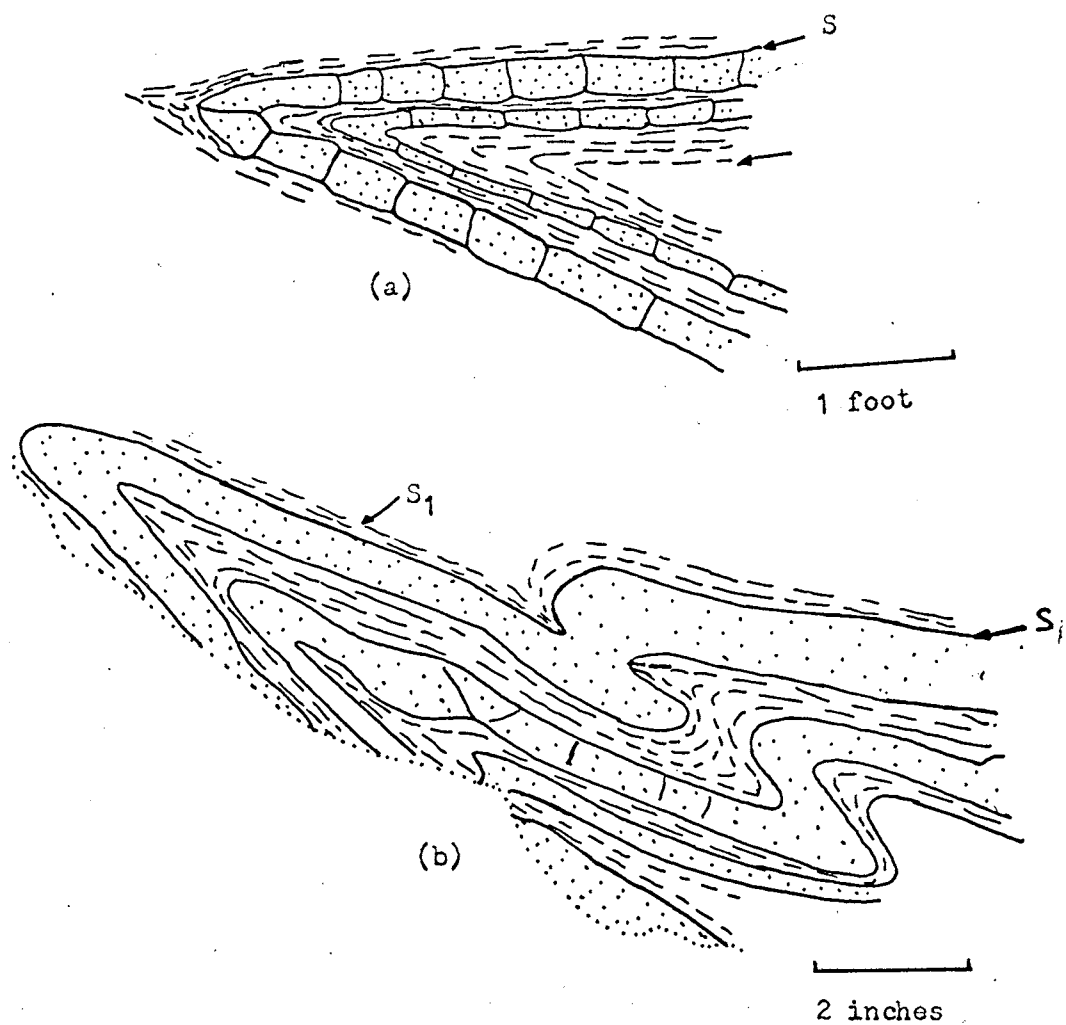
FIGURE 2.19

Style of $B_S^{S_2}$ folds in mica schists:

(a) at Loc. 35100134700, and (b) at Loc. 36700138300 (both drawn from photographs).

Both folds are outlined by quartz-plagioclase layers (stipled) in sillimanite schists (a) and quartz-muscovite schist (b); both dashed parallel to the trace of S_1). The lower limb of (a) gradually curves away to nearly parallel the upper limb 10-12' to the right of the hinge shown.

deformation indicates that B_2 folds post-date both the metamorphism and B_1 folding, in a separate episode of folding.

The redistribution of the lineation L_2 in $B_2 \frac{S_2}{S_1}$ folds is unusual. The lineation, after folding, is disposed in a plane whose normal is at an angle to the fold axis (Fig. 2.20). The style of $B \frac{S_2}{S_1}$ is concentric, and the kinematic model generally conceived to account for concentric folds envisages slip on the folded surface. A lineation in the unfolded surface is distributed on the surface of a cone whose axis is concentric with the fold axis; the semi-angle of the cone is the angle between the old lineation and the fold axis (Ramsay, 1960). Redistribution of a lineation in a plane is consistent with slip folding to produce similar folds.

Ramsay,(1960) has investigated the effects of flexural slip folding followed by slip folding on the distribution of a lineation in the unfolded surface. On a stereographic nett, the lineation is first distributed on a small circle by the flexural slip folding and then, as slip folding proceeds, is rotated so as to plot approximately on a great circle. The final distribution may be indistinguishable from one produced by slip folding alone. It is suggested that B_2 folds have developed by slip on S and S_1, and that as folding has proceeded the slip has approximated more closely to slip on an axial surface (as the fold became more isoclinal). It is doubtful if folds evolved in this manner could be very penetrative or regular, which seems to agree with the nature of B_2 folds.

(a)

• Lineation L_2

⊙ $B_{S_1}^{S_2}$

◼ Axis of great circle that contours the lineation.

(b)
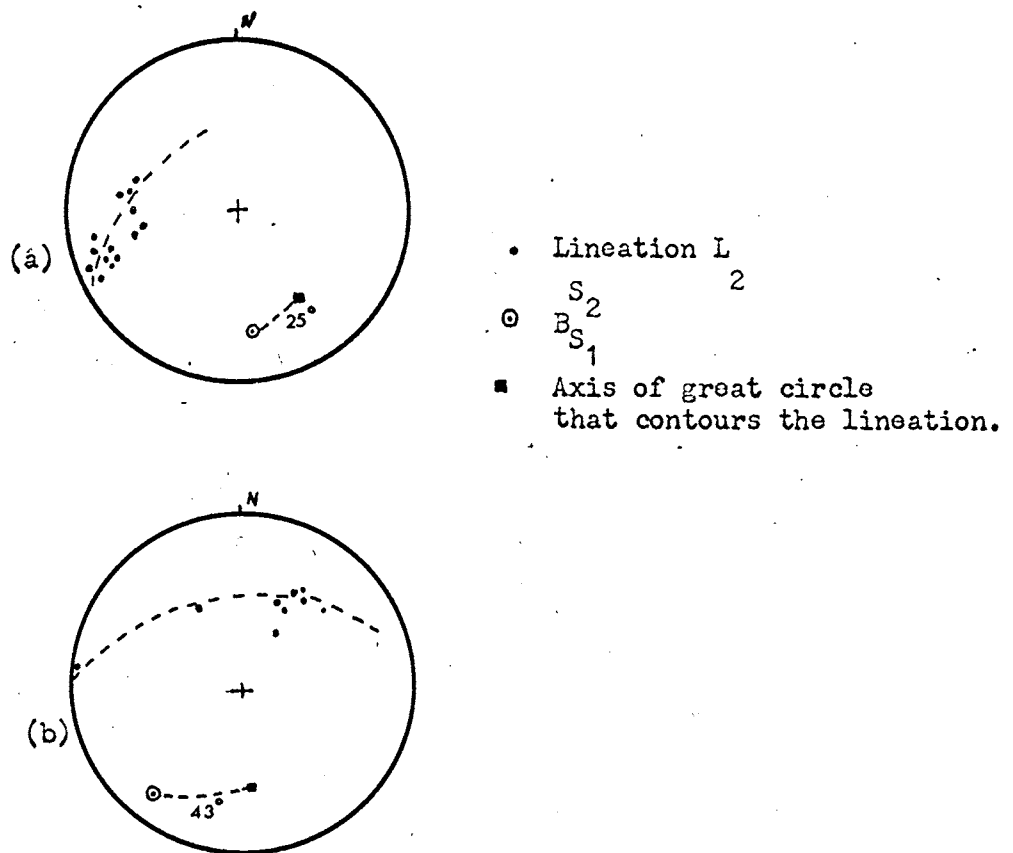
FIGURE 2.20

Distribution of lineation L_2 in two $B_{S_1}^{S_2}$ folds. Both folds are in rodded sillimanite schist and are almost isoclinal; the lineation is represented by the long axes of sillimanite rods:

(a) fold at Locality 285001 32200,

(b) fold at locality 46200125000

The angles between $B_{S_1}^{S_2}$ and the normal to the plane in which the lineations are distributed are 25° and 43° respectively.

CHAPTER 3

B$_3$ AND B$_4$ FOLDS

3.10 Introduction

The folds classified as B$_3$ and B$_4$ folds are a complex group of kink folds and concentric folds which exhibit a great diversity of style and orientation. B$_3$ and B$_4$ folds both possess the same characteristic axial structure: a system of microscopic kink bands in the hinge region of the mesoscopic fold.

B$_3$ and B$_4$ folds are distinguished from relationships observed at one single locality (see Sect. 3.26). At this locality the orientation of the kink bands, and hence the axial surfaces of the mesoscopic folds they parallel, fall into two non-overlapping groups. Folds of one orientation-group (B$_3$) are constantly overprinted by folds of the other group(B$_4$). The style of both the mesoscopic folds and the microscopic kink bands of both groups (B$_3$ and B$_4$) are identical at this locality, and B$_3$ and B$_4$ can only be distinguished by the orientation of their axial surfaces. Elsewhere in the area the microscopic kink bands and mesoscopic folds are variable in style, but the variation cannot be related to orientation. Rather, the style of both is dependent on the bulk lithology of the rock and the presence or absence of lithological layering. When, for example in the laboratory, specimens are divested of their geographic orientation, it is impossible to discriminate between B$_3$ and B$_4$ folds.

Instead of duplicating the definitions of the structural elements of B$_3$ and B$_4$ folds, a single set of definitions will be given for B$_4$ folds; similar definitions for B$_3$ folds can be obtained by substituting 3 for 4 in the appropriate place.

3.20 S$_4$, L$_4$ in homogeneous mica schists

In mica schists with a homogeneous composition S$_4$ surfaces (kink surfaces)

are axial surfaces to a system of microscopic kink folds. Usually the kink folds occur in pairs sharing a common limb, thus forming a kink band. An example of a schist in which kink bands are well developed is illustrated in Fig. 3.1.

At the microscopic scale a kink surface is represented by a domain of acute flexure between the planar, or nearly planar, limbs of a kink fold. This domain is always thin compared to the width of a kink band, and most closely approximates an ideal surface in very micaceous layers. Where the structure of S_1 is less regular or a micaceous foliation is not prominent, the domain representing the kink surface is a broader zone of flexure. However, when viewed in hand specimen the kink surfaces always appear as discrete surfaces. Also it is noticeable that the kink bands are less regular in rocks with poorly developed micaceous foliation compared to rocks with well developed S_1. Kink surfaces are not developed in rocks which lack a micaceous foliation, even where adjacent rocks are intensely deformed by kink bands. A fracture cleavage parallel to S_3 and S_4 appears in thin units of quartzose rocks but there is no surface that can be identified with kink surfaces in the amphibolites or calc-silicates.

There is no tendency for micas to have a preferred orientation parallel to S_3 or S_4, or for transposition of S_1 parallel to S_3 or S_4. Also there is never any sign of displacement on the kink surfaces where the kink bands cross metamorphic laminae. The kink bands are symmetrical within a few degrees with respect to the angle between the kink surface and S_1 on either side.

FIGURE 3.1 (PLATE 1)

Polished hand specimen of a B_4 tectonite (quartz-muscovite-andalusite schist) from outcrops on the northern slopes of Mt. Franks. The kink bands appear as dark bands passing diagonally from left to right across the photograph. S_2 in the kink bands is nearly vertical and S_2 outside the kink bands horizontal. The porphyroblasts are altered andalusite.

(Section is normal to kink axes. Close to natural size)

The angle between S_4 and S_1 in each limb of a kink may vary not only with position along the trace of axial surface in a section perpendicular to L_4, but with different kinks in the same tectonite. All of the kinks illustrated in Fig. 3.2a are taken from a single specimen (3760087400) from Mt. Franks. The angles range from 20-55°; angles of 40-50° seem to predominate in most specimens examined.

It is not as easy to determine the variability of the angle S_1 kink surface parallel to the kink axis but it appears to be much less than that perpendicular to the axis. The angle is almost constant over a distance many times the width of the kink band, except where the kink bands terminate (parallel to L_4) by a rapid decrease in amplitude, a change that occurs in a matter of millimetres.

Fig. 3.2b emphasises another important aspect of the style of the kink bands. The basic "kink-style" is independent of the relative angle of rotation of the limbs; the kinks are not transitional to continuous flexures with decrease in the angle of rotation of the limbs. However the intersection of two kink bands produces a fold which is not a kink but a continuous flexure (Fig.3.3)

One aspect of the morphological properties of systems of kink bands is illustrated in Figs. 3.4, 3.5, 3.6. One feature of sections normal to L_4 is distinct changes of orientation of the trace of S_4 on the plane of the section (Fig. 3.4, 3.5). A more detailed analysis of this variation is presented in Fig. 3.6 which contains all the trace of the axial planes of kink folds present in a large thin section. The figure was prepared from an enlarged photograph of a thin section. The figures beside each trace relate to the angle between the trace and an arbitrary direction OY. The frequency of the various orientations is given in the histograms accompanying the figure. The fact that emerges is the presence of a distinct grouping of the traces of the S_4 surfaces

Figure 3.2.

Variation in style of kink bands in a section normal to the kink axis:

(a). Variation in the angle between S_1 and S_4 in each limb at different

points along a kink surface, and in different kink bands (detail traced from

photograph, measurement of the micas with a Universal stage indicates the

kink axis is normal within a few degrees to the plane of the section).

(b). The kink style is independent of the actual angle between S_1 and S_4.
In the left hand example the angle between the two limbs is constant, but the

domain forming the kink surface changes from a narrow, sharp zone at the bottom

to a broader zone of curvature near the top of the fold. The situation is

reversed in the right hand example. Note also the same style of basic kink

in all examples on the page, although the angle $S_1 \wedge S_4$ varies between 20° and

50°.   (Approx. X 5   )

29 30

S_4

50 50

37 40

49 48

38 38

(a)

S_4

S_4

S_4

30 30

29 28

20 21
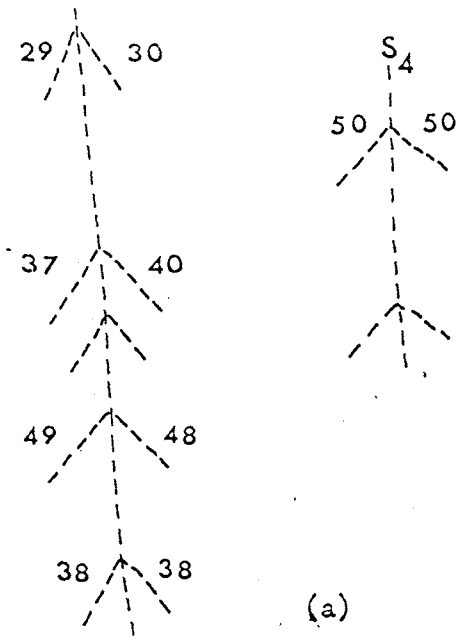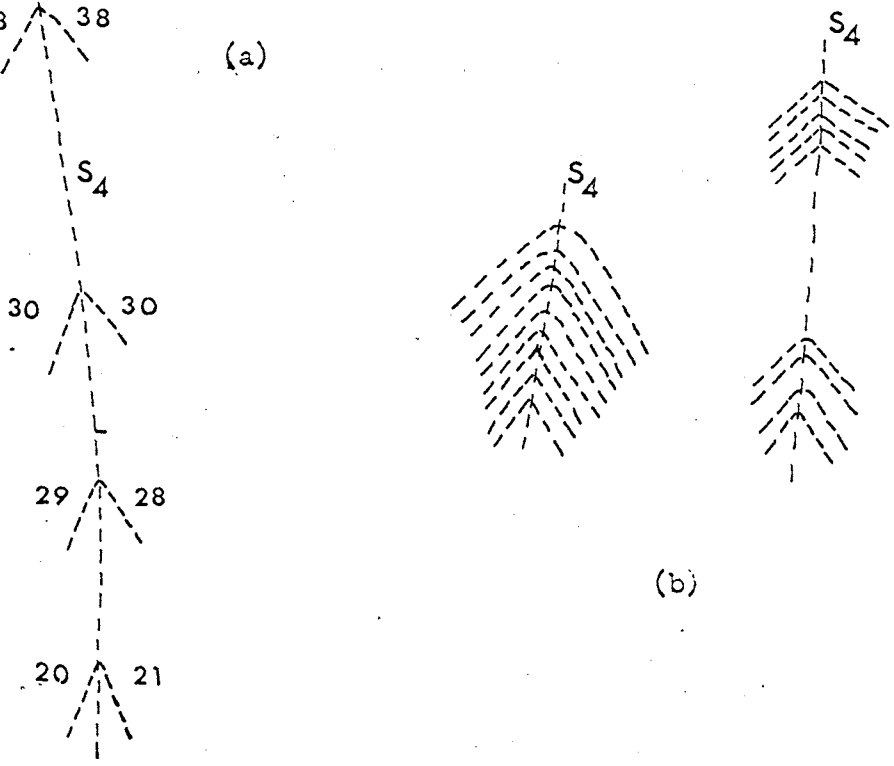
(b)
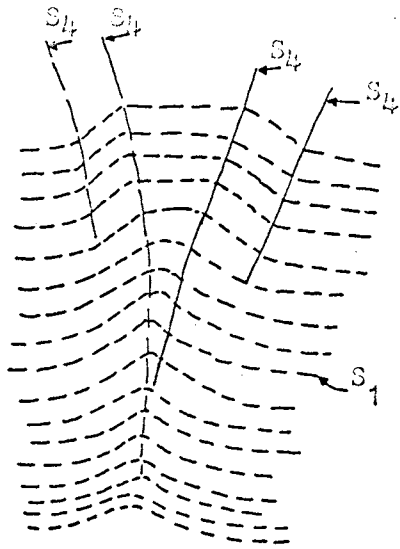
<u>FIGURE 3.3</u>

Fold formed at the intersection of two kink bands in S_1. The lower portion of the fold is an open flexure that dies out rapidly downwards.
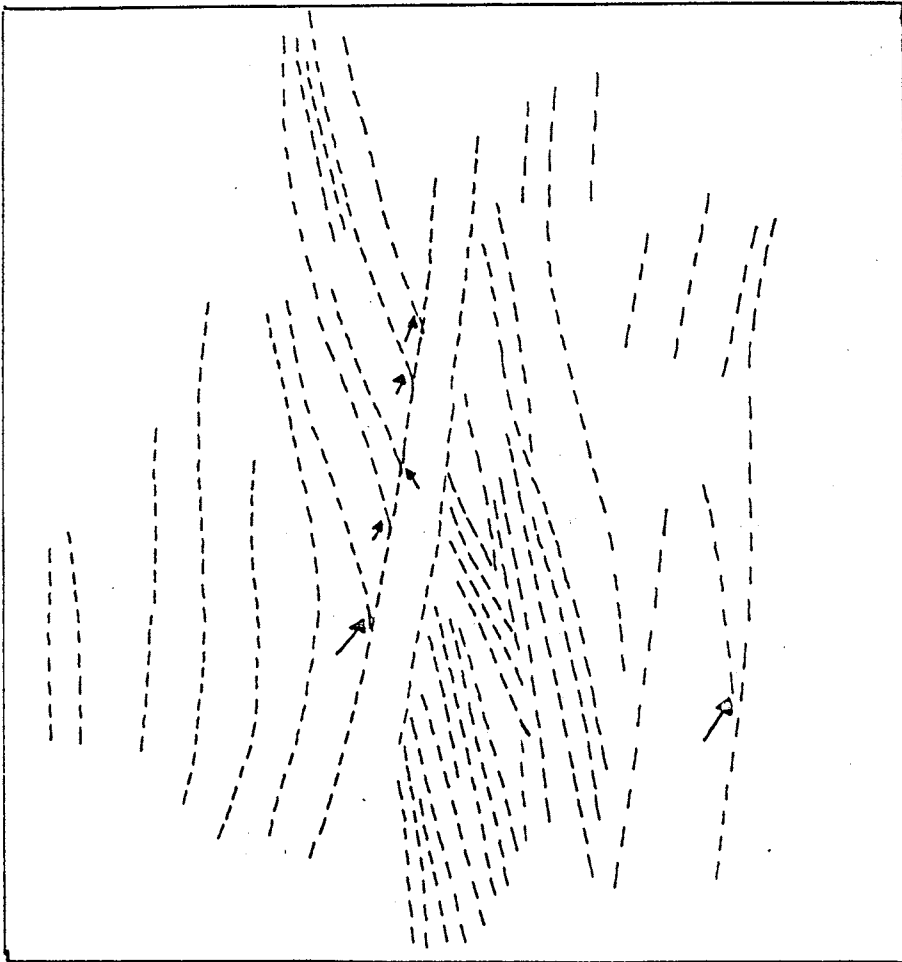
FIGURE 3.4

Well developed conjugate pair of kink bands. The traces of the kink bands
are shown on a polished surface normal to L_4 from a quartz-mica schist from Mt.
Franks. Arrows point to conjugate kink bands forming a fold of the type illus-
trated in Fig. 3.3 (data traced on photograph, twice natural scale).
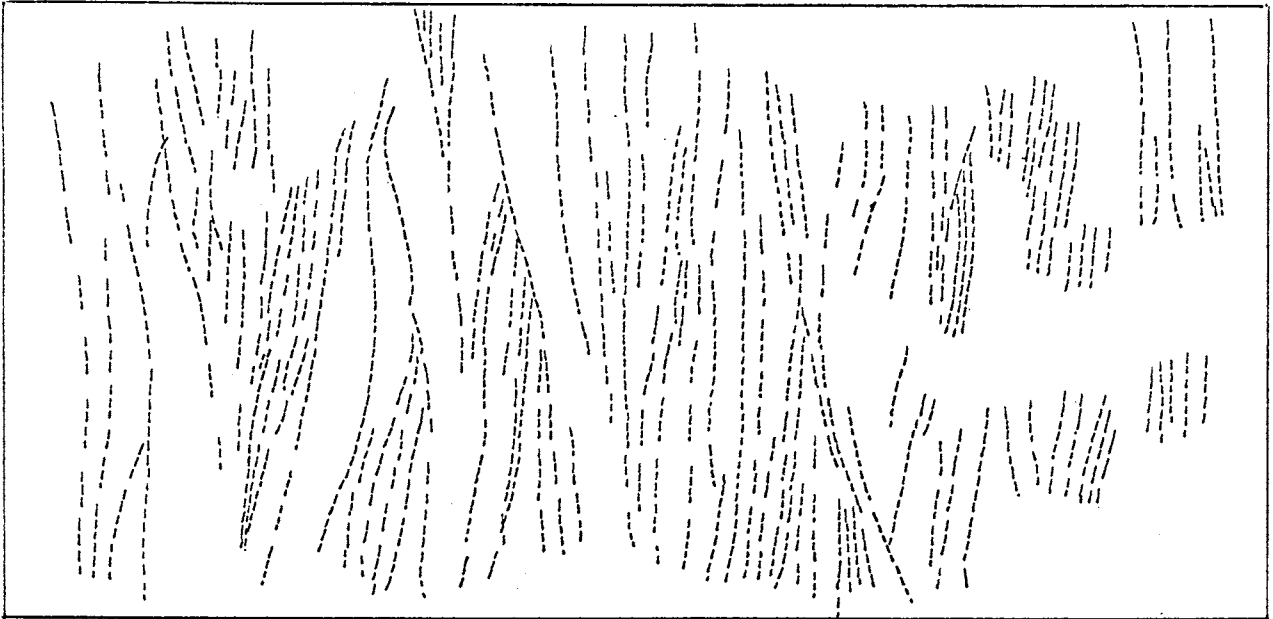
Fig. 3.5

Variation in the orientation of kink surfaces in a section normal to the kink axes. Diagram shows traces of S_4 on a polished face of a quartz-muscovite schist from Mt. Franks (data traced from photograph, approximately natural scale).

to form a conjugate pair, separated by an angle of 10-20°. The pair is
not equally developed throughout the specimen. The total variation in
traces of the kink bands is nearly 90°, but the traces at an angle of 40°
to the left of OY in Fig. 3.6 can probably be neglected, reducing the range
to 55°.

The second point of interest is the grouping of traces of a single
orientation into domains (Fig. 3.6). The extent of the domains is suggested
in Fig. 3.6.

A second pattern of variation is evident in many of the tectonites sectioned.
This is observed as a variation in the trend of the kink axes (Fig. 3.7, also
Fig. 3.16a) as observed on the folded S_1 surface. The angle between extreme
trends is about 15°, and single kink axes may change continuously between
these orientations.

It appears that the geometry of the kink bands can be conceived of as
rotation about two axes at right angles, roughly parallel and normal to the
kink axes in the specimens studied. Sections at intervals through specimens
on which the trace of the kink axes is homogeneous still reveal the full range
of variation about an axis parallel to the kink axis. If the geometry could be
described by rotation about one axis oblique to both sections, then change in
the trace on one section must be accompanied by a change in the trace of the
other. That this is not always true is demonstrated by a section through a
mica schist from Mt. Franks (Fig. 3.8); the traces change orientation indep-
endently in the two sections. In hand specimens the variation about an axis
normal to the average kink axis is usually much subordinate to variation
about the other axis.
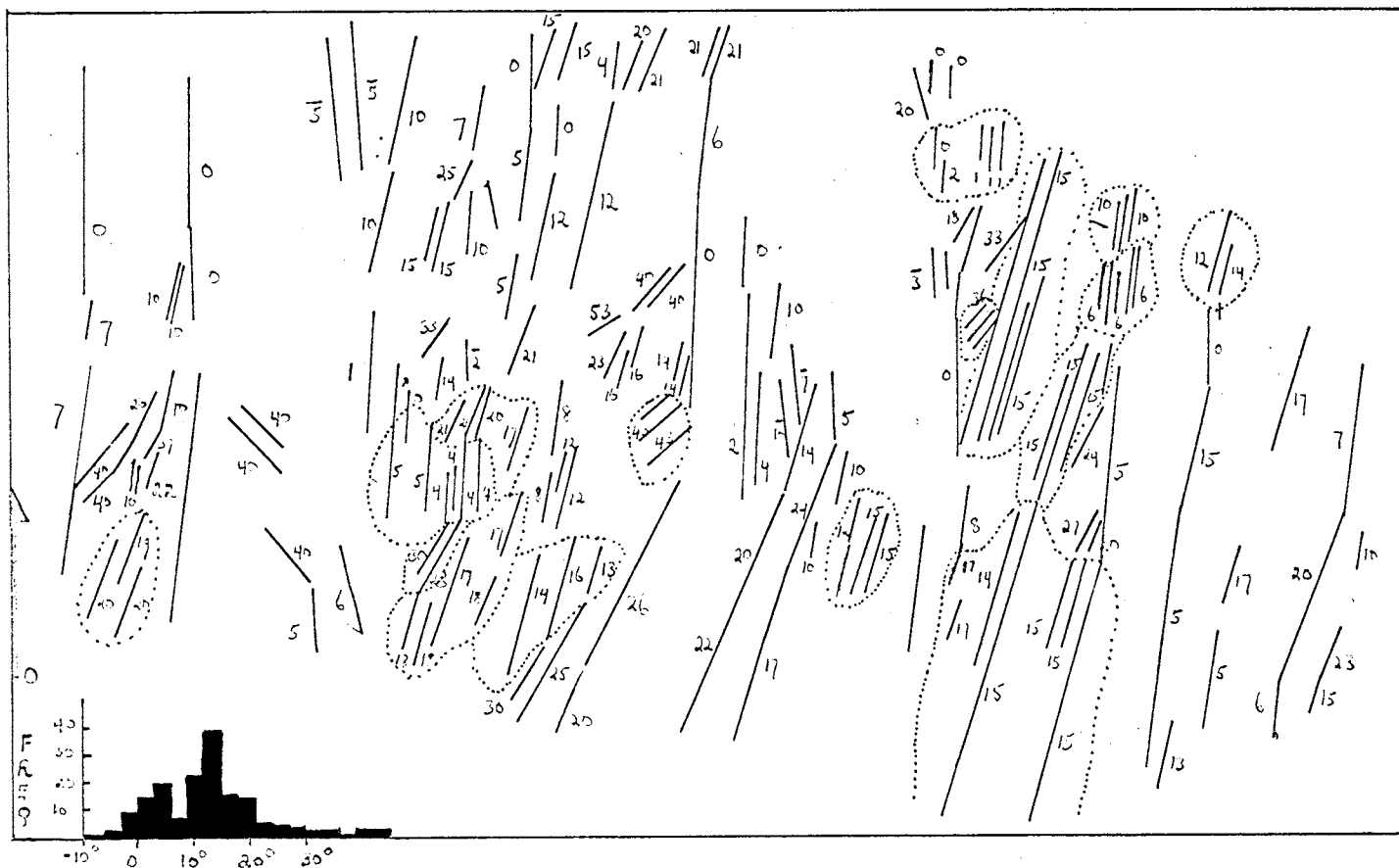
FIGURE 3.6

Traces of S$_4$ on a section normal to L$_4$ in a quartz-muscovite schist from Mt. Franks. The numbers beside the traces (solid lines) refer to the angle the trace makes with the vertical edge (OY) of the diagram. The dotted lines outline some domains in which the traces have similar orientations. The histogram gives the frequencies of the various angles made by the traces with OY and indicates two main groups at 5° and 15°. The area covered by the diagram is approximately 2x3 inches (Data added to enlarged photograph).
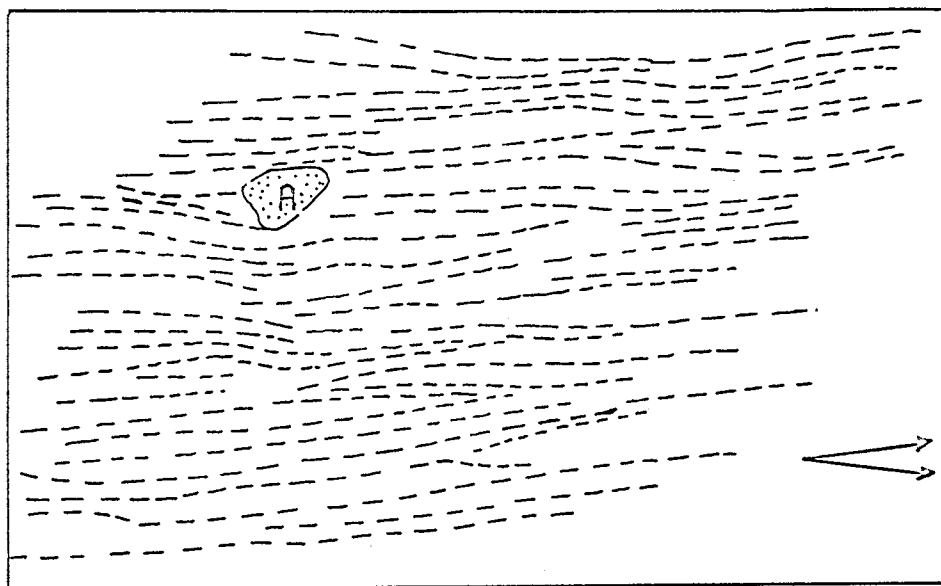
Figure 3.7

Traces of the kink surfaces on a slab polished parallel to the kink axes. (i.e. as might be seen on a finely crenulated schistosity surface). Two trends of the kink bands are indicated by the two arrows in the lower right hand corner. Note how continuous individual·kink bands are parallel to the kink axes (A = andalusite porphyroblast; natural size).

FIGURE 3.8

Geometry of kink bands as deduced from the trace of the kink bands on surfaces normal and parallel to the mean kink axis.

(a)   Orientation of sections I and II with respect to the mean kink axis for diagrams (b), (c) and (d).

(b)   Traces of S_4 are constant in section I, but vary in II. Geometry can be described in terms of rotation about an axis normal to the mean kink axis.

(c)   Commonest situation encountered; the traces of S_4 are constant in Section I but vary in Section II.

(d)   Traces have variable, but consistent pattern of orientation in Section I and Section II.

Diagrams (b) and (d) are from serial sections of a mica schist from Mt. Franks. Diagram (c) is from a mica schist from Loc. 46200125000. Data drawn from projected images or photographs..
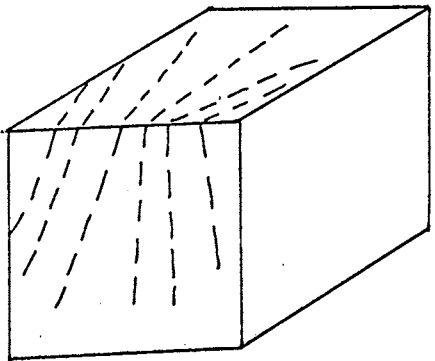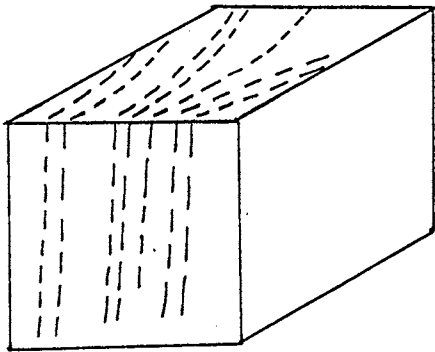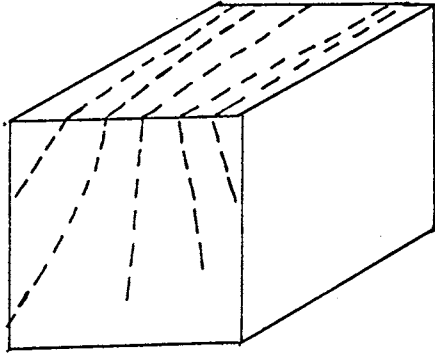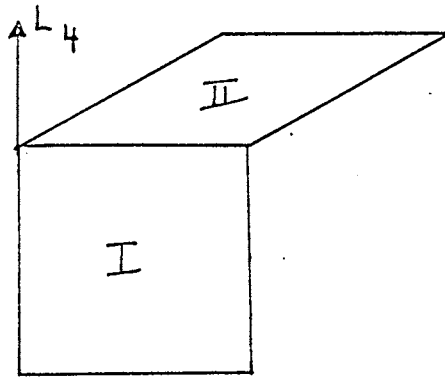
3.21 $B_{S_1}^{S_3}$ and $B_{S_1}^{S_4}$ folds in schists of uniform composition

Mesoscopic folds in S_1 with S_3 or S_4 parallel to their axial surfaces in schists which lack lithological layering are very similar in style to the microscopic kink bands (Fig. 3.9). The folds are simple kinks, often with slight curvature of one limb, with a bundle of kink bands (S_3 or S_4) concentrated in the hinge region with rare kink bands in the limbs. The angle between the two limbs is fairly constant throughout the whole area and fall within the range 75-90° (stated as the acute angle).

The folds are symmetric with respect to the angle between their hinge surface and each limb, but are asymmetric if the length of the limbs is considered. Within small domains the size of the folds may be nearly constant and their spacing approximately periodic, indicating a very uniform strain throughout that particular domain.

3.22 Combined $B_S^{S_3}$ and $B_{S_1}^{S_3}$ folds and combined $B_S^{S_4}$ and $B_{S_1}^{S_4}$ folds in layered schists

Mesoscopic folds in schists that are layered (S) which have S_3 or S_4 as axial surface differ in a number of respects from $B_{S_1}^{S_3}$ and $B_{S_1}^{S_4}$ folds in unlayered schists. In general (because of the transposition of S during B_1 folding) $B_S^{S_4}$ and $B_{S_1}^{S_4}$ (and $B_S^{S_3} - B_{S_1}^{S_3}$) are co-axial and the style of the fold in the schistosity agrees with that in the layering. This case will be discussed first.

The main points of difference between combined $B_S^{S_4}$ and $B_{S_1}^{S_4}$ (and $B_S^{S_3}$ and $B_{S_1}^{S_3}$) folds as compared to $B_S^{S_4}$ folds in unlayered schists are:

(1). The combined folds typically occur as single folds or a group of several folds in which the size of each fold is considerably different. The approximation to a periodic array is lacking in the combined folds.
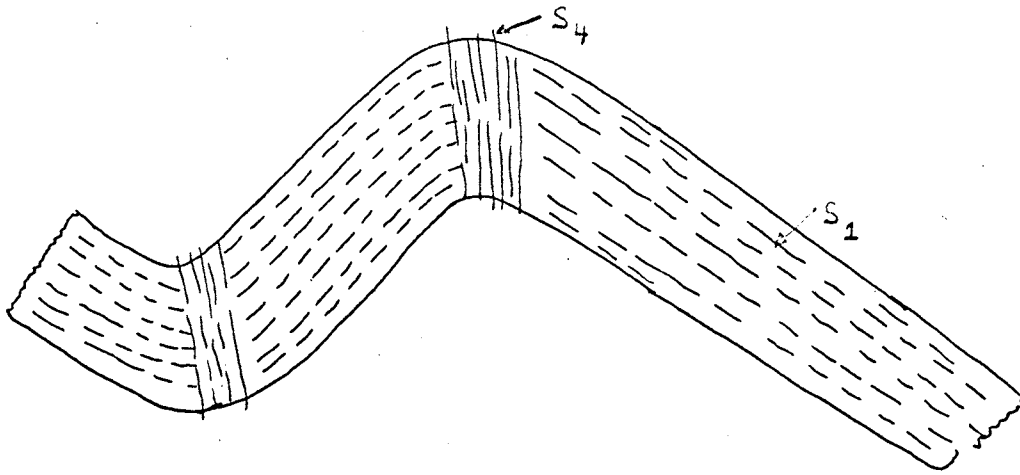
FIGURE 3.9

Example of a $B_S^{S_1}$ fold in unlayered schist. The fold is a simple limb

with kink bands concentrated in the hinge. The limb sloping to the left is the

longer limb. (Sketch: $\frac{1}{2}$ scale; drawn from photograph)

(2). The combined folds vary quite markedly in their style (Fig. 3.10), even

in the same outcrop. Also the angle between the limbs is not as constant as

that of $B_3^{S_4}$ folds in unlayered schists.

(3). Unless the differences in composition of the various layers are minimal

and all layers contain more than 20-30% mica, the combined folds do not form

simple kinks. The combined folds are always concentric folds.

Examples of folds in which the axes in S and S_1 are not parallel are very

rare, even in outcrops which contain abundant folds in adjacent areas where S

is parallel to S_1. A more common situation, particularly at Mt. Franks

is illustrated in Fig. 3.11. Inhomogeneities in the S_1 surface seem to

result in the creation of kink bands with a different orientation from those

in the adjacent schists. Thus in Fig. 3.12b, in the left-hand limb of the fold

the continuity of the fabric is disturbed by the termination of one layer, the

crossing of S_1 by another and the presence of an andalusite porphyroblast. The

set of conjugate kink bands in this limb, nearly at right angles to S_4 have an

orientation different to that of any kink band in the surrounding schists.

Similarly, fine nests of kink bands, with a different than average orientation,

are sometimes found around andalusite porphyroblasts (Fig. 3.12).

3.23 $B_{S_2}^{S_4}$ folds

A single outcrop, in the creek at the hut in Little Aller Creek, contains

$B_{S_2}^{S_4}$ folds (Fig. 3.12c). Single grains of muscovite bent about the hinge of

the B_2 folds clearly distinguish them from B_1 folds. The kink bands in this

area are all S_4, and no example of a $B_{S_2}^{S_3}$ fold has been discovered. However,

B_4 folds, at least, post-date B_2 folds.

3.24 L_2 lineation in kink bands and B_4 folds

Where the lineation L_2 crosses a kink band or a mesoscopic B_4 fold it is

FIGURE 3.10

Style of folds in S and S$_1$ with S$_3$ or S$_4$ as axial surface as seen in profile. In every instance, the fold axis in S is parallel to that in S$_1$ (dashed).

(a)   Pegmatite layers (stipled) in quartz-biotite schists from Eldee Creek (53400107000, drawn from polished slab, 1/3 actual size).

(b)   Quartz-plagioclase layers (stipled) in quartz-muscovite schists (Loc. 41200132300; sketch, ¼ scale).

(c)   Quartz-plagioclase layers (stipled) in mica schist (Loc. 36700138300; sketch, 1/5 scale).

(d)   Quartz-plagioclase layers (stipled) in mica schist (Loc. 44600128000; sketch, 1/5 scale).

(e)   Quartz layers (stipled), quartz-mica layers (stipled and dashed) and mica-schist (Loc. 22400128000, drawn from polished slab, half scale).

(f)   Quartz-plagioclase layer (stipled) in mica schist (Loc. 46200125000; drawn from polished slab, 1/3 scale).

Note how in (f) and (g) domain boundaries for S$_4$ and S$_3$ often correspond with lithological boundaries.
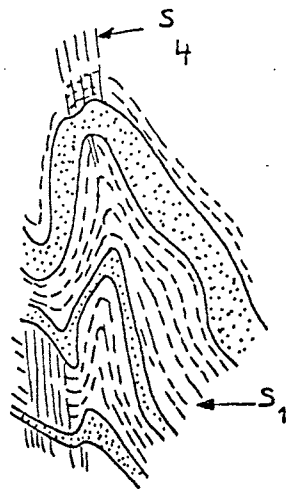
(a)
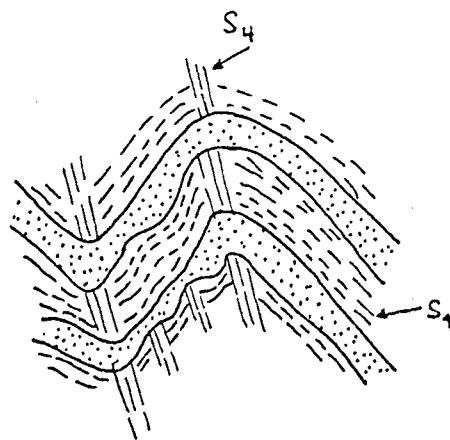
(b)
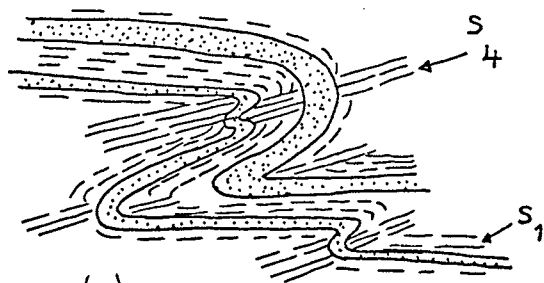
(c)
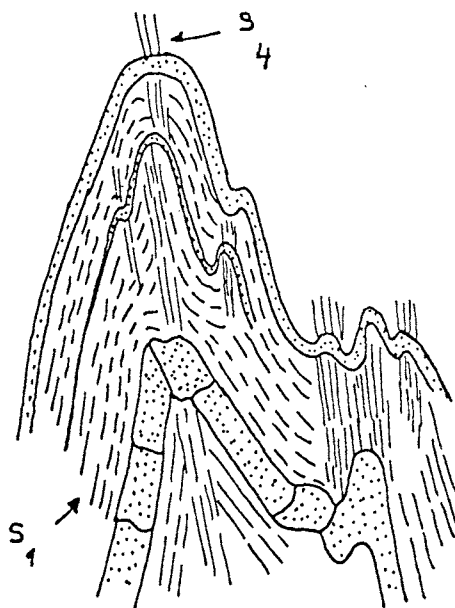
(d)
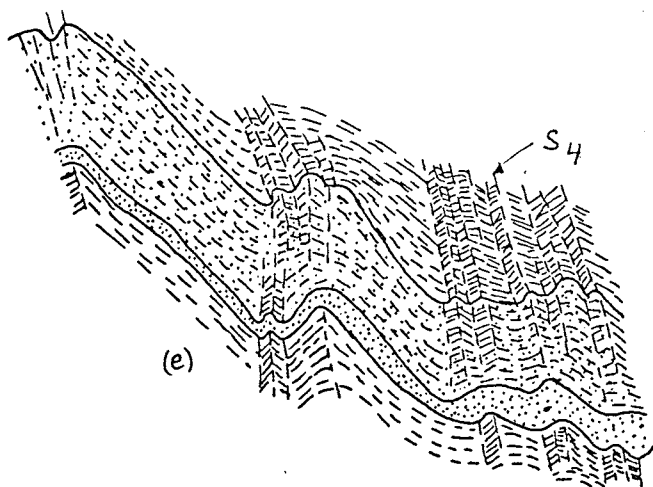
(e)
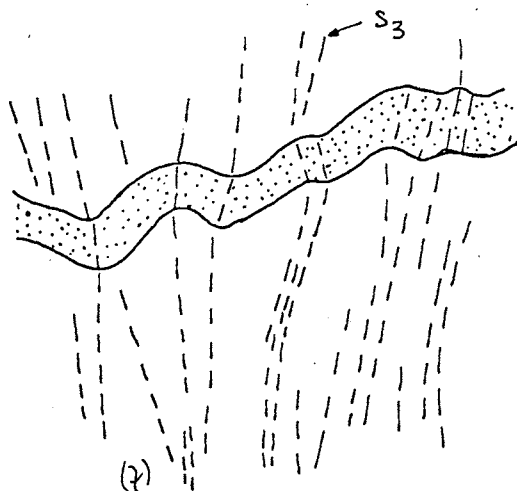
(f)

FIGURE 3.11   (PLATE 1)

B$_4$ folds where lithological layering cuts schistosity. The contact between quartz-mica schist (top portion of plate) and more micaceous andalusite schists (lower portion) passes diagonally across the plate just above the match box. A fold in S$_1$ in the quartz-mica schist (which can be seen closing near the match box) has an axis oblique to the contact between the schists (15°). The vertical foliation in the andalusite schist is S$_4$ and not S$_1$ and the structure is discontinuous. Kink axes in the andalusite schist parallel B$\frac{S_4}{S_1}$ in the quartz-mica schist. The contact is unaffected by the mesoscopic B$\frac{S_4}{S_1}$ fold. The complete discontinuity of structure across a lithological boundary is typical (Mt. Franks, loc. 3640087200).

Figure 3.12

(a). Kink bands appearing on the limb of an S_4 kink (stipled layers are quartz rich; muscovite layers shown by dashes parallel to S_1; A is an andalusite grain; detail drawn from photograph). Conjugate pairs of kink bands are developed at an angle to S_4 in the left limb of the main (S_4) kink band (X 20).

(b). Nests of kink bands around andalusite porphyroblasts (drawn from a photograph of a polished slab; andalusite schist from Mt. Franks).

(c). $B^{S_4}_{S_2}$ fold. Nearly isoclinal B_2 folds outlined by pegmatitic layers (stipled) versus micaceous schist (dashed) are folded about an open fold with S as axial surface. Single grains of muscovite are bent around the hinge of the B^{S_2} folds. Note the discordance of the pegmatite on the far left of the specimen.

(Drawn from polished slab, actual size.)

(a)

(b)

S_4

S_1

(c)

S_4

S_1

S

37.
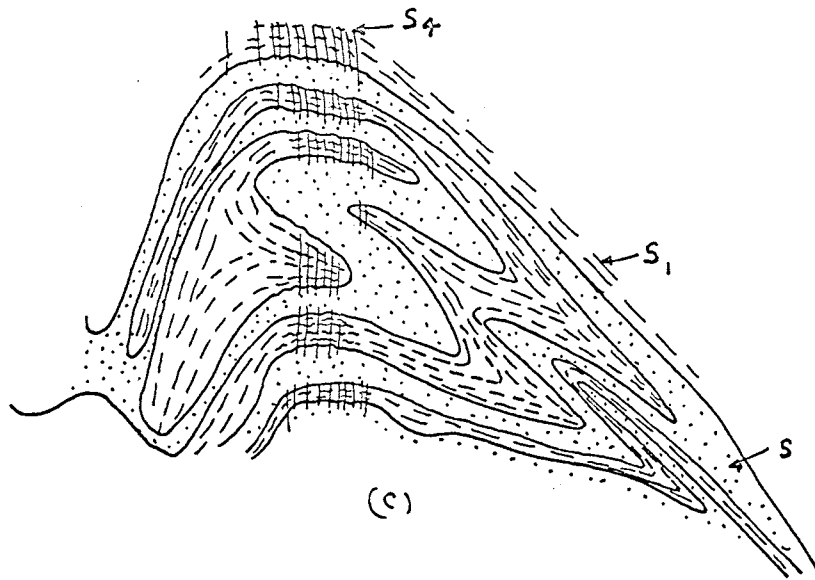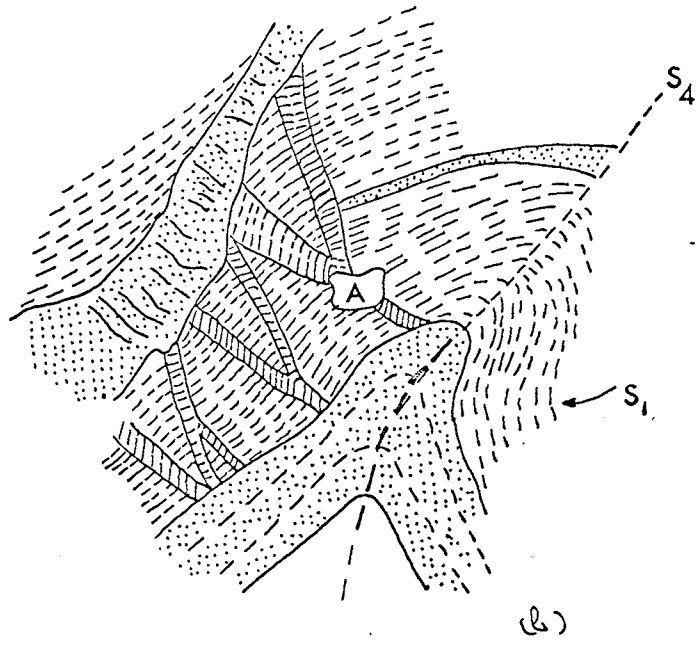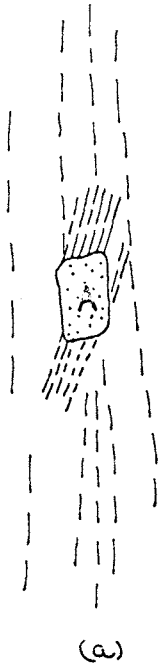
located on the surface of a cone whose axis is concentric with the kink
or fold axis (Fig. 3.13). Rotation of an old lineation by folding in this
manner is consistent with flexural slip folding by slip on S and S_1 (Ramsay,
1960) with no significant change in the area of the slip surface. The
redistribution of the lineation is equivalent to simple external rotation of
the lineation about the fold axis.

3.25   Preferred orientation of quartz in a B_4 fold.

Fig. 3.14 presents the results of the determination of the preferred
orientation of (0001) in quartz in each limb of a B_4 fold collected at a
locality north of the Silver King Mine (Spec. No. 28390, Locality No.22400127900).
The angle between the two limbs, which are sensibly planar is 77°. The grains
were measured only in a quartzose layer from sections normal to B_4 and parallel
to S_4 in each limb. L_2 is not obvious in the hand specimen, but in this general
area L_2 and L_4 are separated by only a few degrees.

Rotation of the plot for limb 2 (Fig. 3.14c) through an angle of 77° would
bring the main features of this diagram to coincidence with those of the plot
for limb 1. The rotation, as with the lineation L_2, is equivalent to external
rotation about the fold axis. The implicit assumption that S_1 and L_2 were planar
and linear respectively before folding is reasonable (Turner and Weiss, 1963,
p.516). Both elements are homogeneous (in orientation) around the margin of
the domain in which the kink folds are developed.

(a)

kink axis

(b) S₄
    B
    S₁
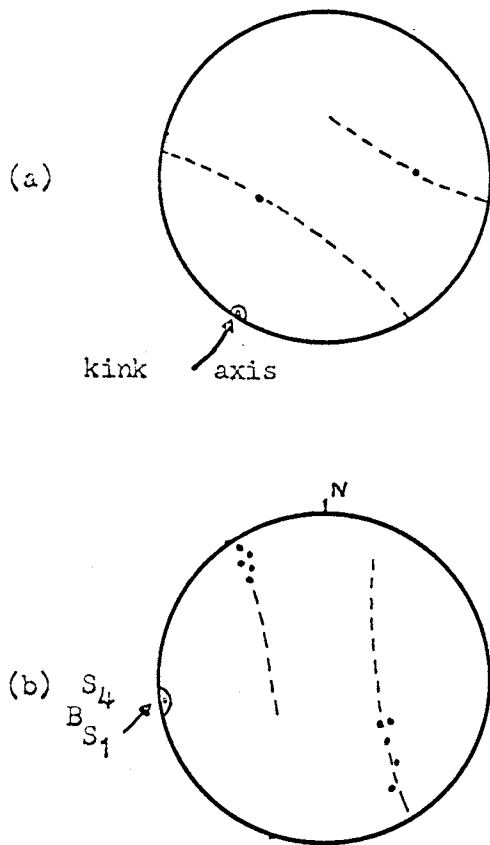
FIGURE 3.13

The distribution of the lineation L₂ across:

(a). A single kink band, in a specimen collected 300 yards north-east of the Black Prince Shafts. Data measured in the laboratory with the kink axis horizontal. The lineations are located on a 60° radius small circle (on the nett) concentric with the kink axis.

(b). In an open $B_S{}^{S_4}{}_{S_1}$ fold just to the south of the Silver King Mine. The data have been rotated to bring the fold axis to the horizontal. The lineations are distributed on a 65° radius small circle (on the nett) concentric with the fold axis.

FIGURE 3.14

Preferred orientation of c-axes of quartz (b, c) in each limb of a combined $B^{S_4}_{S}$ and $B^{S_4}_{S_1}$ fold (a) from locality 22400128000. The fold is outlined by a thin quartz layer concordant with S_1 from which most of the grains measured come. Data were measured for each diagram from two sections, one normal to the fold axis and one parallel to S_4. The data are projected on a section normal to the fold axis. L_2 is nearly parallel to $B^{S_4}_{S_1}$. The two diagrams are shown in their correct orientation with respect to each other. Note that both diagrams retain the essential form for the c-axes of quartz in B_1 folds, although there is some departure from orthorhombic symmetry. The diagrams also differ in detail, but rotation of 77° about $B^{S_4}_{S_1}$ bring the diagrams to approximate coincidence.
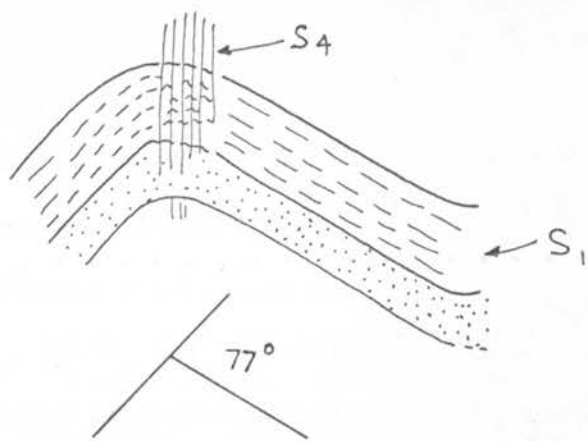
(a)

500 grains (Cont. 3, 2, 1, ½%
per 1% area)

(b)
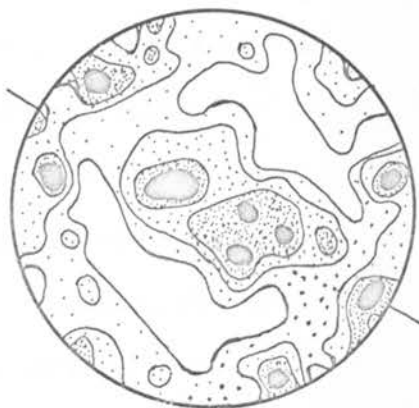
500 grains (Cont. 3, 2, 1, ½%
per 1% area)

(c)

3.26 Distinction of S_3 and S_4

The further discussion of B_3 and B_4 folds requires some data that really belongs with the macroscopic analyses. However, rather than spread the discussions in a disconnected fashion over two chapters, this data will be presented here. S_3, and S_4 are the last two imposed surfaces in the area, and since the discussion is largely confined to these surfaces alone (and not the orientation of say L_4 and B_4), no real knowledge of the macroscopic geometry of the area is necessary at this stage. The possibility that S_3 has been disturbed by B_4 folds will be considered during the course of the discussion.

The distinction of S_3 and S_4 rests on the interpretation of a small area (200-300 square yards) of effectively continuous outcrop at locality 46200125000. The rocks are well foliated quartz-muscovite-(biotite) schists which are only poorly layered (S). L_1, L_2 and B_1 folds are absent. The schists are enclosed (in plan) on three sides by massive pegmatite and thin sheets of pegmatite have penetrated the schists near their margin.

The geometry of the area is summarised in Fig.3.15 . The plotted poles to the kink surfaces form two non-overlapping girdles (Fig. 3.15, a, b). Kink bands belonging to the NE-SW girdle have axes that plunge shallowly to the NW or SE (Fig.3.15c). These kink bands are concentrated in the hinge region of a group of mesoscopic folds ($B_{S_1}^{S_3}$), which have a fairly constant amplitude of 2-3 feet and a wavelength of 12-15 feet over much of the area. L_3 is visibly parallel to the axes of these folds.

S_4 is not usually accompanied by distinct mesoscopic folds, and appears as kink bands of more uniform density crossing the B_3 folds at angles close to 90°. The poles to S_4 form the maxima in the NW-SE quadrants of Fig.3.15f. L_4 are distributed in a great circle (Fig. 3.15d), the two maxima in the girdle correspond to lineations lying in the two limbs of the B_3 folds. The great
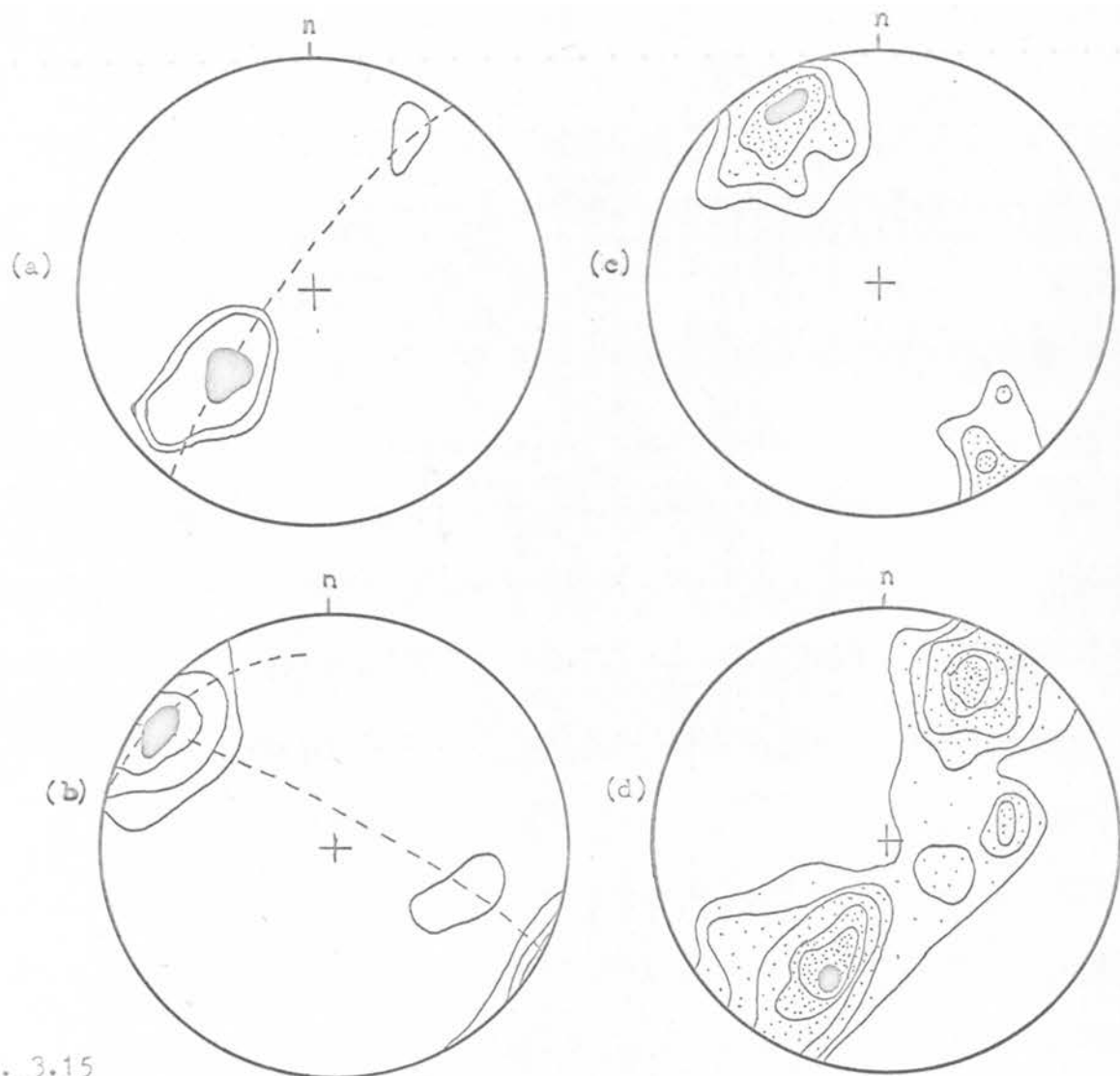
FIG. 3.15

The geometry of the area at which B_3 and B_4 folds are defined (see text)

(a). 49 poles to kink bands which are defined as S_3 (Contours: 33, 5, 1, % per 1% area).

(b). 89 poles to kink bands which are defined as S_4 (Contours: 19, 10, 4, 1, % per 1% area).

(c). 96 kink axes (L_3) of S_3 kink bands (Contours: 12, 6, 3, 1, % per 1% area).

(d). 214 kink axes (L_4) of S_4 kink bands (Contours: 15, 12, 6, 3, $1\frac{1}{2}$, $\frac{1}{2}$, % per 1% area).

(Note that the shape of the maximum in diagram (b) is considerably distorted by the properties of the equal-area projection near the primitive circle. The spread on the nearly vertical and horizontal great circles is $65°$ and $50°$ respectively).

circles containing S_3 and S_4 poles intersect at $82°$; all angles of inter-section between $60°$ and $90°$, indicating intersection of kink surfaces from different parts of the girdle, can be observed in the field. A second great circle, with a nearly vertical axis, is evident in the spread of S_4 (Fig. 3.15b).

The interaction of S_3 and S_4 follows a number of different patterns. One situation of frequent occurrence, in which the interference of the two sets of kink surfaces is minimal, is illustrated in Fig. 3.16, Plate 1. L_4 appears on the nearly planar limb of a B_3 fold and where L_3, is prominent (left-hand edge of the plate) the L_4 lineations are absent. A slightly different form of the same general type is shown in Fig. 3.16, Plate 2. Where L_3 and L_4 are equally developed in the hinge of a B_3 fold, the interference patterns of the type illustrated in Fig. 3.17 are prominent. Very rarely S_3 and S_4 are both concentrated in the hinge of equally sized mesoscopic folds, to produce a "basin and dome" structure.

Fig. 3.18 depicts some of the features of the interference of S_3 and S_4 where they are of equal development. It is noticeable that L_3 (see text beneath figure) is disturbed in such a way as to correspond with L_4 antiforms and synforms in the limbs of the L_3 kinks. If we follow a single S_4 kink surface across a L_3 kink we notice that an antiform on the horizontal limb of L_3 corresponds with a synform on the steeper limb (see for example arrowed S_4 in Fig. 3.18) and vica-versa (this is most obvious across the L_3 synform on the left of Figure 3.18). Often an S_4 surface terminates at an L_3 hinge and only a minor indentation in the other limbs near the hinge (corresponding to the fold in the hinge line) is apparent. The pattern is consistent with the super-position of S_4 and S_3 tectonites. If S_4 had pre-dated S_3, the antiforms on one limb would continue, along the one S_4 surface, as an antiform on the
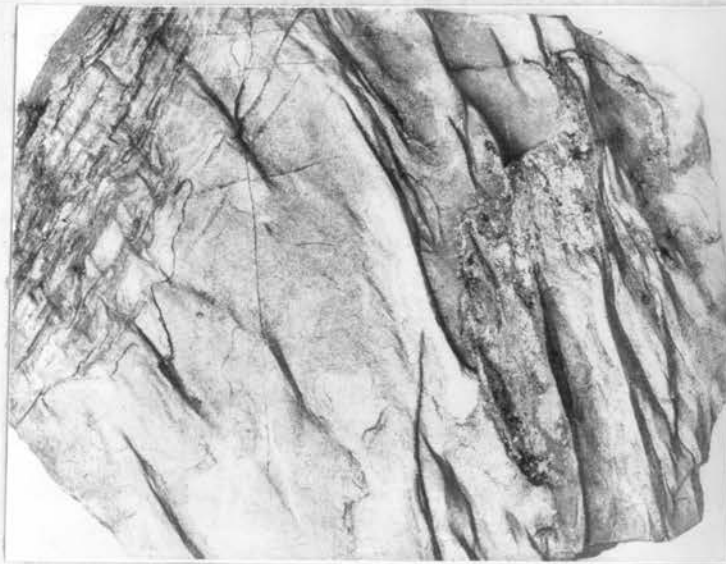
(1)
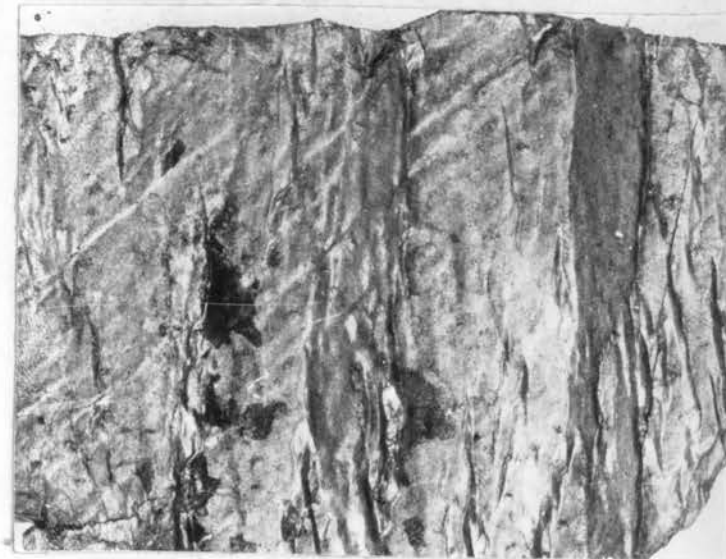
(2)

FIGURE 3.16

PLATE 1:   L$_4$ lineations on the limb of a mesoscopic B$_{S_1}^{S_3}$ fold. L$_3$ lineations concentrated in the hinge of the B$_{S_1}^{S_3}$ fold, pass diagonally across the top left hand corner of the plate. L$_4$ is only significantly developed in the limb of the B$_{S_1}^{S_3}$ fold. Note the very variable trend of L$_4$.

PLATE 2:   Very weakly developed L$_4$ kinks (diagonal) crossing L$_3$ lineations (vertical). Note that the L$_4$ lineations are obviously disposed in a plane across the L$_3$ folds.

(1).
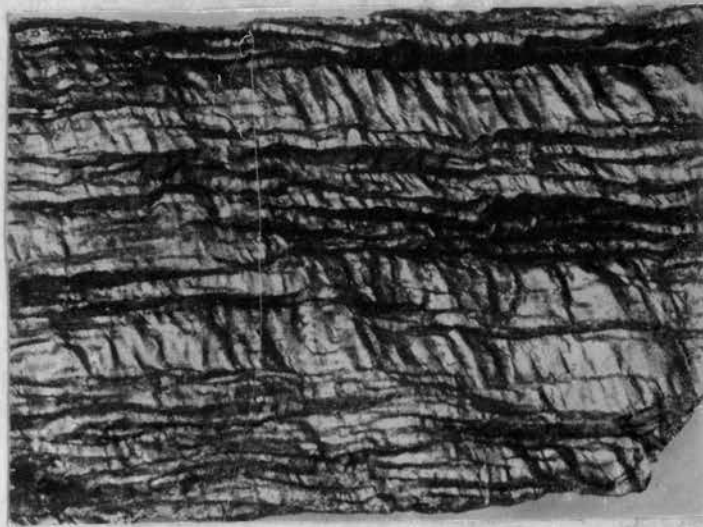
(2)

FIGURE 3.17

PLATE 1 and PLATE 2: S_3 and S_4 equally developed.

In both plates L_3 lineations are horizontal and L_4 lineations cross L_3 at a high angle. Note how L_3 is crenulated in parts of the tectonite illustrated in Plate 2.
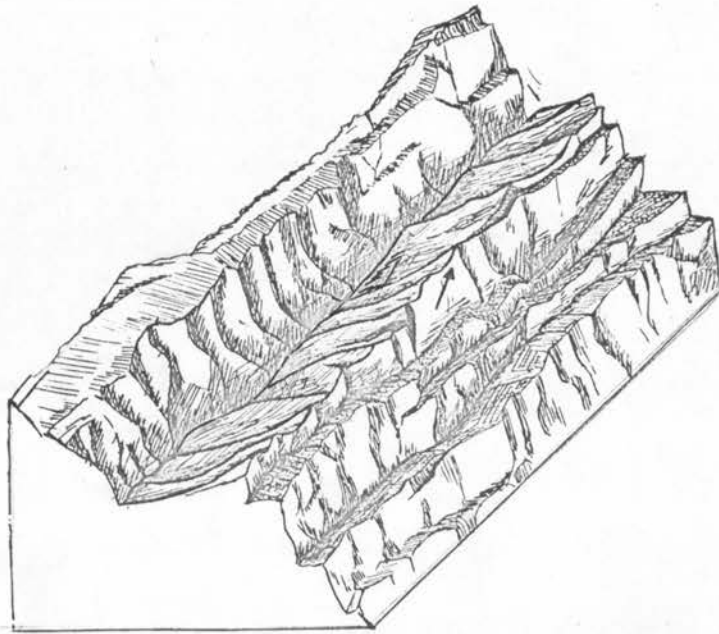
Figure 3.18

Oblique view of the same tectonite as illustrated in Fig. 3.17, Plate 2. L_3 passes diagonally from bottom left to top right across the figure; S_4 is parallel to the front face of the block. The arrow in centre of block points to the change of an antiform to synform across a L_3 hinge on a single S_4 surface (see text for description, sketch at natural scale).

other limb. The contrary nature of the structure in each limb, and the

folding of the L_3 hinge, prove that S_4 has post-dated S_3. Wherever these

criteria (in combination) can be applied in the area, then the same chrono-

logical order is found. It is also true that where L_4 can be measured crossing

L_3 folds (as in Fig. 3.16, Plate 2) it is distributed in a plane (as expected

of a superposed lineation; Ramsay, 1960, Weiss, 1959a)and not in the "small

circle" pattern of L_2 on B_4 or L_4 kinks (Sect. 3.24). On a grosser scale,

this is evident in the total distribution of L_4 axes at the type area (Fig.3.15d).

Interference of kink bands of different orientation does not occur outside

the small area just described (referred to simply as the 'type area' in the

following text). It follows that, since there is no significant variation of

style with orientation of either kink bands or associated mesoscopic folds,

the distinction of S_3 and S_4 and hence B_3 and B_4 depends on orientation alone.

The concentration of the kink bands in discrete domains is a general

feature of the macroscopic fabric. A domain may be no more than several

hundred square yards, or may be as large as 20,000 - 30,000 square yards (Mt.

Franks). The orientation of the poles to kink bands in 55 such domains is summ-

arised in Fig. 3.19. The main feature of the diagram, a girdle about an axis

plunging at $30°$ towards (030), has no counterpart in the plots of the poles to

kink bands in the type area. The source of the girdle in the total diagram

is revealed by inspection of the plots from individual domains. The latter

exhibit several different patterns:

(1). The poles to the kink surfaces fall within the limits of the S_3 or S_4

maxima as defined at the type area (Fig. 3.15). The poles form either a

maximum,an ill-defined scatter or a definite girdle (great-circle) within these

<u>Figure 3.19</u>

Poles to 486 kink bands measured throughout the mapped area (Maximum, 16%, contours 10, 8, 6, 4, 2, 1, $\frac{1}{2}$% per 1% area). Great circle represented by the dashed line has an axis plunging at 50° towards 030°.

limits. The girdles may be about a sub-horizontal or a sub-vertical axis (Fig. 3.20).

(2). The poles are located on a great circle that nearly bridges the S_3 and S_4 maxima in the plot for the type area (Fig. 3.21). Scattered points, not resolvable into a great circle, also appear in the region between the maxima. Where a girdle is formed, the points cluster in the main S_4 maximum, and thin out towards the S_3 maximum.

Of the 55 domains measured, 33 can be identified with S_4, 8 with S_3 and 14 fall into the second category above.

The axes of the great circles containing the poles to the kink bands are plotted in Fig. 3.21a; the labelling is in accord with the key diagram underneath (Fig. 3.21b). For example, an axis designated B is the axis of a great circle containing poles which fall within the limits of the S_4 maximum at the type area, and corresponds with the spread of the S_4 poles in a great circle with a sub-horizontal axis at the type area. The interesting fact that emerges is the apparent continuity between C and D (the two groups have been divided arbitrarily on the diagrams at the horizontal). The results indicate, that by continuous variation, great circles corresponding to the spread of S_4-poles at the type area pass into great circles that contain (at least potentially) both S_3- and S_4-poles as defined at the type area. If we consider that in some domains - because of chances of exposure or limitations of sampling - only poles measured in that part of a great circle passing through S_3 and S_4 in the limits of S_3 (at the type area) are measured, then an unambiguous classification outside of the type area is not possible. Also, are great circles bridging the S_3 and S_4 maxima at the type area and poles located between the maxima to be classified as S_3 or S_4?
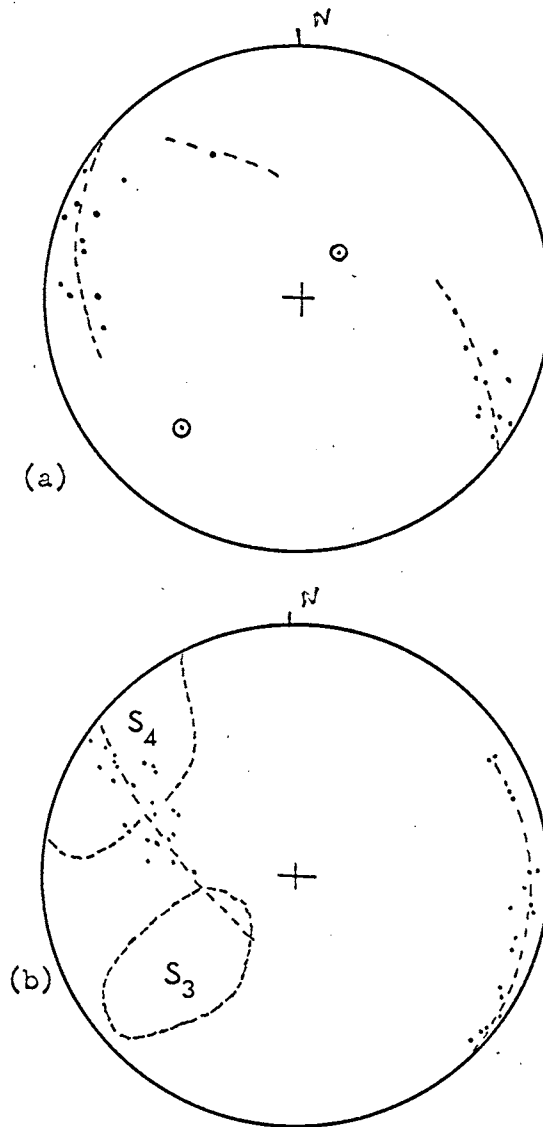
Figure 3.20

Orientation of kink bands in two domains:

(a). Poles to 22 kink bands in a domain 300-400 square yards in area, (Loc. No. 36700138300). A peripheral and a vertical girdle are developed simultaneously. The peripheral girdle has an unusual orientation, but nevertheless lies within the limits of S_4 at the type area. The vertical girdle is similar to the spread of S_4 at the type area.

(b). Poles to 42 kink bands in the area between the Black Prince and Consolation Shafts. Note the girdle tending to bridge the S_4 and S_3 maxima (limits shown by dotted line) at the type area. A peripheral girdle is also prominent.
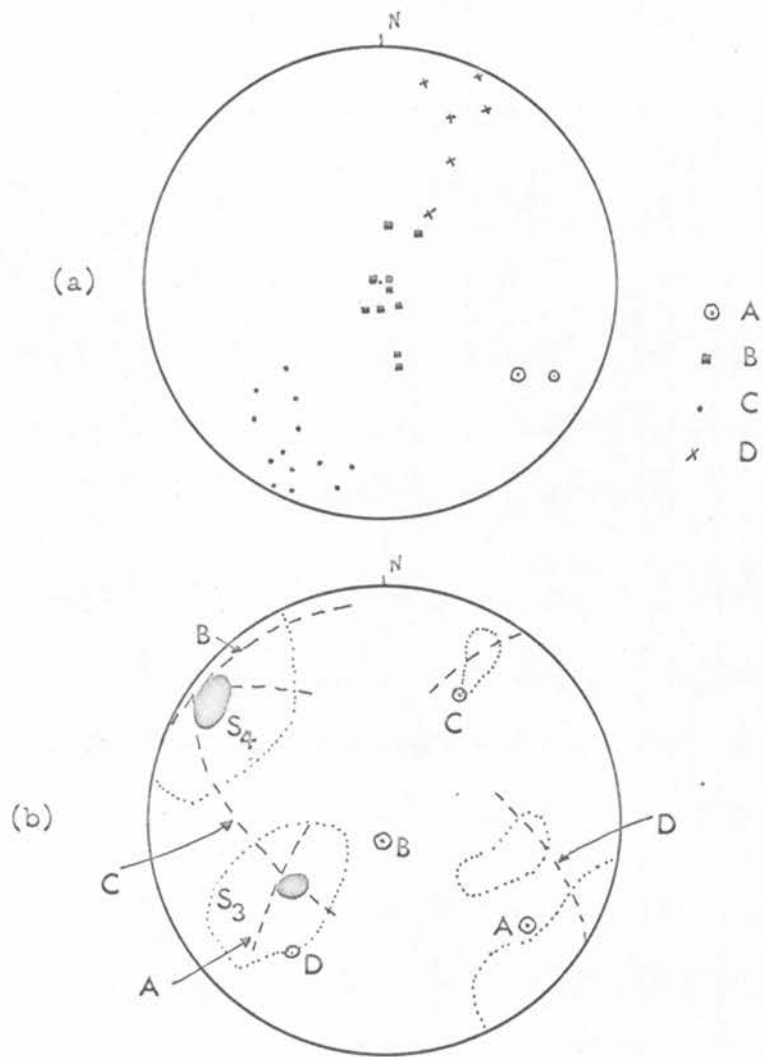
Figure 3.24

Axes of great circles containing poles to kink bands in 31 domains.

(a). Axes of great circles

(b). Key diagram, showing how axes are classified as A, B, C, and D, with

respect to the limits (marked by dotted lines) of S_3 and S_4 at the type area.

There are two courses that can be followed. The first is to classify the
domains as best as possible, acknowledging that the number of instances in
which ambiguity is present, or error may occur, are relatively few. The
second course is to question the nature of the type area in light of what is
known of the distribution of kink bands throughout the whole of the mapped area.

Are the relationships observed at the type area anomalous? Conceivably, at
the type area, a set of kink bands and associated mesoscopic folds (correspond-
ing to S_3 and B_3) may have brought the initial fabric (S_1) to an orientation
at which it became susceptible to deformation by a second set of kink bands,
still in the same stress field (this is analogous in some respects to the
deformation of a single crystal by slip on one glide system which bring the
lattice to an orientation suitable for slip on a second system; Turner and
Weiss, 1963, p.353). In this view, a system of kink bands and mesoscopic folds
of an extreme orientation (B_3 and S_3) were imposed and then later deformed - in
the same applied stress field - by kink bands of another orientation (S_4).
This view is clearly different to the first case, where any overlap is incidental.
Here, the geometry has resulted from a single continuous process and kink bands
of different orientations may have formed simultaneously in different domains.
The factors most likely to have influenced the orientation of the kink bands
are the geometry and mechanical properties of S_1 in each domain before deformation
(see next section). Any peculiarity in the initial fabric of the type area may
then be reflected in its geometry.

Several facts seem to oppose the alternative just advanced. The spread of
S_3 poles at the type area is along a great circle nearly at right angles to
great circles joining the S_3 and S_4 maxima. In order to generate this pattern
it is necessary to have a large number of S_4 girdles, with poles occurring only
in a restricted portion of the girdles. This is contrary to the experience

other domains, where poles are confined to a single narrow girdle. Also this takes no account of the subsidiary maximum in the S_3 girdle, and the fact that similar girdles occur in three other domains. Consequently the division of kink bands into two distinct groups will be adopted. Domains in which there is any ambiguity are specifically noted in the macroscopic analysis of the area; however, it is probably fairly safe to include the girdles joining S_3 and S_4 maxima (at the type area) as S_4 since, wherever any number of measurements have been made, the majority fall within the limits of S_4 at the type area.

It is worth noting that folding of S_3 by $B_c^{S_4}{}_{S_3}$ cannot have contributed significantly to the distribution of S_3 at the type area. The great circle about the intersection of the mean S_3 and S_4 surfaces along which poles of S_3 would be distributed by such folding passes through the main S_3 maximum at nearly right angles to the girdle actually observed (Fig. 3.22). Folding may, however, have caused the slight spread of the maximum in this direction (about 35°, compared with 75° along the main girdle). The shallow reversals of plunge of L_3 (and B_3) probably result from the effects of B_4 folding.

Finally, one point should be clarified at this stage; namely the use of two different reference systems for the description of the variation in orientation of the kink bands. The mean kink axis was chosen as a reference axis in hand specimen, whereas the geometry of the macroscopic domains has been referred to geographic axes. Normally these two reference axes are coincident; fanning about a sub-horizontal axis is the same as fanning about the mean kink axis in hand specimen. The orientation of the kink axes varies considerably from domain to domain but at any one domain tend to form a point maximum in projection. Where the kink axes are steep the correspondence above is reversed.

Path of S_3 poles
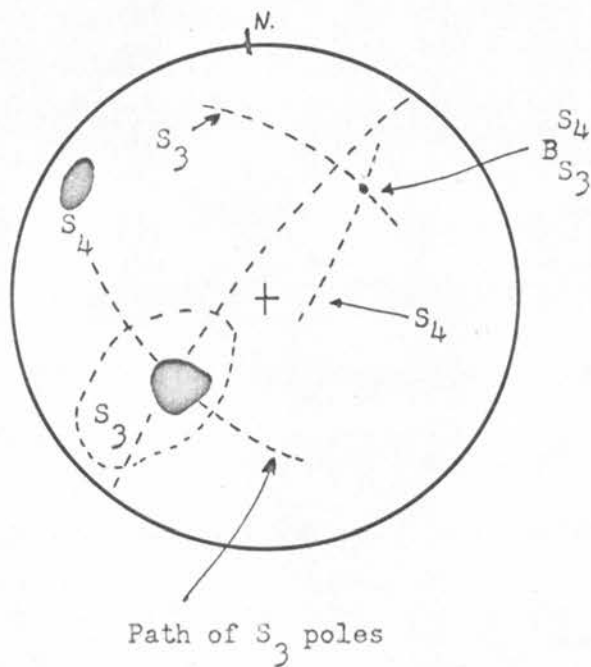
FIGURE 3.22

Folding of S_3 by $B_{S_3}^{S_4}$ folds. The path on a stereographic projection along which poles to S_3 should be spread by folds with S_4 as axial surface is shown. The path is a great circle whose axis is $B_{S_3}^{S_4}$ (calculated from the intersection of average S_3 and S_4 planes) passing through the S_3 maximum. The path is at nearly 90° to the great circle along which S_3 poles actually spread.

The sub-horizontal and sub-vertical axes tilt in a sympathetic manner with the average kink axis.

3.27   The formation of the kink bands

The style of the kink bands in B_4 and B_5 tectonites is very similar to kink bands in experimentally deformed single crystals of metals and minerals (Orowan, 1942; Barrett, 1952, p.375; Turner, Griggs and Heard, 1954; and in biotite crystals, Griggs, Turner, and Heard, 1960) and, more importantly, to kink bands in well foliated phyllites and mica schists deformed experimentally by Paterson and Weiss (1962). The last experiments reinforced the kinematic model suggested by the analogy of kink bands and kink folds in tectonites with kink bands in single crystals by demonstrating that slip is possible on an existing micaceous foliation, and that kink bands can arise as the result of this type of deformation. Kink bands in crystals develop at an angle to slip planes in the lattice and result in the external rotation of material in the kink band about an axis which is parallel to the intersection of the slip plane and the kink boundary. Unless there is slip in the kink boundary itself, the slip direction in the slip plane must be normal to the axis of external rotation.

The micaceous schistosity of many of the metamorphic rocks is an obvious potential slip-surface, and it is significant that kink bands are only found in rocks possessing such a foliation.

The kinematic model proposed is consistent with the redistribution of the lineation (L_2) and the preferred orientation of quartz in the kink bands and mesoscopic B_3 and B_4 folds (Sect. 3.25). One implication of the model is that the kink boundary can only approach an ideal surface if slip can take place on infinitesimally spaced surfaces. As slip becomes less penetrative, the kinks must degenerate into continuous flexures (unless faulting occurs). The differences of style in kink bands in well foliated (S_1) schists and less micaceous rocks are obviously in accord with this prediction. Also the less angular form of mesoscopic B_3 and B_4 folds in layered schists as contrasted

with unlayered schists is no doubt dependent on this factor.

Inhomogeneities in S_1, such as andalusites or the intersection of S with S_1, results in inhomogeneous strain, as is evident from the creation of supplementary kink bands (Sect. 3.23). But the irregular array of B_3 and B_4 folds in layered schists is probably not dependent so much on inhomogeneity of slip as the influence of the varying mechanical properties of the different layers. The gross strain in any portion of a deforming body is prescribed by the constraint of the material bounding that portion (Paterson and Weiss, 1962). In a body of unlayered schist the constraint was produced by boundary layers of amphibolite, pegmatite, layered schists, etc. Because of its homogeneous mechanical properties, the portion of unlayered schist would have to respond in a consistent way to produce the gross strain. The gross strain in a body of layered schists will also have depended on the constraint exercised by adjacent amphibolite layers etc. However, at a finer scale the constraint varied from point to point as the mechanical properties of the different layers (a function mainly of composition and thickness) changed. This secondary influence can be thought of as producing perturbations in the gross strain, and may have caused the irregular nature of the folding. However, from the consistent manner in which L_2 is redistributed in B_3 and B_4 folds, the presence of the layering did not significantly modify the movement picture of the folding.

In the following arguments it is assumed, because there is no evidence of any movement in the kink boundary and the kinks are continuous over relatively large distances parallel to their axes, that the slip direction in S_1 is always strictly normal to the kink axes. The pattern of the kink bands in hand specimens and different domains consists of two separate geometrical elements;

(i) the poles to the kink bands are distributed in two great circles in projection, and (ii) the orientation of these great circles varies from domain to domain. Insofar as the former is a property of every domain and is found in rocks of different composition and compositional homogeneity, it is apparently an intrinsic property of the deformation. Certainly lithological layering may affect the local distribution of domains, as witnessed by the coincidence of domain boundaries and lithological boundaries, but the domainal structure has an existence in its own right. In contrast, the second pattern is a property of each domain independent of its size (Sect. 3.26) and hence must be dependent on much more general influences. For the moment we shall consider only the first case above.

Clearly in the first case, the measurements are reproducing the variation of the kink bands observed in hand specimen. As long as sufficient data could be obtained in each domain these trends will appear (this is true of the data gathered). Whereas the spread about the mean kink axis is discernible in most hand specimens, the variation about an axis normal to the mean kink axis is usually not. Still, the latter spread is often just as prominent in the total diagrams for a domain (especially if it is fairly large) as variation about a sub-horizontal axis. This suggests that a domainal structure, with a size larger than can be easily viewed, produces the variation about an axis normal to the mean kink axis.

The fanning of the kink bands about an axis coincident with the mean kink axis is very similar to the structure of kink bands produced experimentally by Paterson and Weiss (1962). Very prominent sets of conjugate pairs of kink bands are visible in some of their illustrated specimens (Fig. 1, 2, 3,4).

Unequal development of each set of kink bands (in different portions of specimen) in the experimental tectonites occurred where the constraint was

supplied by rubber jackets, rather than by thick brass or copper jackets capable of supplying a more uniform constraint. Applied to natural tectonites, this signifies that the constraint is never entirely uniform in detail, even in unlayered schists. Each domain, with its own orientation and number of kink bands, apparently represents a domain of homogeneous strain, and the manner in which these domains are totalled, to yield the gross strain in any portion of the deformed rock, is dependent on the nature of the constraint applied. However, the gross strain is also dependent on the mechanical properties of the deformed rock and applied stress. We can gain some information concerning the latter from a study of the deformation lamellae in B_4 tectonites.

Deformation lamellae in quartz are commonly found to be preferentially concentrated in the hinge of B_4 folds, but may be absent from the limbs. The relationship implies a genetic connection between the development of the lamellae and B_4 folding. The recent experimental work of Carter, Christie and Griggs, 1964, and Christie, Griggs and Carter, 1964, has shown that deformation lamellae sub-parallel to $\{0001\}$ in quartz originate by slip on $\{0001\}$. The optics of the experimental lamellae can be explained in terms of arrays of basal edge dislocations (Christie, et al, 1964). From a study of the orientation of the basal lamellae in a polycrystalline aggregate (initially with random orientation) it is possible to deduce something of the orientation of the stress axes causing the deformation, since the lamellae form in planes of high resolved shear stress. In the following section the natural lamellae and the experimentally formed lamellae are assumed to be identical structures and have the same significance (see Christie, et al, 1964).

3.23   Deformation lamellae in a B$_4$ fold

The deformation lamellae in the quartz grains have the characteristic

morphological and optical properties summarised by Christie and Raleigh,

1959; they are narrow, planar or slightly lenticular structures which occupy

a part or the complete area of a grain. The lamellae have a slight, but

definite, difference in extinction position to the host grain and are slightly

brighter than the host in plane-polarised light. The lamellae (in rocks from

Broken Hill) are always found in grains with marked undulose extinction.

Individual grains with lamellae of more than one orientation, although

not common, are found. These grains can be resolved into two types;

(1). Grains in which the angle between the c-axis and the pole to the

lamellae in each sub-grain has a constant value for the whole grain. The

sub-grains correspond with undulatory extinction bands in the quartz and are

sub-parallel to the c-axes of the grains.

They are of the type usually referred to as "discontinuous" undulose extinct-

ion in natural tectonites (Christie and Raleigh, 1959), and resemble deformation

bands in experimentally deformed quartz crystals (Carter et al, 1964). However,

Carter et al (1964) note several differences between the two structures, the

most significant of which is the presence or absence of deformation lamellae

adjacent to the band boundary. The association of deformation lamellae and dis-

continuous undulose extinction is apparently uncommon (Christie and Raleigh, 1959)

whereas lamellae are common in grains with deformation bands in both natural and

experimental tectonites (Christie and Raleigh, 1959, Carter et al, 1964). Carter

et at (1964) suggest that deformation bands in quartz are equivalent to kink bands

in metals and originate by slip on a plane (hence the presence of
deformation lamellae) and "bend-gliding" or kinking of the plane. On the
other hand Bailey et al (1958) suggested that discontinuous undulose
extinction develops by polygonisation of continuous undulose extinction
bands. The climb of dislocations out of the slip plane would tend to remove
deformation lamellae.

It seems therefore that the sub-grains are a type of deformation band,
although the walls separating the sub-grains are too irregular to measure,
a feature typical of discontinuous undulose extinction. The boundaries of
deformation bands are generally planar and easily measurable. However the
genetic difference (indicated by the presence or absence of deformation lamellae)
is probably more important than the morphological characteristic of the
boundary of the bands.

(2). Some grains contain more than one set of lamellae, with a different
angle between the c-axis of the grain and the pole of each set of lamellae.
The lamellae usually do not intersect but rather occur in different portions
of a grain in which the c-axis is essentially homogeneous (differences range
up to 5°; probably a combination of measurement error and slight straining
of the grain). Most of the measurements given below are from grains of this
type. Less commonly, a small zone in a grain may have a concentration of
lamellae in which the c-axis of the quartz is different to that in the surround-
ing grain. The angle between the c-axis and the pole to the lamellae is also
different to that in the host grain.

lamellae in a grain. The second set is either only poorly developed or in an
orientation (at a high-tilt on the U-stage) not easily accessible to accurate
measurement. Some results are presented in Table 1 of Fig. 3.24.

FIGURE 3.24

Measurement of the angles between two sets of lamellae in one grain. The figures in the two left hand columns of Table 1 give the angle between the pole to each set of lamellae and the c-axis of the host grain. Where this is close to an angle between the c-axis and a common form of quartz (Table 2), the form is noted in brackets after the angle. The right hand column of Table 1 gives the angle between the two poles of each set of lamellae. The angle between the poles of the forms suggested in the left hand columns is also given (to the nearest degree).

TABLE 1.

	Angles between c-axes and poles to lamellae.		Angles between the two poles of the lamellae.
1.	58°	26°	60°
2.	16°	38°	24°
3.	67° (s,s')	25° (d,I$\bar{1}$)	88° s$^\wedge$d = 87° s'$^\wedge\bar{x}$ = 85°
4.	54° (r,z)	66° (s,s')	71° r$^\wedge$s,s' = 75° z$^\wedge$s,s' = 75°
5.	23°	66° (s,s')	86°
6.	66° (s,s')	90° (a,m)	69° a$^\wedge$s,s' = 64°
7.	52° (r,z)	64° (s,s')	27° z$^\wedge$s,s' = 29° r$^\wedge$s,s' = 29°
8.	47° (ξ,ξ')	58°	30°
9.	55° (r,z)	15°	54°

COMMON FORMS IN QUARTZ AND THE ANGLE C AXIS TO POLE OF FORM.

(to the nearest degree)

	Form.	C$^\wedge$L Form.
c	- {0001}	0°
m	- {10$\bar{1}$0}	90°
a	- {11$\bar{2}$0}	90°
r	- {10$\bar{1}$1}	52°
z	- {01$\bar{1}$1}	52°
d	- {10$\bar{1}$2}	32°
π	- {01$\bar{1}$2}	32°
s,s'	- {11$\bar{2}$1}{2$\bar{1}\bar{1}$1}	66°
ξ,ξ'	- {11$\bar{2}$2}{2$\bar{1}\bar{1}$2}	48°

Table 2.

There is a good correlation in some instances of the angles between the c-axis of the grain and the poles to lamellae and the angles between the c-axes and some of the common forms of quartz (see lower table), and also of the angle between the poles of the lamellae and the angle between the forms (in brackets in second column) suggested in the first column. Hence the lamellae are often parallel to some of the lower index lattice planes in quartz.

Fig.3.25 presents the results of the measurement of the preferred orientation of deformation lamellae in a B_4 tectonite. The measurements were made in a medium-grained (4-6mm.) quartz-pegmatite vein 1 cm. thick. The vein is concordant with S_1 in the enclosing schists and is deformed into microscopic-mesoscopic folds with an axial plane and axis coincident with micro-kinks in the schist.

Initially attempts were also made to determine the preferred orientation of deformation lamellae in quartz grains in the schist. However these attempts were frustrated by observational difficulties. Undoubted deformation lamellae exist in the quartz grains, generally in the form of fine swarms confined to part of a grain. During measurement it was found that in many grains the swarms of lamellae could apparently be brought to maximum sharpness in two different tilt positions of the E-W axis of the stage. It is not possible to distinguish any difference between these two positions, although possibly some fine distinction is blurred by the use of high magnification (X320) necessary to see the lamellae. The reason for this phenomena is not understood. A second difficulty is that many grains appear to contain a multitude of parallel, fine "fractures" that are difficult to distinguish from deformation lamellae. These "fractures" may be extremely fine lamellae, but if so, their thickness is beyond the limits of resolution of the microscope. These difficulties are absent from the measurement of lamellae in the pegmatite vein.

<u>Figure 3.25</u>

Deformation lamellae in a B_4 tectonite:

(a). Histogram relating the angle between the pole to a set of lamellae and the c-axis of the host grain to frequency, for lamellae in 182 quartz grains.

(b). Poles to 182 lamellae (contours: 5,4,3,2, and 1% per 1% area) measured from three sections at right angles. In this and the following diagrams the plane of projection is normal to the fold axis in the pegmatite layer, $B_{S_1}^{S_4}$ and L_4. The diameter through the index arrow is approximately the average orientation of the trace of S_4 on this section.

(c). Poles to 62 lamellae whose angle to the c-axis of the host grain is less than $20°$ (contours: 10, 8, 4, and 2% per 1% area). Small circles with a radius of $43°$ are shown as dashed lines.

(d). C-axes of 200 quartz grains of grains without and with lamellae, measured in three perpendicular sections (contours 4,3,2,1, and $\frac{1}{2}$% per 1% area).

(b)

(c)

(a) Angle c-axis ⊥ to lamella

Frequency
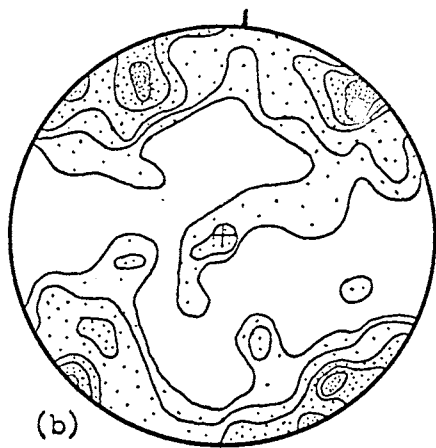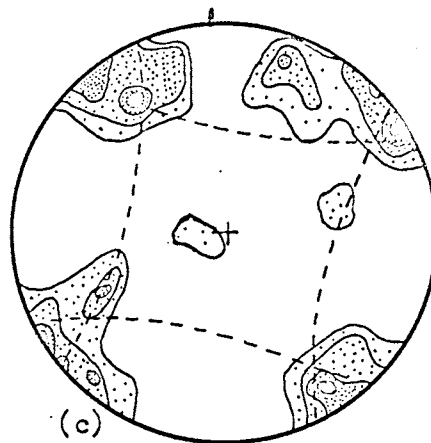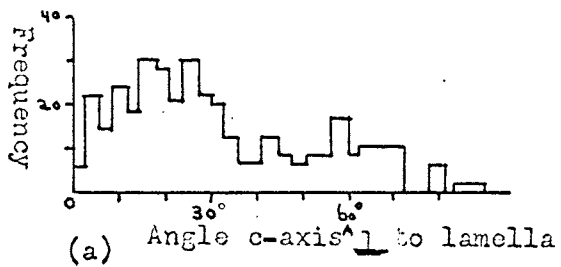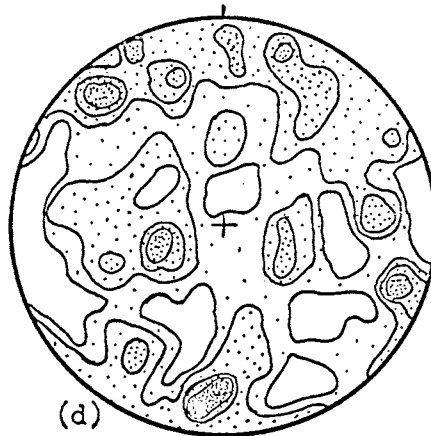
(d)

A histogram of the angle between poles to lamellae and the c-axes of the host grains for 182 quartz grains from the pegmatite is given in Fig. 3.25a. The angles are distributed through the whole range 0-70° with a few angles at 80° and 84-90°. The wide distribution of the angles compares well with the measurement of the same angles in other natural tectonites (Fairbairn, 1941; Christie and Raleigh, 1959). Carter et al (1964) have pointed out significant differences for the distribution of the angle between the poles to lamellae and the c-axes in naturally and experimentally deformed tectonites. Experimental lamellae tend very strongly to form in an orientation close to the basal pinacoid, so that angles (c-axis to poles to lamellae) form a maxima in the range 0-12°. A lesser maxima occurs at about 35° (Carter et al, 1964, Figs. 3 and 6). For two examples deformed in the cube apparatus 80% and 57% of the lamellae lie within 1-6° of the basal pinacoid, compared with 7.7% for the Broken Hill sample. A concentration of the lamellae at angles of 10-30% is much more evident in the Broken Hill example.

In one specimen deformed in their cube apparatus (Spec. C-127) Carter et al (1964) found that increase in the angle C$\wedge$pole to lamellae could be correlated with increase in strain and temperature in the central portion of the specimen. There is no indication in the shape of the grains to confirm that the lamellae have rotated out of their basal orientation by another active slip system.

The orientation of the poles to lamellae is shown in Figs. 3.25a, b. Fig. 3.25b is for lamellae whose poles are at an angle of less than 20° to C in the quartz. The distribution of poles is essentially a double maxima, with possibly a weak tendency for poles to lie on two small circles with radius of 43°.

An additional 48 measurements of lamellae in a thin section specially oriented

so that basal lamellae whose poles (in projection) would plot on one of these

small circles (the E-W axis small circle) away from the maximum should be

prominent, revealed no further basal lamellae. The plot has some affinities

with those published by Riley (1947); Christie and Raleigh (1959, Fig. 4);

Hansen and Borg (1962, Fig. 5) and perhaps Fairbairn (1941, Fig. 1). The

experimental work of Carter, Christie and Griggs (1964) has shown that for

rocks subjected to a general state of stress (maximum stress $\sigma_1 > \sigma_2 >$ minimum

stress σ_3) the strongest concentration of poles to lamellae may be expected

to form, in projection, two maxima in the $\sigma_1 - \sigma_3$ plane at 45° to σ_1 .

σ_1 and σ_3 are not uniquely specified by the plot in Fig.

However, consideration of the axes with respect to the geometry of the kink

bands removes the ambiguity. Fig.3.26 indicates the relationship of the stress

axes deduced from Fig.3.25c , with respect to the geographical orientation of

the kink axes in S_4. One axis is normal to a plane that falls between the two

sets of conjugate kink bands in the specimen, and is at an angle of 64° to the

pole to the schistosity (outside the kink bands)at this locality. Kinking

could not have occurred on S_1 unless this axis was the maximum compressive stress;

had this axis been σ_3 , presumably kinking would have occurred about kink

axes normal to those developed. The position of the stress axes inferred from

the deformation lamellae agrees in a general way with the experiments of

Paterson and Weiss (1962). They observed that the main compressive stress was

located in the oblique angle between the two conjugate sets of kink bands.

Also the kinking of biotite flakes in specimens of the Westerly Granite deformed

by Griggs, Turner, and Heard (1960) occurred preferentially in those flakes

with their cleavage oriented at 32° to the maximum compressive stress.
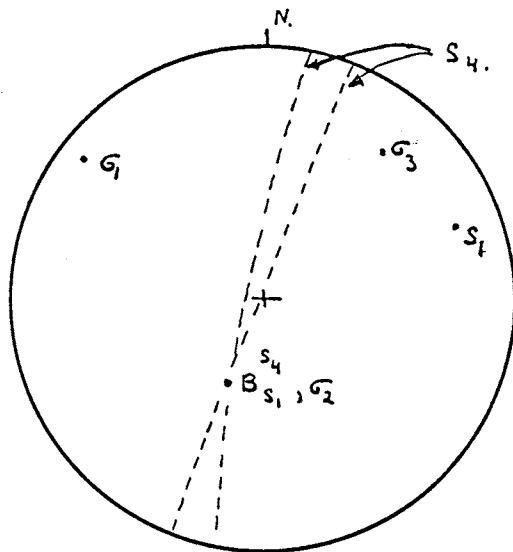
Figure 3.26

Geographic orientation of the stress axes deduced from Fig. 3.25c and the elements of the B_4 fold. The orientation of the three stress axes are:

σ_1 plunges at $10°$ towards $306°$

σ_2 plunges at $60°$ towards $203°$

σ_3 plunges at $28°$ towards $040°$

The angle between σ_1 and the pole to S_1 is $64°$ measured in the plane containing both elements.

Active elements in the kinking are S, S_1 and L_2. The last involves either the surface structure of S_1 (intersecting foliations) or causes local inhomogeneities in S_1 (quartz rods). In schists where L_2 is virtually absent (e.g. even-grained mica schists) the symmetry of the array of kink bands in B_3 or B_4 tectonites is, because of the unequal development of the congugate set, monoclinic. A monoclinic fabric may result from the imposition of a stress system with orthorhombic symmetry, on a fabric with axial symmetry (S parallel to S_1) with one plane of symmetry in common (Paterson and Weiss, 1961).

Where L_2 is present and at an angle to L_3 or L_4, which is the general case, the final fabric is triclinic and the movement picture for the deformation must also have been triclinic. Much of the irregularity of the kink bands in less perfectly foliated schists (which usually corresponds to increasing prominence of L_2) is no doubt due to the presence of L_2 as a kinematically active element in the movement picture.

The plot of the 182 poles to lamellae (Fig. 3.25b) is not very different to the plot of basal lamellae (Fig. 3.25c), although the latter contains only one third the number of poles. This suggests that the lamellae of orientation other than nearly parallel to (0001) also form in planes of high shear stress. However, the few lamellae in the centre of the stereogram are anomalous.

We might expect that extensive gliding on a second set of slip planes would cause rotation of the first set out of a rational orientation. The fact that the two sets seldom develop in the same portion of the grain, and the poor development of one of the sets, suggests that slip on one plane had only just

begun or was limited.

In conclusion, we can note that the results given in Fig. 3.24 indicate that lamellae may parallel $\{11\bar{2}0\}$, $\{10\bar{1}1\}$, $\{01\bar{1}1\}$, $\{01\bar{1}1\}$, $\{10\bar{1}2\}$, $\{01\bar{1}2\}$ and $\{11\bar{2}1\}$ or $\{2\bar{1}\bar{1}1\}$. However, it is not certain that lamellae are parallel to all these forms, since it is impossible to distinguish between two possibilities in some instances (e.g. $\{10\bar{1}1\}$ or $\{01\bar{1}1\}$ if the second set of lamellae is parallel to $\{11\bar{2}1\}$, see right hand of column of Table 1, Fig. 3.24.)

The kink bands are always symmetrical. To maintain symmetry during progressive deformation either the kink boundary must rotate (with respect to external axes) or equal slip in opposite senses must occur on each side of the kink boundary (Christie, $\underline{et.al}$, 1964). The fact that there are marked changes in the angle between the kink boundary and S_1 without significant change in the orientation of the boundary (e.g. see Fig. 3.2α) suggests the former is the case.

The fanning of the kink bands about an axis normal to the mean kink axis implies that the direction of slip in S_1 has varied systematically in direction over fairly large areas of each macroscopic domain. Since the variation is about an axis normal to the kink axes, it is also about the normal to S_1 in its orientation before deformation. This would seem to rule out any variation in S_1 relative to the principal stresses as a cause. Possible causes are curvature of the lineation L_2 in S_1 or indeed, any inhomogeneity in the structure of the actual surface of S_1.

We can now return to the second type of variation in the geometry of the kink bands. In order to explain the different orientation of the girdles (in projection) in which the poles to kink bands spread, it is only necessary to account for changes in the orientation of the mean kink axis. The rest

of the geometry then follows. Since the kink axes are constrained to lie in S_1, simple changes in the initial orientation of S_1 in the various domains is implied. This certainly seems to be the case for the domain at the Black Prince Shafts (see discussion of sub-area 4, next chapter). The axes of the girdles (in projection) for both types of variation about the kink axis tend themselves to spread in a plane that is vertical and strikes 030°.

The kink axes are normal to the direction of slip on S_1 in its initial orientation. Thus the variation in S_1 must have been such as to cause differences in the direction of slip. The nature of the variation could only be found if the absolute magnitudes of the principal stresses were known, for it is the resolution of the stresses on S_1 that determine the direction of slip (assuming that slip is equally possible in all directions on S_1). There is no grounds, for instance, for assuming that the different orientation of the kink bands has resulted from superposition of S_4 on a surface (S_1) previously folded about a horizontal axis striking 120°.

Summary of mesoscopic structures

It is useful at this point to summarise the nature of the various meso-scopic structures described. The mesoscopic structures, when style is used as a criterion, can be divided into three separate groups. The groups can be distinguished by the following criteria:

(1). B_1 folds are characterised by the presence of a foliation (schistosity) parallel to their axial surfaces. The folds are isoclinal and development of mullions in more competent layers is usual. Lineations in B_1 folds lie in the axial surface at some angle to the fold axis.

(2). B_2 folds lack any penetrative surface parallel to their axial surfaces. The only lineations visible in B_2 folds lie in the folded surface and are

disposed in a plane whose normal makes a variable angle with the fold axis.

(3). B_3 and B_4 folds (as defined here) are concentric folds with an angle of 60-90° between the limbs. Microscopic kink bands are concentrated in the hinge region of the folds. There is always in the hinge region, a "crenulation" lineation parallel to the fold axis. Other lineations in the folded surface are disposed on the surface of a cone co-axial with the fold axis.

Weiss and McIntyre (1957) have given criteria for recognising different generations of mesoscopic structures. They state that:

"(i) structures of similar style and with similar patterns of preferred orientation (not necessarily with same directions of preferred orientation) are assumed to be of the same generation; (ii) structures of consistently dissimilar style and consistently dissimilar patterns of preferred orientation are ascribed to separate generations".

Clearly B_1 and B_2 folds are sufficiently different in style and pattern of preferred orientation (e.g. S_1 and L_2 with respect to $B_1^{S_1}$ and $B_2^{S_2}$) to be regarded as separate generations by the above criteria. Overprinting criteria indicate that B_2 folds formed after the completion of B_1 folding.

B_2 folds differ from B_3 and B_4 folds by the absence of kink bands and a lineation parallel to the fold axes in B_2 folds. Overprinting criteria indicate that B_4 folds formed after B_2 folds. The relationship of B_2 folds to B_3 folds is more difficult to assess. If we ignore the microscopic kink bands, then B_2 folds can be regarded as a tighter form of B_3 folds. From the arguments advanced in Sect. 3.40 , the different disposition of lineations (other than crenulations) is then only a matter of the degree of folding. Evidently, however, we cannot ignore the kink bands, for there is no way that they could be obliterated without trace during progressive deformation. The kink bands

are a persistent style difference between B_2 and B_3 and B_4 folds and must reflect some vital difference in the conditions of formation (since both folds seem to depend on slip on a surface that is folded during the deformation).

The grouping of folds with the same kind of style into separate generations is, in the first instance, a matter of geometrical convenience. Each generation has a reproducible kink of geometry which facilitates the breakdown of a complex fabric into simpler geometrical units during analysis. Thus the separation of B_3 and B_4 folds, even though they have similar styles, is convenient, provided the overprinting relationships seen in only one area are valid everywhere.

The results gained earlier in this chapter suggest a valid and useful orientation-criteria can be erected and two generations of kink folds distinguished.

The chronological relationship of B_2 to B_3 folds is not known, since no example of interference of the folds has been discovered. Considering the scarcity of mesoscopic folds of both types, this is perhaps not surprising. Some reasons for believing B_3 folds are probably closely associated with B_4 folding, and post-date B_2 folds, will be advanced in Chapter 7.

It is obvious that style is much more than a "matter of geometrical convenience". B_1 folds, except where parasitic folds occur in quartzite layers, usually have a very constant style whether the folds are a few inches or many feet across. One limb is parallel to the schistosity and the other limb curves away gradually from the hinge to nearly parallel the schistosity. The constancy of the shape of the folds implies the existence of a fundamental,

if heterogeneous, unit of strain for the deformation. The size of the

unit of strain varies from point to point, but the propagation of such a

unit is very basic to the deformation. A further implication is that

variation of the mechanical properties of the rock are not, in general,

important.

CHAPTER 4

THE MACROSCOPIC STRUCTURE

4.1 Introduction

Map 1*, which embodies the results of the lithological mapping of the area,
reveals that the metamorphic rocks have a very complex macroscopic fabric.
(Most of the pegmatites and certainly all the larger bodies are intrusive
rocks not present before the first phase of metamorphism and deformation;
Chapter 5). The nature of exposure within the district allows the location of
most lithological boundaries to within less than 5 feet. Initially the
boundaries were fixed in air photos at a scale of 400 feet = 1 inch, and later
reduced to the scale of the map presented. Hence the final map is a very
accurate picture of the macroscopic fabric, and because of this and the complex-
ity of the fabric, the extrapolation of boundaries across areas of no outcrop
has not been attempted.

The macroscopic structure has been analysed by a method similar to that used
by Weiss and McIntyre (1957) in their study of the Loch Levin area. The
mapped area is divided into sub-areas in which the structure is homogeneous.
In the present study, the geometry of the schistosity rather than S has been
used to delineate the sub-areas. Because of transposition, the geometry of S
is the same as that of S_1 over large areas. The large-scale structure of the
area is mainly determined by folds that post-date the formation of S_1. Since
S_1 is more penetrative and usually more prominent than layering, it is more
sensitive to changes in the homogeneity of later structures. Obviously, where
the geometry of more than one surface is to be considered in a complex fabric,
the sub-areas for one surface may not be convenient for other surfaces.

* In pocket in back cover of thesis.

One of the most important sub-areas (1) is at Mt. Franks, where major
lithological units form an open fold. From east to west across the sub-
area five units can be mapped:

(i)   poorly schistose, fine-grained, quartz-plagioclase-muscovite rocks
with some fine laminae rich in biotite,

(ii)   fine-grained grey schists (quartz-muscovite-plagioclase-biotite with
minor andalusite); often finely layered. This unit and (1) are often deformed
by small B_1 folds,

(iii)   purple chiastolite schists, with minor andalusite schists, often well
layered,

(iv)   poorly foliated, quartz-muscovite-biotite-andalusite schists, with
numerous fine layers (< 1 foot) richer in quartz and biotite,

(v)   even-grained quartz-muscovite-andalusite schists, with thin layers
(< 3 feet) of quartz-plagioclase rocks and quartz-plagioclase-biotite schists.
The thin layers in this unit provided most of the information of transposition
described in Chapter 2.

The lithological layering in the sub-area is homogeneously folded about an
axis plunging at 40° towards 185° (Fig. 4.1a); S_1 is folded about an axis
plunging at 30° towards 230° (Fig. 4.1, 1b). Over almost all of the area
occupied by unit (5) in the sub-area, S_1 is deformed by microscopic kink bands;
the mean kink axis plunges at 35° to 225°, which is coincident with the fold in
S_1 (this is also the plunge of the mesoscopic folds with the kink bands as
axial surface; where the plunge of the mesoscopic folds is visibly parallel
to a set of kink axes, the mesoscopic axes are included with L_3 or L_4. β is
used for fold axes determined from a stereographic plot of the surface denoted
by the subscript). The kink bands plot in projection, along a great circle

(Fig. 4.1, 1b) and can be classified as S_4 by comparison with the type area.

Thus the kink bands and kink axes are S_4 and L_4 respectively. The spread of

the kink bands in a sub-horizontal plane is not very evident in the plot of

the S_4 poles, but the distribution of L_4 in such a plane (Fig. 4.1, 1g) suggests

some bias in sampling may have masked the effect. Evidently $\beta_{S_1}^{S_4}$ equals $B_{S_1}^{S_4}$.

However the fold in S is not a $B_S^{S_4}$ fold, since the orientation of β_S

coincides with only 1% of the measured L_4 lineations. Also the average S_4

surface dips at 75° towards 315° (Fig. 4.1, 1f), and this cannot possibly give

the trace of the axial surface (on the topographic surface) of the fold in S.

The trace of the axial surface is best judged from the smaller fold on the

eastern side of the mountain, for the hinge points of this fold are all

approximately the same topographic level. In contrast the hinge points on the

larger (western) fold are separated vertically by about 750 feet, and this has

the effect of displacing the northern-most hinge in the surface between units

(4) and (5) westwards (as viewed on the horizontal surface of the map). The

shape of the whole fold is considerably distorted by the topography. The trace

of the axial surface and the fold axis are located in a plane that dips at

about 80° towards 270°. Now along the eastern side of the sub-area S_1 changes

its strike from $000-020^\circ$ in the elbow of Eldee Creek to $340-360^\circ$ in the south

eastern portion of the sub-area. Thus the trace of β_S is closer to the

average orientation of S_1 than S_4, and S_1 ,in a general way, follows the trace

of the axial surface. Also the plunge of β_S is parallel to the few L_1 lineat-

ions measured in the sub-area (Fig. 4.1, 1c). The fold in S_1 is apparently

a macroscopic $B_S^{S_1}$ fold.

Possibly S_1 forms a large fold on the north-western side of the sub-area

where lithological layering is virtually absent. Otherwise, S_1 can only be

folded locally, since there is no pronounced girdle in the plot of S that

corresponds to the fold in the schistosity.

The Mt. Franks sub-area contains the clearest examples of macroscopic B_1 folds. The folds correspond in style with parasitic folds on the limbs on some of the larger B_1 macroscopic folds (e.g. Fig. 2.6a).

The five units described above can be traced continuously to the northern boundary of sub-area 2. Numerous amphibolite bodies outcrop along the western side of these units, and with S_1, trace out a macroscopic structure with a hinge just to the south of the Black Prince Shafts.

β_S and β_{S_1} plunge at 80° towards 240° (Fig. 4.1, 2a, b). Kink bands are not prominent in this sub-area, but at two localities, kink bands corresponding to S_4 are found. The axes of the kink bands at these localities have a mean plunge of 75° towards 225° (Fig. 4.1, 2g). Kink bands at several other localities cannot be identified as either S_3 or S_4. The three main concentrations in the plot of L_2 are located (approximately) on a small circle of 35° radius about β_{S_1}.

The structure in sub-area 2 abutts a similar structure in sub-area 4. However, in the latter case, β_{S_1} plunges at 60° towards 262° (Fig. 4.1, 4b). The whole area west and north of the Black Prince Shafts is deformed by kink bands. The kink bands whose normals form the sub-vertical great circle in Fig. 4.1, 4f, have shallow axes plunging to the north. These kink bands are mainly found to the north of the Black Prince Shafts. Some kink bands in this area, still with shallowly plunging axes, have normals that plot on the peripheral great circle (Fig. 4.1, 4f). Kink axes plunging steeply to the south-west are mainly found in the area to the west of the Black Prince Shafts. Geometrically, then, it is possible to sub-divide the area into two domains, but there is no spatial discontinuity in the development of the kink bands.

The vertical great circle in the projection of the normals to the kink

bands in Fig. 4.1, 4f are tentatively designated S_4 , although the girdle

nearly bridges the S_3 and S_4 maxima at the type area (see Fig. 3.20b). Kink

bands whose poles project on the peripheral great circle are difficult to

classify, although the poles of many of them fall within, or are very close

to, the 1% contour for S_4 poles at the type area (Fig. 3.15). Consequently,

they too are identified as S_4 .

None of the kink axes have a plunge near that of β_{S_1} . When this is added to

the sympathetic variation of S_4 and L_4 as S_1 changes from a northerly to a

westerly strike, it appears that S_4 and L_4 post-date β_{S_1} . The changing orient-

ation of S_1 then has affected the ultimate orientation of the kink axes as well

as the kink surfaces in a systematic manner (hence the spatial continuity of the

domain). In this case the structure in sub-area 4 pre-dates B_4 folding.

The pegmatites have obscured the actual junction, between sub-areas 2 and

4 but some discontinuity must be involved. This is most evident just to the

south of the Black Prince Shafts. The amphibolites in sub-area 4 are inter-

calated with even-grained andalusite schists with some quartz schist (and quartz-

plagioclase schist) horizons. On the eastern side of this unit are schists

similar to those of unit 4 at Mt. Franks. Scattered outcrops of purple schists

similar to unit 3 at Mt. Franks have been found to the east of the above unit.

The eastern edge of the mapped area at the Black Prince Shafts corresponds to

the edge of a sandy plain drained by Gun Creek and its tributaries. Hence, it

is impossible to completely trace out the pattern of these units. Still, the

units in sub-area 4 can be correlated with those of sub-area 2; an interpre-

tation of the relationship of the structures in sub-areas 2, 3, and 4 is given

in Fig. 4.2.

The actual location of the fault shown in Fig. 4.2 to the west of the Black
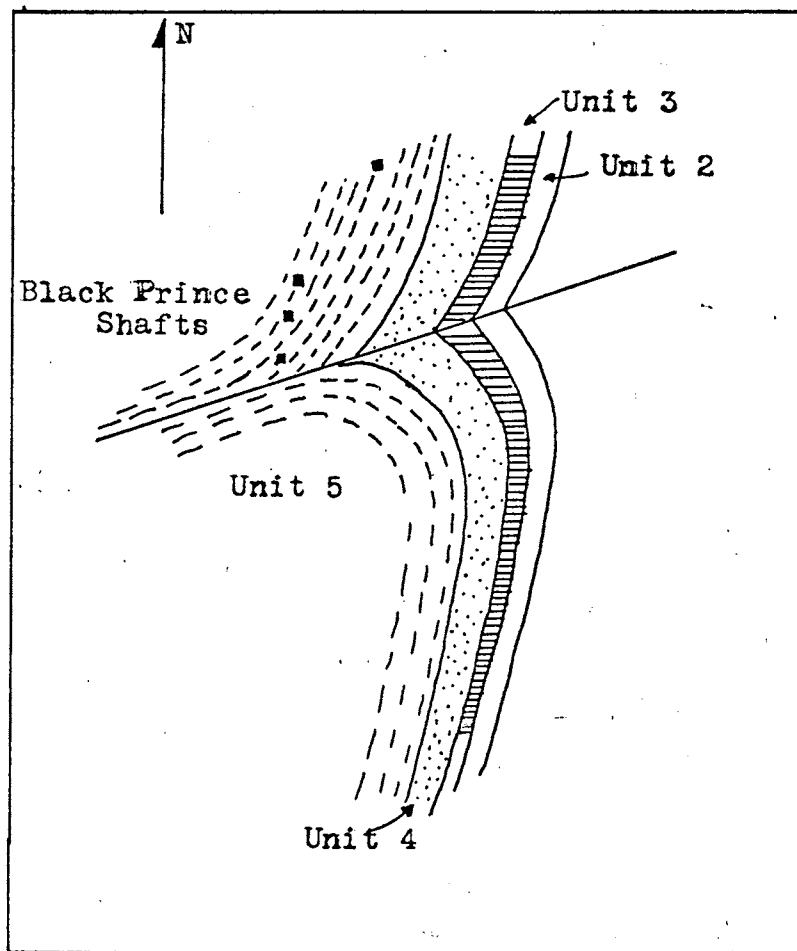
FIGURE 4.2

   Interpretation of the distribution of lithological units in the vicinity of

the Black Prince Shafts. The units referred to are those defined at Mt.

Franks. S is shown as broken lines. Amphibolites and pegmatites are
       1
omitted (Scale: 1 inch = 1 mile).

Prince Shaft can only be guessed, since the pegmatites and strong retrogression of the schists and amphibolites (virtually obliterating S_1 and L_2) have obscured the situation. From Fig. 4.2 it seems clear that the structures in sub-areas 2, 3, and 4 are parts of a single, inhomogeneous structure. The structure may have been initiated as a fold-like structure, but faulting must have occurred early in the development, so that the "folds" on either side of the fault could form about different axes. The axis of the "fold" in sub-area 2 is close to the orientation of some of the kink axes developed in the hinge, but this may be a coincidence, resulting from the imposition of S_4 on the already folded surface.

Sub-area 5 contains the Mt. Robe Synform; a fold in S and S_1 plunging at 50° towards 230° (Fig. 4.1; 5a, b). The shape of the fold is outlined by a broad band of amphibolites, composed of numerous layers of amphibolite broadly parallel to S_1. From the Consolation Shafts to the hinge of the fold, the eastern edge of the band of amphibolites coincides more or less with the edge of the sandy plain mentioned above. However, an aero-magnetic map published by the Bureau of Mineral Resources (Canberra) - which faithfully traces out the outcrops of amphibolites in the Mt. Robe District and elsewhere in the Willyama Complex (by comparison with the 24,000:1 field sheets of Zinc Corporation) - indicates that there are no further amphibolites to the east. Also, if amphibolites were present to the east, it is likely that they would form ridges similar to those formed by amphibolites along the eastern margin of the area. The band of amphibolites constitutes a mappable form surface.

The schists on the eastern limb of the Mt. Robe Synform can be correlated with units in sub-areas 1, 2, and 4. The amphibolites in the limb of the synform are intercalated with even-grained andalusite schists that closely resemble Unit

5 at Mt. Franks. The presence of numerous thin layers of quartz schist is a further point of resemblance. Thicker units of quartz-schist are also prominent in the eastern limb of the Synform, and although such units are absent from Unit 5 at Mt. Franks, their presence is not inconsistent with the general nature of the unit. Along the eastern edge of the unit above there is a layer of schists resembling Unit 4 at Mt. Franks. Further again to the east, and largely obscured by alluvium, are sporadic outcrops of purplish andalusite schists and andalusite schists correlatable with unit 3 in Sub-area 1. As in sub-areas 2 and 4, the amphibolites are found mainly in Unit 5.

In the hinge of the synform, the andalusite schist of Unit 5 is transitional across a metamorphic zone boundary to rodded sillimanite schists. The content of quartz schist in the unit decreases westwards. The other units have not been traced around the hinge of the synform. The amphibolites in the eastern limb of the Mt. Robe Synform (away from the pegmatite) form regular units with contacts strictly parallel to quartz schist versus andalusite schist boundaries. The persistence and regularity of thin quartz schist units between and in the amphibolites suggests they are sedimentary rocks. There is evidently a fault just to the north of the Silver King Mine, offsetting the amphibolites on the northern side to the east. There is a complication in the pattern of amphibolites just on the northern side of the fault in the hinge of the Mt. Robe Synform. An interpretation of the actual distribution of the units across areas occupied by pegmatite and alluvium is given in Fig. 4.3 . The pattern can be interpreted in terms of isoclinal folding if the fold dies out to the north-west. The appearance of numerous mesoscopic B_1 folds in the schists, suggesting that layers in the schist are also trending across S_1, supports this idea. But, since the amphibolites may be intrusive rocks, there is always the chance that the structure may be a modification of a cross-cutting portion of the original.

A

S

A

S

A

A

S 4'

A

A

A

A

A

S

A

A

A Amphibolite.
S Schist.

Scale I in. = 600 ft.

(?) F

A   A   A

S| S| |S| ||
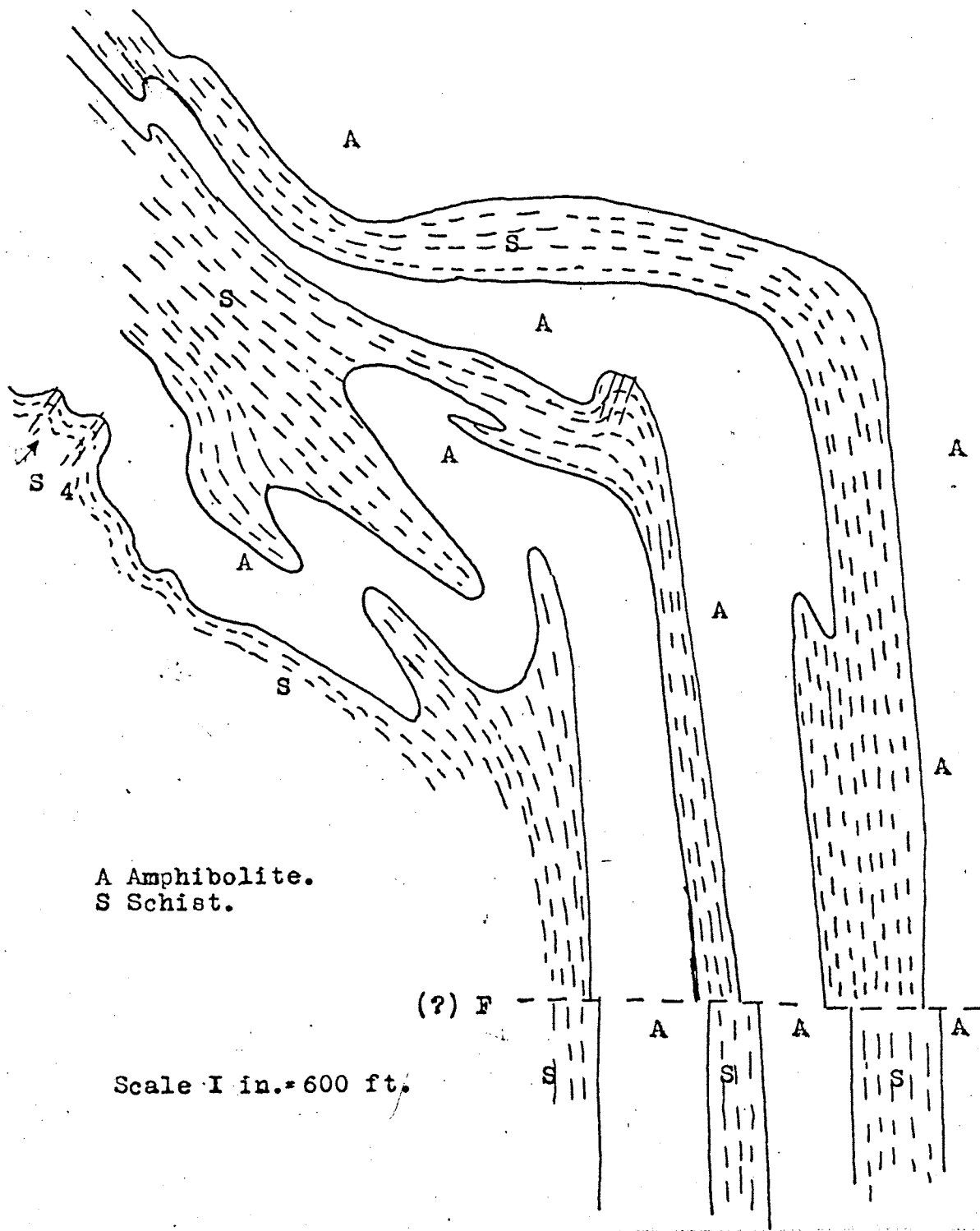
FIGURE 4.3

Interpretation of the outcrop pattern north of the Silver King Mine. The

amphibolites pattern suggests the existence of a fold with S (dashed

1

intrusion. In dealing with the amphibolites it is difficult to avoid circular arguments by using structure to determine origin and vica-versa. Those difficulties are a definite handicap in attempting to interpret the macroscopic structure. It is unfortunate that amphibolites provide the only form surfaces over a great part of the mapped area.

Kink bands are found in scattered domains along the eastern limb of the fold, but the greatest concentration of kink bands is found in the hinge region of the fold. The kink bands measured over the whole sub-area form a fairly homogeneous great circle in projection that corresponds to S_4 at the type area (each individual domain can also be identified as S). The kink axes (L_4) form a maximum (in projection) corresponding to a plunge of 45° towards 216° (Fig. 4.1, 5f). The shallowly plunging kink axes came almost exclusively from domains just inside the southern edge of the sub-area and are continuous with similar kink bands in sub-area 4.

The trace of the axial surface of the Mt. Robe Synform on the map cannot be fixed with much precision. Nevertheless it is clear that the axial surface of the fold - calculated from the trace shown and the fold axis - must be close to the mean S_4 surface. The value calculated is a plane dipping at 70° towards 280°.

The lineation L_2 has a plunge very close to β_{S_1} in the hinge of the fold and a different plunge in each limb. The more central maximum in Fig. 4.1, 5d is made up of lineations in the hinge. Concentrated measurements of L_2 in an area on the eastern limb of the Mt. Robe Synform in which S_1 is homogeneous, indicate that L_2 varies considerably (up to 25°) in pitch in S_1. As shown in Fig. 4.1, 5d, the main concentrations of L_2 fit on a small circle on the projection with a radius of 15° about β_{S_1}. Similarly B_{S_1} and L_1 are located on a small circle on the projection with a radius of 25° about β_{S_1} (this means, at least statistically,

that B_1 (L_1) and L_2 could not have been parallel over the area in which the B_1 folds occur. This covers most of the area of the hinge of the synform and part of the western limb. The actual discrepancy observed is often less than 10°).

Mesoscopic B_4 folds in amphibolite-schist contacts are abundant in the hinge region of the Mt. Robe Synform. The folds appear as indentations in the boundary of the amphibolite with S_1 (in amphibolite and schist) faithfully tracing out the folds. Kink bands are common in the indentations. The folds are occasionally transitional to faults and much of the irregularity of the outcrops of amphibolite are due to the combined action of folding and faulting. Pegmatite dykes in the amphibolite form a pronounced radial pattern in the hinge of the Synform.

The Mt. Robe Synform is a fairly open fold with two almost vertical limbs, with slight overturning on the eastern limb. Since it is not known which way is up in the sequence of units, the fold is better referred to as a synform (a fold in a form surface that closes downwards) than a syncline. The coincident of S and S_1 with L_4 and the axial surface of the macroscopic fold with S_4, the distribution of the lineation (L_2) and the concentration of kink bands and mesoscopic B_4 folds in the hinge, all indicate that the Mt. Robe Synform is a macroscopic $B^{S_4}_S$ and $B^{S_4}_{S_1}$ fold. As has been pointed out by Ramsay (1960) and Weiss (1959a) the distribution of a lineation on a small circle

about the fold axis in projection is indicative of flexural slip folding (as

a kinematic model). Before folding, L_2 must have plunged at an angle between

35° and 65°. Similarly B_1 could have plunged before folding at an angle

between 25° and 75°.

$B^{S_2}_{S_1}$ folds have been found only on the western limb of the Mt. Robe Synform.

They are particularly common at one locality(31800130900   ) on the northern

end of the limb. Here they have steep plunges and cause local reversals (in

one limb) of the plunge of L_2. In the same area L_2 sometimes changes plunge,

with only a minor variation ($< 10^\circ$) in the orientation of S_1, in strips

several hundred feet long. The effect is assumed to indicate the presence of

macroscopic $B^{S_2}_{S_1}$ folds with nearly isoclinal limbs, of which the hinges have

not been found. This is in accord with the style of the observed $B^{S_2}_{S_1}$ folds.

β S_1 in sub-area 6 is essentially a sheet dipping to the north-west (70°

towards 304°; Fig. 4.1, 6a, b). The considerable variation in strike evident

in the plot is present in much smaller domains than the sub-area.. L_2 plunges

to both the north and south; the plunge to the south prevails over most of the

sub-area, whereas the northerly plunges are very local. As in the preceeding

sub-area, the latter are believed to be due to undetected B_2 folds.

Kink bands are scattered in numerous small domains and cause only minor

folding of S_1. Except at one locality (35600138300), where the kink bands are

not obviously S_3 or S_4, they can be classified as S_4 (Fig. 4.1, 6g). Kink axes

have a wide variety of plunges to the north and south (Fig. 4.1, 6f). Many of

the kink axes plunging more steeply to the north are found at the terminations

of amphibolite bodies, especially in the extreme northern corner of the sub-area.

S in this sub-area is usually parallel to schistosity, with a few notable

exceptions. In the central portion of the sub-area (around point 38000132000

on Map 1), the amphibolites are apparently isoclinally folded with S_1 as axial

surface. In the hinge of these structures S_1 in the schists passes continuously (in orientation) into the foliation in the amphibolites, at a high angle to the amphibolite-schist contact. Consequently, S_1 in the schists and the foliation in the amphibolites have identical significance. Similarly L_2 is continuous in orientation across the amphibolite contact.

As before, there is a chance that the 'folds'above may be modified pre-metamorphic structures (e.g. bifurcating dykes or sills). However, as the number of these structures increase, all with the same basic and regular style similar to mesoscopic B_1 folds, it becomes increasingly probable that they are simply macroscopic B_{S}^{S1} folds. They will be accepted as such here (other examples will be cited below). Accurate plunges cannot be found for any of the folds in the amphibolite, but it is fairly certain that most plunge at $60-70^{\circ}$ to the south. The mapped shape is then approximately a profile.

The total structure in the above area is not very clear. If we assume that there is only one amphibolite layer, then it is necessary to introduce a complicated system of faults sub-parallel to S_1 to explain the observed fabric. Even so, the results are not very satisfactory, although faulting of this type might be predicted from a study of mesoscopic B_1 folds. It seems probable that more than one layer was present before folding.

S_1 in Sub-area 7 is folded homogeneously about an axis plunging at 40° towards 340° (Fig. 4.1, 7b). Both limbs dip towards the north-west. L_2 is distributed in a great circle on the projection, with an axis at 64° to the fold axis. The distribution of L_2, and the style of the fold, strongly suggests that the fold is a macroscopic B_{S1}^{S2} fold. No kink bands are found in the hinge region.

The folds in sub-area 8 (in S_1) plunge uniformly at 30° to 010° (Fig. 4.1, 8b). This is parallel to a set of kink axes in the sub-area (Fig. 4.1, 8f), and kink bands are poorly developed in the hinge region of the folds. The kink bands are classifiable as S_4. Apparently the macroscopic folds are B_4 folds developed mainly on the lower limb of the B_2 fold in sub-area 7. L_2 is not sufficiently developed to be measured.

There is in the south-eastern corner of sub-area 8 a single mesoscopic B_3 fold (Fig. 4.1, 8h). The poles to the kink bands plot exactly in the S_3 maximum at the type area.

Sub-area 9 is only a small area penetratively deformed by kink bands. The kink axes have a shallow plunge northwards (Fig. 4.1, 9f). The kink bands are distributed in two great circles in projection parallel and normal to the kink axes (Fig. 4.1, 9g). One of these great circles is coincident (within a few degrees) to the sub-vertical great circle of S_4 at the type area. The other passes through the S_3 and S_4 maxima, although no poles actually coincide with poles to S_3 at the type area. Since the kink bands are developed in a continuous domain, and there is no evidence of the interference of kink bands of different orientation, all the kink bands can be regarded as S_4.

The structures in sub-area 10 are mainly outlined by numerous sheets of pegmatite parallel to S_1 and fine layers of quartz-plagioclase rock. The prevailing trend of S and S_1 over the sub-area is sub-horizontal, a fact that is not very clear from the plot of the surfaces (Fig. 4.1, 10a,b, most of the steep dips are found near the eastern edge of the area). S and S_1 are folded about an axis plunging at 30° towards 210°. Folds with kink bands parallel to their axial surface abound. The kink bands can be identified as S_4 (Fig. 4.1,10g) The kink axes generally plunge shallowly to the south (Fig. 4.1, 10f).

Sub-area 11 is bounded on its southern side by a fault. β_{S_1} for this sub-area plunges at 25° towards 230° (Fig. 4.1, 11b). Kink bands, which are only developed in the hinge of the fold, are classifiable as S_4. L_4 is parallel to β_{S_1}. Several possible B_1 folds in amphibolites are present in the sub-area and, on the eastern side of the sub-area, the total array of amphibolites seems to form a layer crossing S_1 at an angle.

The fault on the southern margin of the sub-area is marked by an abrupt change of dip of S_1 and the truncation of amphibolite layers, including one folded isoclinally. There is also a discontinuity in the gross structure between sub-areas 11 and 12. S_1 in sub-area 12 is virtually a plane sheet dipping 35° towards 180° (Fig. 4.1, 2b). L_2 plunges uniformly at about 30° towards 210° (Fig. 4.1, 2d). Lithological layering in this sub-area is either parallel to S_1 or is deformed by visible $B_S^{S_1}$ folds. The fold axes and L_1 are generally at a high angle to L_2. Kink bands are not developed, but a few B_2 folds are scattered throughout the sub-area.

Sub-area 13 lies along, or close to, the trace of the axial surface of the Mt. Robe Synform. The poles of S_1 fall on a great circle in projection (Fig. 4.1, 13b) with an axis plunging at 20° towards 216° but there is little evidence in the trends of S or S_1 of a major fold. Form surfaces are only poorly developed Along the summit ridge of Mt. Robe a distinctive layer of quartz-muscovite-biotite schists overlies muscovite schists. The contact dips uniformly at a low angle southwards and the two units are underlain and overlain by rodded sillimanite schists. The last typically contain numerous fine (<1 foot) layers of quartz-plagioclase rock just to the west of the Mt. Robe Mine. Further westwards the fabric of the schists is totally linear and, as a consequence, the structure is undefined. A few scattered bodies of amphibolite provide the only other form surfaces.in the sub-area. Except in mesoscopic $B_S^{S_1}$ folds,

S is parallel to S_1 throughout the area.

Only sporadic kink bands are present. These can be identified as S_4 (Fig. 4.1, 13g). Kink axes plunge shallowly to the south (Fig. 4.1, 13f; 20° towards 190°). The maximum in the projection of L_2 represents a lineation plunging at 40° towards 237°.

The direct relationship between S and S_1 in sub-areas 5 and 13 can only be seen in the area near the huts at Mt. Robe. In this area there is an abrupt change in the orientation of S_1 across a fault.

The fault is marked at one point by a narrow zone characterised by a new phyllitic cleavage (point 39800122400 , the zone is marked on Map 1). The phyllitic foliation dips at 70° towards 200°. S_1, and the amphibolites, seems to swing slightly westwards on the western limb of the Mt. Robe Synform as the fault is approached from the north. Clearly neither the amphibolites nor S_1 in sub-area 6 can form a continuous structure with the same elements in sub-area 13. To the east and west of the huts at Mt. Robe the course of the fault is largely obscured by the pegmatites. However the dips between S_1 in sub-areas 6 and 13 appear to be discontinuous across the extrapolated trace of the fault for a considerable distance eastwards. The fault separating sub-areas 11 and 12, and 5 and 13 are continuous in orientation and position and are apparently parts of a major fault crossing the mapped area. It is proposed to call this fault the Mt. Robe Fault.

If the Mt. Robe Fault is continuous to the east, it must eventually intersect the eastern limb of the Mt. Robe Synform somewhere near Gun Creek. The fault has not been located in this area, but unfortunately there is a gap where Gun Creek crosses the band of amphibolites. There is, however, no apparent lateral displacement in the limb across the gap. The strike of the amphibolites and other units in this area is nearly normal to that of the
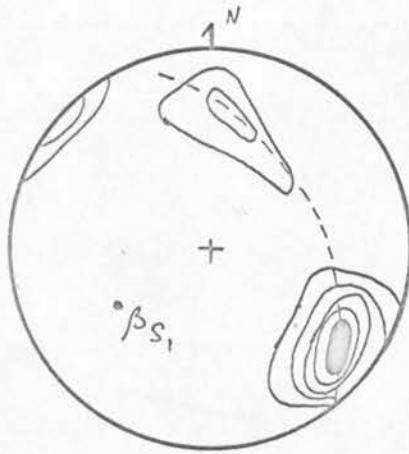
FIGURE 4.4

Poles to S$_1$ in the western limb of the Mt. Robe Synform and the sub-area 6. The poles are distributed in a great circle of the projection with an axis plunging at 40° to 230°.

(200 poles; Cont. 20, 15, 10, 5, $\frac{1}{2}$, % per 1% area).

fault and the dips are nearly vertical. Hence only a large lateral movement on the fault would produce any lateral displacement of the units.

The band of amphibolites along the north-western edge of the mapped area can be tentatively correlated with the amphibolites in the western limb of the Mt. Robe Synform. As noted before, the latter seem to swing westwards just before reaching the Mt. Robe Fault towards sub-area 11. From sub-area 11, the amphibolites can be traced, albeit discontinuously, to the north of Big Aller Creek where they again form a band similar to that in sub-area 5.

Acceptance of the correlation leads to the recognition of a second fold to the west of the Mt. Robe Synform, with a western limb dipping more or less parallel to the eastern limb of the Mt. Robe Synform. If the poles to S_1 in sub-area 6 are plotted on a stereogram with the poles to S_1 in the western limb of the Mt. Robe Synform, then a fold plunging at 40° towards 230° is obtained (Fig. 4.4). This is close to the plunge of the Mt. Robe Synform. The dip of S and S_1 in the two limbs of the proposed fold indicate an antiform.

If the above correlation is invalid, and S and S_1 are merely changing dip about the vertical on the western limb of the Mt. Robe Synform, the north-western band of amphibolites should close to the north of the mapped area around the Mt. Robe Synform. The mapping of Zinc Corporation (King and Thomson, 1953) and Leslie and White (1955) and the aero-magnetic map cited previously all indicate that this is not so. Consequently a major fold - to be called the Western Antiform-- can be postulated with some confidence.

There remains one difficulty. Over much of the area covered by the Western Antiform (sub-areas 6,7,8,9,10, and 11) there are kink bands identified as S_4 with kink axes plunging at various angles to the north. From its

association with the Mt. Robe Synform the Western Antiform should be a B_4 fold, in which case the kink axes are anomalous. Sub-area 8 is critical for it lies very close to the hinge of the antiform. However, S_1 in sub-area 8 has an orientation controlled by a macroscopic B_2 fold that closes in sub-area 7. The orientation of S_1 before B_4 folding in what is now sub-area 8 may have been different from the average and resulted in the appearance of kink bands of a different orientation. Similar arguments can be applied to all of the kink bands plunging to the north in sub-area 6. The kink bands with axes of this direction of plunge are all found around the termination of amphibolite layers where S_1 may have been disturbed before B_4 folding. In sub-area 11, which is located in the hinge of the fold, and in parts of sub-area 6, L_4 plunges nearly parallel to S_1 for the Western Antiform (the plunges are slightly shallow in sub-area 11, see below). The situation is not very different to that in the Mt. Robe Synform, where kink axes near the Consolation Shaft are sub-horizontal, although the kink surfaces have a similar orientation to those in the hinge of the fold with more steeply plunging axes. Near the Consolation Shafts, S_1 differs only slightly in orientation from S_1 further to the north in the eastern limb of the Mt. Robe Synform.

The kink axes in sub-areas 9 and 10 are less critical, for the flat dips of S and S_1 across both these sub-areas might indicate the presence of another macroscopic fold along the western edge of the mapped area. It is not possible to confirm this idea, for the area to the west is covered by the alluvium of the Mundi Mundi Basin.

The trends of S_1 in sub-area 14 indicate the presence of a macroscopic fold. There is no form surface to delineate the fold as a whole. In general the sub-area is composed of rodded sillimanite schists and often, especially along the

western side of the area, linear fabrics and poor outcrop limit the structural interpretation. β_{S_1} plunges at 55° towards 210° (Fig. 4.1, 14b). The calculated axial surface dips at 72° towards 276°. Lithological layering commonly cuts S_1 in this sub-area, but in most cases the intersection is too fine to allow meaningful calculation of L_1 (L_1 here, and elsewhere in the area, is seldom exposed as a lineation that can be measured directly. This is partially because of the character of the schists and partially due to the nature of exposure). L_2 lineations plunge southwards, and appear to plot on a small circle on the projection with a 15° radius about β_{S_1} (Fig. 4.1, 14d).

Kink bands are not very prominent anywhere in this sub-area, and are notably inconspicuous in the hinge of the macroscopic fold. Those found can be identified as S_4 (Fig. 4.1, 14). While the orientation of the axial surface of the macroscopic fold and the geometry of L_2 suggest a B_4 fold, the lack of kink bands is unusual.

Scattered bodies of amphibolite outcrop on the southern side of the Mt. Robe Fault in sub-areas 13 and 14, but there is nothing comparable to the band of amphibolites north of the fault. This would seem to set a limit on the direction of movement of the fault. The limited amount of lateral movement on the fault means that sub-areas 13, and 12 and 14, are extensions of the Mt. Robe Synform and Western Antiform respectively. The limb between the two folds on the southern side of the fault is not easily detected, because of the predominance of rodded sillimanite schists lacking proper foliation to the west of Mt. Robe.. If the fault had moved upwards on the southern side then the hinge and limbs of the Western Antiform would be repeated somewhere on the southern side of the fault. If the amphibolites near Mt. Eltie are considered as equivalent to the hinge of the Western Antiform in sub-area 11, then amphibolites should stretch back to the fault from the hinge. A sufficient portion of the area south of the fault has been mapped to eliminate this possibility.

Down movement of the fault on the southern side means that the rocks on this side of the fault are part of a sequence not seen on the northern side of the fault. The sequence on the northern side might then correlate with portions of the sequence displaced by pegmatite in the hinge of the Mt. Robe Synform and covered by alluvium on the western side of the Western Antiform.

The Mt. Robe Fault is apparently located in a region where the plunges of the two major folds to the north of the fault flatten. The dips of S_1 in sub-area 13 cannot be fitted to a fold that has a plunge of 50° and a direction of plunge of 230° (note the last two elements must be considered simultaneously, since we do not know which part of the fold the dips are in). Rather, S_1 in sub-area 13 are folded about an axis plunging at 20° to 216°.

The plunge of the Western Antiform is 15° shallower than the plunge calculated between sub-areas 5 and 6. The dips in sub-area 12 on the southern side of the fault are compatible with a shallower plunge. In sub-area 14 the plunge is again steep. Therefore, the Mt. Robe Fault can be viewed as a steep normal fault, downthrown on the southern side, probably resulting from inhomogeneous movements where the plunge of the two major folds changed.

A model of the shape of the Mt. Robe and Western folds is provided by a hand specimen from an outcrop in Little Aller Creek (Fig. 4.5). The mesoscopic fold reproduces the open hinge of the Mt. Robe Synform and the more acute hinge of the Western Antiform, even down to the concentration of kink bands in the area of the former and their relative absence in the latter. The radical pattern of quartz segregations in the larger vein of pegmatite approximates the radical pattern of pegmatites in the hinge of the Mt. Robe Synform.

In one respect the macroscopic and mesoscopic fabrics do not compare very well. There is less isoclinal folding (B_1) and less evidence of transposition in the macroscopic fabric than may have been expected from a study of the meso-
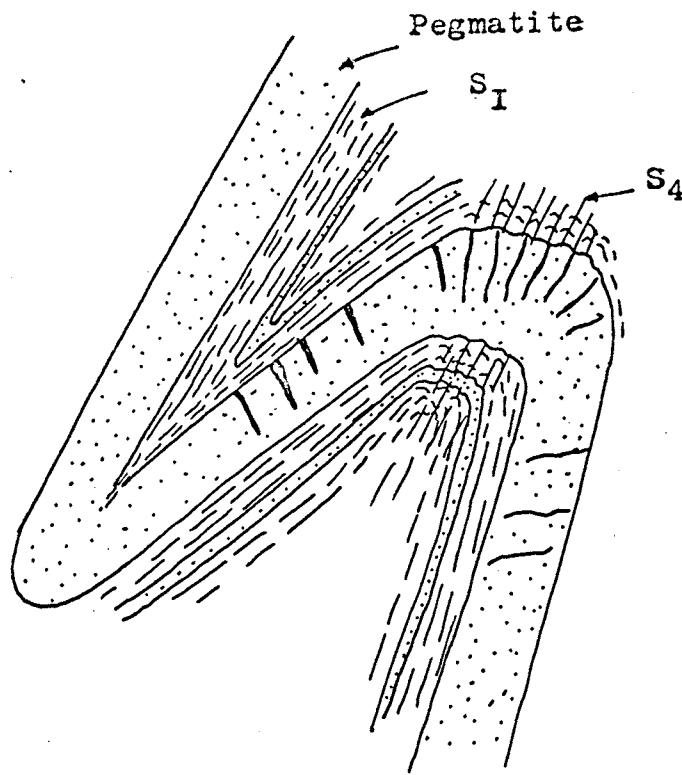
FIGURE 4.5

Style of B_4 folds in a hand specimen from Little Aller Creek. The layers are pegmatites concordant with S_1. Note the radial quartz "veins" in the pegmatite (drawn from polished slab perpendicular to fold axes, actual scale).

scopic fabric. Indeed there seems to be no major isoclinal folds in the
mapped area that cause a complete reversal of the layers. The length the band of
amphibolites traces out around the Mt. Robe Synform and the Western Antiform is
about 14 miles and in this distance there is no sign of an isoclinal closure
in the band of amphibolites as a whole. Certainly there is some isoclinal
folding of the amphibolites in sub-areas 6 and 11, and perhaps near the Silver
King Mine, but these do not significantly alter the trend of the amphibolites
parallel to S_1. Apparently the gross parallelism of layering and schistosity
at all scales is a feature of the Willyama Complex. Gustafson, Burrell, and
Garretty (1950) and King and Thomson (1953) comment that schistosity is always
parallel to bedding, even in the closure of folds. However, Andrews (1922,Fig.8,
11,28) gives a number of examples, including Mt. Franks, of schistosity
intersecting layering.

Two alternatives can be considered;

(i) there are no isoclinal folds larger than those known. Schistosity has
been imposed nearly parallel to the mean orientation of layering before deform-
ation and it is only where S_1 crossed S (because of some inhomogeneity in the
initial layering) that S became folded. It should be pointed out that S_1 is not
an example of a "concentric" schistosity in the sense used by deSitter (1960,
p.292) with respect to the macroscopic B_4 folds in the area. Although the
schistosity passes around the folds parallel to layering, the folds and the
schistosity belong to two different tectonic and metamorphic episodes (Chapter
3). It may, however, be a concentric schistosity with respect to other macro-
scopic folds of which we are seeing only a portion in the Mt. Robe area. The
concept seems to be implicit in the writings of Gustafson et al (1950) and King
and Thomson (1953). Nor is the schistosity a "load" schistosity since it is
often associated with intense mesoscopic folding (for a more general criticism of

the concept of "load" schistosity see remarks by deSitter, 1960, p.278;

Turner and Weiss, 1963, p.455, concerning imposed fabrics in such regions).

There are some difficulties in reconciling this hypothesis with the

symmetries of the various sub-fabrics. The schistosity in this model is

wholly an imposed element and, as noted previously (Sect. 3.25), it is difficult

to see why the symmetries of the quartz and mica sub-fabrics should then differ.

(ii) the Mt. Robe Synform and the Western Antiform are superposed on one limb

of a large B_1 fold in which transposition equivalent to that observed in the

mesoscopic fabric has acted to bring S parallel to S_1. Areas such as Mt. Franks

represent parasitic folds on the limb of the major B_1 fold. It is not possible

to reconstruct much of the details of such a fold without making assumptions

about the orientation of B_1. The difficulties are manifold:

(a) apparently the axes of B_1 folds were not homogeneous at the conclusion of

B_1 folding. Presumably any major B_1 fold would also be inhomogeneous,

(b) the initial orientation of B_1 is not known, for there is no place in the

mapped area that we can be sure is beyond the influence of later folding. It

is not possible to unroll the B_4 folds to find the internal orientation of B_1,

since we do not know the true orientation of any element before B_4 folding.

All we know is that B_1 varied with respect to L_2 in different areas.

It is possible, however, to obtain some idea of the initial plunge of B_1 if

it is at a small angle to B_4. B_1 and L_1 (and L_2) are apparently distributed

on the surface of a cone co-axial with B_4 during folding. Where the angle of

the cone is small, no matter how much B_1 has been rotated, it is still not very

far from its original orientation. Unfortunately the possible error is twice

the angle between B_1 and B_4 so that the usefulness of this criteria is limited.

Still it appears B_1 may have plunged south or south-west over much of the mapped

area

(iii) the plunges in the mapped area, if they are located on one limb of the

B_1 fold are not necessarily relevant to the plunge of the whole proposed B_1 fold.

Obviously only a careful combination of regional mapping and structural analysis can clearly differentiate between the alternatives above for the general relationship of S_1 to S (in this respect the mapping of King and Thomson, 1953, is quite inadequate to resolve the problem).

The first alternative is not very plausible for it demands that layering behave in two contrasted ways in different parts of the deforming body. In a concentric fold, formed by slip on layering and a foliation parallel to layering created by the deformation, the layering is kinematically active. The properties of layering can be expected to dominate deformation and control such factors as size, shape and distribution of folds. If there were any anomalies in the initial fabric by changes in orientation of the fold axes and local heterogeneity in the fold system. In contrast, in similar folds it appears that layering, if not passive, plays a less important role in the deformation. The existence of areas such as Mt. Franks and of sioclinal folding in sub-area 6 proves that layering when deformed macroscopically behaves in a manner similar to that observed in the mesoscopic fabric. There is no reason to believe the same character does not persist to even larger scales. In this case, the gross parallelism of major units to schistosity results from transposition at a macroscopic scale as penetrative and effective as that found in the mesoscopic fabric.

The five units of schist mapped on the eastern side of the area are no doubt derived from original stratigraphic units. There are no criteria to indicate which way up the original sequence was before folding. Also, large scale transposition, by comparison with the mesoscopic fabric, has probably distorted the thickness of the units considerably.

B_2 folds, as in the mesoscopic fabric, are relatively unimportant in the

macroscopic fabric. Where B_2 folds are present in the mesoscopic fabric their axial surfaces are usually at an acute angle to the prevailing orientation of S_1 in adjacent areas. Thus on the western limb of the Mt. Robe Synform S_2 is steeply dipping, whereas at two localities at Mt. Robe it dips shallowly. The relationship implies that S_2 has been rotated with S_1 by B_4 folding and B_2 folds pre-date B_4 folds.

4.3   Cleavage zones

Zones of retrograded rocks, characterised by a phyllitic cleavage, are sporadically developed throughout the area. One example, located on the Mt. Robe Fault, has already been cited. Otherwise, it is impossible to determine if there is a discontinuous displacement across the zones, and so they will be referred to as cleavage zones rather than fault zones. The zones are linear and up to 50 feet wide (e.g. at the Consolation Shafts) and cut across layering and schistosity. The rocks in the zones are typically phyllitic in appearance with a prominent cleavage parallel to the margins of the zone. A second, more widely spaced cleavage intersects the first at an angle of $10\text{-}20^\circ$ about a steep axis. A faint lineation parallels this axis. Both cleavages are near vertical in the examples known and the lineation plunges vertically. The cleavage develops where the zones cross amphibolites (e.g. near the adit of the Mt. Robe Mine). Kink bands, with an orientation typical of S_4, are found deforming zones at three localities where S_4 is present in adjacent rocks:

(i)   the zone west of the summit of Mt. Robe

(ii) at the Consolation Shafts

(iii) in zones to the north-east of Mt. Franks (loc. 3400078000 and northwards)

Thus, at least some of the zones pre-date the completion of B_4 folding. On the other hand, the zone on the Mt. Robe Fault is probably synchronous with the final stages of B_4 folding. Either the zones have formed at different

stages of B_4 folding or are separated into several distinct episodes. There
is no evidence for the unsupported claim made by Binns (1963) that kink bands
are marginal or transitional to zones of this type. Generally the zones
trend at a high angle to kink bands in adjacent rocks. At Mt. Franks zones
nearly parallel to S_4 are developed, but the zones are separated from the main
concentration of kink bands by rocks in which kink bands are only very spor-
adically developed.

4.4   The Mt. Franks Fault

A fault running along the eastern flank of Mt. Franks and disappearing near
the Terrible Dick Mine was first recorded and named by Andrews (1922) as the
Mt. Franks Fault. King and Thomson (1953) show a similar fault, but extended
a further three miles north on their map. Binns (1963) extended the fault a
further 10 miles north to Brewery Well. None of these authors has demonstrated
any lithological or structural discontinuity that might indicate the presence of
a fault, and in the case of Binns, the extension is unsupported by mapping.
Apparently Binns' main arguments for the existence of a fault are concerned with
metamorphism. He believes that thermal metamorphism associated with the fault
has caused retrogression of a belt of sillimanite schists from south of Mt.
Franks to Brewery Well to andalusite schist. In contrast to the foliated and
lineated fabric of the schists, the same retrogression has caused the destruction
of foliation (S_1) in amphibolites.

There are no compelling reasons to believe a fault of the type envisaged by
Binns or King and Thomson exists. Near Mt. Franks there are a number of cleavage
zones, but the intensity of these dies out rapidly northwards. If we assume, as
in the case of the Mt. Robe Fault, these zones are sporadically developed along
a fault and project the fault northwards (Fig. 4.6   ), then the fault crosses
the units mapped in sub-area 2 at an acute angle. There is no evidence of
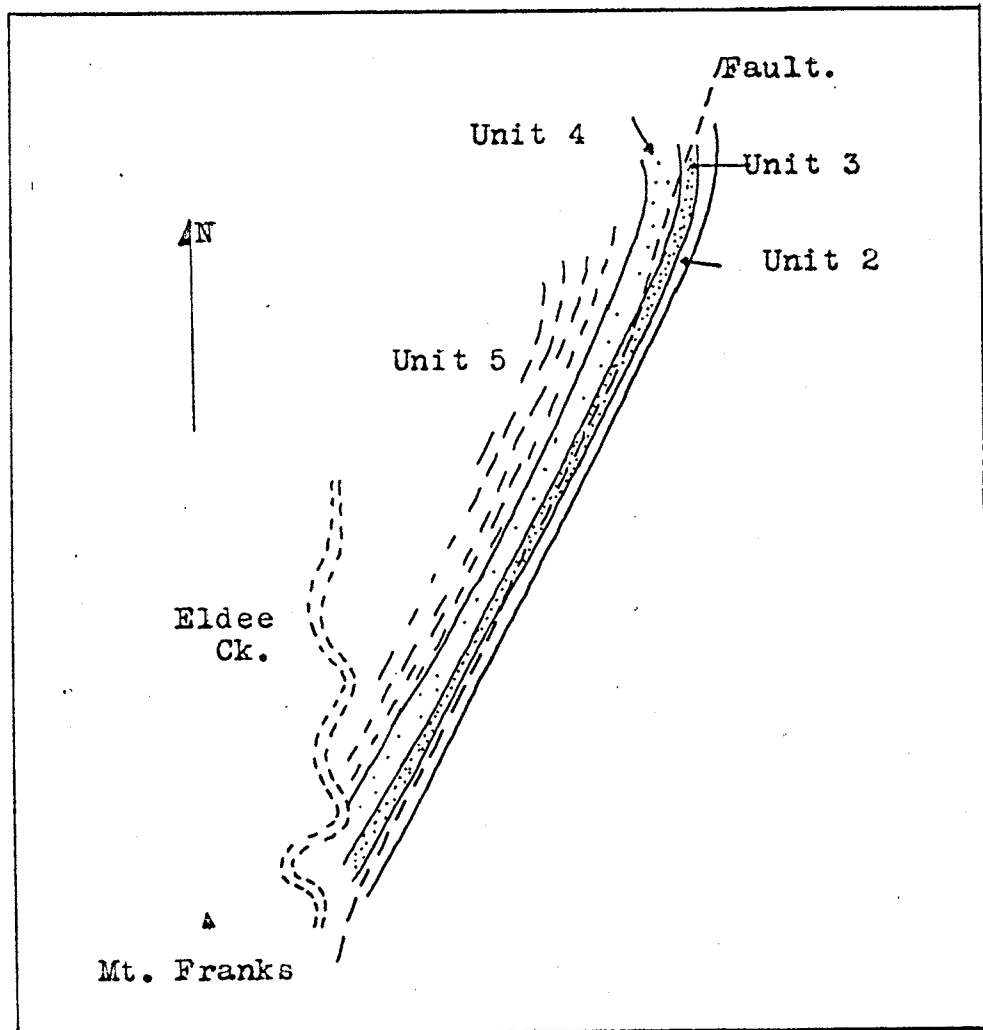
FIGURE 4.6

Location of Mt. Franks Fault proposed by King and Thomas (1953) and Binns

(1963). Note how the fault crosses units of schist at a low angle without

causing any displacement (S_1 dashed; lithological units as defined at Mt.

Franks. Scale 1 inch = 1 mile).

displacement of the units. Nor is there any discontinuity of structure across the proposed fault. It is possible that the cleavage zones near Mt. Franks mark faulting, but there are no reasonable grounds for placing a major fault along the eastern side of the mapped area. The genesis of the andalusite, which does not require a distinctive metamorphism in this region, is discussed at the end of Chapter 5.

C H A P T E R   5

METAMORPHIC PETROLOGY

5.10   Introduction

The contributions of Browne (1922) and Binns (1962, 1963) to the study of the general metamorphic petrology of the Willyama Complex have been noted in the introductory Chapter. A more detailed review of the conclusions of these authors is given below. This review serves to establish the regional setting of the Mt. Robe area, and also to record comments particular to this area.

Browne (1922) recognised three definite stages in the history of metamorphism at Broken Hill:

(i)   A regional high grade metamorphism producing sillimanite schists and gneisses.

(ii)   Local metamorphism associated with the intrusion of igneous rocks. The genesis of andalusite, sericite - and in part - staurolite, kyanite, chloritoid and chlorite is ascribed to this phase of metamorphism.

(iii)   A "stress" metamorphism. Assemblages include sericite, staurolite and kyanite.

A very local metamorphism, concomitant with faulting, is also noted by Browne.

Widespread development of andalusite (including the variety chiastolite) is apparently restricted to the northern portion of exposed Willyama rocks. It is particularly important in the area northwards and eastwards of Mt. Robe and Mt. Franks. Browne was apparently perplexed by the genesis of andalusite. He was clearly unable to reconcile its mode of occurrence with the then (1922) current acceptance of andalusite as only a contact metamorphic mineral; particularly as the only visible

thermal source, the pegmatites, seemed insufficient to create the required intensive alteration. Browne, however, tentatively accepted the contact metamorphic origin.

The even grained mica schists and carbonaceous phyllites (the rocks typically containing andalusite and chiastolite respectively) were believed by Browne to have formed during the same metamorphic period as the sillimanite schists, but in areas of lower temperature.

Binns (1962, 1963) defines four metamorphic periods, designated M_1, M_2, M_3, and M_4, in chronological order.

(i) M_1 :   Regional high grade metamorphism, divided into three zones on the basis of both pelitic and basic assemblages. The N.W. Barrier Ranges lie completely within the zone of lowest grade rocks - Zone A. The critical minerals for this zone are (Binns, 1962);

a. Sillimanite-muscovite in pelitic rocks

b. Pleochroic green-blue hornblende (z) in basic rocks.

(ii) M_2 :   A period of metasomatism, the main expression of which is the growth of unoriented porphyroblasts of muscovite.

(iii) M_3 :   Thermal metamorphism along the Mt. Franks Fault to form andalusite in pelitic assemblages, and pale blue-green pleochroic hornblendes in amphibolites.

(iv) M_4 :   A dynamic metamorphism along "shear" zones; chloritoid is assigned to this phase.

Binns, in common with Browne, records the different habit of sillimanite and the overall intensity of retrogressive metamorphism in the N.W. Barrier Ranges.

A still different origin for the andalusite is postulated by Leslie
and White (1955), as a result of their study of the area around Brewery
Well (Map 1). Although they note that andalusite (chiastolite) may be
related to the Brewery Creek Granite, Leslie and White conclude that
andalusite is probably the product of primary regional metamorphism.

In this thesis metamorphic events are divided into four categories, labelled:

(1). M_1 - regional high grade metamorphism

(2). M_2 - local metamorphism associated with faulting

(3) M_3 - local contact metamorphism associated with the intrusion of
the pegmatites

(4). M_4 - retrogressive metamorphism, irregularly distributed at a regional
scale.

Later we shall have reason to believe that M_3 and M_4 are different aspects
of the same phenomena, but the separation is convenient for descriptive
purposes. The symbols denote a probable chronological order of events.
Again for convenience,the descriptive material is arranged in the order
M_1 (Chapter 5), M_3, M_4, and finally M_2 (Chapter 6).

5.21 The mineralogy of M_1 rocks

The rock types included in this group are the schists and unfoliated
quartz-muscovite-biotite rocks and minor unfoliated quartz-feldspar rocks.
Most rocks which contain more than a few percent of mica are sufficiently
foliated to be termed schists, even though in certain sillimanite schists
the foliation may be very poor and the fabric mainly linear. Other
exceptions are fine-grained sillimanite (andalusite)-

muscovite-biotite-quartz rocks containing 20-30% of micas, but in which

the mica sub-fabric is virtually isotropic. Similar rocks lacking either

sillimanite or andalusite also occur. The fabric of the schists has

already been described in Chapter 2.

Assemblages typical of M_1 schists are:-

(1). Sillimanite-muscovite-biotite-plagioclase-quartz

(2). Sillimanite-muscovite-garnet-biotite-plagioclase-quartz

(3). Sillimanite-muscovite-biotite-quartz-($\pm$ garnet)

(4). Andalusite-muscovite-biotite-quartz-($\pm$ garnet)

(5). Andalusite (chiastolite)-muscovite-quartz-graphite

(6). Quartz-muscovite-garnet

(7). Quartz-muscovite-biotite-($\pm$ garnet)

(8). Quartz-muscovite-biotite-plagioclase-($\pm$ garnet)

5.22   The sillimanite schists

The sillimanite in the schists invariably occurs as fine fibres up to

-1 cm. long and less than 0.01 mm. in diameter. The organisation of the

fibres to form cylindrical aggregates is typical of most schists. More

rarely the sillimanite is dispersed as felted laminae parallel to the

schistosity or in wisp-like aggregates.

The mode of occurrence and the dimensions of the cylindrical aggregates

of sillimanite have been described previously in Chapter 2. At some point

along the length of each cylinder there is a slight bulge which contains a

few grains of biotite, muscovite and quartz, about which the fibres form a

swirling mass. Away from this bulged region the c-axes of the sillimanite

are co-axial with the cylinder axis. The muscovite and biotite crystals in

the bulge distinctly lack the preferred orientation of the same minerals in

the enclosing schist, but have the same optical properties. A variety of the sillimanite schist has finer rods than those described above, approximately 1 mm. in diameter and a mean length of 1 cm. Muscovite and biotite crystals have not been observed in rods of this type and the fibres parallel the length of the rod throughout the aggregate.

The rods are restricted to sillimanite-rich schists, and as the sillimanite decreases, which can be correlated in a general way with an increase of quartz and feldspar compared with micas, the sillimanite is distributed in the felted laminae and wisps mentioned above. Fibres of sillimanite also appear as inclusions in quartz and to a much less extent in biotite and muscovite. Muscovite is generally the predominant mica in sillimanite schist. The muscovite forms small tabular flakes (0.05 mm.long) which define the foliation of the rock. Some sillimanite schists also contain a few porphyroblastic flakes of muscovite; further details of these and the discussion of their origin will be delayed until Sect.6.43. . The smaller grains of muscovite seldom contain inclusions, and then only sillimanite.

The biotite of the sillimanite schists, and indeed in all M_1 rocks, is essentially dichroic with Y and Z a vivid red-brown and X a pale straw yellow. The tints of the colours vary very little from rock to rock. The biotite has a $2V_x$ of only a few degrees in thicker flakes separated from the rock, and in thin section is often sensibly uniaxial. Biotite usually tends to be porphyroblastic (up to 2-3 mm.) and more weakly oriented than muscovite. The larger flakes, commonly contain inclusions of sillimanite, quartz, and regularly arranged inclusions of skeletal (?) rutile. Haloed zircons are rarer inclusions.

Plagioclase is only a minor constituent of schists which bear only a small percentage of sillimanite and is entirely absent from those richer in sillimanite. The plagioclase is untwinned and is either andesine or labradorite. Plagioclase, like quartz, has an average grain size of 0.2 mm.

A pinkish garnet is present in many schists as small idioblastic grains but never forms more than 1% of the rock. The garnet grains intersected in thin section are generally less than 0.2 mm. in diameter, but a few coarser grains (1-2 mm.) have been observed in hand specimens.

A black tourmaline (Schorl), pleochroic from olive-brown to colourless is a common accessory in the sillimanite schists. Traces of tourmaline in the schists may have been derived during the metamorphism from detrital material present in the parent rock. However, tourmalinisation of the schist, post-dating M_1 metamorphism, is widespread in the Mt. Robe District (Chapter 6) and hence accessory tourmaline might also mark the incipient stages of boron metasomatism, particularly as the accessory tourmaline is optically identical with that produced by the tourmalinisation.

5.23 Andalusite schists

The typical andalusite schist is composed of porphyroblasts of andalusite set in a fine-grained, well foliated matrix of quartz and muscovite and minor biotite. Metamorphic lamination is usually prominent in the andalusite schists. The andalusite is generally confined to quartz-rich laminae.

The andalusite is strongly idioblastic in all but a few schists and may be up to 7 cms. long, although 1 cm. is a more typical size. Cross twins on (101) are common. Optically the andalusite is colourless with a negative 2V of 70-80°. The porphyroblasts always contain numerous inclusions

of quartz and occasionally plagioclase, garnet and biotite. Biotite inclusions have the same pleochroism and 2V as biotite external to the porphyroblasts.

The optical properties and mode of occurrence of the biotite, plagioclase, muscovite, garnet, and accessory tourmaline are the same as the corresponding minerals in the sillimanite schists. On the whole the andalusite schists are finer and more uniformly grained than the sillimanite schists. Grains of quartz have a mean diameter of 0.1 mm. Garnet is very rare. It is possible to distinguish two distinct varieties of andalusite schist; quartz-muscovite-biotite-andalusite schist, and quartz-muscovite-andalusite schist with only minor biotite. Biotite may compose as much as 30% of the first, and at Mt. Franks forms delicate layers 1-5 mms. thick. In contrast, the second variety which is the commoner of the two, contains less than 3% of biotite and generally more andalusite. The two varieties can be mapped as distinct lithological units.

Chiastolite forms in schists which are rich in a black opaque mineral. Determinations by Browne (1922) indicate that the opaque mineral is graphite. Chiastolite schists are also well foliated and very well laminated. The chiastolite typically forms "finger-shaped" porphyroblasts up to 7 cms. in length. The average grainsize of quartz in the chiastolite schists examined is 0.01 mm., which is much less than the grainsize of quartz in intercalated andalusite schists.

5.24   Andalusite in sillimanite schists

Isolated andalusite crystals are sporadically distributed throughout the schists in which sillimanite is the dominant Al-silicate polymorph. The texture of andalusite in these schists is very distinctive; the andalusite

is always surrounded by a partial or complete "ruff" of muscovite. The ruff is composed of clear flakes of muscovite with a grain size (1-2 mm.) slightly larger than muscovite elsewhere in the schist. The mica composing the ruff is noticeably free of inclusions of sillimanite but may contain numerous inclusions of quartz and sometimes tourmaline.

The ruff is only absent where the andalusite is in contact with a quartz-rich lamina containing no trace of sillimanite. Otherwise the ruff forms a complete shield between the andalusite and any nearby sillimanite.

The aggregate of muscovite plus andalusite in Fig. 5.1 (Plate 1), has a square outline about which the schistosity diverges, with a structure similar to that of andalusite in the ordinary andalusite schists. In this particular example small inclusions of andalusite in the muscovite with an optical orientation the same as that of the core of andalusite extend almost to the edge of the square. The total shape of the aggregate (mica plus andalusite) is the same as that of a basal section of andalusite and thus it appears that muscovite is replacing the andalusite.

Apart from the presence of andalusite the assemblages of the rocks are the same as normal M_1 sillimanite schists.

5.25 Other rocks

Schists or non-schistose rocks composed of quartz, plagioclase and micas, but bearing no sillimanite and andalusite, are only minor constituents of the body of metamorphic rocks. The most important of these are the quartz-muscovite schists that outcrop along the eastern edge of the area north of the Black Prince Mine. These rocks usually contain quartz and muscovite in the proportions of 2:1 and sometimes minor biotite (the proportions vary quite
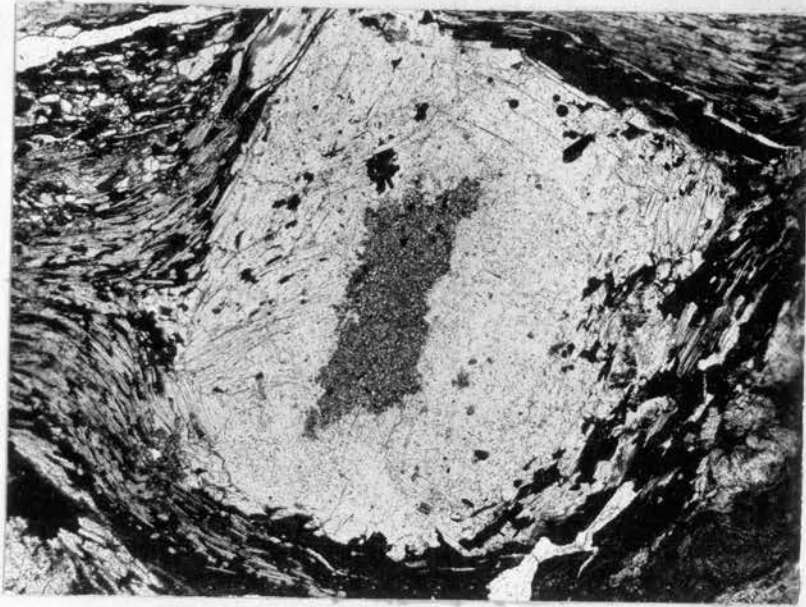
FIGURE 5.1 (PLATE 1)

Andalusite porphyroblast partially replaced by muscovite (Spec. No. 28279). The section is normal to {001} in the original grain and the rectangular outline of the andalusite in this section has been preserved. The core of andalusite (high relief) is surrounded by coarse flakes of muscovite (mainly with their basal cleavage sub-parallel to the section). (Field of view is 2 x 1½ cm., crossed nicols)

considerably from specimen to specimen) and have grainsizes comparable to the andalusite and sillimanite schists.

Garnet is never more than a minor component, and then is mainly found in quartz-muscovite layers often with a higher biotite content than is usual in sillimanite schists. At Mt. Franks andesine and biotite are more common in the quartz-muscovite schists than elsewhere, but still only constitute 10-15% of the total volume of the rock.

To the north and east of Mt. Franks there is a unit of much finer grained (0.01 mm.) poorly foliated quartz-andesine-muscovite rocks which may be finely layered (1.5 mm.) with layers of biotite and andesine. Muscovite is only 10-20% of these rocks and quartz and plagioclase in equal amounts make up the bulk of the rock. ·

Rock which might be classified as true quartzites are very rare.

5.26   Petrography of the foliated amphibolites.

It is only the well foliated amphibolites that have simple mineral assemblages combined with simple arrays of grain boundaries and an even grain size. These amphibolites are interlayered with andalusite and sillimanite schists that show a minimum of retrogressive effects. This association, combined with the fabric of the rocks and the assemblages indicate that the foliated amphibolites are a result of the primary high-grade metamorphism.

The foliation is due to a planar preferred orientation of the hornblendes and is further emphasized in some rocks by a crude layering of quartz and feldspar. The amphibolites are fine-grained with hornblende grains of 1-2.5 mm. long and a cross-sectional diameter (average), of the same order as plagioclase and quartz, i.e. 0.1-0.5 mm. Plagioclase grains

are slightly elongate parallel to {001} (0.5-0.6 mm.), but in general

grains of plagioclase and quartz are equant.

Assemblages of the foliated amphibolites are:-

1. Hornblende-plagioclase

2. Hornblende-plagioclase-quartz ($\pm$ minor epidote)

3. Hornblende-plagioclase-quartz-garnet

4. Hornblende-plagioclase-quartz-biotite*

5. Hornblende-cummingtonite-plagioclase-quartz-biotite*

6. Hornblende-cummingtonite-plagioclase-quartz-garnet-biotite*

7. Hornblende-cummingtonite-plagioclase

8. Hornblende-plagioclase-epidote

9. Hornblende-plagioclase-quartz-sphene *

The modal composition of three typical varieties of amphibole are:

Volume percentage composition

	(1)	(2)	(3)
Hornblende	50.9	73.2	34.1
Plagioclase	48.1	15.5	46.7
Cummingtonite			16.1
Quartz		9.9	
Opaques	0.9	1.4	3.2

3,000 points counted in each specimen. Apatite (0.1%) is present in all

specimens.

(1). Specimen No. 28389 , typical amphibolite,

(2). Fine grained, dark coloured variant of amphibolite, (28377)

(3). Two amphibole amphibolite. (28317)

*Apatite and opaques (mainly ilmenite) are present as accessories in all
assemblages, except (9), examples of which contain no opaques. Biotite is
only a minor member of assemblages (4), (5), and (6).

the hornblendes of the amphibolites are pleochroic with X=pale yellow, Y=medium-dark green (brownish) and Z=medium-dark green or, medium-dark green (bluish) or, medium-dark vivid blue-green. The absorption is always Z=Y X.

The Z^c angles in the hornblende lie in the range 18-24°, measured on a flat stage in {010} sections. A few values determined with a Universal Stage agree with those measured on the flat stage. Due to the strong absorption of the hornblendes, the former are probably no more accurate than values determined with a flat stage (See Turner, 1947).

The $2V_Z$ vary from 102-106°. The hornblende is generally nearly idioblastic and contains only rare inclusions of quartz and feldspar.

Amphibolites with a second amphibole are not widely distributed and examples (5), (6), and (7) are from specimens taken at three localities (37200132800, 23000123200, 28500111300). The cummingtonite in one specimen sectioned (28281) forms lamellae in the hornblende (Fig. 5.2, Plate 1) as well as discrete grains. The latter contain no inclusions or lamellae of hornblende. The cummingtonite is a pale green variety, non-pleochroic, with a $2V_Z$ of 80° ($\pm$ 1.5°) and a Z^c angle of 17° ($\pm$ 1.5°) - (averages of 6 measurements). Lamellar twins parallel to {100} in the cummingtonite are common. There is a distinctive relationship between the optical orientation of the cummingtonite lamellae and the host hornblende grain. Both minerals share common {110} cleavages and also X and Z axes within the limits of measurement* ($\pm$ 3° in the hornblende, due to absorption). The only difference in the optics of the two minerals is the location of the optic axes, with a $2V_Z$ of 106° ($\pm$ 2°) in the hornblende and 80° ($\pm$ 2°) in the cummingtonite. One set of cummingtonite lamellae have poles that make an angle of 4-5° (four measurements) with Z in the hornblende and cummingtonite, and at the same time are

*Average of measurement in four different grains with cummingtonite lamellae
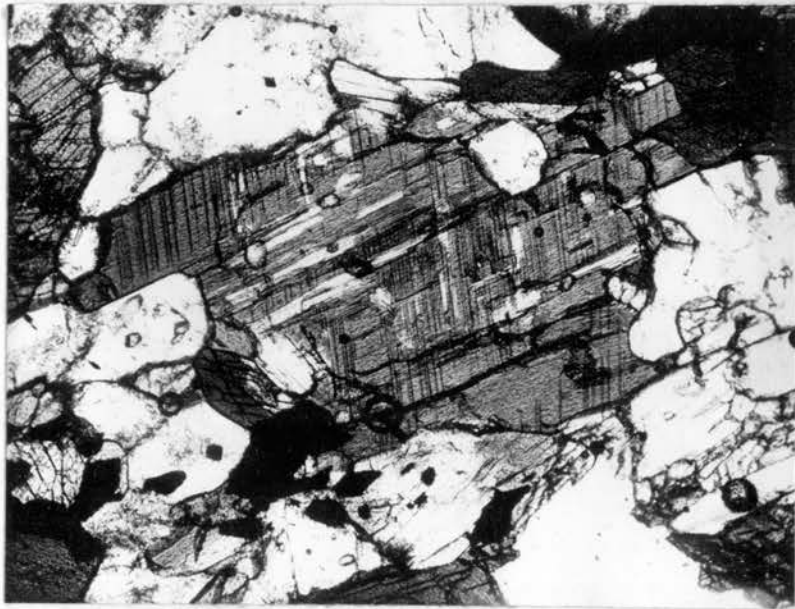
FIGURE 5.2 (PLATE 1)

Cummingtonite lamellae in hornblende. The fine cummingtonite lamellae crossing the hornblende grain vertically (appearing mainly as fine black lines resembling cleavage) are probably parallel to {001} in the hornblende. The broader lamellae slanting along the diagonal of the plate (and parallel to the trace of the cleavages) are parallel to {100} in the hornblende. (The field of view is 8 x 6 mm., crossed nicols, Spec. No. 28281)
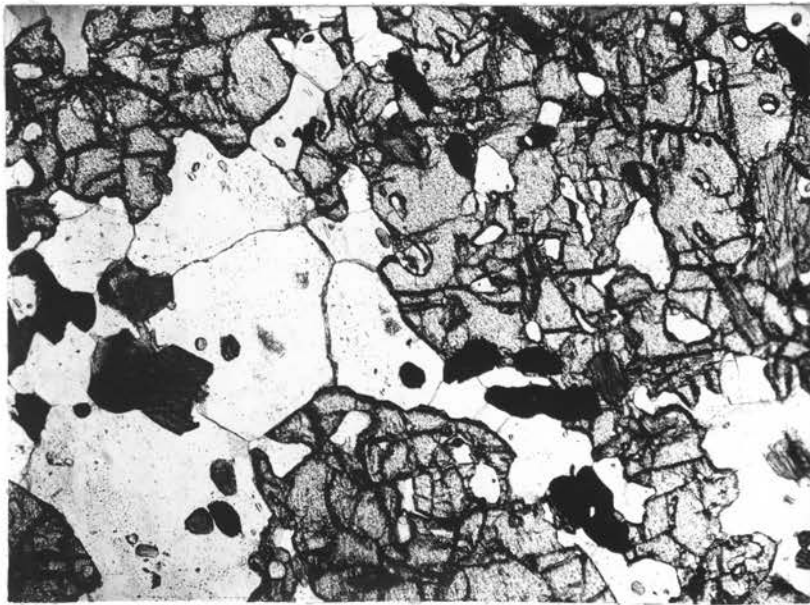
FIGURE 5.2 (PLATE 2)

Sieve structure in a garnet porphyroblast in amphibolite. The garnet
(high relief) contains inclusions of quartz (white), hornblende (dark
grains in quartz cluster), biotite(far right) and opaques.
(Field of view approximately 1 x 0.75 mm., nicols uncrossed, Spec. No. 28285)

at an average angle of 17° to c (Fig. 5.3), suggesting the lamellae

are parallel to {001} in the hornblende. The second set of lamellae

are parallel to {100} in the hornblende.

The composition of plagioclase is very variable (An_{10} - An_{55})* (Binns,

1964, gives a range of An_{40} - An_{93} for plagioclases of Zone A amphibolites.

However, this includes many amphibolites from outside the area studied).

All plagioclase determined are low-temperature varieties. Twin types

recorded include albite-ala, albite-carlsbad and carlsbad. Albite twins,

with one or two broad lamellae crossing the whole grain, are probably the

commonest type. A large percentage of grains are untwinned.

Garnet is widespread in the amphibolites bearing quartz and a minor

quantity of biotite. The garnet forms scattered xenoblastic porphyroblasts

(5-10 mm.). The grains often give the impression of a matrix (sieve

structure), pervading the quartz rich portions of the rock (Fig. 5.2,

Plate 2). Quartz and opaques are the commonest inclusions, but the garnet

may include all other components of the amphibolite except plagioclase.

As mentioned previously, variation in the internal composition of the

foliated amphibolites is uncommon. A few important instances are described

below.

An outcrop of amphibolite in the creek just below the adits of the Mt.

Robe Mines contains, over a limited area 10-12 feet long and 2-3 feet wide,

numerous prism shaped fragments of a biotite-andesine-quartz rock. The

fragments are usually 10-15 cm. long and have an approximately square end

section of 3-5 cm., and are not systematically aligned. The portion contain-

ing the fragments is close to contact of the amphibolite with sillimanite

*Determined optically by Universal Stage, using data given by Slemmons, (1963)
by the method of Turner (1947).
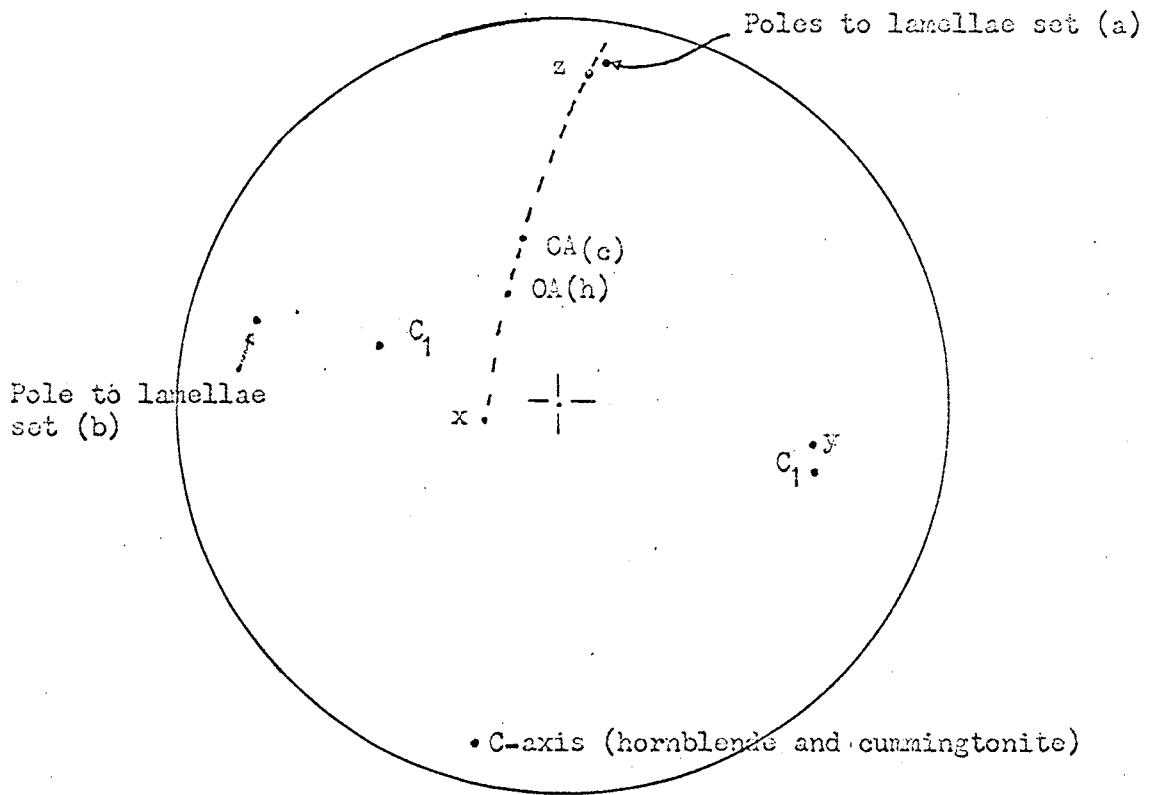
FIG. 5.3

Optical orientation of cummingtonite lamellae in hornblende. (Data from grain in Fig. 5.2, Plate 1.) The pole to one set of lamellae (a) makes an angle of $5°$ with the z axis of the hornblende (and cummingtonite) and is at $17°$ to the c-axis of the grain, suggesting the lamellae are parallel to {001} in the hornblende. The pole of the second set of lamellae is located mid-way between the poles of the {010} cleavages of the hornblende, and hence the lamellae are parallel to {100} in the hornblende. (Lower hemisphere Wulf Nett; C=pole to {010} cleavage in the hornblende, OA(h) and OA(c) = position of one optic axes of the hornblende and the cummingtonite respectively)

schists. Unfortunately the amphibolite is partially retrogressed, but in the specimen sectioned (Spec. 28,324.) the effects are not extensive enough to cause any real ambiguity. The principal effect is the replacement of plagioclase (in the amphibolite and fragment) by sericite and very fine (?) clinozoisite.

The mineral assemblage of the amphibolite is hornblende, plagioclase and biotite (red-brown), and accessory apatite and opaques. The fragment is composed of andesine (extensively sericitised), biotite, quartz, hornblende, and minor chlorite. Most grains are untwinned and a few grains are indistinctly zoned. The texture and grainsize of the rock are the same as those of quartz-feldspar layers in the schists. The biotite (3-5%) is the usual vivid red-brown variety and is apparently little altered, and the flakes are roughly aligned to define a foliation that is continuous with the weak foliation of the amphibolite. (The foliation in the fragment cannot be seen in hand-specimen, and an attempt in the field to decide if the foliation is independent of the orientation of the fragments was inconclusive. Presumably the parallelism of the foliation in the fragment and the amphibolite in the above specimen is typical.) Small needles of hornblende (0.5 mm. long, similar to that in the amphibolite, are disseminated throughout the fragment. Hornblende is also concentrated in strings that sweep across the contact between the fragment and the amphibolite and penetrate the former for a distance of several millimetres, along surfaces parallel to the foliation of the amphibolite. Chlorite is only a very minor component and may well be due to local retrogression of the biotite.

There is an increase in the hornblende content of the amphibolite near its contact with the fragment with the hornblende forming distinct clusters. A

fine "halo" of hornblende can be observed around most of the fragments.
The amount of biotite in the amphibolite is a little unusual (particularly
as quartz is absent); and a specimen several feet from the fragments, although
strongly retrogressed, contains no trace of biotite or anything that might be
interpreted as altered biotite (Spec. 28325).

Layers of quartz-andesine-garnet (pink)-biotite rock are sparsely disseminated
throughout the amphibolite bodies. The layers are usually less than 2" thick
and a few feet or less long. The proportions of quartz and andesine in the
layers varies widely from approximately equal volumes to 70% quartz. Scattered
grains of pink garnet, exhibiting pronounced sieve structure, are always present;
flakes of red-brown biotite are sometimes abundant enough to impart a foliation
to the rock (S_1) but are often entirely absent. Hornblende, identical with
that in the enclosing amphibolite, is an important component (10%-15%) in some
layers (e.g. Spec. 28337). Unlike the fragments from Mt. Robe just described
there is no concentration of biotite and hornblende in the amphibolite near the
layers. The texture and grainsize of the layers are similar to those of
quartzose layers in the schists.

The recognition of retrogression in the calc-silicate rocks that outcrop
in the area is hampered by their lack of a distinctive (imposed) fabric
similar to that in the schists and their mineralogy. Many of the minerals
that characterise these rocks (e.g. diopside, epidote, clinozoisite) appear
in the retrograde amphibolites. Because of uncertainties in distinguishing
M_1, M_3 and M_4 metamorphism, the calc-silicates contribute little to our
knowledge of the metamorphic history of the area; consequently their description
is deferred until the end of Chapter 6, where they can be discussed in the
light of the metamorphic history deduced from the schists and amphibolites.

5.30   Microstructure of M$_1$ Rocks

The configuration of grain boundaries in many M$_1$ rocks is very similar

to that of certain metals, ceramics and rocks recrystallised experimentally.

In metals, where the details of microstructural changes during recrystallisat-

ion have been much more extensively investigated experimentally than in rocks,

microstructures of the type we shall be interested in are commonly formed

during annealing of cold worked metals. The microstructure is the result

of migration of the grain boundaries in the aggregate under the sole influence

of differences in interfacial energies, and tends to minimize the interfacial

energy of the aggregate as a whole. Recrystallisation of this type (during

the annealing of cold work metals) is usually referred to by metallurgists

as grain growth (recrystallisation) (Beck, 1954). The characteristic geometry

of grain boundaries that is created during grain growth, and its dependence on

interfacial tensions was first noted by Desch (1919) and later generalised

by Harker and Parker (1945) and, in particular, Smith (1948, 1954).

In addition to the empirical studies a sound theoretical understanding of

this type of microstructure is also available (Smith, 1948, Herring, 1951,

1952, Maclean, 1957, Swalin, 1962). Since the theory is couched in terms of

macroscopic thermodynamic quantities it can be applied equally to rocks or

metals, even though knowledge of the structure of grain boundaries between

silicate minerals is almost totally lacking. Before describing the micro-

structure of M$_1$ rocks a brief review will be given of the equivalent micro-

structure in metals and the thermodynamics necessary for understanding its

formation.

The important features of an aggregate resulting from grain growth recryst-

allisation is the array of strain-free grains with planar, or very slightly

curved boundaries; three boundaries intersect in line (a triple junction) and four boundaries intersect in a point (Smith, 1948).

The condition for the stable configuration of three grain boundaries intersecting along a line is given by Herring (1952, p.157) as:

$$\sum_{i=1}^{3} \left(\gamma_i t_i + \frac{\partial \gamma_i}{\partial t_i} \right) = 0 \qquad\qquad (i)$$

where γ_i is the interfacial tension in the ith face and t_i is a vector in the ith surface normal to the triple junction (and pointing away from it). If the term $\frac{\partial \gamma_i}{\partial t_i} = 0$, that is if the interfacial tension is independent of the orientation of the interface with respect to the crystal lattice, then equation (i) for the three interfaces between three phases reduces to the usual form (Smith, 1948):

$$\frac{\gamma}{\sin \alpha} = \frac{\gamma}{\sin \alpha} = \frac{\gamma}{\sin \alpha} \qquad\qquad (2)$$

where $\gamma_1, \gamma_2, \gamma_3$ are related to the interfacial angles $\alpha_1, \alpha_2, \alpha_3$ as shown in Fig. 5.4.

If the values, or the relative values, of the interfacial tensions are known then measurement of the interfacial angles can be used as a criterion of the completeness of grain growth.

Surface energy and surface tension (and the corresponding terms for interfaces*) are macroscopic thermodynamic quantities which are independent of the atomic structure (or type of bonding) of the surface region. Here independence means that the physical nature of the thermodynamic quantities is not a function of these properties, although the numerical values of the quantities will depend on these properties of the material, and possibly also the structure of the interface.

*Some authors, in the discussion of solids, (Swalin, 1962, Maclean, 1957) retain the term 'surface' for the external boundaries of a solid (solid/ liquid, solid/vapour) and 'interfaces' for the internal boundaries between grains of the solid. This convention is used here, although it should be noted that there is no difference in the physical nature of the thermodynamic quantities. Grain boundary is synonymous with interface.
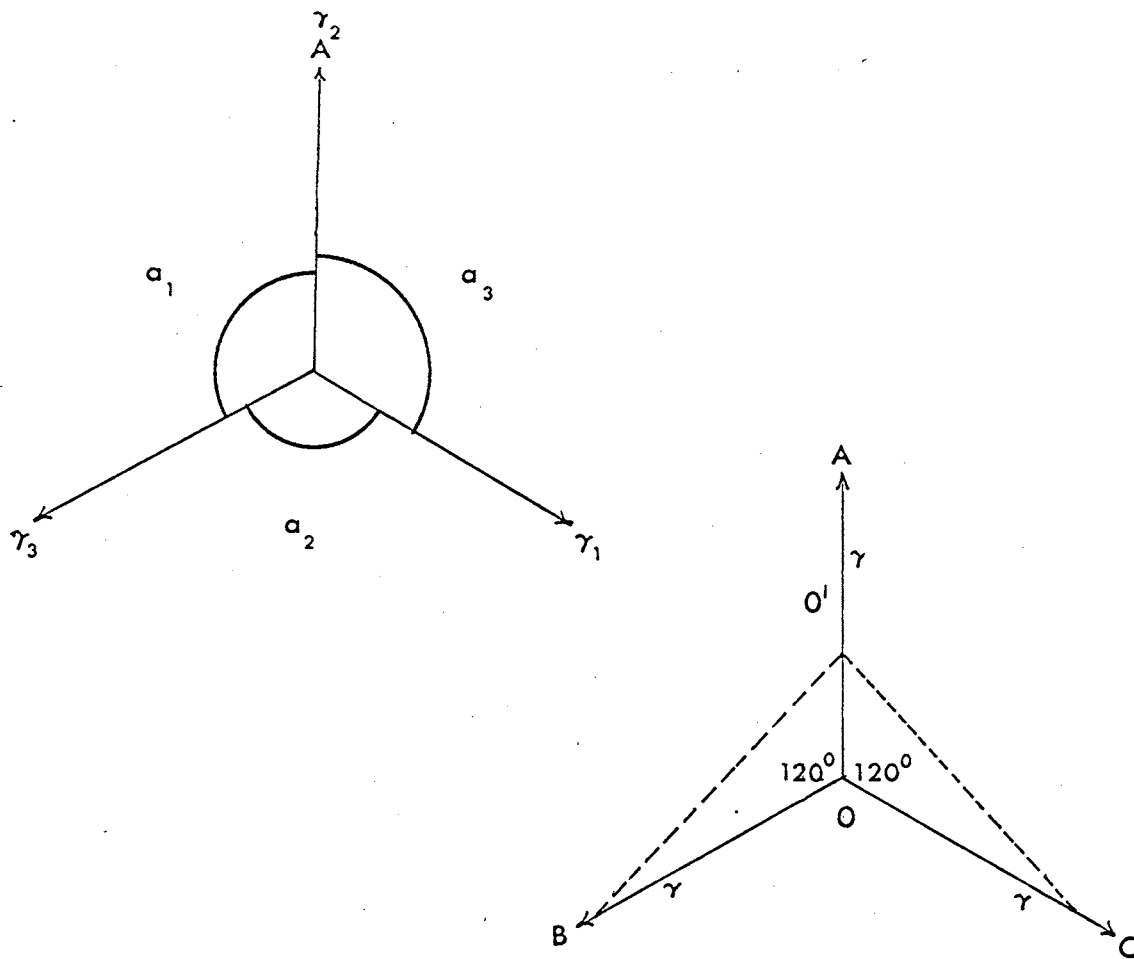
FIG. 5.4

(a). Relationship between the interfacial angles a, a_2, and a_3 and the interfacial tensions γ_1, γ_2 and γ_3 at a triple point. The line of intersection of the two boundaries is normal to the page.

(b). O is a triple junction between three grains of the same phase, at which the three boundaries AO, BO, and OC meet at $120°$ (the faces and triple junction are normal to the page). The interfacial tension is assumed to be independent of orientation of the lattice of the phases. Movement of the triple junction to O', with a corresponding change in the three interfacial angles leads to an increase of the total interfacial energy of the system if the points A, B, and C are fixed (at triple points). The increase is demonstrated by the greater length of AO'+ BO'+OC' (4.7 units) compared with AO+BO+OC (4.4 units), and is equivalent to an increase in area in three dimensions.

Some confusion in the use of the thermodynamic quantities associated with solid surfaces particularly in the definition of surface or interfacial tension is apparent in the metallurgical literature. The surface tension defined by Gibbs (1906) is a scalar energy-function, while that devised by Shuttleworth (1950) is a symmetrical second-rank tensor which only reduces to a scalar in special circumstances. Part of the difficulties is due to terminology and part to the comparison of solid surfaces with liquid surfaces, for which the surface free energy, the surface-tension and the surface stress are all numerically equal, whereas for solids this is not generally true. The circumstances in which the quantities can be considered equivalent can be seen from the equations defining the quantities.

Gibbs (1906, p. 221) showed how to assign definite quantities of energy (U_s) and entropy (S_s) to an interface between two phases. The Helmholtz free energy (F_s) of a surface at temperature T is then:

$$F_s = U_s - TS_s \qquad \text{--------- (4)}$$

Gibbs (1906, p.228, p.315) then defined the surface tension γ for both solid and liquid surfaces as:

$$\gamma = F_s - \sum_i \mu_i \eta_i \qquad \text{--------- (5)}$$

where η_i is the surface density of the ith phase and μ_i its' chemical potential.

The surface energy is a measure of the difference in total energy between a homogeneous phase with no surface and the same phase with a surface introduced. The surface energy of all crystalline solids is positive (Shuttleworth, 1950). The mathematical specification of γ is dependent on a convention for locating the surface (Gibbs, 1906, p.315). The term "Helmholtz surface free energy" of Shuttleworth (1950) is equivalent to defined as above. The "surface tension" derived by Shuttleworth for solid surfaces is

a particular case of the surface stress of Gibbs (1906) or the surface stress tensor σ_{ik} used by Herring (1952). Changes in σ_{ik} measure the work required to deform a surface. In general σ_{ik} is a symmetrical second-rank tensor with two principal components in the surface layer.

For the very special case of a crystal surface with a normal axis of three-fold or greater symmetry the tensor can be reduced to a scalar (Shuttleworth, 1948). Surface stress is related to surface tension for the reversible deformation of a surface by the equation:

$$\sigma_{ik} = \gamma + A\left(\frac{\partial \gamma}{\partial A}\right) \qquad \text{------(3)}$$

Thus the two quantities are numerically equal if $\frac{\partial \gamma}{\partial A} = 0$; that is if the atomic mobility is sufficient to keep the separation of surface atoms constant during deformation of the surface. This is true for a liquid and may be approximately true for solid interfaces at temperatures approaching the melting point of the solid, in which atoms can move to the surface at a rate comparable to the ra te of expansion of the surface.

It is a result of the above discussion that equation (ii) should not be literally interpreted as a tension tending to pull grain boundaries into equilibrium configurations during grain growth. Triple junctions compatible with equation (ii) are stable because any motion of the triple junction requires the creation of a positive amount of new surface; and hence an increase in the interfacial energy of the system around that triple junction. A simple graphical demonstration of this, for a system in which $\gamma_1 = \gamma_2 = \gamma_3$ is given in Fig. 5.4b .; the demonstration can easily be extended to cases in which $\gamma_1 \neq \gamma_2 \neq \gamma_3$. It is only when $\frac{\partial \gamma}{\partial A}$ in equation (i) is not equal to zero that there is a "torque" tending to rotate the boundary.

5.31 Description of the Microstructure of M_1 rocks

The minerals of M_1 rocks, in which there is no trace of retrogression, are strain free. Quartz is free of undulose extinction, the cleavage of the mica grains is planar and free of kinks. None of the other minerals have any micro-structural features that could be interpreted as evidence of strain in the aggregate. At the conclusion of M_1 metamorphism, any recrystallisation* that was proceeding, was taking place in a strain-free aggregate. Many rocks that show minimal traces of retrogression also show signs of intra-granular strain. The main expression of this is slight undulatory extinction of the quartz. However, the invariable association of the intra-granular deformation with retrogression, proves that it is not a primary feature of M_1 rocks (Chapter 6).

Aggregates of quartz grains best exhibit the features to be expected from grain growth recrystallisation. The grains (in section) are usually five or six sided polygons whose diagonals tend to be equal (equiaxial polygons). Three edges invariably meet in a triple point. The commonest deviation from this situation is for the polygons to become less regular (yet still with the same number of sides) and for angular bends to appear in the boundary between two triple points. However triple points are universal in quartz aggregates; the intersection of four boundaries at a point has not been encountered.

With a Universal stage, it is simple to show that the grain boundaries are generally planar in three dimensions, and hence the line of intersection of three boundaries must be straight. On a flat stage the angles at the triple

*Recrystallisation is used here in the sense of Beck (1954) who proposed "......all boundary migration phenomena connected with the movement of ordinary high angle grain boundaries are designated by the generic term 'recrystallisation' ". Apparently this is the sense intended for the term "annealing recrystallisation" of Griggs, Paterson, Heard and Turner, (1960).

point are often near 120°; angles more acute than 80° are exceptional.

To avoid effects of the orientation of the slide with respect to the triple

junction, the determination of the interfacial angles is best made with a

Universal Stage.

5.32 Measurement of interfacial angles at triple junctions between quartz
grains

The interfacial angles between three quartz interfaces were determined by

use of a Universal Stage by the measurement of each interface. The inter-

facial angles were then calculated on a stereographic nett. Grains were

checked simultaneously for undulose extinction by testing the homogeneity of

the extinction of the grain.at the optic-axis position.

An estimate of the error involved in the measurements can be gained from the

"triangle of error" formed at the intersection of the three great circles

representing the interfaces on the nett. Where the sides of the triangles

exceeded three degrees the measurements were usually rejected, unless some

very obvious error had been made. This means that the probable error in the

measurements of the interfacial angles is less than 2°. The failure of the

three great-circles to meet at a point may be either the result of a

proceedural error or measurement in an oblique section through a slightly

curved triple junction. Each interfacial angle was determined separately,

and the sum checked against 360°. Specimen 28371 (a quartz-plagioclase-

garnet rock) was traversed at regular intervals and all the triple junctions

crossed were counted. The results are given in Fig.5.5a . 48% of the inter-

facial angles lie within the range 113° to 127°; 16.6% are within 2.5° of 120°.

The distribution is slightly skewed about 120°, a feature that results from

the absence of one angle near to 120° at some triple points. However, at least

(a)

(b)
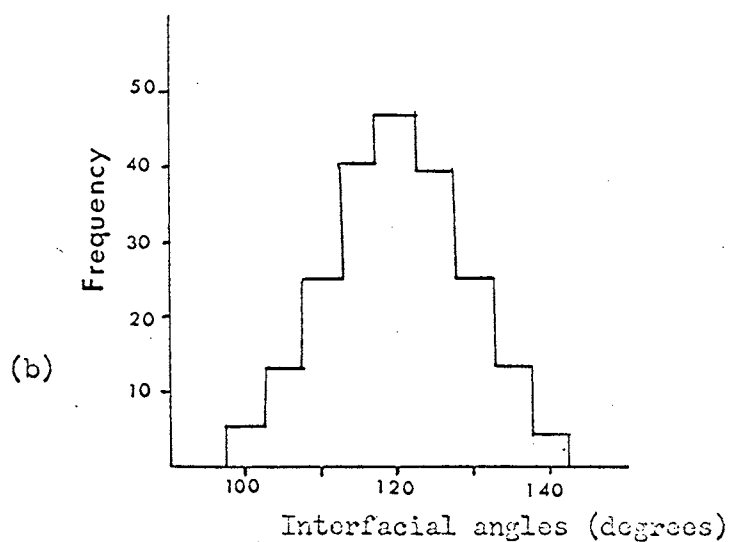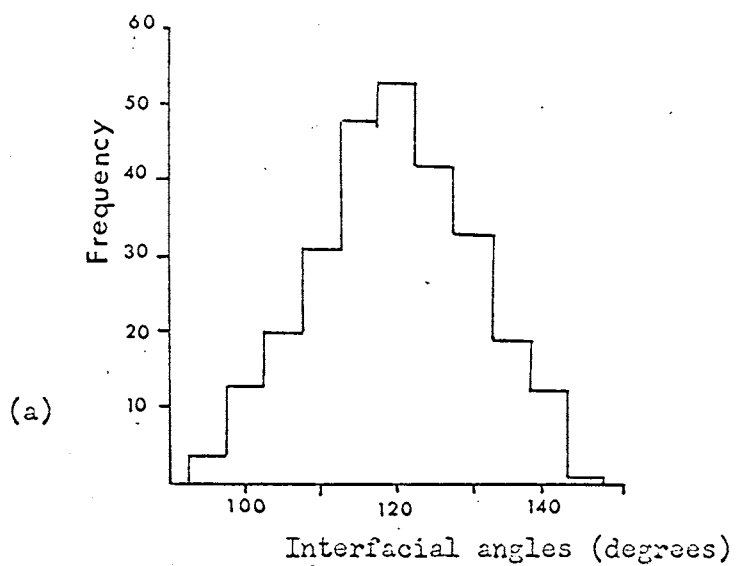
Fig. 5.5 (a, b). Frequency of interfacial angles between the grain boundaries of three quartz grains at a triple junction. The angles are summed over $5°$ intervals centered on $120°$;

(a). Measurements at 92 triple junctions.

(b). Measurements at 71 triple junctions.

(See text for description)

one angle of 120° appears at most triple junctions. The Universal Stage

revealed that the homogeneity of the grains in this specimen was not as

good as the preliminary examination had implied. Curvature of the boundary*

is also more common than in the rocks measured below.

The results expressed in Fig. 5.5b , have been obtained by measurement in

quartz aggregates with well developed triple junctions in a number of spec-

imens, mainly quartz-muscovite schists. (Sections from Specimens 28291, 28297

from the Silver King Mine provided the bulk of the results). The distribution

in the second plot is more symmetrical, and 55% of grains lie in the range

113° to 127°. The quartz grains at the triple junction in the second case

are free of strain.

The following points are relevant in evaluating the significance of the

plots (in terms of interfacial tensions):

(1). Adjustments of the grain boundaries under the influence of interfacial

tension is complete; ultimately all the interfacial angles would closely

approach 120°.

(2). The interfacial tension of quartz is not independent of the orientation

of the underlying lattices at the boundary. If the term $\frac{\partial \gamma_i}{\partial t_i}$ in equation (1) is

not zero, then the equation expands into three equations with five independent

unknowns. Determination of the unknowns depends, in part, on determining the

orientation of an interface with respect to the quartz lattice. Knowledge

of the orientation of the c-axis, the only easily determined direction in

quartz, is insufficient. Nevertheless, measurement of the angle between the

boundaries and the c-axes of quartz grains (in the first case) at triple

junctions whose interfacial angles are close to 120° ($\pm$ 3° as determined)

showed that no simple relationship existed. A complete, and apparently

*Triple junctions at which curved boundaries intersect were not measured.

haphazard, scatter of angles was obtained. Further determination of the
angles for grains at another 26 triple junctions (for all ranges of inter-
facial angles), when combined with the above, indicated that the boundaries
between the quartz grains are general high angle boundaries.

Brace and Walsh (1962) made direct measurements of the surface energy of
quartz in known lattice planes. The surface energies varied by a factor of 5,
so that the surface energy of quartz is anisotropic. However, these results
cannot be applied immediately to aggregates, since the situation in aggregates
is much more complicated. Across a boundary between two solid phases of the
same composition there exists the possibility of a compromise structure forming,
so that the interfacial energy may be less than the energy of the two juxtaposed
surfaces taken by themselves (unless the interface consists of a fairly thick
zone with a completely chaotic, and hence structureless, nature; MacLean,
1957). The structure of high angle boundaries in metals is not properly under-
stood, even less is known of silicates. The "island" theory of Mott (1948)
and Smoluchowski (1952), in which the boundary is conceived as a thin region
broken up into areas of complete mis-fit of the adjacent lattices and isolated
regions of good fit, is the only model that has some acceptance. Bubble rafts
constructed by Lomer and Nye (1952) approximate to this structure. However
the model has failed to predict adequately other experimental results, such as
grain boundary sliding rates; MacLean, 1957). The interfacial energy will then
depend in a complex fashion on the orientation of the contiguous lattices, and
the extent of anisotropy on the nature of the compromise structures.

(3). Assuming the interfacial tension of quartz is isotropic, the nature of
other boundaries adjacent to the quartz aggregate (e.g. quartz-plagioclase,
quartz-muscovite) because of their different interfacial tensions, necessitate
compromises at nearby all-quartz triple junctions. This effect should

disappear with the possibility of prolonged adjustment of the boundaries.

Still, even allowing for these uncertainties, the results obtained point
to one conclusion. The approach of the interfacial angles to 120° is close;
and no matter whether the departure from 120° is due to imperfect annealing
or anisotropy of the interfacial tensions, these effects are subsidiary to
this general trend. If the spread of the interfacial angles is due to
anisotropy of the interfacial tension, the total variation is only small
compared to the mean value of the interfacial tension.

5.33 Plagioclase aggregates and quartz-plagioclase aggregates

Aggregates of plagioclase grains also tend to form polygonal grains with
good triple points, especially in the amphibolites. However, the impression
is given that the polygons are generally less regular than those of quartz.
Mixed quartz-plagioclase aggregates are similar to aggregates of either
mineral by itself; except that acute angles (mainly in the quartz) are more
abundant. However triple points with the interfacial angles approaching
120° seem to be the rule. Hence the interfacial energy of general quartz-p
plagioclase boundaries must be of the same order of magnitude as plagioclase-
plagioclase boundaries, which in turn, are of the same order as quartz-quartz
boundaries.

Measurement of the interfacial angles between three plagioclase grains at
a triple junction (Spec. 28371, Fig. 5.6) indicates a wider distribution
about 120° than that of quartz in the same rock. The prevalence of angles
around 90° often corresponds to the intersection of boundaries against a
surface nearly parallel to the cleavage in the third grain. Triple junctions
between combinations of quartz and plagioclase grains have not been measured.

5.34 Quartz-mica interfaces

Voll (1960) suggested that the interfacial energy of a quartz-muscovite

Frequency

40
30
20
10

100   120   140

Interfacial angles (degrees)
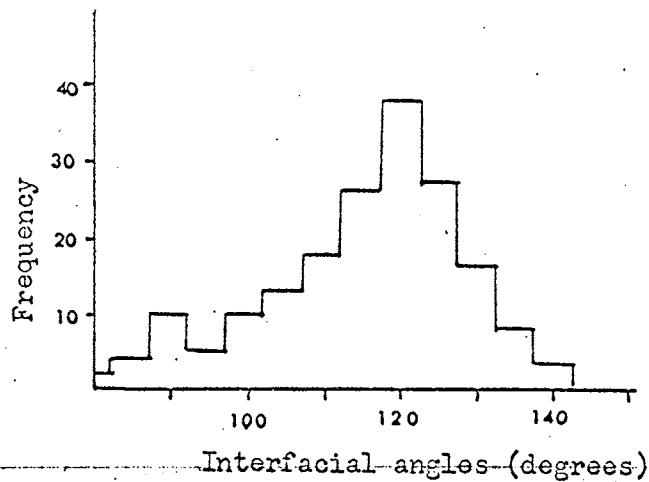
FIG. 5.6

Frequency of interfacial angles observed at a triple junction between
(a) three plagioclase grains and (b) two quartz grains and a muscovite
flake. Angles are summed over 5 degree intervals centered on 120°. Angles
measured at 192 triple junctions.

interface parallel to {001} in the mica is infinite compared with the energy of a quartz-quartz interface. Thus, at a triple junction between two quartz grains and a mica grain the quartz-quartz interfaces will tend to meet the {001} plane of the muscovite at right angles.

Triple junctions between two quartz grains and a muscovite flake are very prominent in the Broken Hill schists. The interfacial angle in the muscovite (opposite the quartz-quartz interface) is always 180° ($\pm 1^\circ$)(by measurement at 100 triple points*) and the quartz-mica interface is parallel to {001} in the mica within the limits of observation. The angles between the quartz-quartz interface and the two quartz-muscovite interfaces are given in Fig. 5.7 . Since the two angles must be symmetrical about 90° only 100 of the 200 measured angles are plotted. 74% of the interfacial angles are situated in the range 90° to 97° and 90% within the range 90° to 101°.

The boundaries involved at the triple junction are general high angle boundaries (from measurement c-axes of quartz and {001} in the muscovite).

Again the spread in the results may indicate insufficient annealing for the attainment of a stable configuration, or anisotropy of interfacial tension. If the latter is the cause, the anisotropy of the quartz-muscovite boundary is probably more significant than that of the quartz-quartz interface (since the latter is only a very small proportion of the energy of a general quartz-muscovite boundary).

Quartz-mica interfaces trending at an angle to {001} in the muscovite are much less regular than the corresponding quartz-muscovite boundaries parallel to {001} in the muscovite. Boundaries of the former type are found at the ends of single grains of quartz and quartz laminae one grain wide. Although the boundary trends as a whole across {001} in the mica, closer examination

*That the angle is sensibly 180° can be observed in almost any M_1 schist on a flat stage. The angle is unaffected by variation in the orientation of the plane of the section.

Frequency

40
30
20
10

100   120

Interfacial angles (degrees)
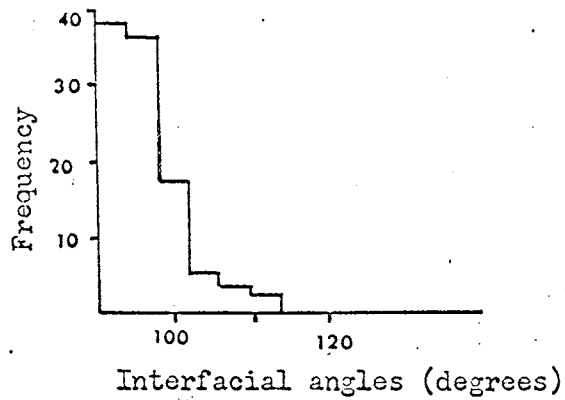
FIG. 5.7

Interfacial cycles between quartz-muscovite and the quartz-quartz boundary, summed over four degree intervals from 90°. The histogram must be symmetrical about the vertical frequency axis passing through 90° (see text). Angles measured at 101 triple junctions.

reveals numerous fine "tongues" of quartz penetrating along the basal

cleavage of the mica (Fig. 5.8a). Strong curvature of the trend of the

quartz-mica boundary is also common. Both types of structures can be

observed in schists in which boundaries between quartz grains meet at good

triple points. Often the termination of the quartz grain by a boundary

transverse to the muscovite cleavage is avoided, by formation of wedge-

shaped grains as illustrated in Fig. 5.8a.

Where a single grain of muscovite forms a triple point with two grains

of quartz the interfacial angles often take the form depicted in Fig. 5.9. .

Actual values have not been determined, mainly because of the imperfect

nature of the quartz-mica boundary across $\{001\}$ in the mica. Angle θ_3(in

section) is usually of the order of 100-110°; angles less than 90° have not

been observed. Contrary to the experience of Voll (1960), quartz-quartz

boundaries are seldom attached to the ends of muscovite flakes, except

where the situation is unavoidable (e.g. where muscovite grains are separated

in a quartz matrix). The quartz-quartz interfaces in the Broken Hill schists

are normally attached to the central portion of the muscovite grain.

If we accept the configuration in Fig. 5.9 as an approximation to stability,

then by resolving the interfacial tensions parallel to ox, we obtain[*]

$$\gamma_2 (\cos(180 - \theta_3) + \gamma_3\cos(180 - \theta_2) - \gamma_1 = 0 \qquad (6)$$

Now γ_3 is very small compared to γ_1 , so that, to a first approximation

$$\gamma_1 = \gamma_2\cos(180 - \theta_3) \qquad (7)$$

Thus, if θ_3 is more than 90° - as is observed - γ_2 is greater than γ_1 . The

conclusion is supported by the penetration of quartz along the basal cleavage

of muscovite grains, thus reducing the total interfacial energy of the aggregate.

The above results have immediate implication in the study of some of the

features of the micaceous schists; some details of quartz-muscovite aggregates

[*]Note that in using this equation we are assuming there are two very distinct
minima in a function describing the variation of against direction for quartz
-muscovite boundaries.

(a)

(b)

(c)
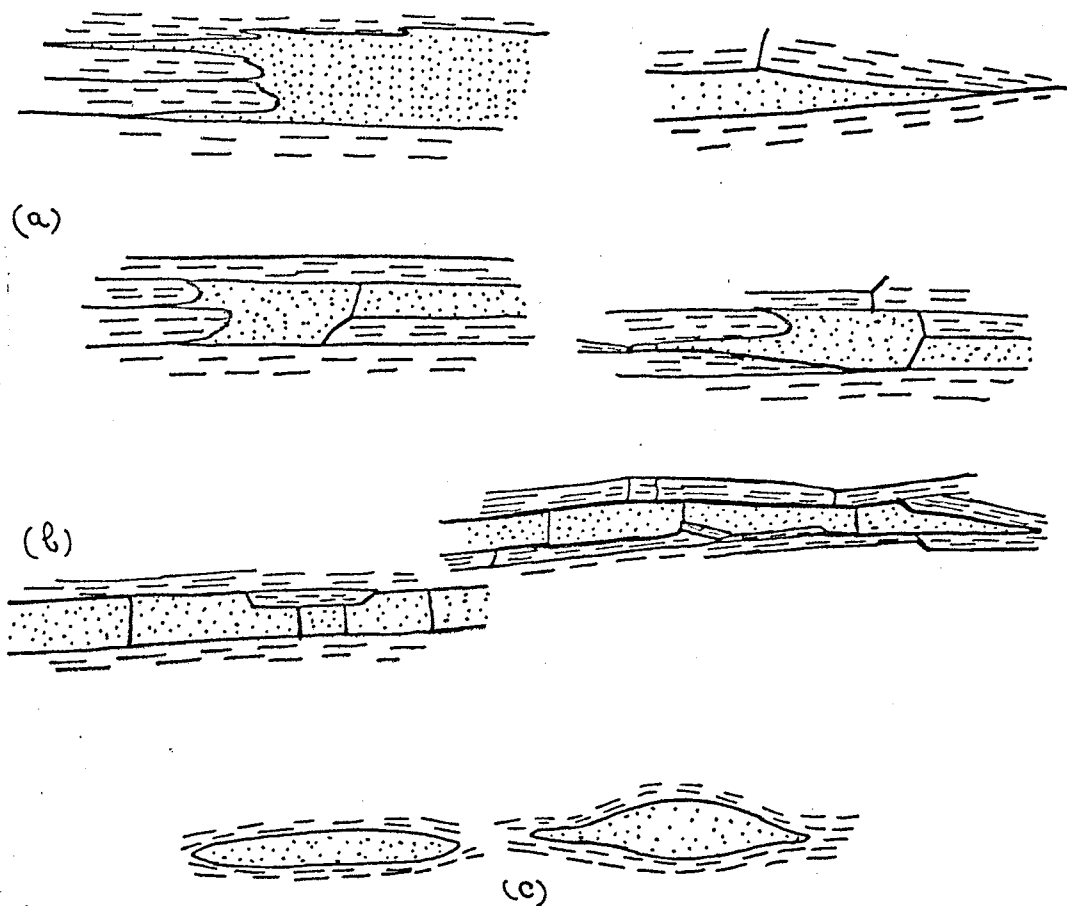
Figure 5.8 (a, b, c).

Features of quartz-muscovite aggregates in M_1 schists (sketched from thin sections; quartz grains stipled, muscovite dashed parallel to traces of {001} cleavage). Of importance is the conformity of the quartz-muscovite boundaries to the basal cleavage of the muscovite, except where the irregular, and strongly curved boundaries cross the mica grain:

(a). Examples of quartz-muscovite boundaries(from Specimens 28372, 28350).

(b). Layers of quartz grains in muscovite aggregates (Spec. 28372).

(c). Shape of quartz aggregates composed of many grains (Spec. 28372); section normal to L_2).
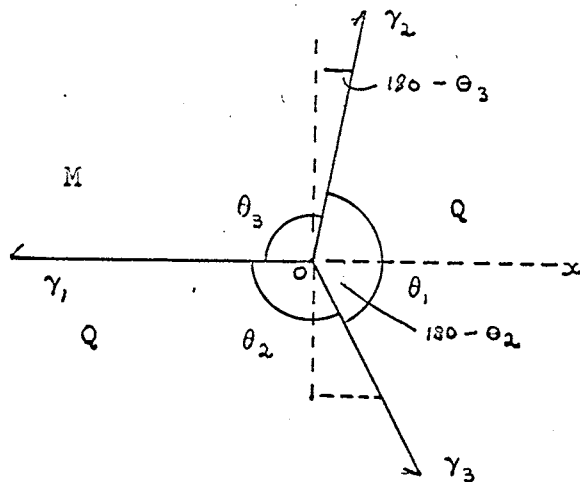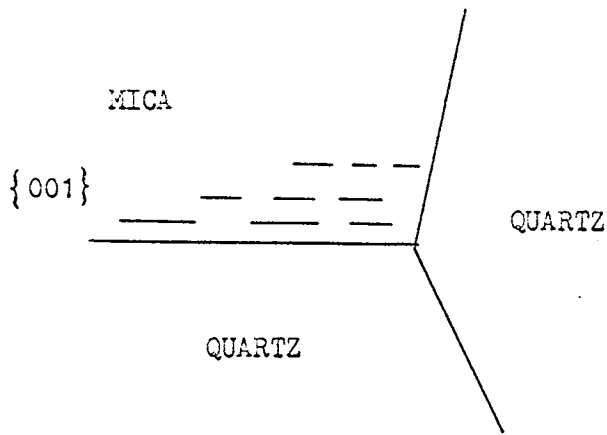
FIG. 5.9

(a). The frequently observed arrangement of interfaces at a triple

point between two quartz grains and a muscovite flake. The trace of 001

in the muscovite is shown as a dashed horizontal line.

(b). Relationship of interfacial tensions and interfacial angles for the

calculations in equations (6) and (7). The arrangement of the various

interfaces is as shown in (a).

in rocks of this type are given in Fig.5.8b. Single grains of quartz in a matrix of muscovite grains are dimensionally elongate in section; ratios of width/length of between 1/15 to 1/20 are common (see especially Spec. 28372). All values from 1/1 up to 1/20 can be found, obviously the location of the plane of the section with respect to the shape of the grain will be a major factor in determining the ratio. Loose sampling of the various specimens has not revealed ratios in excess of 1/20). The dimensional elongation is always parallel to the schistosity of the rock. Elongation of the grains is similar in sections at right angles from the same specimen. Sections sub-parallel to the foliation of the schists suggest - when combined with the above - that the grains are very roughly disc-shaped. Development of this shape might reflect the balancing of the interfacial tension of boundaries across the cleavage of the muscovite flakes at the ends (in section) of the quartz against that parallel to the cleavage of the muscovite. The two tensions will be balanced when the area of the side of the disc is in the same proportion to the area of the circular ends as the values of the two interfacial tensions. (If the grains are considered as ideal discs, and the ratio of 1/20 represents an average for thickness to diameter of a stable disc, then the ratio of the area of the edge of the disc to the area of two circular ends is close to 1/10. Substituting this value in equation (4) gives a value of θ_3 equals $96°$. A ratio of 1/15 for the thickness/diameter ratio yields θ_3 equals $99°$. These angles are of the same magnitude as the interfacial angle frequently observed in the muscovite flake at a quartz-quartz-muscovite triple junction).

It is noticeable that elongate grains of quartz (in section) never transgress the cleavage of the mica flakes they contact, except at their lateral termination. Again this probably reflects the interfacial tensions

of the various quartz-muscovite boundaries.

Of very common occurrence in the schists, are laminae one grain thick (Fig. 5.8b) composed of dimensionally elongate quartz grains. The laminae are strictly parallel to the schistosity. The width/length ratio of the individual grains is usually 1/5 to 1/10. Except for the internal boundaries and their overall dimensions, the laminae are very similar to the single grains of quartz just described; and have - with one difference - probably developed in a similar fashion. The much smaller tension of a quartz-quartz interface compared to quartz-muscovite interfaces parallel to the mica cleavage, mean that thickening of the laminae normal to the schistosity, with corresponding reduction of the area of quartz-muscovite boundary, is a favourable process. The result is a lowering of the total grain boundary energy of the aggregate. However the thickening increases the area of quartz-muscovite interface that transgresses the micas (at the ends of the laminae); hence, the ultimate dimensions of the laminae will depend on a balancing of these three tensions. Since the area of the quartz-quartz interfaces is relatively large, the contribution of these interfaces may be significant.

There is a marked contrast between the shapes of quartz grains in layers many grains thick and the two structures just discussed. The quartz grains in the layers are polygons with no noticeable dimensional elongation. Measurement of the interfacial angles at all-quartz triple junctions in layers of this type provided the data for Fig. 5.5 . The shape of these layers in a section normal to L$_2$ is shown in Fig. 5.8b (other examples have already been illustrated in Fig. 2.2 of Chapter 2). The slightly lenticular outline is characteristic, and as mentioned previously in Chapter 2, with decrease of the length relative to thickness (using S$_1$ as a reference plane) the laminae

grade into rods. In terms of interfacial tension, the development of the lenticular section allows an increase of the area of quartz-quartz interface without producing any quartz-muscovite boundaries that cut across the muscovite flakes at a significant angle. The area of the ends of the layers are correspondingly decreased.

The behaviour of quartz-biotite aggregates parallels that of quartz-muscovite aggregates, although the dimensional elongation of quartz grains isolated by biotites seems to be less marked. It was noted earlier that the absence of intragranular strain in M_1 rocks, when combined with the knowledge that the rocks have been metamorphosed (i.e. recrystallised), indicates that grain growth recrystallisation was a possibility in M_1 rocks. The micro-structure of quartz and plagioclase aggregates agrees well with the micro-structure of aggregates formed experimentally by grain growth in metals (Smith, 1948, MacLean, 1957, for grain growth recrystallisation of rocks see Griggs, Paterson, Heard and Turner, 1960), and with predictions from thermodynamics. The two strongest points in this connection are the reduction of curved boundaries to a minimum and the creation of triple junctions. The relative interfacial energies of quartz-muscovite interfaces and quartz-quartz interfaces allow a ready explanation of some of the features of quartz-muscovite aggregates. However it is necessary to try to evaluate whether interfacial tension has been the prime cause of the structures observed, or if the grain growth is merely modifying structures inherited from the pre-grain growth fabric. The relevance of this question is indicated by the fact that the lenticular laminae in the schists are part of the imposed schistosity and lineation (L_2) of the schists.

The fabric of M_1 rocks, amphibolites and schists, is dominated by one or

both of the fabric elements, S_1 and L_1 imposed during B_1 folding (Chapter 2). In turn, these fabric elements are dependent on the dimensional orientation of muscovite and biotite and to a much lesser extent discoid grains of quartz (S_1), and for the variation in orientation of micas from point to point to form L_2. Dimensional orientation of sillimanite, andalusite and hornblende also contribute to the lineation L_2. The orientation of these minerals, plus their lack of intra-granular strain, proves that M_1 metamorphism can only have been synchronous with, or post-dated B_1 folding. The grain growth texture of quartz and plagioclase signifies that M_1 metamorphism has concluded after the finish of B_1 folding.

Some aspects of the fabric of the M_1 rocks favour the operation of metamorphism during B_1 folding. This relationship has been proposed previously to explain the closed internal layering in the ellipsoids (Sect. 2.33). The data offered by the preferred orientation of the minerals produced by M_1 metamorphism is less equivocal, since final interpretation must depend on the vexed question of the mechanisms of orientation. All the major phases produced by M_1 metamorphism - except plagioclase and garnet, are known to have a preferred orientation of some sort. Quartz apart, the orientation of the minerals (sillimanite, andalusite, muscovite, biotite, hornblende) is a dimensional orientation; hence mimetic recrystallisation may have played a significant role in the evolution of the pattern. This certainly seems to be the case for tufted aggregates of sillimanite and perhaps twinned andalusites growing with random dimensional orientation in the schistosity.

The reason for the aggregation of sillimanite into rods in the sillimanite schists is not clear, although it seems, at least for the coarser rods, that the presence of the few flakes of mica (unoriented) and grains of quartz are vital for their formation. Binns (1963) has proposed that the aggregates are

replacing kyanite porphyroblasts; this might account for the quartz and mica and also the swirling of the sillimanite around these particles. However the almost perfect cylindrical shape of the rods (and also the finer rods without) a core of quartz and mica aggregate) away from the bulged region might result from the direct influence of stress on recrystallisation; the shape is not one likely to result wholly from replacement of kyanite or any other phase.

We concluded in Sect. 2.35 , that the preferred orientation of quartz in B_1 by tectonites probably reflects the symmetry of the stress field that caused the deformation. This is compatible with the recrystallisation of quartz during the course of deformation; but it is not possible to eliminate critically the growth of the pattern from "seed" crystals developed during deformation in a distinct, and later, episode of metamorphism.

The shape of the discoid quartz grains is almost certainly the result of the action of interfacial tension, as shown by the close conformity of the quartz grains to the dimensional shape of the mica grains (e.g. where the grains form wedges between two mica grains). The fact that the shape of the grains have symmetry elements in common with the other fabric elements of the schists (and consequently might be interpreted as evidence of the symmetry of strain of the rocks) is a secondary effect, resulting from the interplay of interfacial tensio and the pre-existing preferred orientation of the mica lattice. Any influence the deformation may have had on the shape of the quartz grains, either in muscovite or quartz aggregates, has been long since obliterated by the influence of interfacial tension.

The rods and laminae present a different picture. Conceivably the rods may have originated by lateral contraction of laminae to satisfy the requirements of interfacial tension. However several facts contradict this hypothesis. The muscovites and biotites deviate around the rods; the deviation is not simply a

matter of grain shape, but also involves the orientation of {001} in the mica.
While grain boundary adjustment might alter the dimensional elongation of the
grains relative to the lattice, it can hardly alter the actual orientation of
the lattice. Also, the elongation of the aggregates to form rods is a deform-
ation feature. It seems that the rods had much the same shape during the
initial stages of recrystallisation (before the onset of grain growth) as they
have now. Grain growth has probably caused the rods to conform more closely
to the pattern of the surrounding micas and also contributed to some extent to
the lenticular cross-section of the laminae, but it is not an important factor
in their overall genesis. The reason laminae developed (predominantly) in
some rocks and rods in others, seems to depend on some intrinsic property of
the original rocks and its influence on the deformation.

Finally, a comment should be made on the micro-structure of the chiastolite
schists. The grain size of quartz and muscovite in these rocks is much less
than that of the same minerals in the adjacent schists (Sect. 5.24). A
further contrast is provided by the irregularity of the quartz-quartz interfaces
and the shape of quartz grains in the chaistolite schists. The presence of
numerous fine inclusions of (?) graphite in the quartz boundaries suggests
that locking of the grain boundaries during grain growth may have been the
cause of these differences.

There is no change of the microstructure or grainsize of M_1 schists across
glide surfaces (Spec. 28350). Nor is there any sign of straining of quartz or
mica in the vicinity of the glide surface. This indicates the glide
surfaces must pre-date the grain growth phase in the schists and are
thus an intrinsic part of B_1 folding.

5.36   Distribution of the Sillimanite and andalusite schists

The distribution of sillimanite and andalusite schists is given in Fig. 5.10. Data for the compilation of the figure are derived from thin sections and the examination of hand specimens in the field. Areas in which andalusite grains are present in the sillimanite schists are denoted by the overlap of symbols. The latter areas should be regarded as the minimum distribution of andalusite in sillimanite schist. For example in one thin section of a sillimanite schist from north of Eldee Creek (Loc. 5240011500 ; Spec. No. 28385   ), a single grain of andalusite was encountered in the thin section, although andalusite was not evident in the hand specimen (before cutting) or in numerous other hand specimens from the same area.

The area can be divided into distinct zones, as can be seen in Fig. 5.10 in which either sillimanite or andalusite is dominant. The nature of the boundary between the two zones is well illustrated in the hinge of the Mt. Robe Synform. The transition from andalusite schists to sillimanite schists is abrupt and occurs in less than 300 feet. There is a region between the andalusite and sillimanite zones in which sillimanite and andalusite schists are mixed, with andalusite occuring predominantly in the more quartzose layers and sillimanite in the more micaceous layers. However to the west of this mixed region andalusite is either absent or appears only as scattered grains (never more than 1% of the total volume of the rock, as opposed to 15% or more sillimanite) in the sillimanite schists.

Much the same situation is reproduced along the boundary between sillimanite and andalusite schists to the north of Mt. Franks, towards and at, Mt. Robe. In particular, about $1\frac{1}{2}$ miles north of Mt. Franks an outcrop of chiastolite schists and sillimanite schists are intermixed in a region several hundred
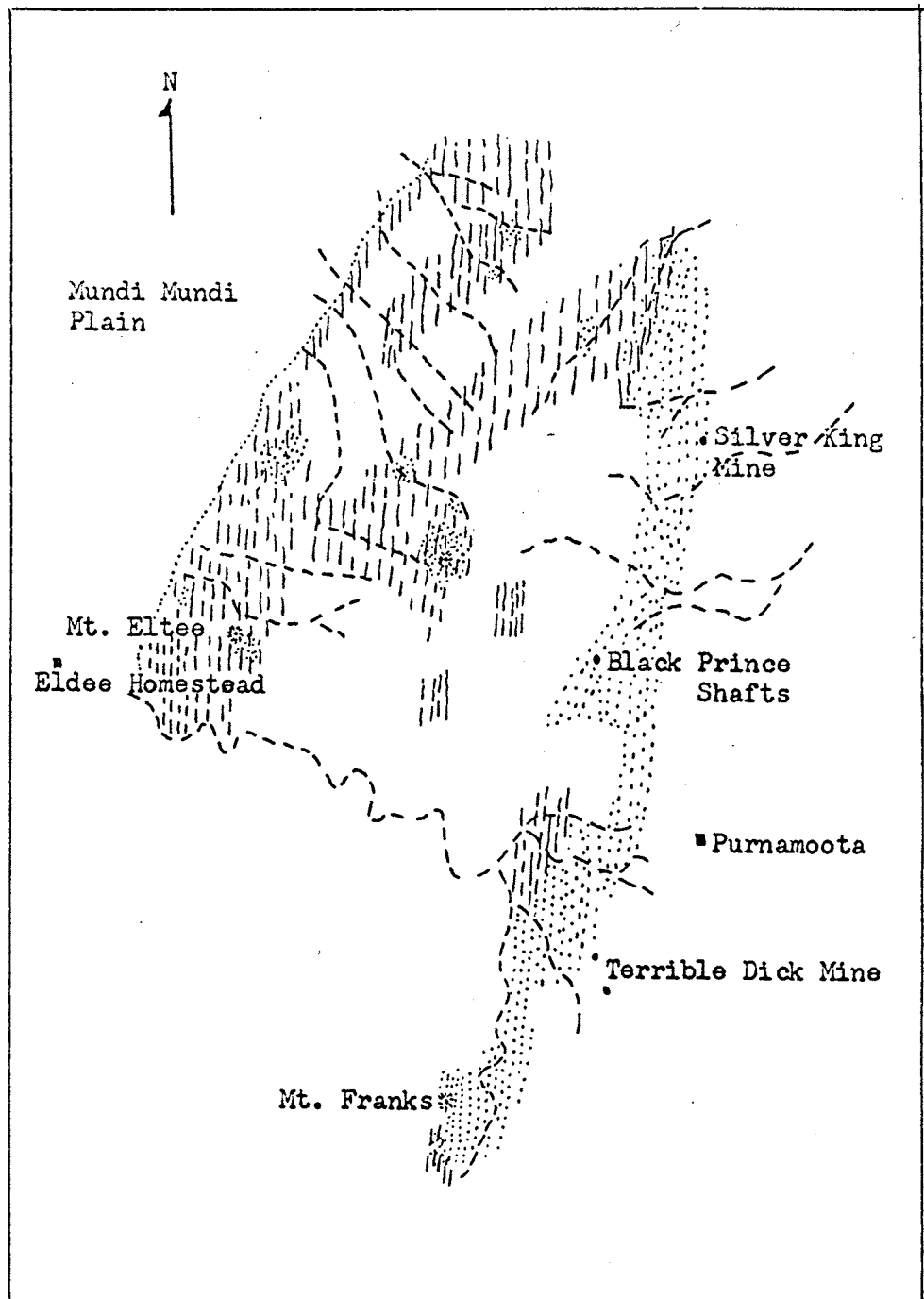
FIGURE 5.10

   Distribution of andalusite and sillimanite schists.

(andalusite;▨ ; sillimanite ▥ ;   scale: 1 inch = 1 mile)

Only areas where andalusite or sillimanite occur are shown.

feet across (normal to the general N-S boundary). On the eastern side of this boundary chiastolite is totally absent from the sillimanite schists.

The reason for assigning the andalusite and sillimanite schists to the same metamorphic event relate mainly to the identity of the fabric of both varieties of schist. The situation is most clear at the locality just to the north of Mt. Franks mentioned in the previous paragraph. Both the andalusite and sillimanite schists are moderately well foliated and the lineation (L_2) although not prominent is clearly recogniseable. The lineation is visible mainly as a "mineral streaking" in the foliation, but there is also a tendency for chiastolites to be aligned parallel to this direction. Sillimanite rods also define the lineation in the sillimanite schists. There is a complete continuity in style and orientation of the schistosity and lineation (as mineral streaking) passing from the andalusite (chiastolite) schists to the sillimanite schists from east to west. The same is true passing around the hinge of the Mt. Robe Synform, although there is a gradual (and continual) change of the gross orientation of the schistosity and lineation around the hinge of the fold.

It is quite clear that the schistosity (S_2) and lineation (L_2 mineral streaking) in the andalusite and sillimanite schists are basically identical, although the lineation is commonly more prominent in the sillimanite schists and foliation is more prominent in the andalusite schists. However even this difference is missing in the quartz-muscovite schists and amphibolites that are intercalated with the andalusite and sillimanite schists; the fabric of these rocks is completely identical in both zones. Finally the microstructure of the rocks which is an intimate part of the fabric of the rocks, is the same in rocks of both zones; and in each case has been created by a metamorphism

that emphasised fabric elements associated with the first phase of folding (B_1).

The crux of Binns' argument for associating the formation of andalusite with the Mt. Robe Fault is a supposed relationship between andalusite and "crenulations" (S_3 and S_4 in this text) in the andalusite schists. This involves (Binns, 1962, 1963):

(1). The identification of the kink bands as a result of the same deformation as the Mt. Franks Fault, and marginal to the fault.

(2). A genetic relationship between andalusite and the kink bands, as a result of which "knots of andalusite often lie at the axes of puckers" (Binns, (1963).

Andalusite is scattered fairly uniformly throughout the andalusite schists, whereas S_3 and S_4 are concentrated in discrete regions. It is only where S_3 or S_4 tends to become penetrative and the andalusite prisms are aligned roughly parallel to L_3 or L_4 that the relationship in (2) is observed. Given that the average cross-section of the andalusite prisms is of the order of 4x5 mm., a high proportion of grains will be intersected by a kink surface in a rock in which the kink bands are less than a centimetre apart on the average. The alignment of the prisms with L_3 or L_4 occurs in areas where L_2 is parallel to L_3 or L_4, and results from preferred orientation of andalusite parallel to L_2. Where L_2 is at an angle to L_3 or L_4, the andalusite prisms can be observed to have a different orientation in each limb of a B_3 or B_4 fold or inside and outside a kink band. The whole range of relationships can be observed passing around the hinge of the fold at Mt. Franks.

The presence of andalusite in the sillimanite schists might imply that the rocks of the sillimanite zone have passed progressively through the andalusite zone (in time). However the aggregates of muscovite replacing the andalusite

are very distinctive, and would be recognised even if the andalusite had been totally replaced. Yet aggregates of this kind do not occur, either in the schists with partially replaced andalusites, or in the sillimanite schists in general. Thus, the number of andalusite porphyroblasts probably never exceeded the number of partially replaced grains now observed. The volume of andalusite in the sillimanite schists is small, and andalusite has never been the dominant polymorph in the sillimanite zone. The preference of andalusite for the more quartzose laminae and sillimanite for the micaceous laminae (in all rocks bearing both or either mineral) suggests that metastable nucleation of andalusite schists in the sillimanite schists has occurred, where the environment has been unfavourable for the nucleation of sillimanite. The sillimanite-andalusite zone boundary predates the main macroscopic folds of the area (Chapter 4). The zone boundary, in fact, may dip quite shallowly under much of the area, and the andalusite in the sillimanite schist might indicate this fact. Finally, it is worth noting that the zone boundary cannot continue very far to the south of Mt. Franks. Reconnaissance mapping by the author in the region south-east of Mt. Franks (not included here) indicates that the boundary swings sharply eastwards or north-eastwards a half-mile to the south of Mt. Franks.

The constantly recurring mineral assemblages hornblende-plagioclase-almandine is recorded by Turner and Verhoogen (1960) as diagnostic of the almandine-amphibolite facies. Cummingtonite can be expected to appear in rocks rich in MgO. The association of sillimanite and muscovite in the pelitic rocks of the sillimanite zone places these rocks in the sillimanite-almandine-muscovite sub-facies of the above facies. The association of sillimanite with orthoclase which marks the upper limit of this sub-facies has not been

found in the area mapped.

No particular difference between the amphibolites of the andalusite zone and the sillimanite zone is discernible. On the basis of the assemblages of the basic rocks, the rocks of the andalusite zone - characterised by the association andalusite-muscovite are also to be classified in the almandine-amphibolite facies. Rocks of a very similar nature in the central Abukuma Plateau of Japan have been placed in the same facies by Miyashiro (1958, 1961)

Binns (1964) has proposed that progressive regional metamorphism of the Willyama Complex passes downwards from the sillimanite-muscovite zone (his Zone A) to a zone characterised by kyanite. The extension into the kyanite zone is based mainly on a supposed correlation between the Willyama Complex and the metamorphic rocks exposed in the Olery Hills of South Australia (50 miles west of Broken Hill); the correlation has yet to be substantiated by mapping to the south and west of Broken Hill. Meanwhile the progressive sequence from Zone A (of Binns) to the andalusite zone is more confidently established, and the relationship of these rocks to the kyanite rocks of South Australia remains as a separate problem. The sequence of zones established in the Willyama Complex (andalusite-muscovite; sillimanite-muscovite; sillimanite-orthoclase^{+}cordierite is very similar to the sequence of zones in the central Abukuma Plateau of Japan established by Miyashiro and co-workers (Miyashiro, 1959, 1961).

5.37   The origin of the amphibolites

The chemical composition and nature of occurrence of the amphibolites throw some light on their pre-metamorphic origin. However, if they are ortho- or para- amphibolites cannot be decided unequivocally at the moment. The chemical analyses of Broken Hill amphibolites published (Mawson, 1912; Browne, 1922; Edwards, 1958; Binns, 1962; a total of 22 analyses, none from the Mt. Robe District) show that

the amphibolites have a composition close to that of an average basalt.
However Binns (1962) comments on two anomalies; the total iron of the
amphibolites is higher and the alkalies lower, than in an average basalt.
The analyses are all of single specimens from widely separated outcrops;
Leake (1954) has pointed out some of the difficulties inherent in using
samples of this type to distinguish ortho- and para- amphibolites. Edwards
(1958) and Binns (1962), from a review of their data, both favour the meta-
morphism of rocks of basaltic composition rather than sediments of unusual
composition.

The regular boundaries of the amphibolites over many miles of contact,
their concentration in a discrete layer (even if transposed) and gross conform-
ity with lithological layering at each point (Chapter 4), would seem to eliminate
intrusive igneous rocks (gabbros) as a source. The general lack of internal
layering (especially relict conglomeratic layers) and the apparent homogeneity
in bulk composition of the amphibolites throughout the area favours basaltic
flows rather than basic tuffs.

The fragments found in the amphibolite at Mt. Robe are compatible with the
reaction between quartzose xenoliths and a basic magma. The modification of
the magma to produce a rim of more acid differentiate (as glass) around the
xenolith and the crystallisation of excess pyroxene in the magma near the
xenolith are typical of such assimilation reactions (Turner and Verhoogen,
1960). On metamorphism, the formation of excess hornblende and of biotite
could mark these reactions. Other quartz-plagioclase layers in the amphibolite
may represent streaks of pegmatitic material generated during crystallisation
of the magma. It seems likely that the amphibolites are basaltic flows repres-
enting (broadly) a stratigraphic horizon in the unmetamorphosed Willyama rocks.

CHAPTER 6

6.10 Introduction

Following M_1 metamorphism the fabric and mineralogy of the schists and amphibolites were modified by metamorphic (metasomatic) changes. If we ignore M_2 metamorphism for the moment the changes can be divided into two groups. It is not certain yet whether these two groups - M_3 and M_4 metamorphisms - represent two distinct metamorphic events, for both are almost certainly connected with the intrusion of the larger bodies of pegmatite. However there are several significant differences between M_3 and M_4 metamorphism and it is worthwhile making the division to emphasise these differences.

M_3 metamorphism is evident as the contact metamorphism (metasomatism) of the schists and amphibolites and can be visibly related to specific bodies of pegmatite. M_4 metamorphism is a general retrogressive metamorphism of the schists; amphibolites and calc-silicates. The correlation of M_4 metamorphism with the intrusion of the pegmatites can only be inferred and not directly observed. One reason for the division is to emphasise the degree of uncertainty in this correlation.

M_3 metamorphism is very local, intense, and has definite (usually sharp) boundaries with the surrounding rocks. In contrast M_4 metamorphism is more pervasive, of regional extent and is usually not very intense. Very few rocks in the area are totally unaffected by M_4 metamorphism. There is no apparent gradation between rocks classified as M_3 and M_4 products. It is possible that M_3 metamorphism was a particular, and very local effect of the intrusion of the pegmatites, the main effect of which was M_4 metamorphism. This, and some other alternatives, will be discussed in Sect.6.47 .

One exception to the classification adopted is certain rocks produced by intense local epidotisation ("patch-epidosites"$ect. 5.43) of the amphibolites. None of the examples discovered can be

connected to a particular body of pegmatite; nevertheless their affinities with the tourmalinised schists are so strong that they are classified as M$_3$ products.

6.21 M$_3$ metamorphism

Contact metamorphism and metasomatism of the schists and amphibolites by pegmatite bodies can be recognised by abrupt changes in the fabric and mineralogy in close proximity to a pegmatite. Distinctive contact metamorphism is only noticeable in the presence of quartz-rich pegmatites bearing some quantity of sulphides (galena, chalcopyrite, pyrites, sphalerite), flourite and tourmaline.

An excellent example of the contact metamorphism of an amphibolite occurs at the Diamond Jubilee Mine. The amphibolite is altered for 40-50 feet about a narrow, steeply-dipping pegmatite dyke located wholly within an amphibolite unit. Intense alteration is confined to within 10-15 feet of the dyke. The intensity of alteration is very irregularly distributed. The amphibolite at some distance from the dyke is a foliated hornblende-plagioclase variety. The first manifestation of alteration is the replacement of the opaque mineral in the amphibolite by sphene, and the introduction of numerous fine "veins" (1 mm.) of epidote and albite and rare tremolite. The sphene forms granular aggregates with occasional cores of the opaque. The veins are surrounded by an area of intensely sericitised plagioclase, interspersed with rare grains of completely clear albite. Away from the veins the plagioclase is moderately sericitised, but it is difficult to determine if this is due to the contact metamorphism or the effects of M$_2$. Even in heavily sericitised grains the outline of the original plagioclase grains can still be distinguished. The veins cut

across individual grains of hornblende and plagioclase grains without disturbing them structurally (Fig. 6.1, Plate 1). Instead a narrow portion of the hornblende grain is replaced by either epidote or, more rarely colourless tremolite. In some instances there is almost complete optical continuity of the tremolite and the host hornblende, but generally there is a difference of 1-2° in orientation of Z in the two minerals. The Z^c angle in both minerals is close to 17°, although the value in the tremolite is probably slightly less (1°) than this value. The tremolite has a negative 2V of 74° ($\pm$ 1°) in contrast to the 2V of the hornblende (76° $\pm$ 1°). Veins of this type are common in the foliated amphibolites throughout the whole area. A discussion of the origin of the veins is given in Sect. 6.30.

Specimens taken closer to the pegmatite have the following mineral assemblages:

(1). Diopside-epidote-sphene (accessory carbonate, quartz and apatite. (Spec. 28321)

(2). Diopside-epidote-actinolite-carbonate-quartz (accessory sphene). (Spec. 28322)

(3). Garnet-quartz-epidote-actinolite-carbonate (Spec. No. 28320)

(4). Epidote-clinozoisite-quartz-garnet (accessory apatite, muscovite, sphene.

The minerals are given in order of abundance, but the distribution varies considerably even within a single thin section. Pods composed of coarse grains of alkali-feldspar and black tourmaline are scattered throughout the rocks near the dyke.

The garnet in Spec. 28230 is a yellow-orange variety and makes up 60-70% of the rock. With the exception of Spec. 28321, which is composed of
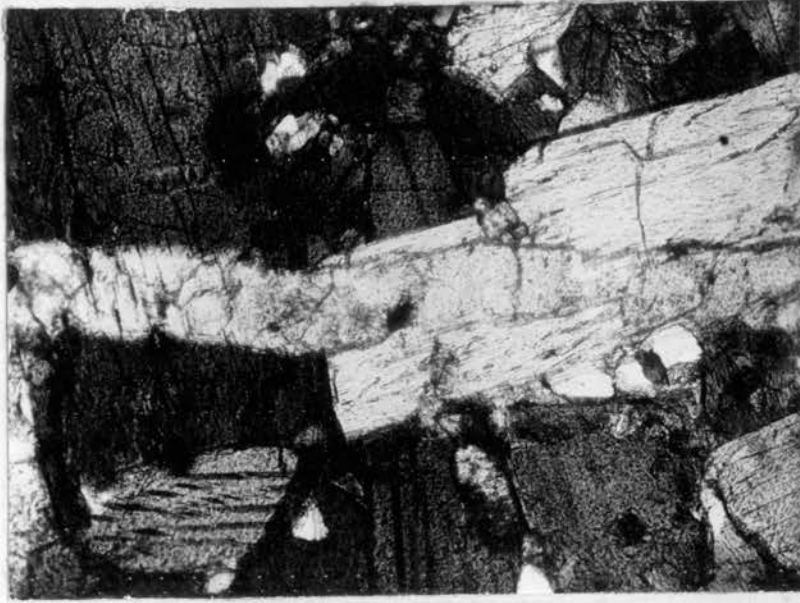
FIGURE 6.1 (PLATE 1)

Tremolite-epidote vein cutting hornblende grains in a slightly contact
metamorphosed amphibolite (Spec. No. 28290). The vein passes horizontally
across the plate and is composed of epidote in the horizontal lath of
hornblende on the right hand side of the plate. To the left of this lath
the vein is composed of tremolite and the cleavage can be seen passing
continuously from the tremolite to the hornblende.

(Field of view is 8 x 6 mm., crossed nicols)

70% diopside grains in aggregates of grains with the shape of equi-axial polygons with well developed triple points, the textures of the rocks are very irregular and the grainsizes variable.

A quartz-rich pegmatite dyke bearing minor copper sulphides is revealed by several shallow shafts 400 feet N. of the main Black Prince Shafts (at the tank and wind-mill). At the margin of the pegmatite the amphibolite has been changed to an albite-epidote-tremolite hornfels. The tremolite (Z=very pale green; Y, X,=colourless, $Z{\char94}c$=20°) appears as fine fibres up to 3 mm. long. Granular epidote is by bulk the main constituent (80%) of the rock and occurs as minute granules or as grains up to 0.5 mm. in diameter. Finely twinned albite laths are concentrated in a few small lenticular aggregates (1% rock). Sphene and opaque minerals, as accessories, are the only other constituents.

The pegmatite itself contains small patches rich (80-90%) in prismatic epidote (1-6 mm.long), which apparently represent fragments of amphibolite incorporated in the dyke.

6.22   Tourmalinisation of the schists

Around the main Black Prince Shafts there is an area of intense tourmalinisation of the schists. The altered zone has an areal extent of several hundred square yards. The tourmalinised rocks have the appearance in hand specimen of dense black, laminated hornfels and are composed almost entirely of alternate laminae rich in black tourmaline and quartz. The lamination in the rock is generally continuous in orientation with the surrounding (unaltered) mica schists; although in places the laminae form structures that are similar to B_1 folds in the schists. Small relict patches of unaltered mica schists are found in the tourmalinised zone.

The former, and the mica schists surrounding the tourmalinised zone are moderately deformed by B_4 folds, but there is no trace of S_4 surfaces in the tourmalinised rocks proper.

The tourmalinised rocks vary between quartz-rich varieties (80% quartz) and tourmaline-rich varieties. In the quartz-rich rocks the tourmaline is dispersed as fine needles (0.1 mm. long) throughout the rock as well as in laminar aggregates. The tourmaline is pleochroic from medium-deep brown (olive) to pale yellow-brown, which combined with its black body colour, indicates the tourmaline contains a high percentage of the schorl (Fe) molecule (Deer, Howie, and Zussman, 1960, Vol. 1). The quartz also occurs in aggregates with fine grains of partially sericitised albite (An_{8-10}, minor quantity). The quartz has discontinuous undulose extinction and fine deformation lamellae. Although the grain boundaries are serrate, the overall shape (in section) of the grain is regular equi-axial polygons with triple points approaching 120 degrees. The size of the quartz is 0.2 mm., which is of the same order as the average schist in the area.

The tourmaline is coarser grained in the tourmaline rich varieties (1-1.5 mm. long) and occasionally has fine cylindrical cores of a bright chrome-green tourmaline. Quartz is also coarser grained (0.2-0.5 mm.) with some very coarse layers (1-2 mm.). Quartz grains are much more ragged in the coarser grained rocks. Flakes of muscovite are scattered through all the rocks.

The rocks are cut by numerous fine quartz-albite veins that carry little or no tourmaline.

Something of the nature of the process of tourmalinisation can be

deduced from a study of two specimens (28269-70) from a locality to
the west of Mt. Robe. Whatever the process is, it is capable of
reproducing many of the features of the structure of the parent rock.
This is beautifully illustrated by Specimen 28269.

The country rock surrounding the tourmalinised schist is a poorly
foliated, rodded sillimanite schist. The foliation of the unaltered
schist (S_1) is emphasised by biotite laminae 1-5 mm. thick and quartz
plagioclase and muscovite laminae.

The completely tourmalinised rock, which outcrops over 100 square
yards, has rods (2-3 mm. in diameter) of the same general dimensions
composed of white microcline, with abundant inclusions of tourmaline
and minor quartz. Often in thin section, the cross section of the rod
is largely occupied by a single grain of microcline (3-4 mm. in diameter)
crowded with inclusions of tourmaline surrounded by a smaller grains
(0.3 mm.) of microcline with fewer inclusions. The larger cylinders in
the altered rock contain the usual bulged region typical of the rods in
the sillimanite schists. In the altered rock this is now the site of a dense
concentration of tourmaline with an overall shape that looks very like
the structure of biotite flakes in rods of sillimanite. The total structure
of the larger diameter rods, except for mineralogy, is identical in style
with the rods in the unaltered sillimanite schist.

The tourmalinised rock is also foliated. Dense aggregates of tourmaline
form irregular black laminae, up to 4-5 mm. thick. Between these laminae
are lighter coloured layers of numerous thin foliae (0.2-1.0 mm.) thick
composed alternatively of microcline and quartz, and tourmaline. The
tourmaline in the laminae and foliae, unlike the inclusions in the micro-

cline, have a strong preferred orientation of their axes parallel to the length of the rods.

The tourmaline (Schorl), both as inclusions in the microcline and in the body of the schist, is black and pleochroic from a medium brown (olive tint) to colourless. The included tourmaline (in microcline) averages one third the size of the grains throughout the schist, which are needles 0.1 mm. in diameter and 1 mm. long.

The microcline is microscopically perthitic and has typical poly-synthetic twinning. A few flakes of muscovite appear as inclusions in the coarser microcline, and are also scattered throughout the rock.

A partially tourmalinised specimen (23270) from the same locality posesses some interesting and peculiar features. The specimen is a poorly rodded sillimanite schist with the following minerals; sillimanite, andalusite, quartz, muscovite, biotite, microcline and tourmaline. Aggregates (not rods) of fibrous sillimanite are concentrated in a thin layer (3-5 mm.) which crosses the foliation of the rock, and only a few rods of sillimanite are scattered through the rest of the schist. The sillimanite is fresh, and apparently unaffected by metasomatism. The biotite, the typical red-brown variety where fresh, generally has a slightly bleached appearance. Fresh biotite and sillimanite go together and tourmaline is less prominent in these portions of the rock. Numerous needles of tourmaline have grown through the altered biotite flakes to give the densest concentration of tourmaline in the rock. The microcline forms grains up to 5 mm. across

and is crowded with inclusions of quartz, tourmaline and muscovite.
The tourmaline and microcline are optically identical to that described
in the previous specimen. In section (parallel to the L_2) the andalusite
forms ragged laths up to 1 cm. long, with numerous inclusions of quartz,
biotite, tourmaline and muscovite. There is a tendency for slightly
coarser muscovite (1-1.5 mm.) to concentrate at points around the margin
of the grains. The andalusite is colourless and shows no trace of
sericitisation. Single grains of andalusite seem to contain whole sections
of the S_1 and L_2 of the original schist (Fig. 6.2, Plate 1). Examination
of the hand specimen reveals that the andalusite grains form rods several
centimetres long. The rods are elliptical in cross-section with the
maximum diameter (1.0-1.5 mm.) in S_2. Andalusite, by volume is about 10%
of the rock. The andalusite grains are apparently oriented with their
c-axes roughly parallel to the length of the rods.

The andalusite is not easy to account for in this environment. It
seems to be a transient phase in the process of tourmalinisation, since there
is no andalusite in the completely tourmalinised rock, and only a few grains
(1%) are present in the untourmalinised sillimanite schist. Its habit
is in no way akin to the usual occurrence of andalusite in the sillimanite
schists; the only point of resemblance is the few grains of coarse muscovite
around the edge of the andalusite grains. Three tentative suggestions are
offered:

(1). The andalusite has grown from pre-existing andalusite grains in the
sillimanite schist. This theory encounters difficulties in explaining the
number of andalusite grains, even if we permit the volume of andalusite to
increase by growth; the number of rods in this schist is far greater
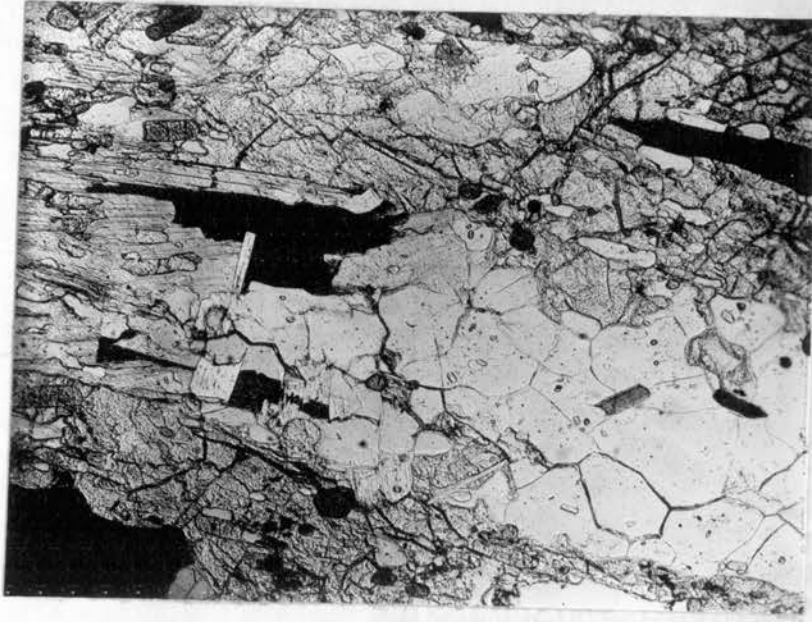
FIGURE 6.2 (PLATE 1)

Details of inclusions in an andalusite grain in a partially tourmalinised sillimanite schist (Spec. No. 28270). The plate illustrates portion of an andalusite grain (medium grey - high relief) containing a lamina composed of quartz grains (white) which passes out laterally into a muscovite lamina (centre-left). A few tourmaline inclusions (high relief - dark grey) are also present.

(Field of view is 6 x 8 mm., crossed nicols)

than the usual number of andalusite grains in the sillimanite schist.

it is necessary to assume that the original rock was a very particular and very local instance of andalusite occurring in sillimanite schist. However this theory might account for the partial ruff of muscovite as a relict from the parent rock.

2. The andalusite represents a stage in the replacement of sillimanite by microcline. This would certainly explain the shape of the andalusite grains and their volume. It fails to fully explain the few remaining rods of sillimanite and the layer of sillimanite. This difficulty is resolved to some extent by the previously noted observation, that the degree of alteration is very irregular and that the sillimanite left is not associated with tourmaline. The layer of quartz crossing the andalusite grain in Fig. 6.2 , may represent the material contained between the two arms of a bifurcating rod in a section slightly oblique to the two rods.

(3. The andalusite is a result of the reversing of the reaction andalusite ————$\Longrightarrow$ muscovite. Andalusite grains nucleated and grew preferentially along the intersection of two trains of muscovite$[1]$, which parallels L_2 in the rock and the orientation of the sillimanite rods. Growth in this fashion would produce the present shape of the andalusite grains. Presumably if the grains also expanded out along the muscovite lamellae in the schists they might enclose rods of quartz, to produce the structure illustrated in Fig. 6.2 . This explanation is favoured, for the rods of andalusite pass laterally into mica-rich bands (in section) of the schist.

With a lack of specific chemical data it is impossible to state definitely which elements have been added and which removed during the metasomatism.

[1]
See Section 2.21 for description of fabric of sillimanite schists.

Certainly boron, iron and water must have been added and possibly

manganese and alkalis (mainly K O). The tourmaline and microcline
$$2$$
have not replaced individual minerals, but the preservation of the

structure of the rock, and the tendency for tourmaline to concentrate

in biotite laminae and microcline in micaceous laminae (in the partially

replaced specimen) and the sillimanite rods suggests that the added

material is fixed by very short-range reactions; that is, the reactions

are governed, to some extent, by the availability of elements already

present in the parent rock. The preferred orientation of the tourmaline

can be explained, if individual tourmaline grains are influenced either
[1]
during nucleation or growth , by the orientation of the lattice of the

enclosing grain.

6.30 The patch epidosites

A type of epidosite occasionally found in the foliated amphibolites

shall be referred to as "patch-epidosites". The patch-epidosites are

small (12-30 cm.) and roughly sub-circular in plan, and are traversed,

particularly in the outer portion of the patch, by numerous veins of

epidote with or without minor albite and quartz. The specimens to be

described in detail are from a small patch of epidosite (Locality

Specs. 28299, 28300, and 28301) in a body of well foliated amphibolites.

A second suite of specimens from Eldee Creek (Loc. 53406107000 .

28350, 28351, 28352) exhibits only minor differences. In neither inst-

ance - as is typical - is the epidosite visibly connected to a

pegmatite dyke, and the enclosing amphibolites show negligible traces of

retrogression. The patch at the first locality, has a bright green

epidosite core, which grades outwards, by decrease in the intensity of

[1] i.e. nuclei of all orientations are formed, but those of a particular
orientation with respect to the surrounding lattice grow preferentially.

colours into the amphibolites. The foliation can be traced from the amphibolite right through the patch of epidosite, although in the core it is less distinctive.

The amphibolite is a normal M_1 type, composed of 50% hornblende, 50% plagioclase (An$_{52}$) and a trace of opaque mineral. The rock in the outer part of the core is composed of an array of hornblende grains similar in shape, distribution, and optical properties to the hornblende in the unaltered amphibolites. The granular epidote (0.1-0.5 mm.) fills all the space between the hornblende grains and laminae of hornblende and epidote define the foliation.

The epidosite in the core of the patch (Spec. 28301) is composed of an amphibole, epidote and sphene. The amphibole, with X=colourless, Y=pale-medium green, Z=pale-medium blue green, has the same general pleochroism as the hornblende in the amphibolites, but the absorption is many times weaker. The Z^c angle averages 14° and the amphibole may be either the hornblende or, more likely, an actinolite. The grains are ragged with the average grainsize (0.5 mm.) much the same as that in the amphibolite. The granular epidote (0.1-0.5 mm.) is slightly greener (pale-green) in thin section than the epidotes encountered in most rocks. Sphene (less than 1%) appears as string-like aggregates. Of some importance is the presence of quartz as scattered grains. Judging from the hand specimen there is every gradation in composition from the epidosite at the core to the amphibolites.

Veins which traverse the patch epidosite are 1-5 mm. thick and are made up entirely of granular or bladed epidote. Blades up to 5-6 mm. long are found in some of the thicker portions of the veins. The margins of

the veins are sharp and truncate individual hornblende grains without any structural disturbance of the grains. A thin layer of very fine epidote (($\angle$ 0.01 mm.) separates the coarser epidote of the veins from the enclosing rocks. The fine and coarse epidote in the vein and the epidote in the enclosing rocks are all optically identical (monoclinic, negative with a 2V of 80-85°) and there is no trace of zoning in individual grains.. In one specimen (28300) where a number of veins intersect, numerous prisms of epidote criss-cross a void. Numerous fibrous projections from the prism suggest they may have grown in a non-solid medium. The open spaces are apparently not due to weathering out of some component, for the rocks are only superficially weathered. Moreover, in one of the specimens from Eldee Creek there is a distinct tendency for the b-axes of the epidote to be aligned normal to walls of the vein.

The specimens from Eldee Creek differ only in that the epidosite and the amphibolite are both richer in quartz than the specimens above. Also veins cutting the rock carry a few percent of clear albite and scattered quartz.

Initially only the plagioclase is replaced by granular epidote with, judging from the optical properties, no participation of the hornblende. The epidote effectively "pseudomorphs" the plagioclase, leaving the structure, and in particular the microstructure, of the rock intact. With more intensive alteration the hornblende is also affected and the opaque mineral (?ilmenite) also reacts. At this stage, the distinctive structure of the amphibolite is only crudely preserved by the alternation of epidote-rich and epidote-poor laminae and the microstructure is largely obliterated.

The fabric of the partially altered amphibolite (Spec. 28300) implies, as a first approximation, that the law of equal volumes (Turner, 1948) can be applied to the reaction plagioclase ———————⟶ epidote. This is most obvious in the case of single grains of plagioclase in an aggregate of hornblendes. By applying calculations of the type similar to those used by Turner (1948, p.111) we can make an estimate of metasomatic changes involved in the reaction. We shall assume the plagioclase is anorthite, since the replacing mineral is calcium-bearing silicate, and this assumption sets an upper limit to the amount of calcium that can be contributed from the replacement of the plagioclase. The data assumed for the reaction are:

epidote, $Ca_2Fe^{3+}_2Al_2O.OH(Si_2O_7)(SiO_4)$, S.G. = 3.49

anorthite, $CaAl_2Si_2O_8$, S.G. = 2.76
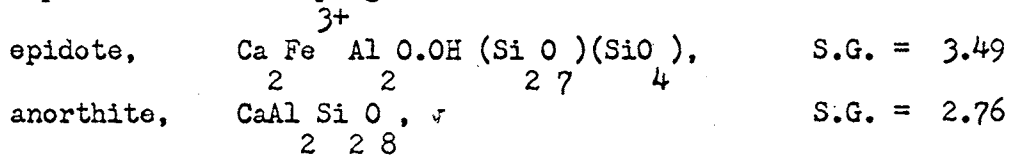
Then the equation representing the equal volume replacement of anorthite by epidote of this composition can be written as;

$$CaAl_2Si_2O_8 + 0.44\ CaO + 0.17\ SiO_2 + 0.72\ OH + 0.72\ FeO \longrightarrow$$
278 gm. 24.9 gm. 10.1 gm. 12.3 gm. 52 gm.

$$0.72\ Ca_2FeAl_2O.OH(Si_2O_7)(SiO_4) + 0.28\ Al_2O_3 \qquad \text{———————— (1)}$$
348.3 gm. 28.3 gm.
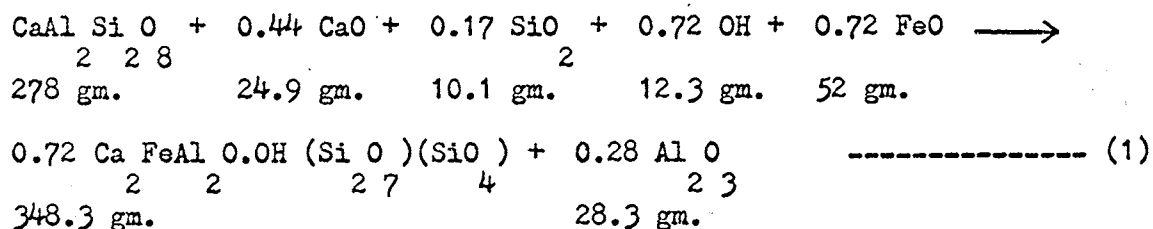
This can be re-written (approximately) as;

$$3\ CaAl_2Si_2O_8 + CaO + \tfrac{1}{2}\ SiO_2 + 3OH + 3\ FeO \longrightarrow$$
$$3\ Ca_2FeAl_2O.OH(Si_2O_7)(SiO_4) + \tfrac{1}{2}\ Al_2O_3 \qquad \text{———————— (2)}$$
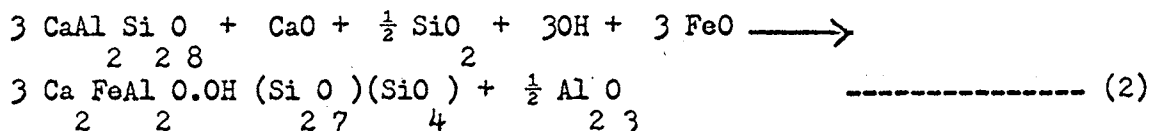
The composition of plagioclases determined in the amphibolites does not exceed An_{55}, so that in natural examples an even greater supply of CaO than that of equation (2) will be required to satisfy the right hand side of the equation. If, as the lack of change in the optical properties indicates,

the amphibole is unchanged during the initial stages of metasomatism,

then the CaO, SiO$_2$, OH and FeO can only be of metasomatic origin.

A source for some of this material can be found in the core of the

patch. For example, the breakdown of the opaque mineral may yield some

iron, but it seems unlikely, particularly if the volume of epidote veins

is considered , that all the material necessary can be derived internally.

It is more difficult to specify the changes in the core of the patch,

for the amphibole is now participating in the reaction, and the precise

nature of the changes in its composition are unknown. If we assume the

change is from hornblende to an actinolite then it is doubtful that the

reaction could supply in any quantity the material on the left-hand side

of equation (2). It may, however, contribute alumina to the right-hand side.

Also the breakdown of the opaque to sphene could supply some iron to the

system, but the total volume of opaque is very small. Considering the

overall volume of epidote in the epidosite and veins it seems fairly certain

that there has been introduction of all the elements (other than anorthite)

on the left-hand side of equation (2). The tourmalinisation of the schists

also signifies the metasomatism of at least iron and water, and in this

respect, the epidotisation is similar to the tourmalinisation of the schists.

In fact, it seems probable that the two processes are genetically related,

and that the elements fixed from the metasomatic agents are dependent on the

bulk chemistry of the rock being metasomatised. This also agrees with the

observation that in the tourmalinisation of the schists, the metasomatic

material is fixed by very localised reactions, apparently dependent in part,

on the chemical composition of the rock at each point.

The explanation in the previous paragraph can be extended to the veins

of epidote, albite and quartz cutting foliated amphibolite and the contact

metamorphosed amphibolites at the Diamond Jubilee Mine. Micro-fractures

cutting the rock and rupturing without displacing individual grains could

provide a path for permeating "volatiles" or fluids carrying lime, silica

and iron.

M_3 metamorphism is found in a number of other localities apart from those

specified in the preceeding discussion. Tourmalinisation of the schists is

fairly common over restricted areas in the strip of rocks along the eastern

margin of the Mt. Robe Stock and in the area northwards and westwards of

Mt. Robe. However, tourmalinisation has not been detected in the whole area

north and west of the Aller Creek Stock. The intensity of tourmalinisation

varies greatly from locality to locality but is more or less uniform at any

one locality. Diopside and diopside-epidote rocks in amphibolite are also

located around a sulphide bearing pegmatite north of Eldee Creek (50000113200)

Numerous other examples of patch epidosites occur in the general area from

which the first suite of specimens described were taken.

6.41 M_4 metamorphism

Two different circumstances are involved with regard to M_4 metamorphism.

The schists and amphibolites throughout the area have been affected by a mild

or even moderately intense retrogressive metamorphism that leaves the original

fabric of the rocks largely unaffected. This type of metamorphism is confined

mainly to the alteration and pseudomorphing of individual grains.

The most obvious evidence of this in the schists is the replacement of

andalusite by a fine mesh of sericite. The idioblastic outlines of the

andalusite porphyroblasts remain, even where replacement is almost complete.

The systematic array of quartz inclusions in the fresh andalusite also persists in some aggregates. Relict cores of andalusite and the distinctive shape of the andalusite porphyroblasts eliminate any problem of identifying the replaced material.

Coincident with fairly extensive alteration of the andalusite is a change in biotite. Fresh porphyroblasts of red-brown pleochroic biotite may exist side by side in a thin section with an altered variant. Relict cleavage is still visible in the altered material and sections of the altered biotite normal to $\{001\}$ are still strongly pleochroic from a dirty brown to a pale (dirty) yellow. However the interference colours in all sections are low first order colours, which are often slightly anomalous. At very high magnification (X1200) the porphyroblasts can be resolved into fine plates of interleaved chlorite, biotite, and muscovite, in that order of abundance. Rare plates of a fine opaque mineral are disseminated in the relict cleavage.

The chlorite is pale green and virtually non-pleochroic, so that the stronger pleochroism of the biotite is seen on rotation in plane-polarised light. However the plates of both biotite and chlorite are apparently very fine, so that the birefringence colours are low, and reflect the anomalous colours of the chlorite. It is not evident whether the muscovite is a result of alteration, since muscovite and biotite are occasionally interleaved in fresh biotites. With progressive alteration distinct laminae of chlorite may appear in the altered biotite.

Discrete flakes of chlorite accompany the altered biotite in many schists, but chlorite never accompanies fresh red-brown biotite. The chlorite is apparently the ultimate product of the alteration, and not a member of the original assemblage.

Alteration of the plagioclase to fine sericite and (?) clinozoisite as with andalusite and biotite, does not obliterate the shape of the grain. The outlines of fairly extensively altered grains of plagioclase forming triple junctions with each other and with quartz grains are easily discernible.

The alteration of sillimanite is more difficult to trace. The original fibrous nature of the sillimanite would make the detection, even if such occurs, almost impossible. However in some sillimanite schists, with well developed rodded structure, part of the rod may consist of a fine mesh of sericite in which only a few fibres of sillimanite are visible. The association of sericite and sillimanite is foreign to the schists in which the biotite and plagioclase (and garnet) are fresh, but is typically found in schists with altered biotite and chlorite. It seems certain that some of the sericite is the product of the alteration of sillimanite.

Garnet is sometimes partially replaced, especially along fractures, by an indefinite chlorite material.

A peculiarity of many slightly retrogressed schists is the presence of porphyroblastic flakes (up to 6 mm.) of muscovite which are oriented with their basal cleavage at a high (but variable) angle to the schistosity. Fine fibres of sillimanite and dimensionally elongate grains of quartz, both oriented parallel to S_1, are usually prominent as inclusions in the muscovite. The quartz grains resemble the isolated quartz grains found in muscovite-rich portions of M_1 schists. The muscovite porphyroblasts themselves are situated in muscovite-rich laminae in the schists and are normally bounded by finer muscovite flakes similar to those in a typical M_1 schist. Only a few scattered porphyroblasts occur in any one specimen and there is a complete contrast in grainsize between the coarser muscovite and the finer

flakes inherited from the M_1 schist. The retrogressive effects in some of the schists bearing muscovite are minimal and consist of little more than mild chloritisation of the biotite.

The retrograde effects described so far are relatively mild and the nature of the original M_1 rock can be discerned without undue difficulty. This type of metamorphism is independent of the proximity of pegmatites. More intensive retrogression in the schists results in the gradual obliteration of S_1 and L_1 fabric by the growth of disoriented flakes of muscovite and chlorite. While it is true that this type of metamorphism is often spatially associated with the pegmatites, the converse is not true. Schists abutting the pegmatites, or enclosed with pegmatites, may show little or no retrogression.

As the intensity of the retrograde metamorphism increases, the choice of a standard for comparison becomes harder. Consequently it is more difficult to distinguish critically between features that may be the sole products of M_4 metamorphism and features that may be due (at least in part) to some variation in the M_1 rocks not previously encountered in the less altered or unaltered rocks. The problem is less acute in the amphibolites, because of their greater initial uniformity of composition.

The most obvious difference between the less altered and more altered rocks is the prominence of unoriented, coarse flakes of muscovite (5-10 mm.). In thin section there is generally a continuous gradation of size of the muscovite from the finest sericite to the coarse flakes. In specimens from the north-east side of Mt. Robe (Spec. Nos. 28262, 3, 4), the coarser grains of muscovite are located in trains of finer muscovite, through which fine wisps of sillimanite can still be discerned. In hand specimen the aggregates

of muscovite (coarse and fine) form a streaky lineation on the crude

foliation present in the specimen, resembling the lineation sometimes

formed by aggregates of sillimanite in S_1 (in unrodded sillimanite schists).

It appears that the coarser muscovite is growing from sericite that replaced

sillimanite. The same specimens as mentioned above have numerous flakes

of muscovite that are the same general size as muscovite in M_1 schists.

Rosette-like aggregates of muscovite are also common (Spec. No. 28263).

These flakes are oriented throughout the rock, and seem to be relict flakes of

muscovite from the M_1 rocks. The muscovite developed during more extensive

retrogression of the schists differ from the porphyroblastic muscovite found

in slightly altered schist in its lack of inclusions and complete gradation

of grain size.

Very often in specimens in which the growth of randomly oriented muscovite

is quite marked, chlorite flakes have a distinct, although poor, preferred

orientation. The chlorite also tends to be concentrated in laminae. The

superposition of these two effects gives rise to a crude foliation in the

rock which parallel any trace of relict S_1. The chlorites in this case seem

to be the end product of the reaction biotite $\longrightarrow$ chlorite, thus retain-

ing the preferred orientation of biotite in the parent M_1 rock. A brownish

tinge in the pleochroism of some chlorites and the similarity of size of the

chlorite and biotite in M_1 rocks support this contention. In other

specimens the chlorite lacks any orientation; but even here there are traces

of what appear to be chloritised biotite (Spec. Nos. 28362, 3). It is

possible that a chlorite fabric of this type could result from the replace-

ment of randomly oriented biotite in a parent quartz-muscovite-biotite rock.

M_1 rocks in which biotite is unoriented were mentioned briefly in Sect. 5.21.

Very little or none of the chlorite then may have been nucleated as discrete

grains.

Quartz in the strongly retrograded rocks has much wider limits of grain-size (0.1 to 2 mm.) and the average grainsize is much coarser (1-1.5 mm.) than in M_1 rocks. Since the coarser grainsize is limited to strongly retrograded rocks, and the grainsize of M_1 or slightly altered M_1 rocks never exceeds 0.2 mm., the coarseness of the grains must be related to the processes of M_4 metamorphism. The nature of the microstructure of quartz aggregates in M_4 rocks contrasts strongly with that of M_1 rocks, this topic is taken up in the next section.

Clear, well twinned grains of albite (An_{4-9} where determined by Universal stage), of much the same grainsize as quartz, are present in some specimens in which coarse muscovite and chlorite abound. Unlike plagioclase in the M_1 schists, the shape of the albite is irregular and the grains are divided into many fine twin lamellae (albite-low). The absence of alteration in strongly altered rocks proves that the albite is a product of M_4 metamorphism.

Chloritoid has only been encountered in rocks at Mt. Robe. In a specimen described previously by Browne (1922, p.305, Spec. No. 13517, the description here is from the authors own examination of the slide), the chloritoid occurs with sillimanite, andalusite, altered biotite, muscovite, garnet, chlorite, quartz, and sericite. Tourmaline and an opaque mineral are important accessories. Retrograde metamorphism is expressed by the almost complete alteration of the biotite to chlorite, and probably sillimanite to sericite. The andalusite is partially replaced by a ruff of muscovite. Garnet is dis-tributed as a few small polygonal grains throughout the slide, and also as rare inclusions in the andalusite and the muscovite replacing the andalusite. Chlorite, only weakly pleochroic in light greens, is only a very minor component. Smaller grains of quartz in the slide (0.1-0.2 mm.) have only slight

undulose extinction. However the larger grains are traversed by fine fractures filled with sericite. Only a few grains of chloritoid are present, with optical properties in agreement with those to be described below.

Chloritoid has also been examined in two specimens (Spec. 28276, 28277) from outcrops a hundred yards west of the Mt. Robe Trig. Station. Both specimens are unfoliated. The chloritoid in both specimens forms ragged, unoriented laths up to 1.5 mm. long, with {001} lamellar twins. Rosettes of chloritoid are visible in Specimen 28277. The mineral is optically negative with a 2V close to 90°*. The pleochroic scheme is X=medium green, Y=medium blue-green, and Z=colourless. Quartz is the only mineral detected as an inclusion in the chloritoid, and then only in minor quantities.

The bulk of both specimens is made up of a ragged collection of grains of chloritised biotite, quartz and muscovite set in a matrix of sericite. The muscovite forms a few flakes up to 2 mm. long but ranges over all sizes down to less than 0.01 mm. The grains almost always exhibit some evidence of deformation, particularly by kinking and flexuring of the basal cleavage. Many of the larger flakes have a peculiar fragmented appearance, in which the muscovite is separated along the {001} cleavage by a fine layer of sericite. Sillimanite fibres are included in some flakes of muscovite.

The quartz, like the muscovite has a very variable grain size (0.1-1 mm.) and is extensively strained (discontinuous undulose extinction) with deformation lamellae in a few grains. The grains are cut by numerous fine fractures filled with sericite. A dirty mixture of chlorite, an opaque, muscovite, and minor biotite apparently represent the last remmnants of biotite porphyroblasts (2-3 mm.) in the parent rock. Chloritoid grains sometimes cut across these altered biotites, but the writer has not seen any evidence, as suggested

* Values measured for a chloritoid from Mt. Robe by Misar (1963) have an average 2Vx of 82 degrees.

by Misar (1963) that the chloritoid is preferentially replacing biotite.

The last two specimens show signs of relatively intense deformation (compared with that normally observed in M_4 rocks), but not of the same kind as observed in rocks from M_2 zones (Sect. 6.4b). These rocks are located in a thin layer (1 foot thick) which is unfoliated; there is in this layer and the adjacent schists considerable development of slickensides on the joint faces. Although retrogressed S_1 and L_2 can be recognised without difficulty in the surrounding schists. The specimen collected by Browne lacks any trace of intensive deformation. Misar (1963) found chloritoid in S_3 or S_4 tectonites to the southwest of Mt. Franks (in hand specimen) in rocks which have definitely not been produced by metamorphism in fault zones. Thus, chloritoid is also a product of M_4 metamorphism and not M_2 metamorphism (as defined in this text); indeed not a trace of chloritoid has been found in known M_2 zones.

If the retrogression of the schists had been carried to its conclusion, the ultimate rock would apparently have been a quartz-chlorite-albite-muscovite hornfels, with, very locally, chloritoid. However, in no specimens examined have all the traces of the original schist been totally obliterated. The ultimate M_4 rock has a mineral assemblage typical of the albite-epidote hornfels facies (Turner and Verhoogen, 1960). The mineral assemblages of the unfoliated amphibolites, to be described in the next section, signify the same facies.

6.42 Unfoliated Amphibolites

In general the study of M_4 in the amphibolites is more difficult than in the schists. The nature of the problem is best outlined by reference to the area extending from the Black Prince Mine to the Silver King Mine, where numerous large units of amphibolite outcrop.

The basic metamorphic rocks within this area consist in part of well-foliated and lineated amphibolites and in part of rocks whose main mafic component is xenoblastic grains of a pale coloured amphibole. A very crude foliation may be detected in some specimens of the latter, but usually they are "mottled" (built up of irregularly shaped aggregates of amphibole and quartz-feldspar).

The amphibole is only weakly or moderately pleochroic according to the scheme -

X = very pale green

Y = pale or medium green

Z = pale or medium blue-green

Absorption   Y=Z > X.

The pleochroism and absorption are weaker than that of the hornblendes in the foliated amphibolites. Also the $Z^{\wedge}c$ angle in the paler amphibole is generally less than that of hornblendes, ranging from 13-18° (18-24° for the hornblendes). The amphibole is optically negative with a large 2V (measured values lie in the range 2V$_z$ = 101-104°). Twinning on {001} is common. X-ray powder photographs of the strongly pleochroic and the less pleochroic varieties of amphibole are virtually identical. The properties of the amphibole lie in the overlap range between members of the tremolite-ferroactinolite series and the hornblende series (Deere, Howie and Zussman, 1962, Vol. 2). Distinction between members of these two series can only be

properly made by chemical analysis.

The remainder of the rock is occupied by grains of plagioclase in various stages of alteration and minor quartz. In some specimens the plagioclase is almost wholly replaced by a mesh of sericite and an epidote mineral (clinozoisite, where the optical properties are determinable), and it is only with difficulty that the relict grains can be distinguished.

In the midst of the altered plagioclase there may be a few grains of clear, unaltered plagioclase, and in one specimen from another locality (1) interstices between the amphibole grains are entirely occupied by clear albite (An$_5$). Unlike the plagioclases of the foliated amphibolites these grains are elongate laths, multiply twinned on the albite law with numerous fine lamellae. The grains are crowded with inclusions of fine acicular amphibole, with the optical properties of the main amphibole, and quartz. A few zoned grains have been detected in Specimen 2833q.

There seems little reason to doubt that the unfoliated amphibolites have resulted from the retrogressive metamorphism of the foliated amphibolites, although details of the changes are lacking. Slight retrograde metamorphism of the foliated amphibolites proceeds by sericitisation of the plagioclase, but leaves the amphibole and the fabric of the rock unchanged. There is a gap between alteration of this type and the more extensive changes necessary to produce the unfoliated amphibolite.

Scattered areas of foliated amphibolite do occur in the bodies of unfoliated amphibolite, testifying to the pre-metamorphic origin of the whole body. Grains of plagioclase in the foliated rocks are heavily sericitised; similar grains, with polygonal outlines exist in the unfoliated amphibolites. The lack of foliation in the unfoliated amphibolites is also significant. It

is unlikely that any rock could have survived B_1 folding and M_1 metamorphism without some imprint of the deformation. Intense retrogressive metamorphism of the schists has occurred in an environment where the new phases were not directly oriented and the final rock is unfoliated. The comparison between the retrograde schists and the unfoliated amphibolites is obvious.

The intensity of alteration of the amphibolites, judging by the extent to which the initial foliated fabric has been destroyed, must have been greater than in most of the enclosing schist. Some poorly foliated muscovite-chlorite schists outcrop between the layers of amphibolite but well foliated andalusite schists, only superficially altered, are also present.

The greatest concentration of unfoliated amphibolites is found in the Black-Prince - Silver King area, and there is an abrupt change from a predominance of unfoliated amphibolite to a predominance of foliated amphibolite in the unit north of the Silver King Mine (around the hinge of the Mt. Robe Synform). Unfoliated amphibolite is fairly extensively developed south and south-west of the Black Prince Mine and in the extreme north-western portion of the area. In both these areas the unfoliated amphibolites are associated with strongly retrogressed chlorite-muscovite-quartz schists.

Units of amphibolite enclosed within the larger bodies of pegmatite are very variable in character. Some amphibolites of this type are well foliated and virtually unaltered; an excellent example is Spec. 28309 a sample from a small bar of amphibolite in Little Aller Creek (403001129300). The only trace of retrogression in this specimen is slight sericitisation of the plagioclase (An_{55}). Many of the amphibolites around Big and Little Aller Creeks are of

are of this type.

Amphibole grains in many of the unfoliated amphibolites exhibit discontinuous undulose extinction. However flakes of muscovite which have grown from the sericite aggregates replacing plagioclase show no trace of deformation. The situation is similar to that in quartz to be described in Section 6.43; the undulose extinction is probably inherited from the deformed foliated amphibolite and does not indicate post-recrystallisation strain.

6.41 The epidosites

Accompanying the unfoliated amphibolites in the eastern limb of the Mt. Robe Synform are large quantities of epidosite. The epidosites form irregular masses in the amphibolite and locally over quite large areas (10-20,000 square yards, e.g. east of the Black Prince Shafts) may make up 50-60% of the amphibolite unit. The contact of the epidosites with the unfoliated amphibolites is sharp and there are no mixed rocks.

Epidosites are not common away from the eastern limb of the Mt. Robe Synform, even where unfoliated amphibolites are relatively abundant. A few examples are found in the north-west limb of the Mt. Robe Synform. Some epidosites in the latter area occur in foliated amphibolite and to some extent resemble patch-epidosites.

In hand specimen the epidosites are fine grained, green rock lacking either foliation or layering. The commonest variety is composed of a mosaic of epidote (monoclinic, negative with 2V close to 90°) and quartz with minor quantities of accessory opaques and sphene. The ratio of epidote to quartz is usually 3 to 1 or more. The quartz and

epidote occur as polygonal, equi-axed grains bounded by almost planar interfaces meeting at triple junctions. However many quartz boundaries are serrate at a very fine scale.

A second variety of epidosite (Spec. 28345) is deficient in epidote compared to the above and contains some amphibole, chlorite and opaques. The amphibole is pleochroic in vivid blue-greens and is apparently an actinolite ($Z^\wedge c = 14^\circ$).

The contact of the epidosite with the surrounding unfoliated amphibolite has not been found in a single hand-specimen in the above area. However the structure of an epidosite of a similar nature from another locality (Locality 30300132000 , Spec. 28336), in contact with a foliated and lineated amphibolite is illustrated in Fig. 6.3 . The amphibolite in hand specimen is a dark, well lineated variety, composed of hornblende, albite, epidote, quartz, clinozoisite, and accessory sphene and apatite. Opaque minerals are conspicuously absent. The hornblende (1 mm. long) grains are bounded by regular faces and have a Z-pleochroic colour of deep green. The albite is universally untwinned and is slightly altered to sericite. Very fine (?) clinozoisite granules are often included in the albite. The albite grains are ragged and variable in size (0.01 - 0.1 mm.) and their texture is quite different to that of the normal M_1 amphibolite. Quartz (10%) and epidote (3-5%) are scattered throughout the rock. A few prismatic grains of clinozoisite are associated with a quartz aggregate in one portion of the slide. There is, in the amphibolite, a slight concentration of hornblende along the contact of the amphibolite with the epidosite.

The epidosite (E) is composed of epidote and quartz in the proportions of 4:1. Sphene (0.02 mm.) is a constant accessory.
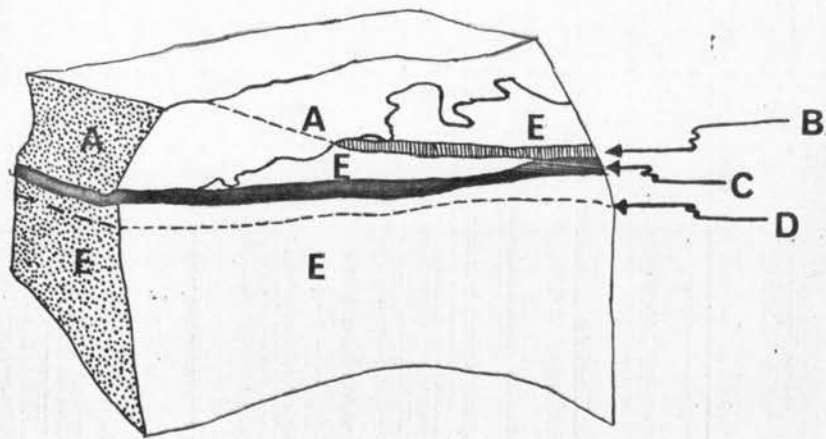
FIG. 6.3

Details of the contact between a foliated amphibolite and epidosite (see text for description and details of various layers).

Layer C which has the appearance of a vein of "pegmatitic" material in hand specimen, is composed of large grains (1-3 mm.) of quartz and orthoclase, with strongly sutured interfaces. The orthoclase is clouded with very fine particles of an unidentified high relief mineral. Clusters of clear, prismatic clinozoisite (up to 1 mm. long) and a few exceptionally large grains of sphene (0.5 mm.) are the only other components.

Layer D, represented by the dashed line in Figure 6.3 has an actual width of 0.5 mm. and is made up of prismatic grains of epidote. The epidotes are arranged with their b-axes at a high angle to the margin of the layer. At one point in the layer a single large grain of quartz (0.5 mm.) is fringed by a number of exceptionally well formed prisms of epidote. Layer B, which slants across the other layers is approximately similar. Although the layer has not been intersected in thin section, examination of the hand specimen leaves little doubt that this is so. Where Layer B reaches the amphibolite-epidosite contact it seems (in the hand specimen) to pass laterally into a thin epidote filled "fracture" in the amphibolite. In thin section the continuation is marked by a fine "vein" (0.01 mm.) containing a fine epidote mineral (? epidote). A series of similar veins almost normal to Layer B also traverse the amphibolite and the epidosite.

The epidosites described in the preceeding Section differ in several respects from the patch-epidosites (Sect. 6.30). Two important differences are the lack of foliation and the small or zero volume of amphibole in the epidosites compared to the patch-epidosites. These differences are most noticeable in Spec. 2%336 where they might be most expected if the epidosites are to be reconciled with the patch epidosites. Also noticeable in Spec. a%336 is the sharp transition between the amphibolite and the epidosite. The amphibolite

in this specimen can hardly be considered a normal M_1 variety, even though the rock is well lineated (L_2). The association of albite and epidote and the ragged texture of the albite are atypical of the M_1 amphibolite (the co-existence of albite and epidote is, of course, inconsistent with the almandine-hornblende facies assemblages of the M_1 amphibolites). Apparently the rock is the result of the retrogression of a well lineated amphibolite, in which the hornblende has survived unaltered.

In considering the origin of the epidosites we are faced with two alternatives:

(1). The epidosites are primary features,that have resulted from the metamorphism of some compositional variant of the rock which yields the amphibolites.

(2). The epidosites are a secondary feature, resulting from epidotisation of the amphibolites of a different kind to that which produced the patch-epidosites.

A number of facts oppose a primary and favour a secondary origin. Of importance are the consistent associations of the epidosites with unfoliated amphibolites and the relative restriction of large quantities of both rock types to a particular area (the Black Prince-Silver King Area). The sudden disappearance of epidosites in the amphibolites to the north of the Silver King Mine is concomitant with a predominance of foliated amphibolite in the amphibolite units. With regard to the epidosites alone, this might be regarded as a simple lateral variation in the environment (igneous or sedimentary) of formation of the amphibolites (metamorphic equivalent).

However, the decrease in epidosites occurs in a number of units, not a single unit. In this light it is very difficult to sustain the idea of a sudden lateral variation in a number of units. The irregular distribution of the epidosites is not a critical factor, for it could arise in three unrelated ways:

(1). Irregular distribution of the primary processes.

(2). The effects of transposition of the regular or irregular primary structure within the amphibolites.

(3). Irregular distribution of a secondary process (epidotisation).

By assuming the epidosites are a result of an epidotisation process we can reasonably combine the two facts which oppose the primary origin.

The differences between the patch-epidosites and the epidosites may be dependent to a large extent on their respective environments. The patch-epidosites are a very local phenomena, whereas the epidosites in the Black-Prince-Silver King area are situated in a much broader environment of retro-gression (marked by the unfoliated amphibolite). It is possible that changes accompanying the epidotisation in the latter instance have proceeded much further, more or less obliterating any influence of the original amphibolite, than in the case of the patch epidosites.

The changes in composition of the amphibolite during its conversion to epidosite must be similar in many respects to changes associated with the formation of the patch-epidosites; although the lack of actinolite in the epidosites may indicate some differences. The sharp but irregular contact in Spec. 28336 , is consistent with metasomatic alteration. Beyond the area

of definite metasomatism, the metamorphism has produced the unfoliated

amphibolites. The effect of this reasoning on the division of M_3 and M_4

metamorphism will be discussed in Sect. 6.52.

6.43   The microstructure of M_4 rocks

One of the more obvious aspects of M_4 rocks in this section is the evidence

of intra-granular strain in the aggregates, whether microscopic-mesoscopic

fabric elements that post-date B_1 folding (e.g. S_4, L_4, etc.) are present or

absent. The intra-granular strain is seen as:

(1). Undulose extinction, either continuous or discontinuous, in quartz grains.

Undulose extinction is also visible in some of the pale amphibole grains in

unfoliated amphibolites.

(2). Bent flakes of muscovite, biotite and fibres of sillimanite. Kink bands

(sub-normal to the $\{001\}$ cleavage) are also common in muscovite.

The microstructure of quartz aggregates in M_4 rocks differ markedly in one

respect from similar aggregates in M_1 rocks; the boundaries between quartz grains

are serrate and often strongly curved. With one exception (the chiastolite

schists discussed in Chapter 5), the presence of undulose extinction in quartz

grains is always accompanied by serrate or curved boundaries between contiguous

quartz grains (this statement is also true of M_2 and M_3 rocks). The converse

is also apparently true, that the curved or serrate boundaries occur only in

quartz grains with undulose extinction. One difficulty in confirming the latter

is due to the observation of undulose extinction. Undulose extinction in M_4

rocks, wheth er continuous or discontinuous, tends to form discrete bands in the

grains. Thus undulose extinction will be invisible, or at least very much

suppressed, in many grains due to the orientation of the bands with respect

to the plane of the section. However it is very rarely that undulose extinction

cannot be observed in one of two contiguous grains with a curved or serrate boundary.

There is a correlation between the intensity of undulose extinction developed in the grains of quartz, the shapes of the grains and the nature of the boundaries between the grains of the aggregate. Where the undulose extinction is continuous and not pronounced, the serrations in the grain boundaries are fine and curvature of the boundary is weak (i.e. the radius of curvature is very large or nearly infinite). An aggregate of this type may retain the most of the details of the equiaxial polygons that are characteristic of M_1 rocks. In contrast, where undulose extinction is predominantly discontinuous (with perhaps deformation lamellae in some grains), the boundaries between quartz grains of an aggregate are coarsely serrated and strongly curved, and the shape of the grains is irregular. Aggregates of the latter type are typical of the coarser grained M_4 schists.

The correlation in the previous paragraph can also be discerned in some B_3 and B_4 tectonites. Discontinuous undulose extinction and deformation lamellae in quartz are more prominent in the hinge region of mesoscopic B_3 and B_4 folds than in the limbs of the folds (Sect. 3.27). The quartz grains (in aggregates) in the hinge region have more strongly curved and strongly serrated boundaries than the less strained grains in the limbs.

Serrations in quartz-quartz interfaces are often found to coincide with the termination of sub-grain boundaries against the grain boundary in grains which possess discontinuous undulose extinction. The same obvious observational difficulty as mentioned above applies. The

interaction of the sub-grain boundary with the grain boundary takes two forms (Fig. 6·4).

Usually the two boundaries produce a triple junction (Fig. 6·4a) that resembles that development at the intersection of three grain boundaries in a grain growth texture. The interfaces near the triple junction are normally curved but nevertheless, the angle opposite the sub-grain boundary (α_1 in Fig. 6·4a) is always significantly less than 120°. Less commonly the situation depicted in Fig. 6·4b is encountered. Curvature of the boundaries along the triple junction in this case is usually strong. The angle opposite the sub-grain boundary is usually much larger (nearer to 270°) than 180°.

The resemblance between the triple junction in the first case (Fig. 6·4) and the triple junction between three grain boundaries suggests an analogous formation. Thus the serration can be thought of as resulting from an attempt to balance the sub-grain boundary energy against that of the grain boundary. With the strong curvature of the boundaries nea r the triple junction the array of boundaries can hardly be stable; nevertheless if the model above is accepted the usually small angle opposite the sub-grain boundary tentatively suggests the sub-grain boundary is much less than the grain boundary energy. This agrees with the experience in metals (see below) and is intuitively very acceptable. The second case cannot be as simply explained, for this would require that the sub-grain boundary energy be negative.

Mullendore and Grant (1961) in a study of serrate boundaries in deformed Al-Mg boundaries also noted the coincidence of sub-grain boundaries with the peak of serrations. However they dismiss.(for the alloys they studied) the hypothesis that the serrations may have resulted from efforts to balance the energies of various b oundaries; the energy of an average sub-grain boundary
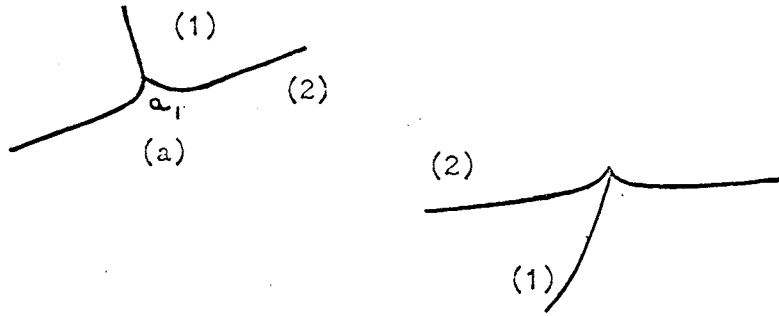
(1)

(2)

α

(a)

(2)

(1)

Figure 6.4

Sketches of the two forms in which sub-grain boundaries (1) intersect grain boundaries (2) between quartz grains (not drawn to scale).

in the alloy is too small to create other than a negligible deviation of the grain boundary. The creep tests performed by Mullendore and Grant (1961) favoured intra-granular slip and grain boundary sliding, and they believe that differential slip in the grain boundaries results in the build up of local concentrations behind the grain boundaries. They further propose that the concentration of dislocation will influence the rate of migration of the boundary (during annealing) at different points; thus creating serrations.

The explanation of Mullendore and Grant is an attempt to provide a mechanism for "strain-induced" boundary migration, a phenomena first documented by Beck, Sperry and Hu (1950). They found that boundary migration could be induced into previously annealed metals by first cold working and then re-annealing the metal. The energy for the boundary migration is derived from residual strain energy stored in the grains (as dislocations) during deformation and released during annealing by replacement of the strained lattice by a homogeneous lattice. Replacement of the strained grain by the more homogeneous grain appears to be proceeding in both of the cases shown in Fig. 6.4.

The reason the serrations develop can be explained if a number of relationships discovered during the investigation of boundary migration in metals also hold for silicates. It appears in most circumstances in metals that the angle of mis-fit of the contiguous lattices across the boundary determines the relative mobility of the boundary; low angle boundaries are less mobile than high angle boundaries.[*] During the measurement of deformation lamellae in Chapter 3, the angle between the c-axes in the various sub-grains of 30 quartz grains with prominent (discontinuous) undulose extinction were determined. The maximum angle measured (from a stereographic plot) between two adjacent sub-grains was 13°, and angles of 8-12° were numerous. Few angles of less than 7° were encountered (no doubt these angles would be found if grains

[*] Beck,(1954),McLean (1957)

exhibiting less prominent undulose extinction had been measured). Thus

a considerable difference of orientation exists between the two lattices

on either side of the line of impingement of the sub-boundary on the grain

boundary. The effect of this additional displacement has been on the

original angle of misfit of the two lattices - by increasing or decreasing

the misfit near the sub-grain boundary, could produce the two different

types of serrations observed. Obviously this hypothesis will require more

experimental information on mobility rates of boundaries in silicate aggreg-

ates before it can be regarded with confidence.

The arguments outlined, concerning the mobility of boundaries of different

misfit, also allow explanations for two other phenomena connected with M_4

metamorphism. The growth of disseminated porphyroblasts of muscovite at a

high angle to S_1 in rocks only superficially affected by M_4 metamorphism is

analogous in many respects to the formation of "duplex" structure in metals.

The argument that follows parallels that summarised by Beck (1954)* for the

formation of duplex structure in metals. The general boundary between grains

in an aggregate with a strong preferred orientation - as occurs in aggregates

of muscovite flakes in well foliated M_1 rocks - will be a low angle boundary.

If then, by accident of nucleation, there are isolated grains in the aggreg-

ates with a lattice orientation radically different to the average, then the

growth of these disoriented grains will be favoured in circumstances favouring

grain growth. This follows from the greater mobility of the high angle

boundaries of the disoriented grains against other grains of the aggregate,

compared to the low angle boundaries throughout the rest of the aggregate.

The presence of dimensionally elongate quartz grains, similar in nature and

size to grains found in the muscovite-rich portions of a normal M_1 schist,

*See also, for a summary, McLean (1957).

probably signify that the volume occupied by the porphyroblast now was originally a muscovite aggregate. The porphyroblasts are located in micaceous laminae. A second explanation of duplex structure (McLean, 1957) depends on the release with prolonged annealing of some boundaries from inhibition of movement by dispersed particles in the interface. If the release of the boundary is independent of the structure of the boundary (i.e. low or high angle boundary), then this process is unlikely to favour grains of any particular orientation. This is, of course, contrary to the observed nature of the porphyroblastic muscovite. If the release is dependent on boundary orientation, then observation of the completed (or arrested) process will not be able to distinguish this from the process above.

In either case, the growth of the muscovite could have occurred during any period (metamorphic) in which muscovite was a stable phase and annealing conditions pertained. These circumstances were probably fulfilled towards the conclusion of M_1 metamorphism (Sect. 5.35.) and perhaps again during M_4 metamorphism. Certainly muscovite was capable of grain growth during M_4 metamorphism[*]. The appearance of the porphyroblastic flakes in schists which have suffered minimal retrogression (given that very few rocks are unaffected by M_4 metamorphism) probably signifies that growth of the porphyroblasts was initiated during M_1 metamorphism.

A similar type of argument might explain the more extensive obliteration of the S_1 fabric in the unfoliated amphibolites compared to the adjacent schists. In well foliated amphibolites which are not well lineated, most hornblende grains are oriented in S_1, but the orientation in this surface is poor. Hence the contact between many grains is a high angle boundary. Grain growth of selected hornblendes, without nucleation of new grains, during the initial

[*]See Sect. 6.44.

stages of M_4 metamorphism could give rise to the relative coarseness of
these rocks and also create the mottled fabric. The mottled fabric, is
then merely a more ragged version of the laminated fabric of the foliated
amphibolite. It is noticeable that hornblende in bodies of well lineated
amphibolite in the Silver King - Black Prince area survive quite extensive
retrogressions without any apparent change in the dimensions or shape of the
hornblende grains (the retrogression is shown by the extensive replacement of
plagioclase - of the same order as that in the unfoliated rocks - by sericite
and clinozoisite; e.g. as in Spec. 28342. . The effect of a similar type of
grain growth in the schists is limited, except possibly for quartz, by the low
angle boundaries between aggregated grains (muscovite, sillimanite) or the
isolation of the phases as porphyroblasts (e.g. andalusite, biotite).
Superimposed on growth of the amphibole by boundary migration must be chemical
and structural changes to produce the optical differences between the pale
coloured amphibole and hornblende. Unless these changes can be made relatively
easily, the process could not proceed as outlined above.

6.44 The relationship between M_3 and M_4 metamorphisms and the tectonic
      history of the area

Relict B_1 folds and associated structures can often be recognised in the
tourmalinised schists, but no instance of a relict B_2, B_3, or B_4 folds or
of a B_2, B_3, or B_4 folds deforming the tourmaline rocks has been discovered.
This is particularly significant in the area around the Black Prince Shafts,
since the schists surrounding the tourmalinised rocks, and relict patches of

schists within the altered rocks are moderately deformed by B_4 folds.

Consequently we may conclude that the tourmalinisation has post-dated B_1

folding, and pre-dated the B_4. The tourmaline rock, although well foliated,

lacks the micaceous foliation necessary to deform by kinking (Sect. 3·a7).

However B_4 folding is recorded in the tourmaline rocks by intra-granular

deformation of the quartz in the rocks at the Black Prince Shafts (See below).

The absence of B_2 and B_3 folds may be fortuitous, since mesoscopic folds of

either generation are not abundant in any schists surrounding a tourmalinised

area.

Kink bands (S_4) in a tectonite from north of the Silver King mine (Spec.

28389,loc.22400128000 are emphasised by a new quartzose layering that cuts

across layering, and metamorphic lamination parallel to S_1. A modal analysis

of the rock yielded the following results:

	Quartz	Muscovite	Tourmaline
(1)	11.6%	84.3%	4.1%
(2)	31.2%	63.1%	5.7%

(1) Area outside the kink bands (1,000 points)
(2) Area inside the kink bands (1000 points)
Data from a section normal to L_4.

The concentration of quartz inside the kink band (relative to muscovite) is

marked. Incipient tourmalinisation of the rock has apparently been concurrent

with the formation of the layering, and probably some of the silica is of

metasomatic origin. Less spectacular layering is visible in a L_4 tectonite

collected several feet beyond the area of tourmalinisation at the Black Prince

Mine. The layering is due to the growth of quartz grains in the S_4 surface in

mica-rich portions of the schist (Fig. 6·5a). Again the layering is at an

angle to transposed S and metamorphic lamination. Because layering of this

type is not general in B_4 or (B_3) rocks elsewhere, we may conclude that

creation of the layering in this instance is also due to M_3 metamorphism. In

Figure 6.5

(a). Development of incipient layering in an S_4 tectonite from near the Black Prince Mine. The layering consists of quartz grains located along the S_4 surface, at an angle to a quartz layer parallel to S_1. All quartz grains in the mica layer that are present are shown (quartz, stipled; orientation of micas indicated by dashed lines).

(b). Evidence for grain growth of muscovite in the domain defining S_4. Note the way muscovite grains of either limb of the kink interlock with each other and with quartz grains with no evidence of strain (Q = quartz; muscovite, dashed).
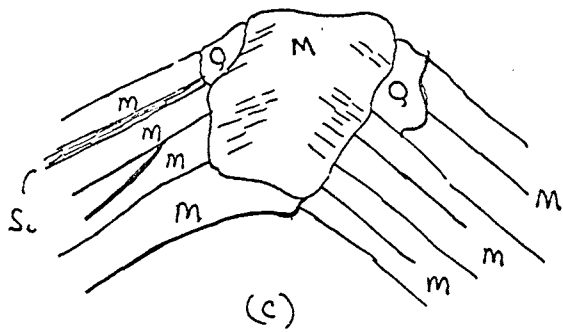
(c). Porphyroblastic muscovite grain, growing across the S_4 surface containing, fibres of sillimanite oriented parallel to S_1 in either limb of the kink (Spec. 28365; M, muscovite; Q, quartz; Si, sillimanite; quartz-sillimanite-muscovite-biotite schist).

(a)
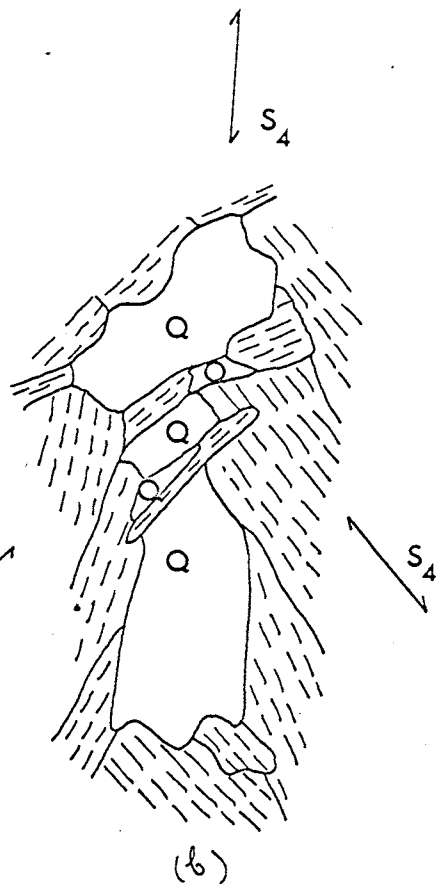
(b)

(c)

both of the cases just described, M_3 metamorphism has been synchronous with B_4 folding.

Nothing can be determined of the relative ages of M_3 metamorphism of the amphibolites, except that it post-dates S_1 and L_2. Nor is the age of B_2 and B_3 folds with respect to M_3 metamorphism known; however, M_3 metamorphism cannot pre-date either episode of folding.

Some recrystallisation of muscovite has occurred after B_4 folding; the evidence for this conclusion is contained in Fig. 6.5b. In the domain that constitutes the S_4 surface there are regions in which there is flexuring of the basal cleavage of the micas across the domain, and other regions in which strain-free micas interlock across the surface. The interlocking is, at least in many cases, due to boundary migration of grains (in S_1) on either side of the S_4 surface that existed prior to the kinking. Some smaller grains, however, may have actually nucleated in the S_4 domain. This type of structure is common in L_4 tectonites affected by M_4 metamorphism, and identical examples can be found in B_3 tectonites. Fig. 6.5c shows a muscovite flake in a sillimanite schist extensively affected my M_4 metamorphism. The flake is located across an S_4 surface and contains fine fibres of sillimanite oriented in S_1 on either side of the surface. Obviously in both cases, M_4 metamorphism post-dates B_4 folding.

The source of the intra-granular strain in M_4 rocks, where it is unaccompanied by visible mesoscopic fabric elements, is not immediately obvious. However it is reasonable to equate this deformation with B_3 or B_4 folding, especially as the same effects are present in B_3 and B_4 tectonites. The rarity of meso-scopic and macroscopic B_2 folds outside of the north-western portion of the area, when contrasted with the more uniform spread of the intra-granular deformation over the whole area, makes it improbable that B_2 folding is responsible for the observed strain. Undulose extinction in quartz grains is

often most evident in rocks which were poorly foliated (in the unaltered state) and, hence, least likely to deform by kinking of S_1 (See Chapter 3 and also Weiss and Turner, 1964, pp. 98, 114, and 475). However, the deformation of the rocks may be accomplished by more diffuse movements throughout the aggregate, giving rise to the intra-granular features.

The close connection between the undulose extinction in quartz and serration of quartz/quartz interfaces proves that the undulose extinction is due to deformation either synchronous with, or pre-dating M_4 metamorphism. The development of distinct sub-grains in the quartz is not incompatible with the general coarsening of the quartz grain size; those grains in which undulose extinction is best developed may grow more rapidly. Homogeneous sub-grains in contact with less homogeneous sub-grains in adjacent grains will tend to replace these grains, with a consequent lowering of the strain-energy stored in the lattice by deformation. The situation is analogous to the growth of homogeneous grains in a strained aggregate, except that many of the internal boundaries are sub-grain boundaries (this situation will probably be transient; it is obvious that we are looking at rocks in which the metamorphic reactions are far from complete).

Before concluding the discussion of M_3 and M_4 metamorphisms it is necessary to examine the pegmatites and their possible role in the metamorphic history of the area.

6.45   The pegmatites

No comprehensive petrological or mineralogical study of the rocks

grouped collectively as the "pegmatites" has been undertaken during the

present study. It should be obvious from the brief discussion that follows

that the pegmatites are a very heterogeneous and complex group and work

necessary to sample and prepare even a summary of their petrology is beyond

the scope of this thesis. The brief review that follows is based mainly on

field observations and is only intended to bring to light the variability of

the pegmatites and their age relative to the tectonic and metamorphic history

of the schists.

The pegmatites are acid rocks composed of various quantities of quartz,

alkali feldspar (usually microcline), albite and pale green or colourless

mica. The microcline, with typical polysynthetic twinning, is commonly both

graphic and perthitic. Tourmaline (Schorl), with the same optical properties

as that in the tourmalinised schists (Sect. 6.22) is always important as an

accessory, and sometimes makes up 3-5% of the rock. Sulphides (chalcopyrite,

pyrite, arsenopyrite, galena and sphalerite), oxides (magnetite), flourite

and very rare beryl are occasional components of quartz-rich pegmatites.

Sillimanite, garnet and epidote have also been discovered in a few pegmatite

dykes, but are fairly obviously derived locally from the schists and amphib-

olites by assimilation.

The grainsize ranges from 0.5 cm. to more than 100 cm.; and extreme contrast

of grainsize between different components is usual. Alkali-feldspar is norm-

ally the coarsest component in any particular sample. The larger pegmatite

bodies locally contain small bodies of acid rocks with a grainsize of 2-5 mm.

and a granitic texture. These rocks contain more albite and less alkali-

feldspar and mica than the coarser pegmatites, and are often rich (5%) in small needles (0.5 x 3 mm.) of tourmaline. One body of this finer grained rock sampled (28360) consists of 97% of perfectly aligned laths of albite and 3% of quartz and a pale green muscovite. The volume of these finer grained rocks is comparatively minor relative to fine and coarse grained pegmatite.

The three stocks of pegmatite are made up of two fractions of different grainsize and structure mixed at all scales. Generally one fraction consists of pegmatite with a grain-size roughly in the range 5-10 cm. and is fairly uniformly grained. The second portion consists of coarse grains of alkali feldspar (a maximum of 100 cm.) with finer quartz distributed between the alkali feldspar. Coarse books of muscovite (10-20 cm. in diameter) and tourmaline (3-15 cm. long) are scattered throughout the coarser fraction. Finer muscovite and tourmaline are also found in the finer grained pegmatite. It is impossible to estimate the comparative volumes of the tourmaline and mica in the two fractions, for the two minerals are not uniformly spread throughout either type of pegmatite. Often there is a distinctive contact between the two types of pegmatite. The coarser pegmatite may appear as small irregular shaped bodies within a fine pegmatite, or the two are separated by a sharp, but irregular contact, with tongues of the coarser pegmatite penetrating the finer pegmatite. Equally often it is impossible to define a sharp contact between the two types of pegmatite, and there is a rapid transition over a short distance (a few feet) from one type to the other. Although the two fractions are apparently mixed on all scales and in differing proportions, some definite trends can be noticed in the three stocks.

Much of the Aller Creek Stock is composed of fine grained material, some of

which borders on, or is slightly less than, the lower limit of the pegmatite size range(in particular the portion of the Stock that is cut by the lower parts of Big and Little Aller Creeks, near the edge of the Mundi Mundi Plain). The composition of this finer pegmatite is fairly uniform and an average composition is: microcline 50%, quartz 40%, albite 5%, muscovite and tourmaline 5%. Tourmaline and muscovite with blue-grey quartz (in roughly equal proportions) are found in small blebs. The blebs which are often sub-circular in section are only a few inches across.

North and South of Big and Little Aller Creek the pegmatite of the stock coarsens and more nearly resembles the character of the other stocks.

The Mt. Robe and Eldee Creek Stocks are composed of a large proportion of coarser material, especially the latter. Tourmaline and mica are evenly dispersed through the portions of pegmatite within which they occur; in contrast to the Aller Creek Pegmatite. There appears to be a higher proportion of fine grained pegmatites and acid rocks (the 2-5 mm. size range) along the northern and north-western contact of the Mt. Robe body than at any other locality. The contact of the three stocks is seldom simple. Passing from the schists there is a zone of ever increasing profusion of pegmatite dykes and sills of pegmatite separating blocks of schist and amphibolite before the solid pegmatite is encountered. Where the dip of the contact of the solid pegmatite can be deduced, it is invariably fairly steep.

Smaller dykes and sills of pegmatite show as much variation in composition as do the larger bodies, although the character of any one body is usually uniform throughout. Many of the dykes are compositionally and structurally zoned. A systematic and constantly recurring example is zoning from a fine grained quartz - microcline - albite margin (5-10 mm.), through a zone of

coarser microcline (10-20 cm.) with less quartz and albite, to a core of coarse grained quartz (10-20 cm.) with little or no microcline.

The volume of pegmatite in the Mt. Robe District is enormous, even if all the larger bodies have shallow bases. By volume, pegmatites are very important components of the Willyama Complex, whereas rocks which might be classified as "granites" are very minor*. The consistent crystallisation of the acid rocks as pegmatites rather than "granitic" rocks myst be attributed to some factor inherent in the source of the rocks. The complex structure of the larger bodies could result from multiple intrusion, but the close intermingling of fine and coarse pegmatite at all scales, with the whole forming a homogeneous body, seems to rule this out. The zoning of the dykes also confirms that the same structure could arise from complicated crystallisation in the pegmatite, rather than multiple intrusion.

The sequence of crystallisation in systems such as the albite-water system, which might represent very crudely the behaviour of pegmatites, is very complex; in all probability the crystallisation of pegmatite magmas will be equally, if not more, complex (Turner and Verhoogen, 1960). A host of different factors may affect the actual path that crystallisation may take at any point during the crystallisation (Turner and Verhoogen, 1960). The complex structure and different distribution of minor phases such as tourmaline and mica in different pegmatite bodies agrees with complexity predicted from experimental systems.

* The petrography or mineralogy of the acid rocks have hardly been touched, except for the pioneering work of Browne (1922). However, there is little doubt that throughout the complex, as in the Mt. Robe District, that rocks with pegmatite grainsize predominate.

6.46   The age of the pegmatites relative to the tectonic history of the metamorphic rocks

No instance of a pegmatite vein folded with S_1 as axial surface has been found. Examples of pegmatite sheets, generally concordant with the schistosity, folded about B_2 folds are plentiful in the area along the western side of the Aller Creek Stock. Thin layers of pegmatite are also commonly folded by B_3 and B_4 folds, but no clear example (at a mesoscopic scale) of a pegmatite cutting a fold of this type has been encountered. However, other evidence suggests that pegmatite has crystallised simultaneously with B_4 folding. Stringers of tourmaline and mica, and to a less extent, quartz, are concentrated in the hinge region of B_4 folds in pegmatites (Fig. 6.6). The stringers are parallel to the axial surface of the folds and resemble (in style) fracture cleavage sometimes developed in quartz-feldspar rocks and suggests that final crystallisation of the pegmatite post-dated the folding. This type of structure is fairly common in pegmatite veins folded about S_3 and S_4 as axial surface.

The Aller Creek and Mt. Robe Stocks are easily dated, for they cut across, and obliterate, the Mt. Robe Fault over much of its length. Consequently they must post-date B_4 folding. The situation of the two stocks in the hinge of macroscopic B_4 folds, and their gross conformity to the shape of the folds probably results from the influence of S_1 and perhaps the amphibolites on the intrusion. Along their margins, partially enclosed by projections from the main body, or within the pegmatite are numerous bodies of amphibolite and schist. The foliation S_1 in these bodies trace out the macroscopic B_4 folds, parallel to S_1 in rocks outside the stock. Moreover it is doubtful that macroscopic B_4 folds, with their dependence on slip on the schistosity could have
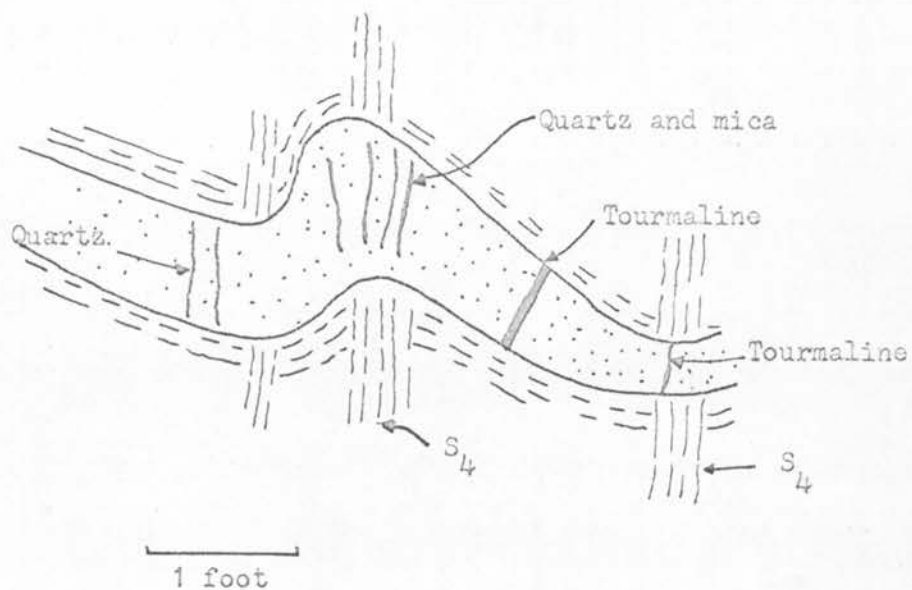
FIGURE 6.6

Arrangement of quartz and tourmaline veins in a sheet of pegmatite (stipled) folded with S_4 as axial surface. The pegmatite is concordant with schistosity in the schists (sketch; Loc. 31200104800).

developed if the pegmatites pre-dated the folds.

The Eldee Creek pegmatite is more difficult to date. It apparently post-dates the macroscopic structure developed at the Black Prince Shafts. The latter structure of course pre-dates B_4 folding (Chapter 4). Insofar as the Eldee Creek pegmatite seems to be continuous with the Mt. Robe Stock, it is tentatively assigned the same age.

From their age relationships, the larger bodies of pegmatite must be of intrusive origin. However, this might have been concluded separately from the nature of their contacts, characterised by tongues of pegmatite penetrating the schists at all angles to lithological layering and schistosity. Any sheet of pegmatite that cuts across S_1 other than in the hinge of an isoclinal fold, can scarcely be considered as pre-dating B_1 folding.

Thin sheets of pegmatite that are concordant with S_1 cannot be dated, although many of these must pre-date B_2 folding (above). However it is unlikely that these pegmatites represent transposed felspathic layering inherited from the pre-B_1 fabric. They are undeformed (mullions, fracture cleavage) and there seems no reason why they should differ significantly in their microstructure and grain size (as they do) from other M_1 metamorphic rocks. Even if we allow that all these rocks originated during the later stages of M_1 metamorphism, it is clear that by far the bulk of the pegmatites has been intruded after B_4 folding. The radio-metric dates of R.Pidgeon (Chapter 1) suggest there has been pegmatitic material introduced over an extended period.

6.47   Discussion of M_3 and M_4 metamorphism

M_4 metamorphism is not a simple contact metamorphism associated with the intrusion of the pegmatite, for, as has already been emphasised, a number of times, there is no simple correlation between the apparent intensity of M_4 metamorphism and proximity to the pegmatite stocks. In view of the discussion

of boundary migration effects in M_4 metamorphism (Sect. 6.43) and the incompleteness of the reactions, comparison of intensity of alteration at different localities are best confined to structurally and compositionally homogeneous rocks. The amphibolites are the only group of rocks that approximate these conditions. There is a very marked discrepancy in the amphibolites in the two limbs of the Mt. Robe Synform, although both limbs are close to pegmatite.

Nevertheless, some degree of correlation exists for bodies of amphibolite enclosed in the pegmatites, if we consider the nature of the pegmatite. Almost all the amphibolites enclosed in the Eldee Creek and Mt. Robe Stocks are intensely altered. Quite intense retrogression is also typical of amphibolites in the southern, coarser portion of the Aller Creek Stock, where the character of the pegmatite is more like that of the other two stocks. The finer grained portion of the last stock is characterised by only incipient retrogression of amphibolites. Intensive retrogression is apparently associated with predominance of the coarser-grained pegmatite.

The rapid variation in M_4 metamorphism in the amphibolites outside the stocks implies that the retrogression is not a "blanket" metamorphism, but rather a localised phenomena recurring over a wide area. Factors which might have contributed to the localisation of the retrogression are; the incidence of strain, variation in thermal intensity of the source, and perhaps availability of metasomatic elements. The close association of strain can hardly be accidental. At low intensity of retrogression, the association is sensible if slight straining assists the initiation of retrogression. For example, the introduction of dislocations into the biotite lattice, by creating regions in which the bonds are distorted, may lower the activation energy for the reaction biotite⟶

$\longrightarrow$ chlorite. The coarser sub-grains in rock intensely affected by M_4 metamorphism may reflect sub-grain growth from sub-grains formed as incipient deformation bands during B_3 and B_4 folding.

The retrogression may involve metasomatic elements. The reactions of M_4 metamorphism (andalusite, sillimanite $\longrightarrow$ muscovite; biotite $\longrightarrow$ chlorite; plagioclase $\longrightarrow$ sericite) favour the replacement of the M_1 phases with more hydrous phases; unless M_1 muscovite were consumed during the retrogression (which is most unlikely) at least water is required from an external source. The epidosites also seem to be at least partially metasomatic in origin. It can be argued that the epidosites would be better classified as M_3 products, in spite of the fact that they cannot be connected with a specific source. In this case the close association of the epidosites with unfoliated amphibolites (Sect. 6.42), implies that M_3 and M_4 metamorphism be considered as a single episode.

There are some advantages in this view. The maximum development of both types of metamorphism in the one area - along the eastern side of the Mt. Robe pegmatite - could point to something inherent in the relationship of the pegmatite to the country rocks (or the pegmatite itself). The same factors were then absent along the north-western margin of the pegmatite. Turner and Verhoogen (1960) have proposed that conditions in the wall rocks adjacent to a pegmatitic "magma" containing volatile phases may exert a considerable influence on the crystallisation history of the magma and the escape of the volatiles.

However, one fact tends to contradict this hypothesis. The dated examples of M_3 metamorphism pre-date B_4 folding, whereas M_4 metamorphism and the intrusion of the pegmatites post-date B_4 folding. The combination of the three events into a single episode is only possible if they are centred about B_4 folding; that is if the sulphide-bearing pegmatites are a preliminary phase of, and genetically related to, the pegmatite stocks introduced just after the conclusion of B_4

folding. M_4 metamorphism (as defined here) has then been produced in a general environment created by the intrusions. As the thermal environment evolved it may have exerted an increasingly important influence on the straining of the rocks. There is nothing inconsistent in the information gathered with this view; but, by the same token, we are justified in considering M_3 and M_4 metamorphism as discrete and genetically unrelated episodes.

In any case, it seems that M_4 metamorphism may be related to the intrusion of the pegmatites on separate grounds. A low intensity thermal environment (from the general nature of M_4 minerals, e.g., chlorite and albite) of variable character, depending on the crystallisation behaviour of the pegmatites at different points (and perhaps expressed by the relative proportions of coarse and fine pegmatite), and combined with variable release of metasomatic agents from the pegmatites could account for the apparently capricious development of M_4 metamorphism.

5.48 M$_2$ metamorphism

The rocks in the cleavage zones contain no trace of the distinctive "high-grade" minerals produced by M$_1$ metamorphism (e.g. sillimanite, andalusite, hornblende), although these minerals (possibly partially retrogressed) may be present in the adjacent rocks. Thus there has been a distinctive metamorphism associated with the cleavage zones. Where the zones cut schists the rocks are usually quartz-muscovite phyllites that may or may not contain chlorite. The muscovites are arranged to form the two cleavages described previously in Chapter 4. In one specimen from near Mt. Franks, hematite is an important component along with minor quantities of tourmaline (Spec. 28250). The rocks are very fine grained ($\angle$ 0.05 mm.). The quartz is often free of strain and may, as in the specimen already cited, form polygonal grains meeting in triple junctions.

However, the quartz in a vein intersected in a specimen from Mt. Robe (Spec. 28265) exhibit discontinuous undulose extinction and individual grains are curved. The sub-structure of the quartz is composed of distinctive polygons with sharp sub-boundaries. Quartz grains with a similar sub-structure have been found in quartz lenses from a cleavage zone crossing amphibolite near the adit of the Mt. Robe Mine. The fine, strain-free quartz grains apparently represent recrystallisation products while the strained grains are inherited from the parent rock.

Where the cleavage zones cut amphibolite the rock produced is composed mainly of chlorite and albite with only minor quartz (e.g. Spec. 28305).

Since the cleavage zones either pre-date or are synchronous with B$_4$ folding, metamorphism associated with their formation pre-dated B$_4$ folding. To what extent the mineral assemblages now observed in the rocks from the zone represent conditions during formation of the zones is unknown. The mineral

assemblages found in schists and amphibolites are consistent in a general way with the tendency of M_4 metamorphism to produce assemblages of the greenschist facies. For zones formed during B_4 folding (e.g. along the Mt. Robe Fault), the actual metamorphic conditions may have been those of M_4 metamorphism. However, because of deformation in the zones, as witnessed by the formation of a new foliation to produce fine grain sizes, the displacement of the M_1 assemblages by greenschist assemblages has been much more complete than in M_1 rocks in general. Still the possibility exists that the zone completely pre-dates M_4 metamorphism and the rocks now observed reflect a distinct metamorphism localised along the cleavage zones.

6.49   The calc-silicates

Although the mineral assemblages of the calc-silicates are often similar
to those produced by M$_3$ metamorphism of amphibolites, the calc-silicates
have a separate existence. The thin layering so characteristic of the calc-
silicates is foreign to the altered amphibolite. The commonest mineral
assemblage in the calc-silicates is diopside and quartz with accessory
apatite and sphene. Variation in the ratio of diopside to quartz and the
grainsize of each component differentiate the layering of the calc-silicates.
Grainsizes range between 0.1 and 1 mm.; a fairly constant size prevails in
any one layer. Plagioclase, now mainly sericitised, is only occasionally an
important component in some of the layers. Overall, diopside usually constitutes
80% or more of the portions of the rocks sampled.

A orange-pink garnet sometimes forms distinct layers in the calc-silicates,
especially in the thinner, boudinaged layers. An amphibole, that is probably
an actinolite (Z^c = 12-14°, pleochroic in brilliant blue-green colours),is
only sometimes important.

Epidote (in thin section pale green slightly pleochroic, monoclinic negative
with a 2V of 75° to 85°) and clinozoisite (colourless, monoclinic positive,
2V of 80-85°) are constantly encountered, often in the same rock. Clinozoisite
is often associated with layers of coarse quartz (up to 4 mm.) that more or
less parallel the quartz-diopside layers. The quartz exhibits marked discon-
tinuous undulose extinction due to the presence of polygonal sub-grains. The
sub-structure is distinctly different to that encountered in quartz in the
schists or amphibolites, but is fairly typical of the pegmatites. Inclusions
of diopside are not uncommon in the quartz, and they and the diopside bordering

the quartz have a peculiar cloudy appearance. The clinozoisite is present in layers laterally continuous with the quartz or along the margin of the quartz layer. Small quantities of epidote and/or clinozoisite are found in the diopside rock bordering the quartz layers. It appears that the quartz layers and the clinozoisite represent a type of M_3 metamorphism imposed on the diopside-quartz rocks.

M_3 metamorphism of a different type is evident in a calc-silicate enclosed in pegmatite near the north-western edge of the area (Spec. 28261). The specimen contains layers parallel to the diopside-quartz layers of vesuvianite (up to 3 mm. grainsize). The vesuvianite is riddled with inclusions of quartz and diopside with distinctive"shard-like" shapes. Again the diopside in and near the vesuvianite has a cloudy appearance. The vesuvianite is apparently replacing whose layers of diopside and quartz in the calc-silicate and is a result of M_3 metamorphism.

Clinozoisite and epidote also occur in circumstances which suggest they may have been members of the original M_1 mineral assemblage. Layers composed of clinozoisite and sphene are prominent in the small calc-silicate body at Mt. Franks where neither M_3 nor M_4 metamorphisms are prominent (Spec. 28254). However, clinozoisite (which is more common than epidote) in other specimens (e.g. Spec. 28332) form granular aggregates that have a distinct grain shape. Apparently the clinozoisite is replacing some other phase in this instance. The more quartzose parts of the calc-silicates are composed of up to 50% quartz with biotite (10-15%) and minor garnet (Spec. 28332). In the specimens examined clinozoisite or sericite constitutes the remainder of the rocks, but both minera may be replacing other minerals.

The M_1 mineral assemblages of the calc-silicates were probably diopside-quartz ($\pm$ plagioclase), garnet-diopside-quartz, and actinolite-plagioclase-quartz with minor amounts of epidote, biotite, sphene, and apatite.

C O N C L U S I O N S   A N D   S U M M A R Y

When the fabric of the metamorphic rocks is studied in detail at the mesoscopic and macroscopic scales, a picture of an intensely and repeatedly deformed complex evolves. Due to a combination of circumstances the major structure of the mapped area is dominated by two relatively simple folds. The apparent simplicity of these folds belies the complex tectonic history of the area. It seems possible to divide the history of the mapped area into two broad episodes:

(1) B_1 folding and M_1 metamorphism

(2) B_4 folding, the intrusion of the pegmatites, M_3 and M_4 metamorphisms.

If the radio-metric dates of R. Pidgeon are representative of all the pegmatites, then the two episodes may be separated by nearly 300 million years (further dates are given by Binns, 1963, including some from the area mapped. The dates obtained from a single specimen by two methods or by using two different minerals sometimes show marked discrepancies - up to 600 millions years. The results, because of their internal inconsistency, can be interpreted in a number of ways and are of no value in clarifying the history of the region)

Knopf and Ingerson (1938, p.190) warned of the difficulties of recognising transposition fabrics. Where, as in the area mapped, the transposition is nearly complete the difficulties are particularly evident. However, the persistence of isoclinal folds and fold hooks throughout the area are clear evidence of transposition. The effect of the transposition on the stratigraphic sequence is not very clear. There seems little doubt that useful units can be mapped in the schists, but if macroscopic B_1 folds are similar in style to observed mesoscopic B_1 folds, the compilation of a stratigraphy over large areas may be difficult.

The principal axes of stress for B_1 folding were probably oriented normal and

parallel to schistosity with one axis coincident with the lineation L_2. The axis normal to S_1 may have been the major axis. The analysis of the various sub-fabrics, inherited and imposed, suggest the presence of an earlier generation of folds. Broad concentric folds with fracture cleavage or slaty cleavage in the more shaly rocks best fit the properties deduced from the geometry and the sub-fabrics of B_1 folds. If B_1 folding took place more or less synchronously with M_1 metamorphism - that is at relatively high temperatures of the almandine-amphibolite facies - then it is likely that viscous flow or diffusion were the primary mechanisms of deformation. In this case the mechanical properties of layering and the old foliation may have been suppressed and the movement picture orthorhombic. Alternatively the movement picture may have been monoclinic - and the presence of glide surfaces tends to confirm this - and the preferred orientation of quartz and layering in the boudins are related directly to stress.

M_1 metamorphism outlasted deformation and interfacial tensions played a significant role in determining grain shapes. The very large interfacial tensions of quartz-mica boundaries compared to quartz-quartz interfaces meant that the preferred orientation of mica was the most important influence. The effect of interfacial tensions is to produce an image of the S_1 fabric as determined by deformation. Thus no part of the fabric of B_1 folding has been lost because of grain growth. It will always be impossible to tell if the departure of the interfacial angles from 120° in quartz aggregates is due to imperfect annealing, the effect of boundaries with other phases, or true anisotropy of the interfacial tensions for different orientation of the boundaries with respect to the contiguous lattices and different angles of mis-fit of the lattice. We may suspect that the last is important. Otherwise the boundary

(quartz-quartz) must possess a characteristic structure for all orientations capable of nullifying the influence of each of the juxtaposed lattices. Measurements of interfacial angles in natural quartz aggregates in contact with different phases in a wide variety of rocks (contact and regional metamorphics) would tend to indicate anisotropy, if the interfacial angles have a peak frequency that is repeated and a fairly characteristic spread.

The second generation of folds are not important enough in the Mt. Robe District to be considered a major episode; apparently they represented a minor episode confined to the north-western portion of the area. There is apparently no metamorphic event associated with B_2 folding.

The second major episode is less surely established and the possibility remains that the events added together here may have been separate. The style of B_4 folds contrasts markedly with B_2 folds. However both generations of folds are very widespread. In any case the orientation of the initial fabric is not a factor that affects the style of B_4 folds or associated kink bands (from the wide range of orientation of L_4). The differences in style, then, may reflect a change in the whole metamorphic environment of the complex. By significantly altering the mechanical properties of the rocks between B_2 and B_4 folding, the metamorphic environment may have influenced the manner in which the rocks responded to deformation. (Other factors may be important, such as the magnitude of the stresses and rate of strain).

A change in the thermal conditions was not sufficient to cause retrogression of the schists and amphibolites by itself. The retrogression is partially dependent on the introduction of material from the pegmatites. On the other hand, the occurrence of significant retrogression at a distance from the pegmatites tending to produce mineral assemblages of the Albite-Epidote-Hornfels

facies, must depend on a thermal environment created by more than the local pegmatites.

Apparently other major folds similar to the Mt. Robe Synform and the Western Antiform are not uncommon in the Willyama Complex. King and Thomas (1953) record a large number of synforms in which schistosity (gneissosity) closes around the hinge parallel to layering and with the same open shape (in the hinge) of the Mt. Robe Synform. They note, however, that antiforms seldom have this shape and are usually much tighter and faulted in the hinge region. The first part of this description at least fits the Western Antiform. King and Thomas (1953, p.549) also comment on a lineation "due to mineral elongation which is generally sympathetic with the plunge of the folded structures". Again the Mt. Robe Synform is apparently typical, although the lineation (L_2) is not strictly parallel to the fold axis. The actual distribution of L_2 is on a cone about the fold axis and the results point to the value of the stereographic nett in distinguishing apparent patterns from real patterns.

The schistosity imparted to the rocks during B_1 folding was the dominant factor in the mechanical behaviour of the rocks during B_3 and B_4 folding. One aspect of the influence of S_1 is apparent in the lack of B_3 and B_4 folds in layering and schistosity in areas where they intersect. Thus at Mt. Franks, B_4 folds in the schistosity occur in between the units without folding the units themselves. The discontinuity of the structure of S_1 between two units (e.g. mica-schist and a quartzose mica schist boundary) is sufficient to prevent folding across the contact. It is doubtful that the Mt. Robe Synform and Western Antiforms could have developed if transposition had not been so complete. If this is the general rule then the Willyama Complex may be divided into two types of macroscopic domains consisting of B_3 or B_4 folds on the

transposed limbs of macroscopic B$_1$ folds (as is suggested by the "basin"
and "domes" of Andrews (1922) separated by zones of "intense dislocation and
flowage").

The pegmatites have a long history and may provide the best source for the
determination of absolute ages of the tectonic and metamorphic events. Evidently
throughout the history of the Willyama Complex after B$_1$ folding there was a
ready source of acid material. The recognition of the second major episode
depends on the recognition of M$_3$ metamorphism which pre-dated B$_4$ folding, as a
prelude to the intrusion of some pegmatites during B$_4$ folding and the main
phase of intrusion after B$_4$ folding. To a large extent the structure of the
metamorphic rocks controlled the shape of the intrusions.

Absolute ages from pegmatites from the following situations should clarify
the history of the area:

(1) From pegmatites in glide surfaces in B$_1$ folding.

(2) From pegmatites folded by B$_2$ folds and pegmatites occurring along the hinge
of B$_2$ folds.

(3) From sulphide-bearing pegmatites at the Black Prince Shafts which pre-date
B$_4$ folding.

(4) From pegmatites that have apparently crystallised during B$_4$ folding.

(5) From the Aller Creek Stock where it cuts across the Mt. Robe Fault.

B$_3$ folds have styles that are indistinguishable from those of B$_4$ folds. The
infrequency of B$_3$ folds (and hence the much less penetrative nature of the
deformation) signifies that metamorphic conditions rather than magnitude of
stress determined the style. Thus B folds may have developed in much the same

metamorphic environment as B_4 folds and represent a low intensity deformation prior to the main phase of B_4 folding.

The fault-fold structure at the Black Prince Shafts represents a single, non-penetrative event that occurred sometime between B_1 and B_4 folding. From the distribution of the lineation L_2 in the fold structure on the southern side of the fault (sub-area 2) slip on schistosity was the main mechanism of deformation away from the fault. If vertical, the fault has an orientation similar to some of the cleavage zones in the area (e.g. at the Consolation Shafts) and may be a particular development of a period of faulting after B_1 folding. Many of the cleavage zones pre-date B_4 folding.

R E F E R E N C E S

Andrew, E. C., 1922, The geology of the Broken Hill District: Mem. Geol. Surv. N.S.W. No. 8, p.1-266.

Bailey, S. W., Bell. R. A., and Perry, C. J., 1958, Plastic deformation of quartz in nature: Geol. Soc. America Bull. V.69, p.1443-1466.

Barrett, C. S., 1952, Structure of metals: McGraw-Hill, New York.

Beck, P. A., 1954, Annealing of cold worked metals: Advances in Physics (Philos. Mag. Supp.) V.3, p.245-324.

Beck, P. A., and Sperry, P. R., 1950, Strain induced grain boundary migration in high purity aluminium: J. Applied Physics, V.21, p.150.

Binns, R. A., 1962, Metamorphism in the Broken Hill District, N. S. W., Thesis submitted for Ph.D. Degree, Cambridge University.

Binns, R. A., 1963, Some observations on metamorphism at Broken Hill, N.S.W: Proc. Australian Inst. Min. Metall. V.207, p.239-261.

Binns, R. A., 1964, Zones of progressive regional metamorphism in the Willyama Complex, Broken Hill District, N.S.W: Jour. Geol. Soc. Australia, V.11, p.283-330.

Brace, W. F., and Walsh, J. B., 1962, Some direct measurements of the surface energy of quartz and orthoclase: American Mineral, V.47 (9-10) p.1111-

Carter, N. L., Christie, J. M. and Griggs, D. T., 1964, Experimental deformation and recrystallisation of quartz: Jour. Geol. V.72, p.687-733.

Christie, J. M., Griggs, D. T. and Carter, N. L., 1964, Experimental evidence of basal slip in quartz: Jour. Geol. V.72, p.734-756.

Christie, J. M. and Raleigh, C. B., 1959, The origin of deformation lamellae in quartz: Am. Jour. Sci. V.257, p.385-407.

Cloos, E., 1947, Boudinage: Trans. American Geophy. Union, V.28, p.626-32.

Condon, M. A., 1959, Sedimentary structures in the metamorphic rocks and ore bodies of Broken Hill: Proc. Australian Inst. Min. Metall., No.189,p.47-65

Deer, W. A., Howie, R. A. and Zussman, J., 1962, Rock forming minerals, V.1,

V.2, London, Longmans, Green and Co. Ltd.

Den Tex, E., 1958, Studies in comparative petrofabric analysis: The

Broken Hill Lode and its immediate wall rock: Australian Inst. Min.

Metall. Stilwell, Anniv. Vol. p.77-104.

Desch, D., 1919, J. Inst. Met. V.22, p.241.

de Sitter, L.U., 1964, Structural geology: McGraw-Hill Book Company, New York,

(2nd Edition) 552 pages.

Edwards, A. B., 1958, Amphibolites from the Broken Hill District: Jour. Geol.

Soc. Australia, V.5, p.1-32.

Fairbairn, H. W., 1941, Deformation lamellae in quartz from the Ajibik

formation, Michigan: Geol. Soc. America Bull. V.52, p.1265-78.

Gibbs, J. W., 1906, as published in "The Scientific Papers of J. Willard

Gibbs": V.1, Dover Publications Inc., New York, 1961.

Griggs, D, and Handin, J., 1960, Observations on fracture and a hypothesis

of earthquakes: Geol. Soc. America, Mem. 79, p.347-364.

Griggs, D. T., Paterson, M. S., Heard, H., and Turner, F. J., 1960; Annealing

recrystallisation in calcite crystals and aggregates: Geol. Soc. America

Mem. 79, p.21-37.

Griggs, D. T., Turner, F. J., and Heard, H, 1960, Deformation of rocks at

500° C. to 800° C: Geol. Soc. America Mem., V.79, p.39-104.

Hansen, E. C., and Borg, I. Y., 1962, The dynamic significance of deformation

lamellae in quartz of a calcite-cemented sandstone: Am. Jour. Sci.

V.260, p.321-336.

Harker, D., and Parker, E. R., 1945, Grain shape and grain growth: Trans.

Amer. Soc. for metals, V.34, p.156.

Herring, C., 1951, Surface tension as a motivation for sintering: in "The

Physics of Powder Metallurgy, ed. Kingston, W. E., New York, McGraw-Hill

Book Co.

Herring, C., 1953, The use of classical macroscopic concepts in surface energy problems: p.5-172 in Structure and Properties of Solid Surfaces ed. by Gomer, P. and Smith, C. S., Chicago, University of Chigago Press.

Knopf, E. B., and Ingerson, E., 1938, Structural Petrology: Memoir 6, Geol. Soc. America, 270 pages.

King, H. F., and Thomson, B. P., 1953, The geology of the Broken Hill District, in "Geology of Australian Ore Deposits", p.533-77 (Australian Inst. Min. Metall.)

Leake, B. E., 1964, The chemical distinction between Ortho- and Para-amphibolites: Jour. Petrol. V.5 (2), p.238-254.

Leslie, R. B ., and White, A. R., 1955, The "Grand" unconformity between the Archean (Willyama Complex) and Proterozoic (Torrowangee Series) north of Broken Hill, N.S.W: Trans. Roy. Soc. S. Australia, V.78, p.121-133.

Lomer, W. M., and Nye, J. F., 1952, A dynamical model of crystal structure 4. Grain Boundaries: Proc. Royal Soc. V.212, p.576-584.

Mc. Lean, D., 1957, Grain Boundaries in metals: Oxford, Clarendon Press, 346 p.

Mawson, D., 1912, Geological investigations in the Broken Hill area: Mem. Roy. Soc. South Australia, No. 2, p.211-319.

Misar, S, 1963, Notes on occurrences of chloritoid at Broken Hill, N.S.W;

Miyashiro, A., 1958, Regional metamorphism of the Gosaisyo-Takanuki District in the central Abukuma Plateau: J. Fac. Sci. Tokyo Univ., sec. II, V.11, p.219-272.

Miyashiro, A, 1961, Evolution of metamorphic belts: Jour. Petrology, V.2, p.277-311.

Mott, 1948, Slip at grain boundaries and grain growth in metals: Proc. Physical Society V.60, p.391

Mullendore, A. W., and Grant, N. J., 1961, Grain Boundary serrations developed during creep: in Structural Processes in Creep, Reprint of Symp. Iron and Steel Inst. , p.44.

Orowan, E., 1942, A type of plastic deformation new in metals: Nature, London, p.643.

Paterson, M. S., and Weiss, L. E., 1961, Symmetry concepts in the structural analysis of deformed rocks: Geol. Soc. America Bull., V.72, p.841-882.

Ramberg, H., 1955, Natural and experimental boudinage and pinch-and-swell structures: Jour. Geology, V.63, p.512-526.

Ramsay, J. G., 1960, The deformation of early linear structures in areas of repeated folding: Journ. Geology, V.68, p.75-93.

Riley, N. A., 1947, Structural petrology of the Baraboo quartzite: Jour. Geology, V.55, p.453-475.

Shuttleworth, R., 1950, The surface tension of solids: Proc. Phys. Soc. London, V.63a, p.444-457.

Slemmons, D. B., 1962, Determination of volcanic and plutonic plagioclases using a three - or four - axis universal stage: Geol. Soc. America Special Paper No. 69.

Smith, C. S., 1948, Grains, phases and interfaces: American Inst. Min. Metall. Eng., V.175, p.15.

Smith, C. S., 1952, Interphase interfaces: In "Imperfections in nearly perfect crystals", Ed. W. Shockley, John Wiley Sons., New York, p.377-401.

Smoluckowski, R., 1951, Theory of grain boundary motion: Physics Rev. V.83, p.69.

Swalin, R. A., 1962, Thermodynamics of solids: N.Y., Wiley, 343 p.

Thomas, W., 1961, Unpublished notes on talk given to A.N.Z.A.A.S. conference, Brisbane, 1961.

Turner, F. J., 1947, Determination of plagioclase with the four-axis
universal stage: American Miner., V.32, p.389.

Turner, F. J., 1948, Mineralogical and structural evolution of the metamorphic
rocks: Geol. Soc. America, Mem. 30.

Turner, F. J., and Verhoogen, J., 1960, Igneous and metamorphic petrology:
New York, Mc. Graw-Hill Book Co., 694 p.

Turner, F. J., and Weiss, L. E., 1963, Structural analysis of metamorphic
tectonites: New York, McGraw-Hill Book Co., 545 p.

Voll, G., 1960, New work on petrofabrics: Liverpool and Manchester Geol. Journ.
2 Pt. 3, p.503-567.

Weiss, L. E., 1959, Structural analysis of the Basement System at Turoka,
Kenya: Overseas Geol. and Mineral Resources, V.7, No. 1, p.1-35; No. 2,
p.123-135.

Weiss, L. E., 1959(a), Geometry of superposed folding: Geol. Soc. America
Bull., V.70, p.91-106.

Weiss, L. E., and McIntyre, D. B., 1957, Structural geometry of Dalradian
rocks,at.Loch Leiven, Scottish Highlands, Jour. Geol., V. 65, p.575-602.

The University of Sydney

SYDNEY, N.S.W.

18th April, 1967

Miss J. Alison,
Acquisitions Librarian,
FISHER LIBRARY.

Dear Miss Alison,

I wish to advise that I have forwarded under separate cover, original copies of theses submitted by the following candidates for the degree of Doctor of Philosophy. All the theses have been successful.

D. E. Anderson	Department of Geology & Geophysics
M. Batley	" " Physical Chemistry
J. A. Bishop	School of Biological Sciences (Zoology)
D. G. Blair	School of Physics
D. Britz	Department of Agriculture
I. G. Brown	School of Physics
Mrs Wendy Goodwin	Department of Chemistry
G. B. Guise	Department of Organic Chemistry
P. S. Hallman	" " " "
T. P. Hopwood	" " Geology & Geophysics
A. Mahmood	School of Biological Sciences (Botany)
Mrs Helen Ramsay	School " " " "
R. E. Thomas	Department of Pharmacy
J. N. Ward	Department of Mathematics (Pure Mathematic
R. E. Wass	" " Geology & Geophysics

The Structural and Metamorphic Petrology of the Mt. Robe District,

Broken Hill, N. S. W.   ------   D. E. Anderson.

The tectonic and metamorphic histories of a portion of the Willyama
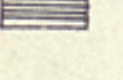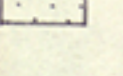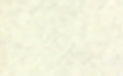Complex are clarified and described.
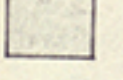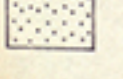
Four generations of folds are distinguished. Folds of the first
generation are isoclinal and are characterised by an axial-surface
schistosity. Two lineations, usually at an angle to each other, are
associated with the folds. Transposition of layering to parallel schist-
osity is almost complete. Analysis of the various sub-fabrics
contributing to the triclinic symmetry of the folds suggests the existence
of an even earlier phase of folding. Folds of the second generation are
also isoclinal, but lack an axial-surface foliation.

The third and fourth generations of folds are characterised by the
development of a conjugate set of kink bands in their hinges. The style
of the folds is very variable and reflects the properties of the initial
fabric. The preferred orientation of basal deformation lamellae in quartz
in a fourth generation fold allows the fixing of the principal axes of
stress for the deformation. The minor and major axes are sub-horizontal
and the intermediate axis plunges steeply parallel to the fold axes. A
study of the geometry of two sets of deformation lamellae in a single grain
indicates that they may be parallel to a number of the common forms of
quartz.

The major structure of the area is determined by one first generation
fold, two fourth generation folds and an inhomogeneous fold-fault structure.

Metamorphism to produce mineral assemblages of the Almandine-Amphibolite
Facies followed or accompanied the first generation of folds. The area can
be zoned with respect to the distribution of andalusite and sillimanite.
Interfacial tension played a significant role in determining the shapes of
grains but probably did not alter the shape of aggregates determined by
deformation. The relative tensions, as determined from the measurement
of interfacial angles at triple junctions, of quartz-quartz and quartz-
muscovite boundaries are the most important factors determining grain
shape. Local metamorphism associated with the intrusion of pegmatites
and a more general retrogression followed the first phase of metamorphism.
The various phases of folding and metamorphism probably represent two
major episodes in the history of the Willyama Complex.

GEOLOGICAL MAP

— OF —

MT. ROBE DISTRICT

BROKEN HILL N.S.W.

MAGNETIC NORTH
7° EAST

0   1000   2000   3000   4000   5000
SCALE of FEET

[Distance between coordinate lines is 10,000 ft.]

Legend:

- QUARTZ – MUSCOVITE – BIOTITE SCHIST
- QUARTZ – PLAGIOCLASE ROCK [1]
- GREY SCHIST [2]
- CHIASTOLITE SCHIST [3]
- QUARTZ – MUSCOVITE – BIOTITE – ANDALUSITE SCHIST [4]
- QUARTZ – MUSCOVITE – ANDALUSITE SCHIST [5]
- SILLIMANITE SCHISTS
- AMPHIBOLITE
- CALC – SILICATE ROCK
- QUARTZ – MUSCOVITE SCHIST
- PEGMATITE

T.S. TOURMALINISED SCHIST

CREEK
H   HUT
MINE
TRACK
WINDMILL

GEOLOGICAL CONTACTS
Fixed
Approx.
Limit of outcrop

- DIP and STRIKE of LAYERING S_o
- DIP and STRIKE of SCHISTOSITY S_1
- PLUNGE of LINEATION L_1 B_1
- PLUNGE of LINEATION L_2
- DIP and STRIKE of KINK BAND S_3 and B_3 LABELLED
- PLUNGE of KINK AXIS S_4 and B_4 UNLABELLED
- F   FAULT
- CLEAVAGE ZONE
- ANTIFORM
- SYNFORM
- S_1 and B_1 SPECIFICALLY LABELLED
- R_1, S_1, S_2, L_2 ETC. AS DEFINED IN TEXT

Map labels:

PLAIN

WESTERN ANTIFORM

DIAMOND JUBILEE

MT. ROBE SYNFORM

BIG ALLER CREEK

LITTLE ALLER CREEK

ALLER CREEK PEGMATITE

MUNDI MUNDI

Approx. contact massive pegmatite

MT. ROBE PEGMATITE

Approx. contact massive pegmatite

Well developed kink bands S_3 and B_3

SILVER KING

GOLDEN CREST GROUP

MT. ROBE CREEK FAULT

Dip 70S

S BEEK

GUN CREEK

MT. ROBE

Epidiorite

V. retrog. schists much peg

CONSOLATION

MT. ELDEE

BLACK PRINCE

Chin-mont. rocks (not fol.)

ELDEE CREEK

Boudins

ELDEE CREEK

PEGMATITE

ELDEE CREEK

TERRIBLE DICK

MT. FRANKS

Coordinate system from Zinc Corp. Mine (1950, Kilns and Thomson 1953)

D. E. ANDERSON 1965

140000 N   130000 N   120000 N   110000 N   100000 N

FIG. 4.1 DATA FOR THE ANALYSIS OF THE MACROSCOPIC STRUCTURE

NOTES.

1. All data are plotted on the lower hemisphere of an equal-area projection. The index mark refers to magnetic north and directions (in the text) refer to this.

2. Sub-areas are numbered from 1 to 14 and their location given on the accompanying map. Each column of the table below presents the data measured in a particular sub-area.

3. Key to stereograms:

Total number of measurements.

Contours - per cent per 1% area.

4. Reference to specific stereograms is by Fig. 4.1,(column)4 (row)a.